Optimization and Ultimate Limitations for Immunoassay and Clinical Diagnostics

by

Christine F. Woolley

A Dissertation Presented in Partial Fulfillment
of the Requirements for the Degree
Doctor of Philosophy

Approved July 2015 by the
Graduate Supervisory Committee:

Mark Hayes, Chair
Joshua LaBaer
Alexandra Ros

ARIZONA STATE UNIVERSITY

August 2015

ABSTRACT

Biological fluids, in particular blood plasma, provide a vital source of information on the state of human health. While specific detection of biomarker species can aid in disease diagnostics, the complexity of plasma makes analysis challenging. Despite the challenge of complex sample analysis, biomarker quantification has become a primary interest in biomedical analysis. Due to the extremely specific interaction between antibody and analyte, immunoassays are attractive for the analysis of these samples and have gained popularity since their initial introduction several decades ago. Current limitations to diagnostics through blood testing include long incubation times, interference from non-specific binding, and the requirement for specialized instrumentation and personnel. Optimizing the features of immunoassay for diagnostic testing and biomarker quantification would enable early and accurate detection of disease and afford rapid intervention, potentially improving patient outcomes. Improving the limit of quantitation for immunoassay has been the primary goal of many diverse experimental platforms. While the ability to accurately quantify low abundance species in a complex biological sample is of the utmost importance in diagnostic testing, models illustrating experimental limitations have relied on mathematical fittings, which cannot be directly related to finite analytical limits or fundamental relationships. By creating models based on the law of mass action, it is demonstrated that fundamental limitations are imposed by molecular shot noise, creating a finite statistical limitation to quantitative abilities. Regardless of sample volume, 131 molecules are necessary for quantitation to take place with acceptable levels of uncertainty. Understanding the fundamental limitations of the technique can aid in the design of immunoassay platforms, and assess

progress toward the development of optimal diagnostic testing. A sandwich-type immunoassay was developed and tested on three separate human protein targets: myoglobin, heart-type fatty acid binding protein, and cardiac troponin I, achieving superior limits of quantitation approaching ultimate limitations. Furthermore, this approach is compatible with upstream sample separation methods, enabling the isolation of target molecules from a complex biological sample. Isolation of target species prior to analysis allows for the multiplex detection of biomarker panels in a microscale device, making the full optimization of immunoassay techniques possible for clinical diagnostics.

DEDICATION

For Tyler, you know why

ACKNOWLEDGMENTS

First I must thank my advisor, Dr. Mark Hayes, for the guidance and support that have helped me through these years of scientific development. Thank you to my committee members, Drs. Joshua LaBaer and Alexandra Ros for your time commitment and the contributions that have helped to improve the quality of my work.

I would also like to thank all of the Hayes lab group members, without whom I could not have made it through graduate school as successfully. A special thanks to Fanyi Zhu for all of your help in device fabrication and collaboration in experiments. Thank you to Jie Ding for entertaining conversations and assistance in the lab. Thanks to Claire Crowther and Ryan Yanashima for their expertise in microscale device design, and to all of the others who have helped along the way.

On a more personal level I would like to thank my husband, Tyler. Thank you for your support and encouragement over the years, for never letting me give up, and for being my best friend. I could not have gotten through these years without you. Thank you to my mom, for pushing me to reach my academic goals, encouraging my passion for science from a young age, and always being there for me. Thanks to my dad, for the support during my years as a student and for cheering me on as I pursued my doctorate. Thank you to my brother, for offer distraction and support from across the country, to my grandparents for always believing in me and encouraging my academic pursuits, and to all the friends and family who have supported me during this journey. I could not have gotten here without you.

TABLE OF CONTENTS

Page

CHAPTER Page

CHAPTER Page

CHAPTER Page

LIST OF TABLES

LIST OF FIGURES

Figure Page

CHAPTER 1

INTRODUCTION

1.1 Disease, and the Role of Biological Species

It is unlikely that one can ever know the origins of medicine exactly, as the practice of treating the sick seems as old as mankind. However, the concept of illness has evolved throughout time, and the foundations of our modern understanding of disease are easier to trace. Historic cultures throughout the world attributed illness to witchcraft, demons, hubris, or the will of gods [1-3]. In these cultures a physician was closely associated with religion and functioned primarily to gather herbs or perform rites believed able to reverse the misfortune of the sick [1-4].

The foundation of modern medical beliefs can be attributed to the ancient Greeks. While Greece still maintained one school of thought based on spiritual beliefs, a second emerged, founded by Hippocrates, stating that treatment should be based on observations of the condition of the human body [1,2]. The emergence of diagnostics based on observation lead to a new belief about the origins of disease. The body was understood to consist of four humors (blood, phlegm, yellow bile and black bile) that must be in balance to maintain physical health [2,3]. While this medicine was more grounded in observation than that practiced in earlier cultures, its treatments functioned only to restore this balance, and disease was primarily attributed to changes in season, climate, or the habits of an individual [3].

For several centuries the humoral theory of medicine persisted, until the 1880s with the emergence of Germ Theory developed by Robert Koch and Louis Pasteur [5-7]. With the evolution to a belief that disease states are produced by molecular

entities foreign to the body, or from a physical event occurring internally, technology has had to evolve to improve the ability to recognize and diagnose disease states. A clear and direct line could be drawn between the Germ Theory philosophy and the development modern diagnostic techniques, including histology and the testing of biological fluids.

1.2 Current Disease Diagnostics

When testing biological fluids, the monitoring of minute changes in disease-indicating species is needed in order to make effective healthcare decisions and allow early disease intervention. In many cases, such as that of myocardial infarction (MI) where early intervention leads to a much better prognosis, the rapid serial monitoring of target species may be required for the positive identification of a disease state so appropriate courses of treatment can be administered [8].

Initial clinical evaluations in the diagnosis of MI have a two-fold objective: to assess the likelihood that observed cardiac symptoms relate to an acute coronary event, and to determine an individual's risk of a experiencing subsequent cardiac event [8]. While it is necessary to consider factors such as a patient's medical history, visible physical symptoms, and results of the electrocardiogram (ECG), cardiac biomarkers are also valuable in achieving the diagnostic objectives.

Optimal sensitivity of blood testing is expected to coincide with the time at which cardiac protein marker concentrations reach a maximum in the blood, which may occur several hours after the initial onset of symptoms [8]. However, by utilizing high sensitive assay approaches and a multimarker strategy for the diagnosis of MI, earlier diagnosis and intervention may be possible. Early diagnosis would require more rapid and, where

necessary, serial monitoring and quantification of specific disease targets. Since blood testing currently takes place in centralized laboratories requiring several milliliters of blood and long assay times for quantitative monitoring [9], achieving these goals compels a change in the way blood samples are treated for testing, shifting away from single-analyte assay requiring long analysis times to those allowing the simultaneous quantitation of multiple targets. Truly optimized diagnostic testing should satisfy several criteria: high sensitivity, low sample volumes, the ability for multiplex quantification, rapid analysis times, and operational simplicity while maintaining a low cost per analysis [10]. Rapid testing in the emergency room for the diagnosis of myocardial infarction should meet the following metrics to be considered truly optimized: sensitivity allowing quantification of samples below the pM range using fingerprick blood and the ability to quantify 3 targets simultaneously in under 30 minutes without the requirement for expensive, complicated or bulky instrumentation.

1.3 Analysis of Complex Biomedical Samples

While there are many approaches to the diagnosis of disease, when analyzing physical samples they can often be too complex for direct analysis, necessitating the rapid isolation and analysis of target species. The study of these complex samples is of primary interest in biomedical analysis where current clinical approaches to diagnosis include both imaging [11-13] and biological recognition techniques [14-16]. Immunoassays have gained in popularity since their initial introduction in 1959 [17] and are attractive for the analysis of complex samples because of the extremely specific interaction between analyte and antibody. While the applications of immunoassay are highly diverse, ranging

from detecting pesticides in soil [18] to the detection of small molecules [19,20], a primary clinical sample of interest is blood [21-23].

Blood is generally considered to be the most important fluid used for clinical diagnostics because it is the most reflective of the physiologic condition of the body and provides a relatively easy source of specific health information [22,23]. Not only does this include classical plasma proteins, but also proteins present through tissue leakage, and many immunoglobulin sequences [22]. While the density of information that can be attained by monitoring the concentration of a biomarker, or set of biomarkers, offers great diagnostic potential, these species are often present in very low concentrations while the protein content is dominated by only a handful of species [24]. These species may interfere with the quantitation of low abundance species, therefore it is necessary to fractionate samples prior to detection [24,25]. Cross-reactivity can be mitigated to some extent through the use of highly specific monoclonal antibodies [25]. Among immunoassay techniques, non-competitive sandwich immunoassays have been generally recognized to allow the most sensitive detection [26]. This has made them an attractive option for both commercial and experimental applications geared towards clinical diagnostics.

1.4 Advantages and Limitations of Traditional Non-Competitive Immunoassays

Non-competitive immunoassays utilize a sandwich-type format and involve the binding of two antibodies to different target sites [27]. This may be accomplished through the use of the same polyclonal antibody for both capture and detection, but is frequently performed with multiple monoclonal antibodies. Compared with competitive immunoassays, this two-site binding allows for better specificity in the assay.

Traditional non-competitive immunoassays have been used experimentally for many years and are available commercially. These techniques have been successful in achieving sensitive limits of detection. Duhau et al. describe a sandwich-type immunoassay utilizing a 96-well microtiter plate for the detection of rat prolactin [28]. In this work, the detection threshold was found to be 0.5 ng/mL (2.2 pM). However, to achieve high sensitivity, incubation times of up to five days were used in a total reaction volume of 150 μL for the quantitation of a single analyte.

Similar immunoassay techniques were used by Boever et al. [29] and by Kratzsch et al. [30] for the detection of samples from biological fluids. Both methods achieved detection limits in the pM range. However, analogous to the work performed by Duhau et al., incubation times were long and sample volumes on the order of 100 μL per target were required to achieve these results. The long reaction times necessary for these techniques can be explained in part by their use of a static solid substrate for the immobilization of capture antibody.

While reactions taking place in solution or on a cell surface are limited by their equilibrium coefficient, those taking place on static solid surfaces have been experimentally shown to differ [31,32]. After the initial stage of a reaction at an artificial surface there is a local decrease in analyte concentration which forces reactants to travel further to participate in binding events [32,33]. This depletion, along with strong antigen-antibody interactions and the high capture antibody concentrations used in reagent-excess assays, produces a diffusion-limited reaction over long incubation times arising from the distribution of analyte in solution becoming less random as more antigen binds to the surface-immobilized antibodies in a reaction considered to be practically

irreversible [31,34,35]. Since separation of the unbound phase from the solid surface takes place before quantification, in a diffusion-controlled reaction setting incubation times must be unrealistically long to produce a quantifiable signal for low-concentration samples [36].

These drawbacks have led to the development of miniature assays and use of forced convection during incubations to alleviate diffusion related limitations and help homogenize the reaction volume near the capture surface [37]. The evolution of the solid phase from microtiter wells to microparticles as a solid surface has also proven to be useful in the elimination of diffusion dependence. Microparticles have a very high surface area relative to a microtiter well and have been demonstrated to achieve solution-phase performance due to their colloidal nature [27].

1.5 Miniaturization in Immunoassay

Miniaturization in immunoassay has resulted in the development of highly diverse platforms, ranging from straightforward downscaling of traditional concepts [38,39], to flow-based techniques [40,41], and those utilizing microparticles as a solid surface [42-45]. These varied methods have improved upon the limitations noted in traditional clinical tests in several ways: lowered analysis time [40,43-45], portability [44], and lowered sample size [40,41,45], while maintaining clinically-relevant limits of detection [38-45]. Miniaturized immunoassays employing a static solid surface, while useful in maintaining high levels of sensitivity, continue to suffer from long analysis times on a microscale [46-48].

To combat long analysis times, alterations in the solid support used for target immobilization have been explored in several ways. Flow-based techniques are capable

of very rapid analysis, ranging from 30 seconds to 10 minutes [40,41]. These rapid assays have maintained clinically relevant limits of detection (pM range) while utilizing small sample volumes (0.5 – 20 μL). However, at present these systems are only able to quantify a single target analyte per assay. In particular, the reverse displacement immunoassay described by Schiel et al. relies on the use of columns containing immobilized analog for the specific target being examined [41]. Label displaced by analyte is eluted from the column past a detector to determine the extent of analyte in a sample (Figure 1.1). While it is possible to redesign a system using a portable analysis device, the redesign would present significant challenges before parallel or multiplexed detection could be possible.

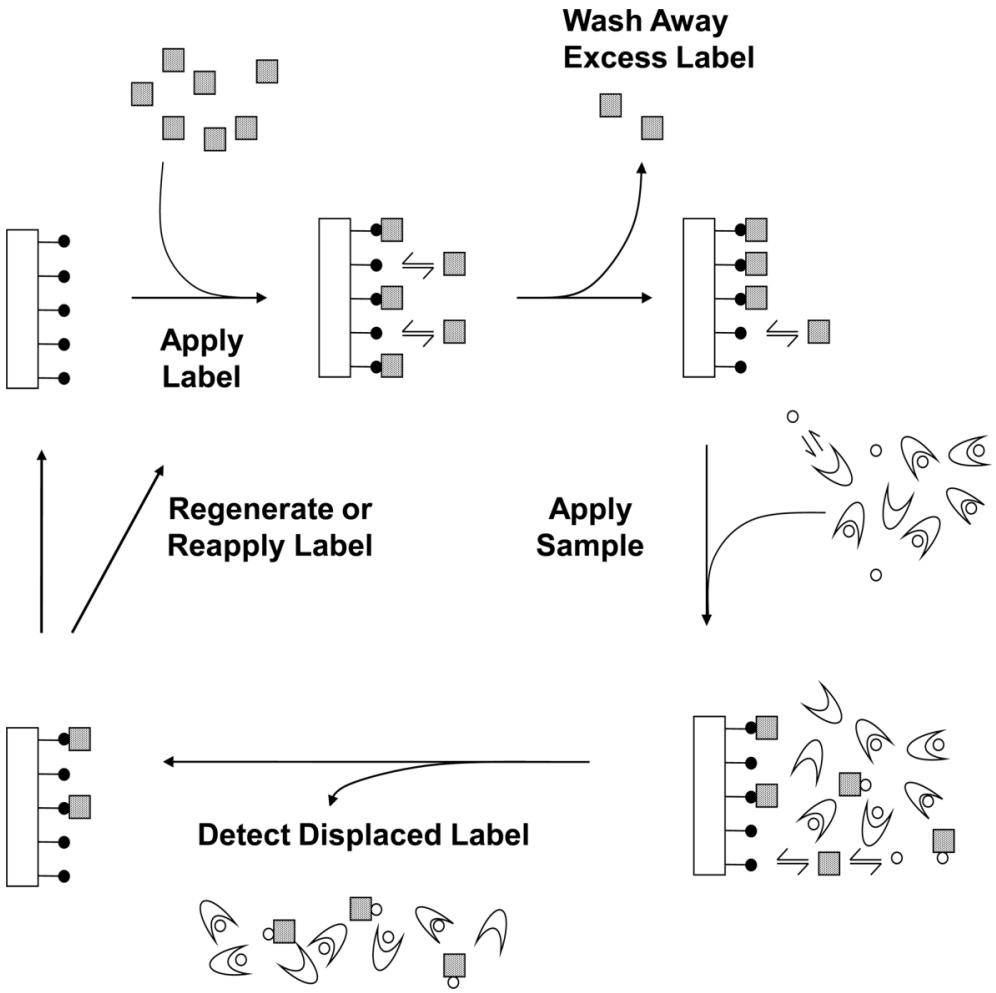

Figure 1.1 Scheme for the reverse displacement immunoassay, where (—●) represents the immobilized drug analog; (shaded □) indicates the labeled monoclonal antibody or Fab fragments; (○) depicts the drug or target analyte; and (half circle), indicates the serum protein or binding agent.

An alternative method to flow-based systems is the use of microparticle-based immunoassays. By incorporating particles as a solid support for immunoassay techniques, several advantages are realized, including both the ease of surface manipulation during wash steps as well as the potential for convective mixing to shorten incubation times. Along with the ability for rapid analyte capture, these techniques are compatible with traditional detection methods, maintaining sensitive limits of quantitation. Microparticles

have been incorporated into assays in a variety of ways, and a subset of this work that is of particular interest involves the use of magnetic microparticles as the solid support.

Magnetic microparticles have been used by the Gijs group for both on- and off-chip incubation methods employing fluorescence detection (Figure 1.2) [49,50]. While incubation off-chip enabled easy manipulation of the capture surface and maintained similar limits of detection to commercial methods, results show that performing on-chip incubations was able to both lower the detection limit and reduce the overall assay time.

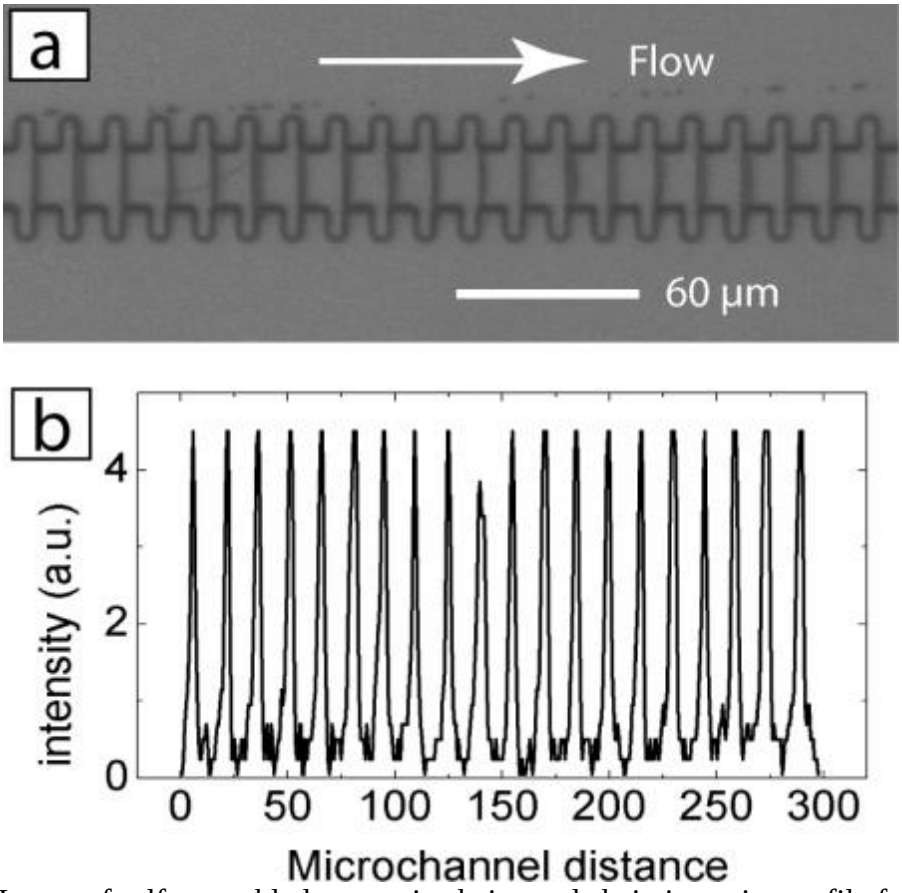

Figure 1.2 Image of self-assembled magnetic chains and chain intensity profile formed on chip [50]. **A)** Image of the self-assembled chains **B)** Intensity profile derived from an image as shown in part A.

Beyond exploiting their unique ability to easily be captured during wash steps or stabilized in the presence of sample flow, an assay based on the incorporation of a period

fluctuation in the applied field was originally developed to improve the detectability of low concentration samples in the presence of a relatively high background signal (Figure 1.3) [51,52]. In addition to utilizing a magnetic field to improve the ease of wash steps, incorporating a periodic fluctuation in the magnetic field during data capture enables this technique to take advantage of coupling signal processing and amplification strategies that allow greater signal power to be extracted from the data [53]. The advantage of extracting a greater signal power from collected video is that it enables improved limits of quantitation for the technique and enables sensitive detection from a small original sample volume.

A methodical optimization of data collection and processing was employed to achieve extremely sensitive quantitation and directly address many of the metrics of an optimized immunoassay stated above. Changes to both optics and acquisition settings allowed improvements to the signal-to-noise ratio (S/N), while data analysis was altered to maximize the signal power obtained from each sample. This enabled the extremely sensitive quantification of cardiac biomarkers myoglobin, cardiac troponin I (cTnI), and heart-type fatty acid binding protein (H-FABP) while maintaining a simple batch incubation approach [54]. While these improvements satisfy the sensitivity needs of clinical assays while utilizing a minimal sample volume, there still exists a need for this sensitive and selective quantitation ability to be applied to the simultaneous detection of biomarker panels. Parallel detection is of particular importance because no single marker has proven to have sufficient diagnostic accuracy for AMI, or a variety of other conditions in which early detection would improve prognosis [8,55,60].

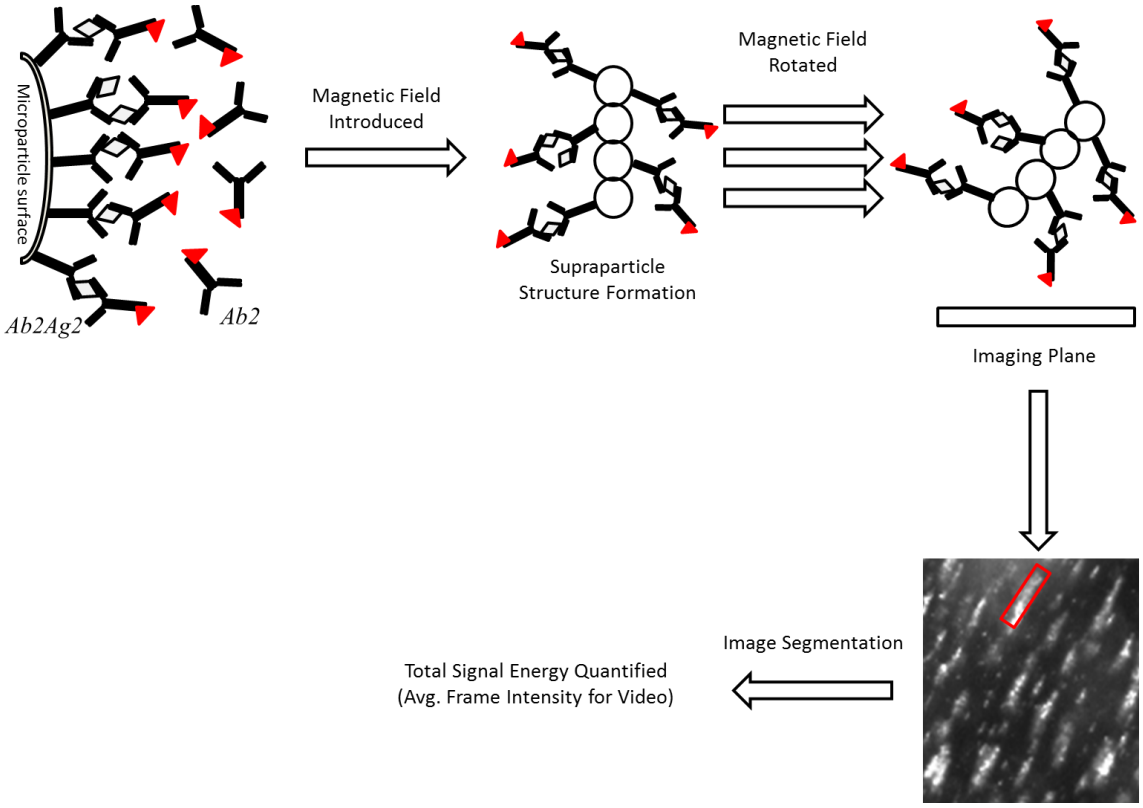

Figure 1.3 Schematic showing method utilized for immunoassay. In the presence of a magnetic field, self-assembled supraparticle structures form and may be manipulated through the alteration of the field producing a periodic change in fluorescence intensity.

1.6 Parallel Detection in Immunoassay

There are many potential advantages to the use of a parallel detection immunoassay system, including increased throughput, simplification of the work performed, reduced overall cost per analyte, and increased sensitivity for disease detection through use of a biomarker panel as compared to a single species [27]. Multianalyte testing has been investigated in two primary ways: through batch incubation with specific antibodies to different target analytes (e.g. Luminex systems or microarray printing) and differentiation during detection, and through separation prior to target capture [57-60]. While multianalyte testing hold the potential to improve diagnostic testing capabilities, it has not yet commercially replaced the singleplexed analyte testing frequently used both

clinically and in point-of-care testing. One of the drawbacks of batch incubation, particularly when utilizing a complex sample such as plasma, is the potential for cross-reactivity [24,25].

Reducing or eliminating the potential for cross-reactivity brings about interest in sample pre-treatment steps to separate components. On a microscale, several options exist for the treatment of blood prior to target quantification. These range from the use of physical barriers to filter sample components [61,62], to differentiation through the use of lateral flow, and the incorporation of electrophoretic separation methods [63-67]. While there are many potential methods for plasma separation, the use of electrophoretic exclusion to separate proteins is particularly attractive because it allows samples to be separated in bulk solution based on their native properties without the need for differentiation based on binding. Differentiation using this method requires the presence of three factors: hydrodynamic flow, the presence of an electric field, and species having an electrophoretic mobility in the buffer conditions used [67]. Electrophoretic exclusion achieves resolution of species based on differences in their electrophoretic mobilities (Figure 1.4) [68]. With the assumption that flow and buffer conditions remain constant during an experiment electric field strengths may be manipulated to separate species. Exclusion is achieved by maintaining a constant electric field across reservoirs in a channel or array, and introducing a sharp gradient to the electric field at channels connecting these reservoirs. When the electrophoretic velocity of an analyte (v_a), based on the relationship:

$$v_a = \mu_a E \qquad 1.1$$

where μ_a is the electrophoretic mobility of an analyte and *E* is the local electric field strength, is equal and opposite (or greater than) the hydrodynamic flow. Under these conditions a species is prevented from entering a channel whereas species with a smaller μ_a (and therefore smaller v_a) will be able to enter and flow through the channel.

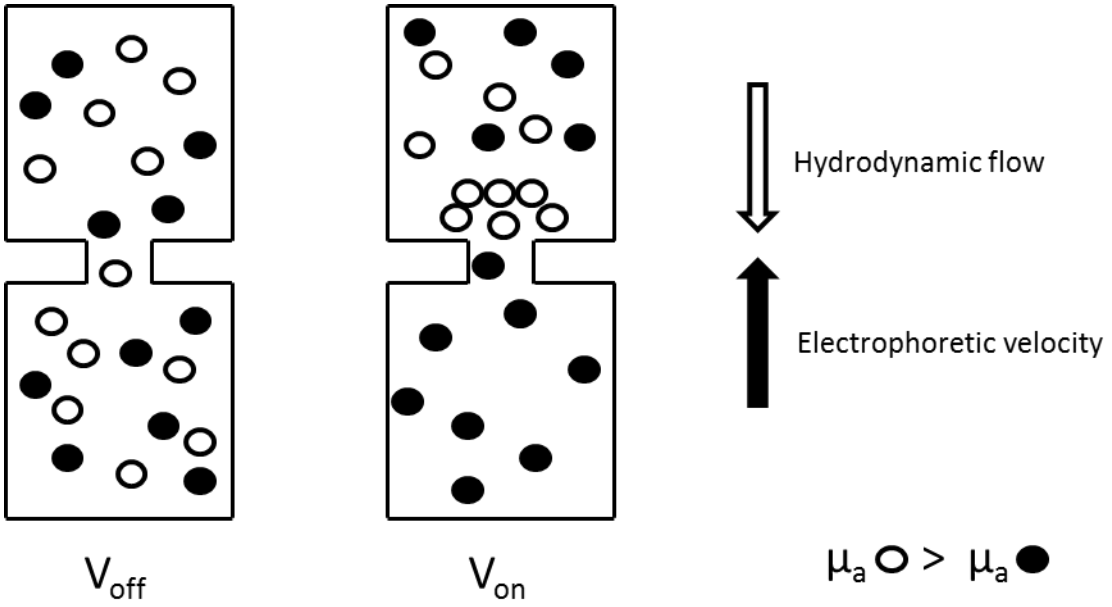

Figure 1.4 Schematic demonstrating the principles of electrophoretic exclusion. When no electric field is applied both samples are allowed to flow through the channel (left), but when the electric field is applied and electrophoretic velocity of one species is equal and opposite to (or greater) than hydrodynamic flow it is excluded from the channel while the analyte with a smaller electrophoretic mobility is still able to enter and flow through the channel (right).

Creation of a microscale analysis system consisting of one primary separation channel (consisting of reservoirs connected by microchannels) connected to many parallel cross-channels with individual compartments for specific target detection makes electrophoretic exclusion ideal for the separation of complex samples prior to the simultaneous quantitation by immunoassay of many isolated species since it not only isolates species, but serves to concentrate individual targets prior to detection. Because separation of components based on other native physical properties takes place prior to

identification based on a binding interaction between the target species and its respective antibodies, there is a reduction in potential NSB from competing species as the sample has been greatly simplified compared to batch incubation approaches. This allows the simultaneous quantitation of species that is theoretically limited only by the size of the analysis system and number of individual compartments as opposed to increasing uncertainty as additional analytes are quantified using batch incubation methods.

1.7 Dissertation Objectives

This dissertation is dedicated to describing the optimization of an immunoassay platform for disease diagnostics and its incorporation into a microscale analysis system envisioned as an accurate, rapid tool for plasma analysis. The novel non-competitive immunoassay platform was initially used to quantify myoglobin concentrations to a limit of 50 pM using a benchtop incubation format and lock-in amplification [52]. However, the bulk of the work presented herein discusses the optimization of data collection and signal processing to achieve superior detection sensitivities for myoglobin, cTnI and H-FABP. A discussion of its applicability as a quantification scheme incorporated into a microscale total analysis system and the limitations of immunoassay quantification are also addressed, focusing on the importance of developing a fully-optimized platform for clinical immunoassay applications.

1.8 Dissertation Summary

To first introduce the field of biomedical analysis, analyte detection carried out both in laboratory settings and utilizing point-of-care devices a review of novel techniques is included as Chapter 2. This chapter covers detection platforms utilizing both imaging and biological recognition and evaluates the capacity of techniques to be used both in clinical

and remote disease diagnostics and monitoring. Articles that are reviewed in this chapter are from January 2010 to January 2014.

To further explore emerging microimmunoassay techniques, a critical evaluation based on their ability to achieve the capabilities of a fully optimized quantification platform is included as Chapter 3. This chapter covers diverse immunoassay platforms including the use of microparticles as an assay surface, flow-based techniques, and the incorporation of a static solid support. Articles that are reviewed in this chapter are from January 2008 to April 2012.

Chapters 4 – 7 present experiments using a novel immunoassay platform and evaluating its utility for incorporation into a microscale total analysis system (μTAS). Chapter 4 presents individual detection and quantification utilizing benchtop sample preparation for three target species: myoglobin, cTnI, and H-FABP. Chapter 5 develops the theory for the limitations of quantitation possible for a non-competitive immunoassay and includes a brief analysis of the results obtained from individual targets. Chapter 6 demonstrates the ability of insulator-based dielectrophoresiss (i-DEP) to act as an initial sample preparation step for the evaluation of whole blood samples on a microscale. Chapter 7 evaluates the capability a current microdevice to manipulate and separate the target species using electrophoretic exclusion. A discussion for adaptation of the assay to a more complete microscale analysis system is also included. Chapter 8 details the development of a prototype total analysis system and includes the preliminary results achieved as well as a discussion of modifications that could improve its ability to process a whole blood sample completely on-chip.

1.9 References

[1] Zuskin, E., Lipozencic, J., Pucarin-Cvetkovic, J., Mustajbegovic, J., Schachter, N., Mucic-Pucic, B., Neralic-Meniga, I., *Acta Dermatovenerol Croat*, 2008, *16*, 149-157.

[2] Vecchio, I., Tornali, C., Rampello, L., Rigo, G.S., Rampello, L., Migliore, M., Castellino, P., Malta, R., Armocida, G., *Acta Medica Mediterranea*, 2013, *29*, 363-367.

[3] Papavramidou, N., Fee, E., Christopoulou-Aletra, H., *J. Gastrointest. Surg.*, 2007, *11*, 1728-1731.

[4] Loukas, M., Tubbs, R.S., Louis Jr., R.G., Pinyard, J., Vaid, S., Curry, B., *International Journal of Cardiology*, 2007, *120*, 145-149.

[5] Berche, P., *Clinical Microbiology and Infection*, 2012, *18*, 1-6.

[6] Koch, R., *Investigations into the Etiology of Traumatic Infective Diseases (The Relations of Micro-Organisms to Traumatic Infective Diseases)*, 1880, 19-39.

[7] Beale, L.S., *Disease Germs: Their Supposed Nature, an Original Investigation, with Critical Remarks (Disease Germs)*, 1870, 1-13.

[8] Morrow, D. A., Cannon, C. P., Jesse, R. L., Newby, L. K., Ravkilde, J., Storrow, A. B., Wu, A. H. B., Christenson, R.H., *Clinical Chemistry*, 2007, *53*, 552-574.

[9] Dimov, I.K., Basabe-Desmonts, L., Garcia-Cordero, J.L., Ross, B.M., Ricco, A.J., and Lee, L.P., *Lab on a Chip*, 2011, *11*, 845-850.

[10] Woolley, C. F., Hayes, M. A., *Bioanalysis*, 2013, *5*, 245-264.

[11] Cheung, K.T., Trevisan, J., Kelly, J.G., Ashton, K.M., Stringfellow, H.F., Taylor, S.E., Singh, M.N., Martin-Hirsch, P.L., Martin, F.L., *Analyst*, 2011, *136*, 2047-2055.

[12] Policar, C., Birgitta Waern, J., Plamont, M.A., Clede, S., Mayet, C., Prazeres, R., Ortega, J.M., Vessieres, A., Dazzi, A., *Angew. Chem. Int. Ed.*, 2011, *50*, 860-864.

[13] Huth, F., Schnell, M., Wittborn, J., Ocelic, N., Hillenbrand, R., *Nature Materials*, 2011, *10*, 352-356.

[14] Song, S. Y., Han, Y. D., Kim, K., Yang, S. S., and Yoon, H. C., *Biosensors and Bioelectronics*, 2011, *26*, 3818-3824.

[15] Garcia-Valdecasas, S., Ruiz-Alvarez, M.J., Garcia De Tena, J., De Pablo, R., Huerta, M. Barrionuevo, I., Coca, C., Arribas, I., *Acta Cardiol*, 2011, *66*, 315-321.

[16] Liao, J., Chan, C.P., Cheung, Y., Lu, J., Luo, Y., Cautherley, G.W.H., Glatz, J.F.C., Renneberg, R., *International Journal of Cardiology*, 2008, *133*, 420-423.

[17] Berson, S. A., Yalow, R. S., *Nature*, 1959, *184*, 1648-1649.

[18] Long, F., Zhu, A., Shi, H., Sheng, J., Zhao, Z., *Chemosphere*, 2015, *120*, 615-620.

[19] Allinson, J. L., *Bioanalysis*, 2011, *3*, 2803-2816.

[20] Verch, T., Bakhtiar, R., *Bioanalysis*, 2012, *4*, 177-188.

[21] Bellei, E., Bergamini, S., E. Monari, S., Fantoni, L.I., Cuoghi, A., *Amino Acids*, 2011, *40*, 145-156.

[22] Anderson, N.L., Anderson, N.G., *Molecular and Cellular Proteomics*, 2002, *1.11*, 845-867.

[23] Fan, R., Vermesh, O., Srivastava, A., Yen, B.K.H., Qin, L., Ahmad, H., Kwong, G.A., Liu, C.C., Gould, J., Hood, L., Heath, J.R., *Nature Biotechnology*, 2008, *26*, 1373-1378.

[24] Tirumalai, R.S., Chan, K.C., Prieto, D.A., Issaq, H.J., Conrads, T.P., and Veenstra, T.D., *Molecular and Cellular Proteomics*, 2006, *2.10*, 1096-1103.

[25] Mitchell, P., *Nature Biotechnology*, 2010, *28*, 665-670.

[26] Ohmura, N., Lackie, S. J, Saiki, H., *Anal. Chem.* 2001, *73*, 3392-3399.

[27] Diamandis, E. P., Christopoulos, T. K., *Immunoassay* (Theory of Immunoassays CH 3, Interfaces in Immunoassays CH 7), 1996, 25-187.

[28] Duhau, L., Grassi, J., Grouselle, D., Enjalbert, A., Grognet, J. M., *Journal of Immunoassay*, 1991, *12*, 233-250.

[29] Boever, J. D., Kohen, F., Bouve, J., Leyseele, D., Vandekerckhove, D., *Clinical Chemistry*, 1990, *36*, 2036-2041.

[30] Kratzsch, J., Ackermann, W., Keilacker, H., Besch, W., Keller, E., *Experimental and Clinical Endocrinology and Diabetes*, 1990, *95*, 229-236.

[31] Werthen, M., Nygren, H., *Journal of Immunological Methods* 1988, *115*, 71-78.

[32] Stenberg, M., Nygren, H., *Journal of Immunological Methods* 1988, *113*, 3-15.

[33] Stenberg, M., Stiblert, L., Nygren, H., *J. theor. Biol.* 1986, *120*, 129-140.

[34] Nygren, H., Werthen, M., Stenberg, M., *Journal of Immunological Methods* 1987, *101*, 63-71.

[35] Nygren, H., Stenberg, M., *Immunology* 1989, *66*, 321-327.

[36] Ekins, R., Kelso, D., *Clin. Chem.* 2011, *57*, 372-375.

[37] Ishikawa, E., Hashida, S., Kohno, T., Hirota, K., *Clinica Chimica Acta* 1990, *194*, 51-72.

[38] Tian, J., Zhou, L., Zhao, Y., Wang, Y., Peng, Y., Hong, X., Zhao, S., *J Fluoresc*, 2012.

[39] Lee, G. Y., Choi, Y. H., Chung, H. W., Ko, H., Cho, S., Pyun, J. C., *Biosensors and Bioelectronics*, 2013, *40*, 227-232.

[40] Casolari, S., Roda, B., Mirasoli, M., Zangheri, M., Patrono, D., Reschiglian, P., Roda, A., *Analyst*, 2013, *138*, 211-219.

[41] Schiel, J. E., Tong, Z., Sakulthaew, C., Hage, D. S., *Analytical Chemistry*, 2011, *83*, 9384-9390.

[42] Fu, X., Meng, M., Zhang, Y., Yin, Y., Zhang, X., Xi, R., *Analytica Chimica Acta*, 2012, *722*, 114-118.

[43] Sakamaki, N., Ohiro, Y., Ito, M., Makinodan, M., Ohta, T., Suzuki, W., Takayasu, S., Tsuge, H., *Clinical and Vaccine Immunology*, 2012, *19*, 1949-1954.

[44] Lee, W.B., Chen, Y.H., Lin, H.I., Shiesh, S.C., Lee, G.B., *Sensors and Actuators B: Chemical*, 2011, *157*, 710-721.

[45] Song, S. Y., Han, Y. D., Kim, K., Yang, S. S., Yoon, H. C., *Biosensors and Bioelectronics*, 2011, *26*, 3818-3824.

[46] Lee, S., Kang, S.H., *Talanta*, 2012, *99*, 1030-1034.

[47] Sloan, J. H., Siegel, R. W., Ivanova-Cox, Y. T., Watson, D. E., Deeg, M. A., Konrad, R. J., *Clinical Biochemistry*, 2012, *45*, 1640-1644.

[48] Vashist, S. K., *Biosensors and Bioelectronics*, 2013, *4*, 297-302.

[49] Lacharme, F., Vandevyver, C., Gijs, M. A. M., *Microfluid Nanofluidics*, 2009, *7*, 479-487.

[50] Lacharme, F., Vandevyver, C., Gijs, M. A. M., *Analytical Chemistry*, 2008, *80*, 2905-2910.

[51] Petkus, M. M., McLauchlin, M., Vuppu, A. K., Rios, L., Garcia, A. A., Hayes, M. A., *Analytical Chemistry*, 2006, *78*, 1405-1411.

[52] Hayes, M. A., Petkus, M. M., Garcia, A. A., Taylor, T., Mahanti, P., *Analyst*, 2008, *134*, 533-541.

[53] Mahanti, P., Taylor, T., Hayes, M. A., Cochran, D., Petkus, M. M., *Analyst*, 2011, *136*, 365-373.

[54] Woolley, C.F., Hayes, M.A., *Anal. Methods.*, submitted.

[55] Macdonald, S.P.J., Nagree, Y., Fatovich, D.M., Phillips, M., Brown, S.G.A., *Emergency Medicine Journal*, 2012, *30*, 149-154.

[56] Molin, S.Da., Cappellini, F., Falbo, R., Signorini, S., Brambilla, P., *Clinical Biochemistry*, 2014, *47*, 247-249.

[57] Jayadev, C., Rout, R., Price, A., Hulley, P., Mahoney, D., *Journal of Immunological Methods*, 2012, *386*, 22-30.

[58] Pereira, A. T., Novo, P., Prazeres, D. M. F., Chu, V., Conde, J. P., *Biomicrofluidics*, 2011, *5*, 014102-1-014102-13.

[59] Granger, J.H., Granger, M.C., Firpo, M.A., Mulvihill, S.J., Porter, M.D., *Analyst*, 2013, *138*, 410-416.

[60] Proczek, G., Gassner, A. L., Busnel, J. M., Girault, H. H. , *Anal. Bioanal. Chem.* 2012, *402*, 2645-2653.

[61] Camerini, S., Polci, M. L., Liotta, L. A., Petricoin, E. F., Zhou, W., *Proteomics Clin. Appl.*, 2007, *1*, 176-184.

[62] Joglekar, M., Roggers, R. A., Zhao, Y., Trewyn, B. G., *RSC Advances*, 2013, *3*, 2454-2461.

[63] Wang, X., Masschelein, E., Hespel, P., Adams, E., Schepdael, A. V., *Electrophoresis*, 2012, *33*, 402-405.

[64] Jubery, T. Z., Hossan, M. R., Bottenus, D. R., Ivory, C. F., Dong, W., Dutta, P., *Biomicrofluidics*, 2012, *6*, 016503-1-13.

[65] Startsev, M. A., Inglis, D. W., Baker, M. S., Goldys, E. M., *Analytical Chemistry*, 2013, *85*, 7133-7138.

[66] Inglis, D. W., Goldys, E. M., Calander, N. P., *Angew. Chem. Int. Ed.*, 2011, *50*, 7546-7550.

[67] Kenyon, S. M., Weiss, N. G., Hayes, M. A., *Electrophoresis*, 2012, *33*, 1227-1235.

[68] Kenyon, S. M., Keebaugh, M. W., Hayes, M. A., *Electrophoresis*, 2014, *35*, 2551-2559.

CHAPTER 2

EMERGING TECHNOLOGIES FOR BIOMEDICAL ANALYSIS

2.1 Introduction

Early disease diagnosis is vital so that more effective intervention strategies may be employed. Because early intervention is essential for improving disease prognosis, in recent years there has been an emphasis on increasing the sensitivity of biomedical analysis methods [1-6]. Stemming from this quest for superior sensitivity, several new technologies for biomedical analysis have emerged on both experimental and commercial platforms. These technologies, in general, take place in one of two formats; biological recognition or imaging.

The area of biological recognition is focused on specifically and sensitively quantifying low-abundance species that are indicators of disease pathways. The platforms are highly diverse, ranging from the immobilization of antibodies on hydrogels[1] or unmodified plastics [7,8], to CD disks for microarray printing [2,9-11], and assays taking place in the traditional microwell format [3]. While some of these assays focus on reducing the non-specific binding associated with long incubation times in traditional assays [3], the primary trends over the last few years have been toward the development of multiplex assays or rapid point-of-care devices [8,11,12].

Work also continues towards improving traditional imaging methods used in disease diagnosis. Imaging approaches analyze the information-rich spectra obtained from tissues to identify characteristic absorptions revealing the underlying chemical composition of the sample and identifying cellular biomarkers [13]. Using these methods both labeled and label-free detection methods have been utilized [13-20]. A main

contribution in this area has been the improvement of resolution in infrared spectroscopy (IR) to overcome the usual limitations imposed by diffraction [13-17].

Although methods that can be used for biomedical analysis in a traditional lab setting continue to be investigated, a primary focus over the last several years has been the development of mobile health (mHealth) platforms that could be used in telemedicine applications or resource-poor settings where access to quality healthcare is limited [21-26]. Mobile health devices have largely been created on one of two platforms: CD discs that have been used as the solid phase for immunorecognition assays and can be read using an unmodified CD player [8,27], and those that take place via a smartphone attachment [9,12,21-23,25,26]. In both cases an emphasis is placed on using simple fabrication procedures, as well as reusable materials, to keep costs low. There is also an emphasis on producing user-friendly applications that allow patients to perform tests independently and upload the results for experts to interpret and determine the best course of treatment [21-23,26]. Advances in this capacity are vital to rapidly identify and address emerging public health threats, as well as to treat chronic diseases that require persistent monitoring [26].

While both imaging techniques and biological recognition assays have been the subject of recent reviews [28-31], the focus of this review will be the application of those new techniques to biomedical analysis and the improvement of early disease intervention published during the time span from January 2010 to January 2014, initiated with literature keyword searches associated with biomedical analysis as well as their references and the later citations of found works. Articles were chosen based on their contribution to new technologies in the area of biomedical analysis and offering

improvements both in terms of shorter test duration and higher sensitivity, as well as improving the mobility of testing platforms to reach resource poor areas. While many tests were described in the context of identifying a particular molecule or disease pattern, they could easily be adapted for the testing of many biological species. The topics addressed are divided into techniques used for biological recognition [Section 2.2] and those used for imaging analysis [Section 2.3]. These sections are further subdivided into laboratory or clinic-based testing and platforms intended for point-of-care diagnostics.

2.2 Biological Recognition

Techniques utilizing biological recognition may further be divided into two main subcategories: (i) biorecognition assays that take place within a laboratory or clinical setting and (ii) portable microarrays allowing point-of-care diagnostic testing. Some of the techniques discussed in this section include magnetic bead-based assays, assays taking place on unmodified plastic substrates (Figure 2.1), and those utilizing a compact disc (CD) as a solid support. CD-based assays have gained popularity for a variety of reasons including the ease of fabrication and established detection methods. The use of computer drives/disc players adapted as a precise optical reading mechanism and employed as a detection instrument allows the assays to be accomplished at low-cost and away from specialized laboratories. Users are able to fabricate high-density microarrays on a CD disc and perform tests for a variety of different targets including DNAzyme assays, antibody-antigen binding, and microorganisms. The recent expansion of this technique to Blu-ray technology has allowed a reduction in feature sizes and a subsequent improvement in assay sensitivity.

2.2.1 Laboratory-Based Bio-recognition Assays

Traditional biological recognition assays employing a static solid support continue to have widespread use both on commercial and experimental platforms [1,3,7,32-36]. Their high sensitivity, versatility in detection methods, and adaptability for the quantification of a myriad of targets continue to make their replacement by other testing platforms a challenge (summary of techniques shown in Table 2.1). While these methods employ diverse tactics, a primary focus over the last several years has been to address a common pitfall of these assays: non-specific binding (NSB) and its limitation of the assays' potential sensitivity [1,3]. Efforts continue to be made toward increasing sensitivity and reducing the characteristically long incubations associated with these techniques so they may eventually be adapted to portable care diagnostics.

Technique	Applications	Sensiti-vity	Analysis Time	Fabrication/Equipment Requirements	Reference(s)
Microwell ELISA	Serum antibody immunoassays, protein detection	-	10 min	Micro-well plate pre-incubation procedure, optical density detection	3
Microarray Assays	Protein detection, diagnostics	1 pM	3+ hours	Protein printing, UV-exposure crosslinking; Biodetect 645® read-out system	1,7
Colorimetric Detection	Sandwich bioassays, DNA and protein detection	0.67 - 10 nM	2+ hours	UV/ozone activation of plastic sheet, 1-ethyl-3-(3'-dimethylaminopropyl)-cabodiimide/N-hydroxy-succinimide coupling; fluorescent microscope	8
Rolling circle amplification Assay	Low-abundance protein monitoring	38 fM	5+ hours	Overnight microplate preparation; electrochemical workstation	37
pH and metabolic monitoring of live cells	Personalized medicine applications	50 cells	Real-time monitoring	Chemical modification of nanowires; extracellular pH probe	38
Amperometric Biosensor	Simultaneous drug detection	1.2-5.5 fM	35 minutes	Fabrication of biosensor probe; electrochemical detector	39
Magnetic Bead Separation Assay	Biomolecule detection	7.1 nM	15 min	Soft lithography fabrication; hemocytometer and microscope apparatus	40
Optically switched dielectrophoretic force	Tissue engineering	-	Days	Photolithography using SU-8 photoresist; CCD equipped microscope	41

Table 2.1 Summary of laboratory-based biological recognition assays.

The reduction in non-specific binding for assays having long incubations was investigated by Farajollah et al [3]. They describe that the most common problem in

microwell assays is the detection antibody binding directly to the solid phase. This can occur if undiluted serum is applied even when using a well that has been chemically or biochemically blocked. To minimize the signal arising from NSB while continuing to provide sufficient signal for the detection of low-abundance species, this work introduces a pre-incubation procedure. Using this technique, a biotinylated capture reagent is first incubated with the serum sample and introduced in a secondary step to a streptavidin-coated well. Detection is enabled with labeled anti-species antibodies. The utility of this technique was investigated and findings show that NSB is time-dependent and both serum as well as purified IgG would bind non-specifically to plastic wells. Blocking provided a slight reduction in NSB, but the blocking agents could be displaced after lengthy incubations. Utilizing the pre-incubation method, along with rapid capture times have allowed for improved sensitivities compared with traditional ELISA (enzyme-linked immunosorbent assay) testing and could potentially help to solve the background noise issue associated with those tests. However, because pre-incubation takes place prior to antibody fixation this technique would be difficult to adapt to the parallel detection of analytes since signals could not be spatially isolated.

The issue of NSB was also addressed by the Ruhe group [1]. In earlier work the single step production of protein microarrays on unmodified plastic substrates is presented [7]. Proteins, along with a terpolymer, were printed at high concentration in surface-attached hydrogels. A single UV-exposure step both covalently immobilizes the protein and modifies the surface, inducing swelling to a 3D surface and increasing its binding capacity. The swelling strongly influences the accessibility of the proteins in the hydrogel. Analyzing this method over a series of analyte standards, it was discovered that

analyte capture increases linearly with antibody concentration up to an asymptotic limit of ~10^8 antibodies/spot while achieving a signal-to-noise value of more than 200 at a concentration of 9 x 10^7 antigens/spot. This technique, through employing more complicated fabrication procedures than assays achieving detection through use of a microwell plate, enables parallel detection of analytes due to the pre-printing of capture proteins prior to analyte incubation and detection. If the fabrication and swelling of the 3D surfaces in the device could be achieved at low cost and with a reasonable shelf life this technique could transition from use in the lab to a portable device.

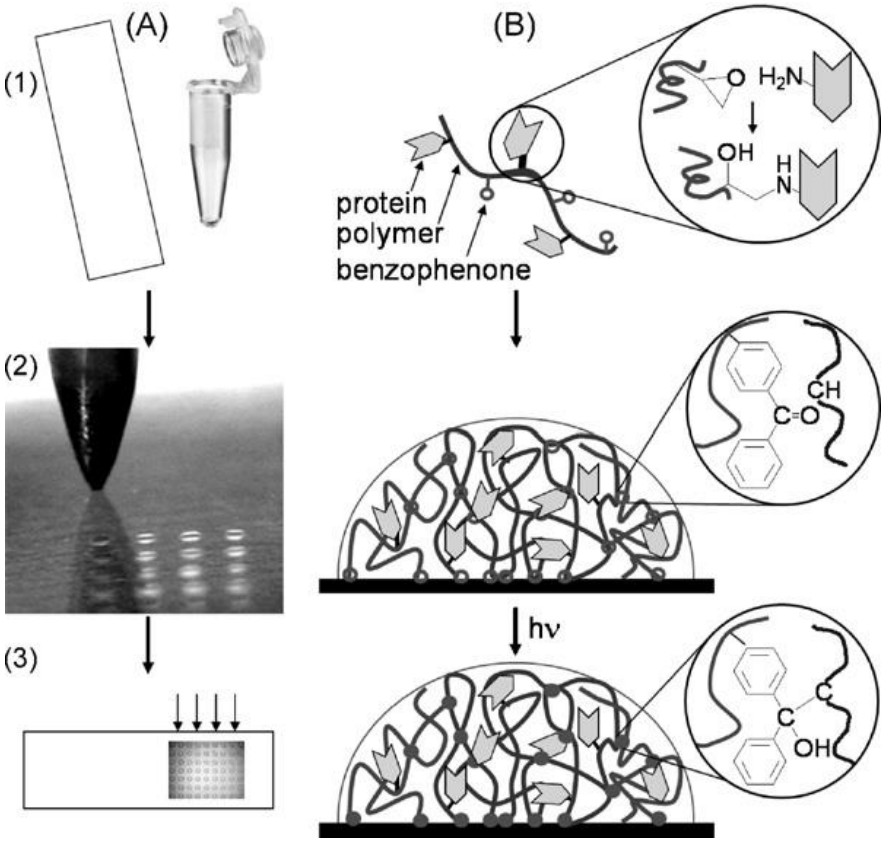

Figure 2.1. Illustration of the process for printing microarrays with mixed polymer protein solutions and immobilization through UV-crosslinking both in the macroscopic (A) and microscopic (B) views.[7] Macroscopic view images show (1) a solution is mixed of buffer and polymer (2) a microarray of the solution is printed onto the provided plastic slide and (3) the chip is irradiated using UV light to crosslink the polymers and immobilize them on the surface. On a microscopic level (B) it is observed that (1) epoxide side groups of the polymer react with primary amino acids, (2) droplets containing these formed complexes form on the surface, and (3) the UV photoreaction crosslinks the polymer, attaching it to the surface and immobilizing the proteins in the network of polymers.

In later work the Ruhe group evaluated assay sensitivity and the extent of NSB observed using these hydrogels [1]. Compared to traditional methods of preventing NSB through blocking procedures the hydrogel has an intrinsically weak binding capacity for proteins. While purified capture antibody is covalently linked to the structure during the UV-exposure step, NSB is essentially eliminated on these surfaces. This method proved effective for the quantification of bovine serum albumin (BSA) between 1 and 500 nM. It

was detected to a limit of 1 pM using this technique. However, at this level the concentration dependence of the signal is too low for quantification. While this limitation is sufficient for the detection of BSA, for adaptation to the detection of other species more sensitive quantitation to the low pM range would be necessary.

Work has also been done on the development of highly sensitive assays by Zhang et al. using alpha-fetoprotein (AFP) as a model protein [37]. This was accomplished by coupling metal surface nanolabels to a silver nanocluster (AgNC)-based rolling circle amplification strategy. Under optimal assay conditions results show a dynamic range of 0.14 fM – 2.9 nM with a detection limit of 0.11 fM and a limit of quantification found at 38 fM. These levels are able to completely meet the clinical diagnostic requirements for AFP. However, the long duration of incubations and specialized detection methods required for the assay prevents its easy adaptation for use outside the clinic.

In an effort to move biochip technology away from labs and hospitals and enable its use as a point-of-care device, Wen et al. describe the development of a novel plastic biochip [8]. The work shows its utility for the sensitive colorimetric detection of both human IgG and DNA. After UV/ozone activation of the plastic substrate probe biomolecules are covalently attached. Signal reporting units are introduced to complete a sandwich-style assay and achieve sensitive detection. Using this label-free recognition system detection limits of 67 pM and 10 nM were achieved for IgG and DNA, respectively. These limits are dependent on staining time and could be adjusted according to assay needs, providing an easy and flexible approach to a portable biochip.

Beyond assays employing a static support, several unique laboratory-based approaches have been developed [38]. Quantitative bioanalysis was accomplished using a

sensitive pH sensor by the Patolsky group. This detection method was performed by evaluating the ratio of electrical signals in ground and excited states to determine the concentration of target species. The device was applied to the real-time monitoring of both intra- and extracellular metabolic activity, with sensitivities down to the signal produced by less than 50 cells, or in the vicinity of single-cell metabolic measurements. Although the assay is not currently carried out on a mobile platform, its ability to provide sensitive and rapid monitoring gives this approach potential for the expansion to detecting specific biological species and its utilization in personalized medicine-oriented diagnostics. However, since detection is based on ratios of electrical signals, modifications to allow the parallel detection of biomarker panels represent a significant hurdle for this technique.

Amperometric biosensors were used in a microfluidic device by Chandra et al. for the sensitive detection of several anticancer drugs [39]. Sensing was accomplished through the integration of preconcentration and separation steps prior to detection. Results show that the detection limit for all four drugs tested was between 1.2 – 5.5 fM with a linear response over the 2 – 60 pM range. This work represents a rapid and sensitive microscale total analysis system whose adaptation to the detection of biomarkers would be beneficial in diagnostics as well as disease monitoring.

Detection on the microscale was also accomplished by Wang et al. who demonstrated the capture and separation of biomolecules using magnetic beads [40]. Taking place on a microchip consisting of two reservoirs connected by a tapered channel, assays were performed in one well using the beads as a solid surface and separated for detection in the second well by an external permanent magnet. Results show the transfer

could be accomplished within two minutes and that carryover was less than 0.002%. This separation was achieved without the use of a pump, giving it potential as a point-of-care device. While this method allows for rapid detection and in the absence of excess detection antibody, the current setup only allows for the quantification of one target molecule at a time. Alterations of the assay to detect markers in parallel would require drastic changes to the chip design as species would need to be separated prior to capture and detection to avoid cross reactivity and allow differentiation of signals.

Microbeads were also utilized alongside and optically switched dielectrophoretic (ODEP) force in bottom-up tissue engineering [41]. Cell-encapsulating alginate microbeads with three different densities were assembled and manipulated using an ODEP force-based mechanism. Manipulations allowed for the formation of a sheet-like cell structure imitating the cell distribution of articular cartilage. Cells encapsulated remained viable to a rate of 96 ± 2%. This system holds promise for the engineering of tissue with a tunable cell distribution and may aid in efforts for developing biological substitutes for the repair of damaged or diseased tissues.

Many commercial methods for bio-recognition assays employing a solid support are available. These include Whatman's FAST® slides, Oncyte-Avid slides, and Unisart slides [6,32-36]. FAST® slides can be used to perform reverse phase protein arrays, traditional protein arrays and antibody arrays utilizing less sample than a traditional ELISA test. They also allow for the parallel quantitation of many samples to a limit of 1 pg/mL [6]. This platform has recently been utilized as a point of reference for new experimental techniques as well as tested in comparison to other commercially available slides [32-34]. The ONCYTE® nitrocellulose slides provide a three dimensional

microporous film designed in three formulations to diversify its use for higher binding capacities, low-fluorescence intensity, or both [35]. This diversity allows for the use of ONCYTE slides in biomarker discovery as well as studies of protein function. The Unisart membranes are utilized in lateral flow immunoassays (LFIAs) by binding the antibodies or capture molecules while preserving their reactivity [36]. These membranes currently enable the analysis of over 60 markers.

2.2.2 Point-of-Care Assays

The compact disc assay is a diagnostic platform that functions without the use of sophisticated laboratory equipment. Utilizing this technique, a microfluidic device is created by modifying a CD so that quantitative biological assays can be performed and detection can take place using a standard (or modified) disc reader or the CD drive in a personal computer (Figure 2.2, Table 2.2). Typically, CDs are prepared by activating the polycarbonate surface with UV/ozone treatment followed by the use of a PDMS stamp to apply surface patterning [2,9,27]. Following CD disc preparation, samples are applied and allowed to incubate for extended periods of time. Once assays are complete, the disc is loaded into a CD-drive where the extent and location of errors in disc reading directly detect and quantify compounds of interest. In addition to their high sensitivity and relatively simplistic fabrication processes, assays using this platform have become increasingly popular due to their low-cost and portability. This makes them an attractive diagnostic option for remote settings as well as use in areas with limited resources.

Technique	Applications	Sensiti-vity	Analysis Time	Fabrication/Equip-ment Requirements	Reference(s)
CD disc bioassay	Lead detection, streptavidin binding, DNA detection, antibody-antigen detection	10 nM – 25 nM	45 – 65 min	Soft lithography fabrications; unmodified disc reader/computer drive and error analysis software	2, 9, 27
CD disc micro-immunoassay	Agrochemical residue quantification	37 pM – 0.28 nM	30 min	Direct attachment of binding groups to disc; silver enhancement/optical disc drive detection	11
CD disc microparticle counting	Measure biomolecules/ cells	1 x 10^6 cells/mL	2.5 hours	Soft lithography fabrication; unmodified disc drive	10
Blu-ray microarray	Competitive microcystin array	0.4 nM	1 hour	Blu-ray disc drive and Nero Disc speed software	42

Table 2.2 Experimental biological recognition techniques that can be used as point-of-care devices for medical diagnostics.

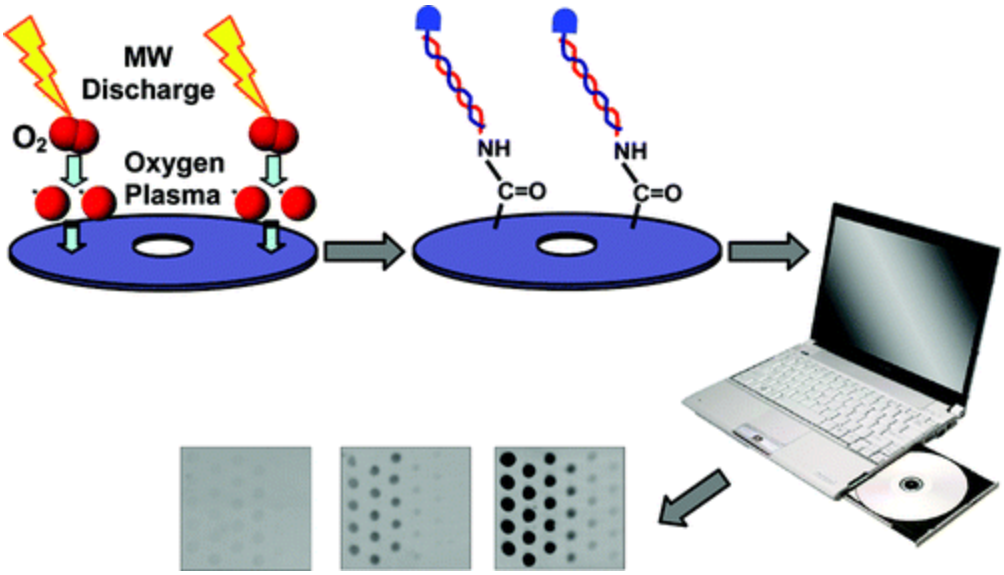

Figure 2.2 is an illustration showing the overall process for performing a DVD-based assay. On the polycarbonate surface of the DVD, activation with oxygen plasma generates carboxylic acid groups which are covalently attached to amino-modified oligionucleotide probes. The use of an unmodified disc reader on a laptop allows for the visualization of spots where binding events occurred and the quantitation of species being investigated. Reproduced from Reference 11 with permission from The Royal Society of Chemistry.

In one experimental incarnation of this technique, Wang et al. have demonstrated the detection of lead at the parts-per-billion (ppb)-level [2]. Lead detection was quantified using a DNAzyme assay where a DNAzyme strand was hybridized to a substrate strand and immobilized on CD. In the presence of lead the substrate strand was cleaved preventing reporter strand binding and reducing CD reading-error rates. The results of this work demonstrate a direct correlation between lead concentrations and error reading signals in the range of 10 nM to 1 mM, with a lead detection limit of 10 nM (2 ppb). This high sensitivity for lead is more than is required for the routine monitoring of its presence in environmental samples. However, while the disc-based assay is adaptable for other targets the detection setup reflects the approach used in a competitive assay, where signal decreases as concentrations of target analyte increase. This method may therefore not

prove to be as sensitive as those for non-competitive immunoassay where signal is directly proportional to sample concentration and could result in an assay with insufficient sensitivity for other low-abundance species. Additionally, the method requires long assay times in excess of two hours, which should ideally be reduced for its application as a point-of-care device.

A similar example of a reading errordetection-based disc assay is demonstrated by Pallapa et al. in the development of a quantitative biotin-streptavidin binding assay utilizing IsoBuster software for the more specific detection of erroneous bits in a frame as opposed to total error number alone [27]. Identifying where errors took place on disc allows the most direct approach for the modification of a CD to biomedical diagnostics and allows various data formats to be used. Using the IsoBuster analysis software, the results depict a clear dependence of reading error on streptavidin concentration. This allowed for a quantitative assay over the tested range of 5.8 nM – 29 nM with high spatial accuracy. Detection was accomplished using an unmodified conventional optical drive, increasing its potential in point-of-care applications. While quantitation was achieved for the tested samples, to adaptto other targets the dynamic range should be expanded and fully evaluated, allowing clinically relevant concentrations of various biomarkers to be detected.

This same approach was used to analyze three trial systems: DNA hybridization, antibody-antigen binding, and ultrasensitive lead detection [9]. The CD-quality diagnostic program is used for detection, which allows a relationship to be generated displaying the reading error on disc as a function of CD playtime. This enables the specific position of the error on disc to be identified, corresponding to the position of the

binding event. The results show that this method is sensitive for all systems tested achieving a 25 nM detection limit of DNA from a sample volume of 2.0 µL (50 fmol of DNA), a 0.17 nM detection limit for IgG, and a 10 nM (2 ppb) detection limit for lead. This platform has been shown to be highly diverse in terms of applicable target molecules and portable for on-site applications due to its use of an unmodified disc reader for detection.

Error reading detection was also employed in microparticle and cell counting [10], providing development of a health diagnostic compact disc (HDCD) aimed at providing rapid and affordable point-of-care diagnostics. While the detection methods employed are simplistic and accessible, the device fabrication is more complicated than that used in similar assays. First, a trench was machined in the polycarbonate surface of the CD and transparency was restored through wet sanding. A PDMS microfluidic layer was fabricated via soft lithography, embedded into the CD trench, and bonded to the CD through an additional PDMS adhesive layer. After sample application, a focused laser beam reflected on the CD data layer is interfaced by the sample suspension. Because the sample is placed directly above the CD data layer, the original digital information is changed through optical interference. The alteration of interaction between the laser and data layer directly relates to the shape, concentration, and optical density of the sample being analyzed. Results show a clear trend with increasing error rates as sample concentration increases. However, incubations of two hours were required between sample introduction and detection. This represents an obstacle to be overcome in the development of a truly mobile device, which would benefit from rapid assay times to increase end user ease of operation.

An alternative CD assay approach was presented by Tamarit-Lopez et al [11]. Haptens were attached to the polycarbonate surface of the CD by direct covalent attachment. Assays were based on an indirect competitive format and utilized silver enhancement solution to display the immunoreaction. Compared to related methods, this assay occurs rapidly, lasting about 30 minutes from sample application to detection. The detection limits for the tested compounds chloropyrifos, atrazine, and 2-(2,4,5-trichlorophenoxy)propionic acid were found to be 0.1nM, 37 pM and 0.28 nM, respectively, an order of magnitude better than classical methods. Along with the use of a conventional optical detector, this illustrates the potential of this assay to be a useful point-of-care diagnostic tool even though it is demonstrated on non-biological samples.

The disc-based assay platform was expanded by this group through its extension to the use of the underlying physicality of DVD technology as the solid support [4]. The disc was activated with oxygen plasma and used to detect the PCR products of *Salmonella spp.* through attenuated analog signal detection. Similar to their previous work the assay time was short, with an 18 minute amplification time to achieve a detection limit of 2 nM with unmodified DVD drive detection.

A further evolution of this technique is illustrated by the introduction of Blu-ray technology in the recent work by Arnandis-Chouer et al [42]. The use of Blu-ray discs presents several advantages over a DVD-based assay: 1) blue laser light is used, so the range of optical detection is expanded and 2) a higher numerical aperture lens is used for greater focusing precision allowing for smaller spot sizes and more information to be stored on disc. As a proof-of-concept experiment Blu-ray discs were compared to DVDs for the same assay, Blu-ray assays were detected by a drive attached to a personal

computer through a USB and analyzed using Biodisk software. Results show the Blu-ray disc has a 6.2 fold improved detection limit versus DVD assays, achieving levels of 0.4 nM for microcystin LR and 10^0 and 10^1 cfu/mL for *Salmonella typhimurium* and *Cronobacter sakazakii* respectively. While these assays have achieved clinically relevant detection limits for the targets investigated, to become a versatile point-of-care device increased sensitivity should be achieved for the detection of varied proteins.

Several commercial methods utilizing mobile platforms are also available through IMTEK, GenePOC, and Gyros [43-45]. These products have been utilized extensively for biomedical analysis investigations. IMTEK is working to develop an automated, user-friendly platform that can integrate micro, nano, and bio components into a multifunctional point-of-care device [43]. The core of this lab-on-a-chip device is its foil-based centrifugal cartridge that can assist in the integration of all operations allowing raw sample to be injected, purified and analyzed at low cost. Although use of this device has not been widespread to date, it's continued investigation and fine-tuning promises to result in a valuable tool for point-of-care diagnostics and personalized medicine.

The Gyros lab has developed a range of Gyrolab Bioaffy™ CD's that are used for nanoliter-scale immunoassays that allowresults to be read in under an hour [44]. This technique was recently validated for the quantification of rituximab in human serum by Liu et. Al [46]. Here, the Gyrolab™ technology was tested and results show validation of the quantification of rituximab between concentrations of0.62 nM – 0.41 µM.. This platform allows for fully automated assays to take place utilizing small reagent and sample volumes. While there are limited examples of fully validated Gyrolab assays, this method holds many advantages that make it an attractive option for point-of-care

diagnostics. While it also lacks significant examples of test validation in literature, the platform developed by GenePOC diagnostics was designed to be user-friendly with only four steps required for performance [45]. This fully automated system generates results in less than an hour with minimal hands-on time.

2.3 Imaging

Imaging-based techniques can be similarly divided into subcategories: (i) those utilizing modified traditional instrumentation and taking place in the laboratory or clinic and (ii) portable platforms allowing remote diagnostics. Some of the techniques discussed in this section include modified Fourier-Transform Infrared Spectroscopy (FTIR) detection, the development of multimodal optical probes, and mHealth monitoring applications. The mHealth platform and others similar to it have gained interest over the last several years because they allow for rapid, sensitive and affordable testing to be accessible in remote settings. It also allows quality healthcare to be possible through telemedicine in regions where access is limited.

2.3.1 Laboratory-based Imaging Technologies

Infrared (IR) spectroscopy has been used extensively for imaging-based biomedical analysis. A major focus in this area has been the improvement of FTIR for high definition imaging [13-20]. Conventional FTIR microscopy has been limited by trade-offs between signal-to-noise ratios (SNRs) and data acquisition times, as well as spatial resolution [17,18]. While IR spectroscopy has long been recognized as a potentially valuable diagnostic tool due to its coverage of regions encompassing characteristic biomolecule absorptions [13], its utility has been limited by these trade-offs and the lower size boundary imposed by the diffraction limit for the relatively long

wavelengths. New experimental techniques have worked over the past several years to overcome those limitations so its full diagnostic potential may be realized (Table 2.3).

Technique	Applications	Resolution	Duration	Fabrication/ Equipment Requirements	Reference(s)
ATR-FTIR	Endometriosis detection	4 cm^{-1} – 8 cm^{-1}	32-45 scans/sample	ATR-FTIR, Bruker Vector 22 FTIR spectrometer, Thermo Nicolet Continuum FTIR microscope	13
Synchrotron FTIR	Lipid detection, label-free imaging	Diffraction limited – 0.54 x 0.54 μm^2	From < 1 min for 30 x 30 µm	Mid-infrared beamline IRENI; multiple synchrotron beam source and wide field detection FTIR	16, 17
Nanoscale Imaging	FTIR, AFM-IR	100 – 200 nm	From 10 min for 100 x 100 pixel image	AFM-IR, novel FTIR system based on s-SNOM	15, 19
Photothermally induced resonance	Organometallic conjugate detection	20 – 50 nm; 10 µM	1 hour	AFM and tunable pulsed laser	20
Multifunctional probes	Detection of cancer cells, estrogen	From 10 cells/mL; 25 µM	2 hours – overnight	TEM, UV-Vis-near infrared laser; synchrotron UV spectromicroscope, FTIR	47, 48

Table 2.3 Laboratory-based imaging techniques that have been modified to improve resolution in biomedical analysis applications.

Work by Nasse et al. introduces the use of multiple synchrotron beams into FTIR [17]. This was able to extend the IR abilities to truly diffraction-limited imaging over the whole mid-infrared spectrum by combining the multiple beams with wide-field detection. This approach was based on the strategy of wide-field imaging with the use of multichannel focal plane array detectors. Results show the successful measurement of ~1

μm polystyrene beads to a limit of 6 ± 1 fmol in a single pixel (0.54 μm^2). In addition to vast improvement in acquisition time (30 minutes to scan a 280 μm x 310 μm area compared to over 11 days using diffraction-limited resolution raster-scanning), this modification to IR holds great promise as a diagnostic imaging technique.

Synchrotron FTIR (sFTIR) was further used to examine lipids in and around amyloid plaques associated with Alzheimer's disease [16]. The primary motivation was to test for elevated lipid presence near recently formed plaques using sFTIR in transmission mode. To archive acceptable SNR ratios, between 64 and 256 scans were co-added. From this analysis a lipid membrane-like signature was found in and around dense core plaques in both advanced and early stage plaque. While analysis suggests that lipid is a common feature of the plaque structure, there are several potential explanations for its origin, which remains unknown.

In addition to the analysis of Alzheimer's disease-related tissue FTIR was recently used by Cheung et al. to discriminate spectral signatures of endometriosis [13]. In this work, both transmission FTIR and attenuated total reflection Fourier-transform IR (ATR-FTIR) were coupled with subsequent computational analysis in an attempt to discern endometrial tissue-specific biochemical-cell fingerprints. Through detailed spectral analysis biochemical differences were identified between healthy tissue and tissue with endometriosis present. While spectral signatures have been observed, this technique requires highly specialized analysis which may limit its utility as a widespread clinical diagnostic tool.

Beyond diffraction-limited resolution lies an interest in the application of FTIR to nanoimaging [15]. As recently discussed by Huth et al., an approach has been developed

based on the superfocusing of thermal radiation with an infrared antenna, detection of the scattered light and signal enhancement using an asymmetric FTIR spectrometer. A semiconductor device was used as the sample and imaging was accomplished within a few minutes. Results show that 10 nm spatial resolution can be achieved. For even more rapid applications spectra with 25 cm^{-1} resolution and an SNR of 10:1 were captured in only 2 minutes. While demonstrated here for the mapping of a semiconductor, imaging of this resolution could become a powerful tool for chemical/biochemical sample analysis. However, as with many imaging techniques, results must be interpreted by an expert adding to overall analysis time. Additionally, the use of highly specialized lab equipment prevents adaptation of this method to a point-of-care device.

Pita et al. also demonstrated simulations aimed at improving the spatial resolution of IR techniques [14]. Results of these simulations suggest that the difference in transmitted and reflected IR energy between a Gaussian reference and a vortex-shaped beam using a confocal microscope could be mapped. This would result in vibrational absorption images with a spatial resolution better than $\lambda/10$. This resolution would enable detection sensitivities great enough for the imaging of organic nanoparticles and would indicate great improvement over classical IR for diagnostic imaging.

In related work toward nanoscale IR spectroscopy, Marcott et al. have coupled an atomic force microscope (AFM) and a tunable IR laser source [19]. Using samples of stratum corneum (SC), results show a spatial resolution of ~200 nm. This technique enables the SC to be spectroscopically characterized in more detail than ever before. These studies may prove useful in diagnostic testing as they are enabling use of this technique for the understanding of penetration pathways for topically applied drugs.

However, data capture requires sophisticated laboratory equipment and data interpretation is performed by specialized personnel limiting its capability for widespread use in diagnostics or disease monitoring.

Another technique for the coupling of AFM to IR to improve near-field resolution is described by Policar et al [20]. It focusses on the development of photothermally induced resonance (PTIR), where AFM is coupled with a tunable pulsed IR laser. IR is attractive for bioimaging because IR probes are stable in biological environments, they are small, and have intense absorption in the 1800-2200 cm^{-1} region where biological samples are transparent. Using PTIR the spatial resolution is improved to 20-50 nm, which is sensitive enough for subcellular mapping. This was demonstrated using an organometallic conjugate whose uptake by breast cancer cells could be monitored. While not currently used in diagnostic biomedical analysis, imaging at this sensitive level illustrates a powerful improvement to traditional IR imaging and could provide valuable diagnostic data in a sophisticated laboratory setting.

Recent work by Guo et al. describes the development of an optical probe used for cancer cell detection [47]. Localized surface plasmon resonance (LSPR) absorption, as well as the fluorescence properties of folic acid-conjugated gold nanorods (F-GNRs) were used as detection systems for the multifunctional probe. The absorption capabilities were explored through the quantification of human cervical carcinoma (HeLa) cells versus African green monkey (Vero) control cells. Results indicate a detection limit using fluorescence detection of 70 cells/mL for HeLa cells with a quantitative range covering 100 – 5000 cells/mL. Using the absorption mode, the probe reduced the detection limit to 10 cells/mL while maintaining the quantitative range for the technique. While this

technique achieves low detection limits for whole cells, the same approach could not be used for the detection of proteins without alteration of the assay procedures prior to detection. Additionally, major adjustments would need to be made to the assay platform in order to achieve parallel target detection.

Another unique multimodal probe was investigated by Clède et al [48]. This probe, called SCoMPI (single core multimodal probe for imaging), was used for the detection of two breast cancer cell lines. Resolution at the subcellular level was achieved, allowing information about the location of the metal conjugated probe within the cell. This capability allows reliable information to be gathered using many imaging techniques. The diverse and sensitive, rapid imaging platform may prove to be a valuable tool for the biomedical analysis of tissues used in diagnostics.

Experimental adaptations to traditional imaging equipment have also been pursued by Neaspec [49]. The NeaSNOM microscope utilized a new technology allowing imaging in the visible, infrared and terahertz spectral regions to a spatial resolution of 10 nm. This technology has been utilized to map insulin fibrils [50] , as well as determine the local dielectric permittivity of a PMMA film [51], among other applications. With a scan speed of up to 20 µm/s and capability for the analysis of sample up to 40 x 50 x 15 mm, this technique offers a desirable balance of sensitivity and speed for the imaging of biological tissues.

2.3.2 Point-of-Care and mHealth Platforms

While improvements to traditional imaging techniques have garnered attention over the past several years, mHealth imaging efforts are growing just as quickly (Table 2.4). This technique takes place with a variety of imaging detection formats attached to

the camera lens of a smartphone. By using the camera to capture data, results can be sent to a central hub in a clinic or hospital so care providers can make treatment decisions without patients having to commute from remote locations. This is also valuable for monitoring health in resource-poor settings where access to healthcare is limited and telemedicine is the only real viable option.

Technique	**Applications**	**Resolution**	**Duration**	**Fabrication/ Equipment Requirements**	**Reference(s)**
mHealth	Fluorescein detection	1 – 10 nM	10 – 15 sec data capture (~85 min sample prep)	Capillary array, fluorescence detector, multiple wavelength LED, computational image stacking program	12, 25
Cell-phone microscope	Detection of micro-particles, red blood cells, white blood cells, parasites	~1 – 2 µm	5 minutes	Specially designed microscope attachment	21
Fluorescent imaging cytometry on cellphone	White blood cell density measurement	2 µm resolution	6 minutes	Specialized optofluidic cellphone attachment	23
Label-free smartphone biosensor	Protein detection	4.25 nM	20 minutes	Photonic crystal biosensor, application for automated data interpretation	24
Rapid diagnostic test reader on cellphone	Immune-chromatographic assays	4x dilution of whole blood	< 1 minute, (0.2 seconds per image)	Specialty rapid diagnostic test reader attachment	26

Table 2.4 Summary of imaging techniques utilized as point-of-care devices for diagnostics.

The Rasooly group has contributed a several studies in the area of mHealth over the last few years. In a first example a capillary tube array was developed to improve the sensitivity of smart phones [25]. An increase in sensitivity was needed since common cellphone cameras are generally not able quantify the weak fluorescent signals present in many mHealth applications. An array using 36 capillaries was developed and illuminated using a multi-wavelength LED directed horizontally to the capillary axis. Fluorescein dilutions were tested between 0-10,000 nM, and a limit of detection was found to be ~10 nM in water. This represents roughly a 100-fold increase in sensitivity over the unmodified phone as well as a vast increase in sensitivity compared to 36 well plates whose LOD was 1000 nM.

In a secondary work from this group, mHealth diagnostic sensitivity was further improved using computational image stacking [12]. This was accomplished by capturing data in video mode, stacking the collected images and averaging the intensity of each pixel to reduce or eliminate random noise. To demonstrate the ability of this system to quantify disease-related biomarkers, adenovirus DNA was labeled with SYBR green or fluorescein. Using computational image stacking signal sensitivity was improved, reducing the LOD to 1 nM. While this technique currently demonstrates sensitivity similar to a standard well-plate reader, its portability, ease of use, and the potential for further increasing the sensitivity while utilizing minute sample volumes makes it an attractive and promising mHealth platform. However, before this technique could be used in diagnostic applications the platform would need to be evaluated for signal arising from

cross-reactivity or non-specific binding in samples which are not present in the current model system and have not been considered in its limit of detection.

Cost-effective microscopy for telemedicine has also been studied extensively by the Ozcan group. The primary focus of this group has been the development of lens-free microscopy (Figure 2.3) [21-23,26]. A microscope-based on digital in-line holography was developed using an light-emitting-diode (LED) and compact opto-electric sensor-array, which allows imaging without the need for lenses or bulky optical equipment [21]. The microscope was tested for imaging performance using a variety of cells and particles. Results show that, in addition to making the platform robust and cost-effective, lens-free imaging was able to achieve subcellular resolution. This work was extended by the imaging of micro-particles, red-blood cells, white blood cells, platelets and a waterborne parasite [22]. The spatial resolution in this application was limited by the pixel size of the sensor.

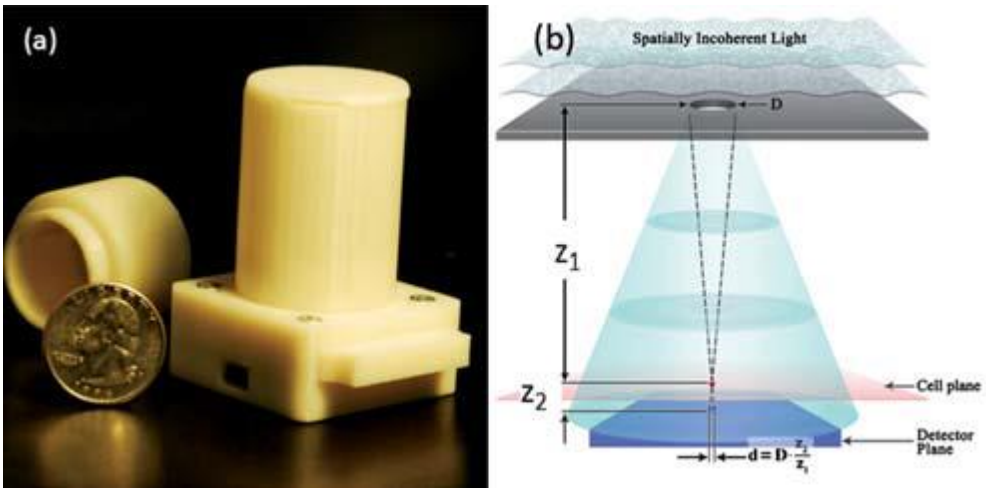

Figure 2.3 is reproduced from Reference 21 with permission from The Royal Society of Chemistry. The figure shows the platform for the attachment of a lens-free microscopy application to an existing cellphone camera. (A) shows an image of the actual device used. Shown in (B) is a schematic of the microscope shown in (A).

Further expansion of these efforts was observed by the integration of imaging cytometery and fluorescent microscopy as an optofluidic attachment [23,26]. This is achieved by inserting a disposable microfluidic channel above the existing cellphone camera to deliver targets of interest to the imaging volume. The captured images are then processed through a smart application that both validates the test and automatically presents the diagnostic results. This provided an imaging resolution of ~2 μm, which highlights this technique's potential as a valuable rapid imaging test for the routine remote monitoring of chronic conditions as well as disease screening in resource-poor areas.

The rapid-diagnostic-test platform was expanded to work with various lateral flow immuno-chromatographic assays to sense a target analyte [26]. In order to accomplish high-contrast imaging, diffused LED arrays were incorporated prior to data processing. The platform was experimentally tested using malaria, tuberculosis (TB) and HIV through detection with gold-labeled antibody-antigen complexes. This technique is capable of rapid, high-resolution screening while providing instant testing results. However, because its format only allows for the analysis of one target species at a time, its use as a diagnostic point-of-care device would require the transport of a library of microfluidic channel inserts which could decrease its ease of use, leaving it better suited to the monitoring of chronic diseases in remote locations as opposed to a diagnostic tool.

Label-free detection on a smart phone was recently demonstrated by Gallegos et al [24]. Broadband light entered through a pinhole and was collimated prior to passing through a photonic crystal biosensor fabricated on a plastic substrate. A custom software application was able to convert the resulting images to transmission spectra and perform

curve-fitting analysis. Results show peak wavelength value shifts could be measured with 0.009 nm spectral accuracy, allowing the detection of an immobilized protein monolayer as well as selective, concentration-dependent antibody binding to a limitof 4.25 nM. The measurement of wavelength shifts above the sensor-specific background noise suggests the LOD is controlled by variations within the assay as opposed to the detector resolution. The development of label-free biodetection on an affordable, sensitive, and mobile platform represents a valuable potential tool for point-of-care diagnsotics, but similar to many cellphone-based techniques is hampered by its limitation to the detection of a single analyte.

The concept of a rapid, affordable point-of-care device has also been explored commercially [52-55]. The most common commercial platform thus far is that traditionally used in glucose monitoring [52,53]. One recent study compares the StatStrip (SS) and SureStrep Flexx (SF) for glucose testing [52]. Results of this show the that the sensitivity of SS was 94.7%, compared to 100% for SF and negative predictive values were found to be 86.1% in both cases. These results were achieved using venous blood samples compared to plasma glucose traditionally monitored, and it was determined that they were of limited use compared to the reading of plasma samples.

The development of point-of-care testing for diverse disease biomarkers has also been explored through a partnership between Texas Instruments and Cnoga Medical [54,55]. Together they have investigated the use of video cameras to measure vital signs like blood oxygen, carbon dioxide levels, blood pressure and pulse rate through skin analysis. Current research by these companies aims to expand this technology toward having capabilities to noninvasively identify biopatterns for diverse diseases.

2.4 Concluding Remarks

In examining the publications over this time span, there was a large emphasis on the development of mobile diagnostic devices both utilizing imaging and biological recognition detection platforms. This focus has evolved from the need to monitor global health issues, as well as treat patients in remote or resource limited locations. While platforms in this arena range from microarrays printed on CD or DVD discs, to the use of a cellular phone camera to image or count cells and interface with applications that allow data to be analyzed centrally through telemedicine, importance has been placed on the need to perform tests rapidly, at low cost, with sensitivity comparable to technologies used in a permanent laboratory, and with user-friendly interfaces. While mHealth and related cellphone applications do not currently share the advantage of parallel biomarker analysis, alterations in the design of the microfluidic cartridges used for testing prior to detection through the cell phone camera should not detract from the sensitivity of detection.

Another broad area of research is modifying traditional infrared spectroscopy equipment to overcome the traditional diffraction-limited resolution capabilities while maintaining reasonable analysis times. These approaches are valuable as they allow for subcellular imaging, pinpointing label locations within a cell, and determination of characteristic spectral signatures for related tissues that may help in the evolution of imaging biomarkers for disease. However, the ultimate limitation to these techniques is the singleplex analysis format they are confined to. While improvements in resolution and reduction in analysis time make these valuable testing platforms, often a great deal of post image-capture analysis is required for the interpretation of results, and only one

tissue may be imaged at a time, presenting a bottleneck to diagnosis of conditions compared to techniques that allow many tests to be performed in parallel in a similar time frame.

Finally, laboratory or clinic-based biorecognition assays have continued to evolve in terms of their sensitivity and capability for the analysis of many compounds simultaneously. While these techniques are diverse, they often require moderate sample volumes and longer incubation times than many of the point-of-care testing devices. In terms of these testing devices, the greatest potential for providing an optimized biomedical analysis device comes from those assays being developed as part of a microfluidic analysis system, where traditional incubation methods are forgone in lieu of convective mixing, as well as sample pre-concentration and purification prior to detection which both reduces cross-reactivity and allows for relatively complete capture of analyte from a sample volume enabling low sample volumes and reduced analysis times.

While many of the biomedical analysis techniques described here have been successful in improving upon on diagnostic capabilities or disease monitoring, there does not currently exist one definitive optimal technique. Progress has been made in the ability of various platforms to be user-friendly, rapid, and sensitive while achieving high resolution and using low sample sizes. However, challenges still remain in adapting many laboratory-based biological recognition assays to a point-of-care format without compromising sensitivity or requiring specialists to interpret results. Future techniques, in addition to being adaptable for the testing of a variety of diseases, should require minimal sample and be capable of quantifying multiple targets in parallel.

While various analysis approaches have specific advantages, combining the rapid analysis capabilities and user-friendly data presentation of the cellphone-based platforms with the high sensitivities and parallel analyte analysis achieved in laboratory-based biological recognition assays appears to present the most realistic path toward optimizing diagnostic and disease monitoring capabilities. Although more work needs to be done toward optimizing microfluidic attachments that may be used in remote locations for multi-analyte detection, developments in this arena over the next few years hold promise in providing optimize tests for disease monitoring tailored to the needs of their specific targets, as well as versatile platforms that may be adapted to the early detection and diagnosis of varied diseases.

2.5 References

[1] Moschallski, M., Evers, A., Brandsetter, T., Ruhe, J., *Analytica Chimica Acta*, 2013, *781*, 72-79.

[2] Wang, H., Ou, L.M.L, Suo, Y., Yu, H.Z., *Analytical Chemistry*, 2011, *83*, 1557-1563.

[3] Farajollahi, M.M., Cook, D.B, Hamzehlou, S., Self, C.H., *Scandinavian Journal of Clinical and Laboratory Investigation*, 2012, *72*, 531-539.

[4] Tamarit-Lopez, J., Morais, S., Puchades, R., Maquieira, A., *Bioconjugate Chemistry*, 2011, *22*, 2573-2580.

[5] Zhang, B., Liu, B., Zhou, J., Tang, J., Tang, D., *Applied Materials and Interfaces*, 2013, *5*, 4479-4485.

[6] FAST® Slide Protein Microarray 2013 KeraFast, Inc. https://www.kerafast.com/c-1-fast-slide-protein-microarray.aspx

[7] Moschallski, M., Baader, J., Prucker, O., Ruhe, J., *Analytica Chimica Acta*, 2010, *671*, 92-98.

[8] Wen, J., Shi, X., He, Y., Zhou, J., Li, Y., *Anal. Bioanal. Chem.*, 2012, *404*, 1935-1944.

[9] Yu, H.Z., Li, Y., Ou, L.M.L., *Accounts of Chemical Research*, 2013, *46*, 258-268.

[10] Imaad, S.M., Lord, N., Kulsharova, G., Liu, G.L., *Lab on a Chip*, 2011, *11*, 1448-1456.

[11] Tamarit-Lopez, J., Morais, S., Manuis, M.J., Puchades, R., Maquieira, A., *Analytical Chemistry*, 2010, *82*, 1954-1963.

[12] Balsam, J., Rasooly, R., Bruck, H.A, Rasooly, A., *Biosensors and Bioelectronics*, 2014, *51*, 1-7.

[13] Cheung, K.T., Trevisan, J., Kelly, J.G., Ashton, K.M., Stringfellow, H.F., Taylor, S.E., Singh, M.N., Martin-Hirsch, P.L., Martin, F.L., *Analyst*, 2011, *136*, 2047-2055.

[14] Pita, I., Hendaoui, N., Liu, N., Kumbham, M., Tofail, S.A.M., Peremans, A., Silien, C., *Optics Express*, 2013, *21*, 25632-25642.

[15] Huth, F., Schnell, M., Wittborn, J., Ocelic, N., Hillenbrand, R., *Nature Materials*, 2011, *10*, 352-356.

[16] Liao, C.R., Rak, M., Lund, J., Unger, M., Platt, E., Albensi, B.C., Hirschmugi, C.J., Gough, K.M., *Analyst*, 2013, *138*, 3991-3997.

[17] Nasse, M.J., Walsh, M.J., Mattson, E.C., Reininger, R., Kajdacsy-Balla, A., Macias, V., Bhargava, R., Hirschmugl, C.J., *Nature Methods*, 2011, *8*, 413-416.

[18] Reddy, R.K., Walsh, M.J., Schulmerich, M.V., Carney, P.S., Bhargava, R., *Applied Spectroscopy*, 2013, *67*, 93-105.

[19] Marcott, C., Lo, M., Kjoller, K., Domanov, Y., Balooch, G., Luengo, G.S., *Experimental Dermatology*, 2013, *22*, 417-437.

[20] Policar, C., Birgitta Waern, J., Plamont, M.A., Clede, S., Mayet, C., Prazeres, R., Ortega, J.M., Vessieres, A., Dazzi, A., *Angew. Chem. Int. Ed.*, 2011, *50*, 860-864.

[21] Mudanyali, O., Tseng, D., Oh, C., Isikman, S.O, Sencan, ., I., Bishara, W., Oztoprak, C., Seo, S., Khademhosseini, B., Ozcan, A., *Lab on a Chip*, 2010, *10*, 1417-1428.

[22] Tseng, D., Mudanyali, O., Oztoprak, C., Isikman, S.O., Sencan, I., Yaglidere, O., Ozcan, A., *Lab on a Chip*, 2010, *10*, 1787-1792.

[23] Zhu, H., Mavandadi, S., Coskun, A.F., Yaglidere, O., Ozcan, A., *Analytical Chemistry*, 2011, *83*, 6641-6647.

[24] Gallegos, D., Long, K.D., Yu, H., Clark, P.P., Lin, Y., George, S., Nath, P., Cunningham, B.T., *Lab on a Chip*, 2013, *13*, 2124-2132.

[25] Balsam, J., Bruck, H.A., Rasooly, A., *Sensors and Actuators B: Chemical*, 2013, *186*, 711-717.

[26] Mudanyali, O., Dimitrov, S., Sikora, U., Padmanabhan, S., Navruz, I., Ozcan, A., *Lab on a Chip*, 2012, *12*, 2678-2686.

[27] Pallapa, M., Ou, L.M.L., Parameswaran, M., Yu, H.Z., *Sensors and Actuators B*, 2010, *148*, 620-623.

[28] Zhu, H., Isikman, S.O., Mudanyali, O., Greenbaum, A., Ozcan, A., *Lab on a Chip*, 2013, *13*, 51-67.

[29] Zeng, Y., Wang, T., *Anal. Bioanal. Chem.*, 2013, *405*, 5743-5758.

[30] Zhu, H., Cox, E., Quian, J., *Proteomics Clin. Appl.*, 2012, *6*, 548-562.

[31] Walsh, M.J., Reddy, R.K., *IEEE Journal of Selected Topics in Quantum Electronics*, 2012, *18*, 1502-1513.

[32] Prashanth, G.R., Goudar, V.S., Raichur, A.M., Varma, M.M., *Sensors and Actuators B: Chemical*, 2013, *183*, 496-503.

[33] Mujawar, L.H., Moers, A., Norde, W., van Amerongen, A., *Anal. Bioanal Chem*, 2013, *405*, 7469-7476.

[34] Mujawar, L.H., Maan, A.A., Khan, M.K.I., Norde, W., van Amerongen, A., *Analytical Chemistry*, 2013, *85*, 3723-3729.

[35] "ONCYTE® Nitrocellulose Film Slides" Grace Bio-Labs, Inc. 2010. http://www.gracebio.com/life-science-products/microarray/oncyte-nitrocellulose-film-slides.html

[36] UniSart® Membranes Consistency by Design http://www.sartorius-stedim.com.tw/Attachment/FCKeditor/Product/file/PDF/lab/filter&membran/Broch_Unisart_Membranes_SL-1522-e.pdf

[37] Zhang, B., Liu, B., Zhou, J., Tang, J., Tang, D., *Applied Materials and Interfaces*, 2013, *5*, 4479-4485.

[38] Peretz-Soroka, H., Pevzner, A., Davidi, G., Naddaka, V., Tirosh, R., Flaxer, Patolsky, F., *NANO Letters*, 2013, *13*, 3157-3168.

[39] Chandra, P., Abbas Zaidi, S., Noh, H.B., Shim, Y.B., *Biosensors and Bioelectronics*, 2011, *28*, 326-332.

[40] Wang, J., Morabito, K., Erkers, T., Tripathi, A., *Analyst*, 2013, *138*, 6573-6581.

[41] Lin, Y.H., Yang, Y.W., Chen, Y.D., Wang, S.S., Chang, Y.H., Wu, M.H., *Lab on a Chip*, 2012, *12*, 1164-1173.

[42] Arnandis-Chover, T., Morais, S., Gonzalez-Martinez, M.A., Puchades, R., Maquieira, A., *Biosensors and Bioelectronics*, 2014, *51*, 109-114.

[43] Disc-shaped Point-of-Care platform for infectious disease diagnosis, K. Mitsakakis, 2014 http://www.imtek.de/laboratories/mems-applications/projects/projects_overview?projectId=8073

[44] Gyrolab Bioaffy CDs 2013 Gyros AB http://www.gyros.com/products/products-optimized/gyrolab-bioaffy-cds/

[45] GenePOC 2014, GenePOC, Inc. http://www.genepoc-diagnostics.com/Technology.shtml

[46] Liu, X.F., Wang, X., Weaver, R.J., Calliste, L., Xia, C., He, Y.J., Chen, L., *Journal of Pharmacological and Toxicological Methods*, 2012, *65*, 107-114.

[47] Guo, Y.J., Sun, G.M., Zhang, L., Tang, Y.J., Luo, J.J., Yang, P.H., *Sensors and Actuators B: Chemical*, 2014, *191*, 741-749.

[48] Clede, S., Lambert, F., Sandt, C., Kascakova, S., Unger, M., Harte, E., Platmont, M.A., Saint-Fort, R., Deniset-Besseau, A., Gueroui, Z., Hirschmugl, C., Lecomte, S., Dazzi, A., Vessieres, A., Policar, C., *Analyst*, 2013, *138*, 5627-5638.

[49] NeaSNOM Microscope, 2013 Neaspec http://www.neaspec.com/products/neasnom-microscope/

[50] Amenabar, I., Poly, S., Nuansing, W., Hubrich, E.H., Govyadinov, A.A., Huth, F., Krutokhvostov, R., Zhang, L., Knez, M., Heberle, J., Bittner, A.M., Hillenbrand, R., *Nature Communications*, 2013, *4*, 1-9.

[51] Govyadinov, A.A., Amenabar, I., Huth, F., Carney, P.S., Hillenbrand, R., *J. Phys. Chem. Lett.*, 2013, *4*, 1526-1531.

[52] Kitsommart, R., Ngerncham, S., Wongsiridej, P., Kolatat, T., Jirapaet, K.S., Paes, B., *Eur J Pediatr*, 2013, *172*, 1181-1186.

[53] StatStrip® Connectivity and StatStrip Xpress Point-of-Care Glucose/Ketone Monitoring Systems 2014 Nova Biomedical Corporation http://www.novabiomedical.com/products/statstrip-glucoseketone-statstrip-xpress-glucoseketone/

[54] Nadeski, M., Frantz , G., The future of medical Imaging http://www.ti.com/lit/wp/slyy020/slyy020.pdf

[55] Cnoga Medical develops diagnostics through skin color, G. Weinreb, 2013 Globes http://www.globes.co.il/serveen/globes/docview.asp?did=1000877563

CHAPTER 3

RECENT DEVELOPMENTS IN EMERGING MICROIMMUNOASSAYS

3.1 Introduction

Over the last several years micro-immunoassay development has focused on replacing existing immunometric assays based on a micro-titer plate format. Notable among these currently existing methods is the enzyme-linked immunosorbent assay, or ELISA. Since its introduction in 1971, ELISA has remained a core, widely accepted practice and remains a common focal point to differentiate and discuss current experimental techniques [1]. Its success stems from the enzyme-based amplification mode and ease of use, along with the specificity and sensitivity of the antibody-antigen interactions common to all immunoassays. Despite the long incubation times and relatively high sample volumes and reagent costs, experimental assays aimed at the replacement of ELISA have universally failed to displace it and few have been implemented commercially. While much of the following discussion is centered on comparisons to ELISA, all immunoassay platforms are included. Over the last five years, efforts to improve upon clinically used sandwich immunoassays have targeted one (or more) of six metrics: increased sensitivity [2-5], reduced analysis time [6-9], reduced cost [10], lower sample volumes [6-11], ability to multiplex [2,6,12-15], or operational simplicity [3]. While many studies improved various aspects of immunoassays, a so-called optimized immunoassay capable of displacing existing tests and significantly improving capabilities for clinical or diagnostic purposes has not been produced. A platform capable of doing so would need to not only meet the critera defined above, but possess high reproducibility and show selectivity for the condition or disease being

investigated. Many of the methods discussed herein have been addressed only in single publications, therefore reproducility of immunoassay results needs to be improved before one may be considered optimal for diagnostics. However, several studies noted here may lay the foundation for a successor to ELISA.

Several groups continue to develop variations on standard immunoassay protocols, notably those of Ko, Gijs, Yang, and Hage. The current article will focus on the ability of these systems (and others) to create sensitive, robust, rapid and cost-effective diagnostic tools with high throughput on a multiplex format. While many of the assays discussed currently take place using singleplex analysis, their ability to be adapted to a high-throughput format will be assessed relative to other formats.

For any assay platform, the ultimate level of sensitivity will depend on the reaction kinetics (K_{eq}) resulting from reagent quality [16]. However, reagent specificity will have differing impacts on the assay outcome depending on the platform in which they are used. An optimized clinical immunoassay format should meet several criteria to be applicable to a comprehensive range of diagnostic tests. First, a sensitivity down to the low pg/mL range is optimal so any plasma protein may be monitored, which allows for ultra-sensitive detection in medical diagnostics [17]. An analysis time should be no more than 1 hour (if samples may be evaluated simultaneously) to permit changes over time to be tracked with ease [18], and sample volumes in the range of 10 μL per analyte interrogated to minimize reagent consumption. Finally, an assay should be able to multiplex for the evaluation of five proteins simultaneously, representing quantification of a group of biomarkers for a specific disease [15], and should take place with minimal transfer/pipetting steps to lessen variation between tests/testing sites [18]. These criteria

represent the desired capabilities of an immunoassay platform such that it may be easily adapted for the detection of a complete range of targets in a clinical setting. The individual assays discussed have been optimized for a particular target (or set of targets), which in some cases have requirements deviating from the desired qualities described above for an optimized clinical assay. While these criteria are not inclusive to all tests, they have been established to provide an organized framework in which to discuss the diverse experimental immunoassay platforms available.

While immunoassays have been the subject of several recent reviews [19,20], the focus of this review is immunoassay platforms aimed at improving diagnostic abilities published during the time span from January 2008 to April 2012, initiated with literature keyword searches associated with micro-immunoassays along with the references and later citations of found works. These articles contributed new techniques to the field by improving limits of detection, decreasing sample analysis time, and refining the ability of assays to accommodate multiple samples in parallel. Many of the designs represent relatively simple fabrication processes and, while demonstrated for specific analytes, could be easily adapted for any number of target compounds. The topics addressed are categorized into three classes: (i) use of micro- or nanoparticles (both magnetic and non-magnetic) as a solid support or to generate signal [Section 3.2], (ii) generation of signal using flow conditions [Section 3.3], and (iii) use of a static solid support to trap antigen and generate signal [Section 3.4]. A summary of these techniques is provided for reference (Table 3.1, Appendix B). Although articles have been divided into these categories for clarity, they are not mutually exclusive and many studies could have been placed in more than one class.

3.2 Assays using micro- or nanoparticles

Assays employing micro- or nanoparticles may be further divided into two categories: (i) those using magnetized particles and (ii) those which use non-magnetic particles. Some of the techniques described here include the fluorescent microsphere immunoassay (FMIA) and its variations, magnetic bead-based immunoassays occurring fully on-chip where beads are manipulated to afford contact with successive reagents and samples, and magnetic bead-based assays which employ batch incubation off-chip prior to on-chip detection. The use of micro- or nanoparticles has gained popularity for a variety of reasons. Chief among these are the ease of manipulation during sample preparations and the ability to tailor the number of beads employed to suit the specific needs of an assay. This allows the solid surface area to be altered and optimized for various targets. Users are able to trap lesser sample concentrations on a small surface area (by employing low bead numbers) which provides signal concentration, allowing sensitive detection. Assays utilizing magnetic particles, in particular, also lend themselves well to coupling with varied signal processing approaches which have improved sensitivities and lowered limits of detection [4,5,21].

3.2.1 FMIA

FMIA is a technique that uses numerous sets of spectroscopically-coded fluorescent microspheres, where each microsphere set is conjugated to a unique antibody or antigen, forming a solid phase for analyte detection [12]. This format was developed with a focus on multiplex analyses and has been used to successfully quantify ten compounds in parallel with detection limits in a clinically relevant range. Antigen-antibody reactions are simply performed in the well of a micro-titer plate. Analysis

follows, on a flow cytometer using Luminex X-Map^{TM} technology, in which separate wavelengths of light excite the microsphere sets and surface-bound reporter dyes [22,23]. The microspheres are labeled with a combination of red and orange fluorescent dyes. The ratio of these dyes acts as an identifier of the target analyte immobilized on the microsphere surface [18]. A separate detector, measuring green fluorescent response proportional to the amount of target, is able to quantify the total analyte present (Figure 3.1) [24]. This technique has been tailored to quantify groups of compounds relevant to a particular disease and possesses the obvious advantage observed in its ability to interrogate up to ten analytes from a single sample. However, in order to achieve clinically relevant levels of sensitivity, this format requires long incubation times and the use of specialized equipment. While verified assays are powerful in the information content they are able to provide, validation studies to ensure specificity represent a time-consuming hurdle for adaptations to limitless biological applications.

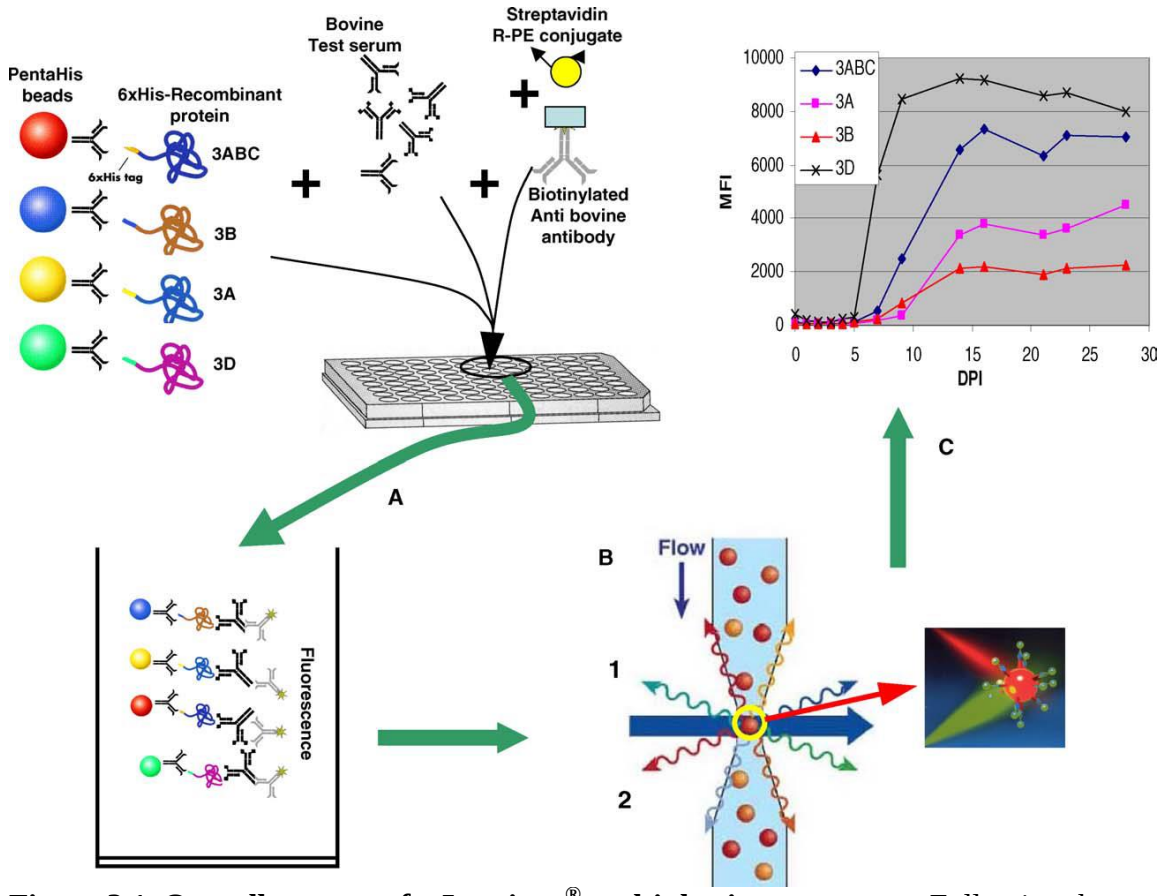

Figure 3.1. Overall process of a Luminex® multiplex immunoassay. Following the immunoreaction shown in **(A)** fluorescence signals from both the reporter-molecule and color-coding dyes are read simultaneously **(B)** and processed digitally to translate signals to quantitative data **(C)**.

The labor-intensive development process for FMIA was demonstrated in one instance by the validation of assays detecting the porcine reproductive and respiratory virus (PRRSV) in both serum and oral-fluid based samples [12,13].This work, done at South Dakota State University, produced an 8-plex FMIA for cytokine detection and requires a single 50 µL sample to quantify the analytes simultaneously [13]. Using the same volume typically required for one ELISA sample, the FMIA assay was able to achieve sensitivities in the pg/mL range. For seven out of the eight analytes studied this detection limit represents between 1.2 – 8.2 fold improvements to sensitivity compared with the analogous ELISA. Follow-up work aimed at replacing serum samples with oral-

fluid resulted in decreased diagnostic capabilities [12]. However, the assay did maintain a clinically-acceptable level of sensitivity and was able to detect the multiple target compounds in a single sample. While this work was successful in producing an assay based around the use of a non-invasive sample (allowing widespread testing), expansion to theoretical capabilities is limited by the quality, in terms of selectivity, of the antibodies employed. Additionally, since the possibility of shorter incubation times was not fully explored, leading to assay times comparable to a traditional commercial ELISA format [24], along with the requirement for sophisticated equipment, this assay carries significant costs both in terms of analysis time and labor for development.

Nonetheless, this technology has been used for various applications including the detection of sera infectious agents [25], matrix metalloproteinases [26], and small molecule drugs [27]. These uniquely optimized assays share the advantage of using a single sample for multiple analytes equivalent to the volume used for one ELISA target. Moreover, owing to reduced sample handling, the multiplexed estimates are less impacted by operator error as compared to ELISAs performed on multiple analytes requiring several trials [26]. These studies were able to achieve sensitivities of 1 μg/mL for sera infectious agents, 17 pg/mL for matrix metalloproteinases and below 1 ng/mL for small molecule drugs. However, like the studies discussed above, antibody cross-reactivity presents a practical limit to the number of analytes that may be interrogated from a single sample and may limit sensitivity.

Using a similar format, but with the added advantage of reduced analysis time, Kuriakose et al. described the use of FMIA for the development of a multiplex assay for avian influenza viruses [28]. The reactions were analyzed on a Bioplex instrument using a

minimum of 100 microspheres in each set. Mean fluorescence intensity calculations for each bead set were used to quantify influenza viruses M, H5, H7, N1 and N2 to 0.04, 0.15, 0.17, 1.56, and 1.15 ng in a 50µl sample, respectively. This represents an average detection limit of 12.3 ng/mL, where the assay can be accomplished within 70 minutes. While the detection capabilities of FMIA are not fully exploited in this effort, the study represents a subset of work where reduced analysis times hold greater importance.

A comparable emphasis on reduced analysis time is observed in the work on glycopolymer quantification by Pochechueva et al, where analysis time totaled 90 minutes [29]. Here, glycoproteins A_{tri}, B_{tri}, Le^x, and H_d were analyzed in both singleplex and multiplex formats to assess antibody cross-reactivity. The mono- and multiplex assay data correlated well, having Pearson's r values ranging from 0.95 to 0.99 for the different analytes, indicating that the six target compounds investigated could be detected independently from a single sample. The lowest concentration tested was detected at 15 µg/mL. While successful under these circumstances, where target compounds have a relatively high relevant range, the full detection capabilities of FMIA were not maximized. Application to other biological targets, where physiological concentrations may be significantly lower, could require longer incubations and negate the time advantage observed here.

In a unique twist on work related to FMIA, Ji et al. reported on the production of quantum dot (QD)-doped microparticles for use in immunoassays [30]. A flow-focusing microchannel with a double T-junction was designed to merge a sodium alginate solution into a hydrogel matrix for trapping QDs. The system affords a series of QD-encoded microparticles to be developed in one step. When tested in an immunoassay on IgG

(immunoglobulin G), FITC-labeled (fluorescein isothiocyanate) IgG could be detected to a minimum concentration of 2.2 μg/mL. Further investigations are needed to separate target and encoding signals and optimize other assay conditions to improve detection sensitivities. Once optimized, this process provides an attractive alternative to the need to purchase fluorescent microparticles commercially for small-scale operations focused on minimizing cost. However, the low cap on bead diversity, as well as the time required to produce the QDs, limit the utility of this platform for large-scale clinical use.

The assays developed using FMIA have, to this point, achieved success in measuring up to ten analytes from a single sample [25]. They require low sample volumes (typically 50 μL), which has permitted the thorough investigation of limited samples by allowing quantification of anywhere from one to ten antigens. Each of the investigations discussed have successfully adapted FMIA to suit their individualized needs. However, they are relatively expensive to perform due to the requirement for specialized analysis equipment and depend completely on antibody specificity for a reliable response. This reliance on antibody quality restricts the flexibility of FMIA in terms adaptation to new target compounds since adjustments require extensive testing to assure minimal cross-reactivity within the assay. This immunoassay format also requires long incubation times, totaling two or more hours, to achieve levels of sensitivity in the pg/mL range. The requirement for these long incubations arises from sample preparation. Samples are incubated in in the absence of convective mixing or sample flow employed by other methods to increase the speed of antibody-antigen recognition events.

Other companies have developed similar commercial products to FMIA, including the cytometric bead array (CBA) from BD Biosciences and the Amplified

Luminescent Proximity Homogeneous Assay (AlphaLISA) [31-33]. Like FMIA, CBA uses small sample volumes (50 µL) and has achieved clinically acceptable limits of detection (3 pg/mL) while operating in the same time frame as FMIA [31]. AlphaLISA has been able to quantify target compounds in a shorter time span using a competitive assay format [32,33]. While AlphaLISA has also attained sensitive detection (0.007 ng/mL) in a shorter time frame using a competitive assay format, signal production depends on an energy transfer between donor and acceptor beads in close proximity to produce a chemiluminescent signal which subsequently activates a fluorophore in the same bead. This method of signal production has resulted in studies that focus on assay development in a singleplex format. Adaptation to a multiplex format would require the ability to distinguish between signals from different acceptor beads. Additionally, because AlphaLISA operates in a competitive assay format, where increases in analyte represent decreases in observed signal, the limits of detection for this platform are not as sensitive as those operating in a noncompetitive sandwich assay design.

3.2.2 Off-chip preparation of magnetic bead-based assay

The use of magnetic particles as a solid support is an attractive alternative to fluorescent microspheres because it allows for easy manipulations and separations both on and off-chip. Off-chip incubation is often employed because it allows sample preparations to be performed in advance of the assay. The initial incubations are simple to perform and can be accomplished using common lab equipment, such as an Eppendorf tube [21], or the well of a micro-titer plate [34]. Magnetic particles may be easily detained by the introduction of a permanent magnet during wash steps, and high sensitivities have been achieved with small sample volumes. In addition to the ease of

manipulations and high sensitivity, use of magnetic particles has gained in popularity because of their compatibility with diverse detection and signal processing systems including, but not limited to, chemiluminescent [34,35], fluorescent [21,36-38], or electrochemical detection [39].

Fluorescence continues to be one of the most popular detection methods, and several protocols used in fluorescence immunoassays (FIA) were described during this time period by the Gijs group from Switzerland [36,37]. In one article, a channel was constructed having periodically enlarged cross-sections used to trap magnetic chains in a homogeneous field [36]. The results showed that off-chip incubation of capture antibody with target analyte under agitation produced uniform fluorescence throughout the channel (Figure 3.2). This approach provided a detection limit of 50 ng/mL, which is similar to classical ELISA. However, the off-chip incubation resulted in the linking of beads via capture antibody interactions creating chain irregularities on-chip. By implementing a full on-chip procedure the issue of chain irregularities was resolved [36,40]. This gave an improved detection limit of a few ng/mL and afforded a reduction in assay time from 2 hours to 25 minutes.

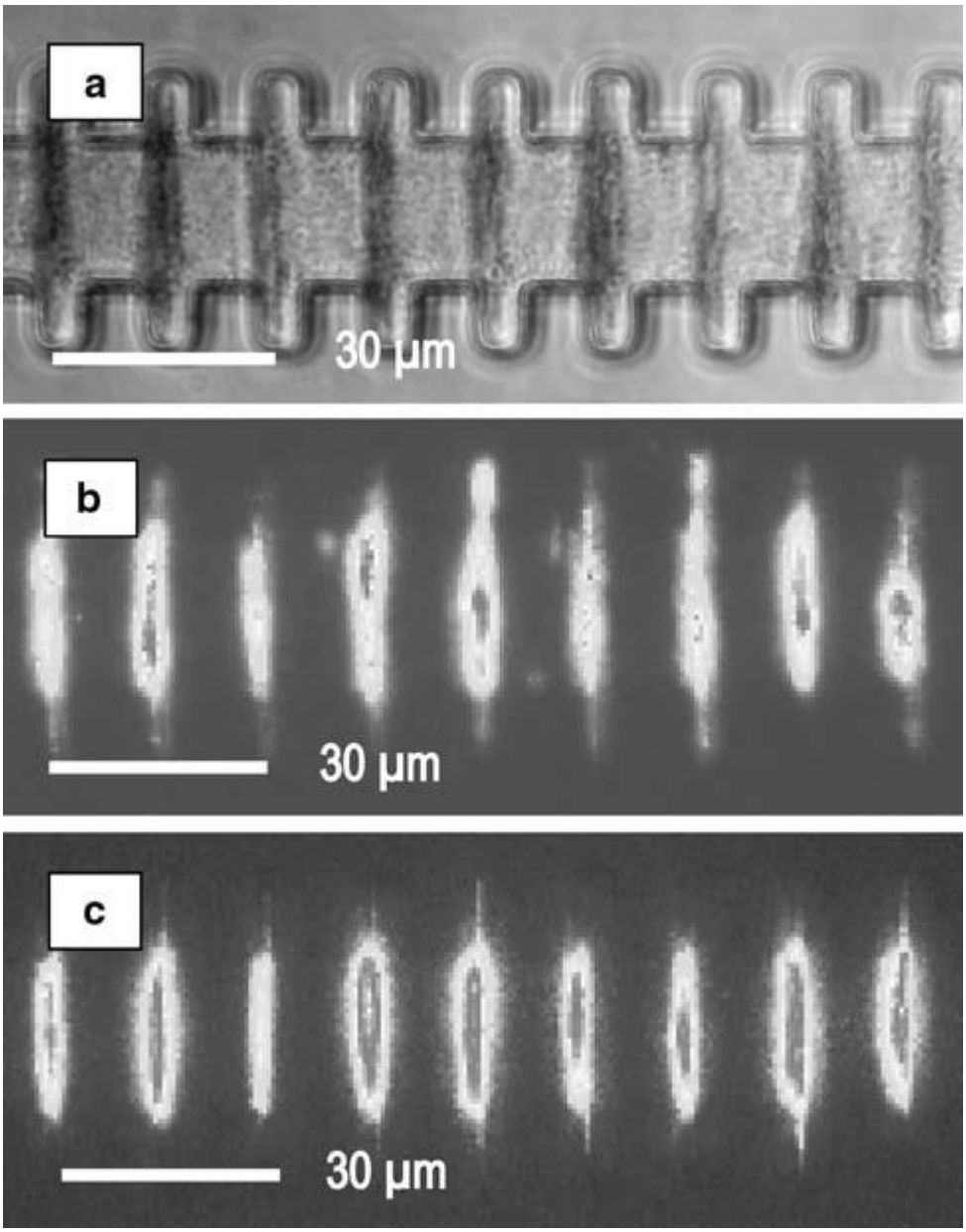

Figure 3.2. Images of the self-assembled chains formed using off-chip incubation, on-chip detection and the full on-chip immunoassay formats. (A) shows an optical image of the self-assembled chains following off-chip incubation. **(B & C)** compare the fluorescence images of the chains after the off-chip incubation and full on-chip assay, respectively.

Building from their work on FIA protocols, an integrated silicon chip was developed by Dupont et al. based on the measurement of photon-induced electrical current pulses in single photon avalanche diodes (SPADs) [37]. This allows for

fluorescence measurements of microparticles without the requirement of a microscope. Here, manipulation on-chip after off-chip incubation of sample is achieved by applying current through microcoils which positions single beads over a SPAD. Once oriented, the fluorescence signal of a single bead could be measured for the detection of monoclonal antibodies down to 1 ng/mL in only 25 minutes using a sample volume of 100 µl. While this assay achieves a comparable sensitivity in the same time frame to the fully on-chip assay described by the group, the sample volume required is much greater (100 µL as compared to 4.1 nL) [36,40]. Additionally, the speed of this assay is an improvement over the 2.5 -3 hours typically required of a commercial ELISA using an identical sample volume. However, the limit of detection is slightly higher than the 0.03 ng/mL limit typically observed commercially for monoclonal antibodies used in analyte capture [101].

A different approach to signal generation in FIA protocols is described by the Hayes group from Arizona State University [4,21]. In these articles, during data acquisition on an inverted fluorescent microscope coupled to a CCD camera, a magnetic field is introduced. By incorporating a periodicity into this field, lock-in amplification was used to selectively quantify surface-localized myoglobin, even in the presence of background noise. Using lock-in amplification, a detection limit of 1 ng/mL was afforded, which is comparable to the methods previously described [21]. By introducing a novel image processing system capable of estimating and eliminating background noise, only the pixels corresponding to the solid surface are used in concentration determinations [4]. Coupling this signal processing to the previously described immunoassay protocol improved sensitivity to a 11.5 pg/mL detection limit for myoglobin using a sample volume of 30 µl. This detection limit represents roughly 100-

fold improvement over previous results and is 2.3-fold more sensitive than the corresponding ELISA.

Off-chip incubation protocols have also been described for methods using varied detection methods. Electrochemical detection was employed both by Proczek et al. [33], and by Piao et al [41]. In the work by Proczek et al. analyte quantification was performed using GRAVI^{TM}-chips from DiagnoSwiss [39]. These chips contain eight independent microchannels, which allows parallel testing. Following off-chip incubation, IgE (immunoglobulin E) could be quantified to a detection limit of 17.5 ng/mL in less than an hour.

Piao et al. used a novel approach to develop an electrochemical immunosensor based on carbon nanotubes coated with enzyme and magnetic particles in combination with an electrically-driven reversible reaction allowing substrate recycling to amplify signal [41]. After off-chip conjugation of magnetic particles and capture antibody to the carbon nanotubes and the binding of target analyte on-chip, the sensing assembly is magnetically guided to a gold electrode. Here, the amperometric responses of the enzymatic reaction were recorded using cyclic voltammetry. Results show a detection limit of 0.19 ng/mL of hIgG after a 30 minute enzymatic reaction. While both methods were able to quantify target compounds with a similar limit of detection to FIA and do not require the use of a fluorescent microscope, sensitivity is afforded through long enzymatic reactions relative to assays boasting the completion of entire protocols within 25 minutes [36,40].

An alternative method employing batch incubation was described by Li et al [34]. Here, the development of a micro-plate magnetic chemiluminescence immunoassay

(MMCLIA) was discussed. This assay uses magnetic particles as the solid support and micro-plate wells as the reactor. The full procedure takes just under two hours to perform. With incubation times similar to conventional ELISA, a detection limit of 0.61 ng/mL for carcinoembryonic antigen was afforded using a sample volume of 35 µl. Although not offering advantages in terms of rapid analysis, and with a format that would be reliant on antibody quality to preserve sensitivity if multiplexing were to take place, this assay affords a competitive detection limit while requiring roughly 1/3 the sample used by current commercial protocols.

This group of assay methods shares the advantage of sensitive detection limits using affordable methods and, in general, low to moderate levels of complexity. They also offer the ability to limit sample use (generally between 30-50 µl is consumed) and reagent consumption. This is afforded by the ability of the magnetic particles comprising the solid support to remain free-flowing during incubations, as well as through convective mixing, which allows the entire sample to be interrogated for antigen capture affording quantifiable signal of low-concentration targets from small sample volumes. Additionally, while many have been evaluated only in a singleplex format, the alteration to these assays allowing the ability to multiplex is straightforward and should not affect assay quality. However, while many of these assays require only simple lab equipment for the initial incubation steps, the chips employed during detection (as well as the detection methods themselves) vary greatly. So, while many methods can be performed with the use of a common fluorescent microscope, there may be initial instrumentation costs depending on the assay platform selected. Furthermore, with off-chip preparation of samples, long incubation times on the order of hours are required. This limits the

capability of these assays to make serial measurements and track concentration fluctuations with time. In addition, some studies have observed issues in the manipulation or non-uniform aggregation, of beads on-chip, following off-chip pelleting protocols during wash steps [36]. Many of these issues can be eliminated through the adaptation of batch incubation procedures to those that take place fully on-chip. The advantages, and limitations, of the on-chip immunoassay format are discussed in the following section.

3.2.3 On-chip assay with sequential introduction to reagents/samples

When immunoassays take place entirely on-chip the magnetic beads employed as the solid support may be manipulated in a variety of ways. Beads can be injected onto the chip at the outset of the experiment, immobilized by permanent magnets, and introduced to reagents and sample by sequential injection [11,36,40,42,43]. They may also be injected onto the chip and manipulated through static plugs of sequential reagents [44], or forced through laminar streams of flowing reagents [8,9]. Relative to their batch-incubation counterparts, these assays are relatively simple to perform, requiring minimal pipetting steps and no transfer of the assay between containers. This minimizes the aggregation issues that have been observed in some off-chip immunoassay applications [36]. Additionally, through the flow of sample and reagents the duration of the assays is minimized. While this is sometimes accompanied by a decrease in sensitivity, some optimized procedures are able to remain competitive with those using longer incubation steps.

The manipulation of magnetic particles through streams or static plugs of sample and reagent was explored by multiple groups [8,9,44]. In the first study, performed by Sasso et al., magnets are placed on both sides of a microchannel [9]. The field is strong

enough to pull magnetic beads to the wall of the channel, but not strong enough to overcome the shear stress from fluid flow required to trap the particles. This allows incubations to occur along the channel walls, and the beads are able to traverse the channel to enter or exit reactant streams. This format allows rapid assay times and requires minimal handling of the sample or reagent. Using an epifluorescence microscopy detection platform a 625 ng/mL limit of detection was realized for biotin-FITC with incubation times of less than five minutes and a sample volume of 90 µL. Despite requiring a relatively larger sample volume compared with other magnetic particle-based assays, this study allows for rapid serial measurements. This could easily be used to track changes in analyte concentration with time, but only for target compounds with a high concentration in plasma. Alterations to the method would have to be made to afford more sensitive detection, and allow this method to be readily ported to additional applications.

A second example of the rapid analysis afforded by fully on-chip immunoassay applications was described by Peyman et al. where IgG quantification was achieved in about ten minutes consuming only 7.5 µl of reagents [8]. In this study several independent laminar flow streams are produced across a rectangular reaction chamber. The functionalized magnetic particles are deflected across these streams, passing through sample, wash, and detection reagents. Once the chip is set up there is only one required pipetting step to perform the assay, minimizing variations between runs. This, in addition to speed, represents a secondary advantage over batch incubation processes. Results show that negative controls used on chip produce little to no nonspecific binding or transfer of reagents between boundaries, evidenced by the lack of fluorescence for these samples. Using this system the detection limit for IgG was 0.1 µg/mL. This high limit of detection

could potentially be improved by increasing the sample volume, or through longer interaction times of the magnetic particles with sample.

A final example of particle manipulation through reagents and sample was developed by Chen et al. from the University of Rhode Island who describe a platform for a microfluidic inverse phase enzyme-linked immunosorbent assay (μIPELISA) [44]. In this format magnetic beads are loaded into a microchannel and transferred sequentially through plugs of sample and reagents separated by oil. This design allows the assay to be set up completely ahead of time and allows the process to be limited to one pipetting step, making operation simple. The oil plugs also prevents the mixing of reagents before, and during, the assay. The beads are allowed to incubate in each plug for 30-45 minutes and fluorescence data are collected for 180 seconds after being moved into the final buffer plug containing a fluorescein diphosphate (FDP) solution. Using this platform digoxigenin-labeled double-stranded DNA (Dig-dsDNA) was detected to a limit of 259 ng/mL. However, at higher sample concentrations the μIPELSIA was less capable of detecting analyte compared to traditional methods. This was proposed to be a product of carry-on water between plugs bringing free detection antibody into the exposure plug. Although slightly more sensitive than similar on-chip methods, this assay loses the advantage of rapid analysis and does not compare to the sensitivities achieved with similar incubation times off-chip. Additionally, adaptation of the current assay to a multiplex format would involve use of all four parallel channels available in the current chip design. This would allow analytes to be quantified simultaneously but would quadruple the consumption of sample and reagents compared to the current system.

The other predominant assay structure for on-chip protocols involves maintaining magnetic beads in a single position by employing a homogeneous magnetic field and sequentially introducing reactants by flow, which has been explored extensively [2,11,40,43]. Keeping particles trapped in a magnetic field prevents undesirable aggregation and reduces the loss associated with particle transfers using batch incubation. Also, sample and reagent exposure times can be varied simply by altering flow rates to optimize signal under minimally required assay durations. This minimizes assay times while affording limits of detection competitive with assay formats requiring long incubations. This approach was used by Do et al. from the University of Cincinnati to design a new lab-on-a-chip facilitating an enzyme-labeled electrochemical immunoassay (ECIA) [11]. The chip uses a magnetic microarray as a bead separator and an interdigitated array (IDA) microelectrode as a biosensor. Results show IgG could be detected to 16.4 ng/mL in 35 minutes using 5 µl of reagent.

In another study magnetic nanoparticles were used as labels on microbeads to detect bound analyte by isomagnetophoretic focusing [2]. An external magnetic field causes particle movement to a denser or sparser field until its magnetic susceptibility is equal to the surrounding gradient. This is important because it allows small changes in concentration to be detected by utilizing a low concentration of gadolinium paramagnetic diethylenetriamine pentacetic acid (Gd-DTPA), used to create the magnetic susceptibility gradient. This low concentration allows a narrow dynamic range with high resolution. However, by employing a higher concentration of Gd-DTPA solution, a wider concentration range may be interrogated, making the assay flexible for diverse target compounds. Using this set-up rabbit IgG-biotin could be detected to a limit of 3.2 fg/mL.

The use of fluorescent microbeads allowed for a multiplexed assay with the detection of three analytes while maintaining pg/mL sensitivity and requiring 200 µL of sample. This represents improved sensitivity compared to commercially available ELISA, but required double the sample volume and similar assay duration. With the flexibility of tailoring the Gd-DTPA gradient, and using long incubations during sample preparation and specialized equipment to prepare and analyze samples, a low limit of detection was achieved for this assay.

Many of the fully on-chip immunoassays afford users rapid results and consume low volumes of sample [8,9,11]. Rapid analysis is allowed by manipulating the solid phase through reagents or by holding the solid surface in place while flow is used to direct sample to the assay surface, decreasing the depletion zone observed with diffusion-mediated incubations. Large depletion zones, which reach a sensor-size dependent steady state during incubations dependent upon diffusion, can be combated by convective mixing or flow which accelerate mass transport and actively decrease the thickness of the depletion zone near a sensor surface [45]. This allows the assay time to be dependent upon the speed of the reaction itself as opposed to mass transport limitations. However, this rapid analysis is frequently accompanied by higher limits of detection. While non-specific binding is not a large problem because the particles are in contact with sample and reagent for short time periods, the entire population of antigen may not be trapped causing an increase in limits of detection. In other cases long incubation times have allowed for sample analysis with high sensitivity, and the interrogation of multiple analytes [2]. Where optimal incubation times are employed these assays require less sample manipulation than their corresponding off-chip counterparts and have shown

equal, or greater, sensitivities. Similar to their off-chip counterparts many of these assays may be accomplished using a fluorescent microscope as the detection element. Nonetheless, due to the diversity of assay platforms, many formats require specialized equipment to perform. This, along with the need to fabricate chips on a large scale, could increase the initial cost and time investment in adaptations of the techniques to a large scale. The full on-chip assay structure holds promise both in terms of assay sensitivity and rapid analysis. However, in order to produce a truly optimized assay these considerations must be balanced to afford a test capable of interrogating any biological sample of interest, regardless of the targets' physiological concentration.

3.2.4 Other Techniques

Several studies have employed micro- or nanoparticles in creative ways that do not fit into one of the above categories. These include rapid analyses where particles are spiked directly into a sample for target quantification [3], protein-functionalized microparticles capable of electrostatic self-assembly [46,47], and fluorescent microbeads that employ simple detection methods [48]. These varied techniques hold individual advantages specific to their applications. Some have been tailored for the rapid analysis of target compounds, while others have been simplified to allow ease of use. The preeminent disadvantage associated with the assays described below is their vast differences from other microbead assays, requiring large adaptations in the average laboratory for widespread implementation.

In the study by Ranzoni et al., a new technology based on magnetic nanoparticles in a pulsed magnetic field was investigated [3]. This method uses a small spike of nanoparticle probing reagent, pre-coated with monoclonal antibodies, which is directly

injected into a sample. The particles are free to move within the sample to capture antigen without the presence of a magnetic field. By introducing a pulsed magnetic field the particles are concentrated and allowed to form clusters mediated by biomarker-induced inter-particle binding. These clusters are then detected by applying magnetic rotation frequencies and using optical scattering to determine cluster size, which correlates with antigen concentration.

Using this technique, after only one reagent addition step, an assay can be performed in a total time of 14 minutes. Using this scheme prostate specific antigen (PSA) was detected to a limit of 13.6 – 17 pg/mL in plasma. This format allows for the sensitive and rapid quantification of a single analyte, in a format greatly simplified compared to ELISA testing. The analysis of multiple compounds would depend on the specificity of antibodies, comparable to FMIA. It would also require detection to be altered so that clusters possessing different targets may be identified without the addition of sophisticated analysis equipment.

Another study based on the manipulations of magnetic microparticles was described by Afshar et al. in the development of a microfluidic magnetic actuation system that allows the 3D focusing of magnetic beads for agglutination assays [49]. The system was designed with a magnetic microtip, used as a field concentrator, to focus magnetic beads in a microchannel. A single lateral sheath flow positions and aligns individual beads in the center of the flow. This allows a small number of beads to be counted in an observation window by automated image reading. Having the individual beads 3-dimensionally focused in the flow center allows reliable counting of single beads versus agglutinated bead doublets which allows biotinylated bovine serum albumin (bBSA)

concentrations to be determined. It was demonstrated that bBSA could be detected to 400 pg/mL (6 pM) with the fully on-chip assay in about 20 minutes with the consumption of 2 µl sample. This format, while rapid, would be difficult to multiplex due to the quantification of signal arising from the counting of aggregate numbers.

As an alternative to the use of magnetic beads, the Gijs group contributed several immunoassay articles investigating electrostatically self-assembled micropatterns performed on-chip [46,47]. Electrostatic forces were used to mediate bead self-assembly in a channel formed by reversibly sealing PDMS onto an (aminopropyl)triethoxysilane (APTES) patterned glass substrate. As opposed to external magnets which create dense bead plugs on-chip, the fabrication of positively-charged APTES-patterns results in low fields where beads align. This allows the formation of self-assembled chains that are stable during both flow-based and static incubation steps. Performing the immunoassay in stop-flow mode, where the channel is sequentially filled and incubated with sample and reagents afforded IgG was quantification to a lower limit of 15 ng/mL in 30 minutes using 560 nL of sample.

A second contribution investigated the effect of continuous-flow versus stop-flow conditions for the assay [46]. The results show that mouse Antigen (m-Ag) could be detected under continuous flow to a limit of 250 pg/mL, representing roughly a 60-fold improvement over stop-flow limits and requiring only 10 minutes to perform. This procedure was performed using 1.3 µl. The advantage of reduced analysis time is afforded using continuous flow because diffusion associated depletion of analyte around the bead chains does not occur as observed under stop-flow conditions. This allows more analyte to be successfully captured onto beads in a short time span, analogous to analyte

capture in affinity chromatography utilized during protein purification. Additionally, high specificity antibodies allowed for two-analyte detection on a single chip. In both cases the rapid analysis and small sample size provide advantages as compared to ELISA without sacrificing the limit of detection. By decreasing the flow rate, thereby increasing analysis time, the second assay could potentially reach a more sensitive limit of detection. This would maintain its advantage of small sample requirements and rapid analysis while increasing its ability to compete with more sensitive analysis techniques.

Several studies employed simple polystyrene spheres in unique ways to produce fluorescent signals. In the study by Fu et al., a bead-trapping/releasing flow cell for a fluidic assay was developed [50]. This device integrated a pillar-array and pneumatic valve to provide flow injection/sequential injection analysis. Using the valve, beads could be manipulated in the device to perform the immunoassay in ten minutes with a detection limit of 0.80 ng/mL for 3,4,6-trichloropyridinol (TCP) using a competitive assay format and 15 µl of sample. This assay could later be altered to perform a noncompetitive assay, which would improve the sensitivity but increase the time required for analysis. Even with these alterations, the current detection method does not lend itself easily to multiplexing and would have to be altered to distinguish between signals arising from different compounds in order to quantify multiple antigens in parallel.

A second example of polystyrene microsphere use is the cross-talk-free duplex FIA for the simultaneous detection of carcinoembryonic antigen (CEA) and neuron specific enolase (NSE) described by Cao et al [14]. A sandwich immunoassay was developed using multiple quantum dots as detection elements, which yield a tunable, symmetrical, and narrow emission band. Each color QD conjugate was capped by a

capture antibody, and polystyrene microspheres (PSM) brought antibodies proximal to the QD surface in a diffusion-driven incubation, allowing both antigens to be specifically identified simultaneously to a limit of 0.625 ng/mL, which is comparable to many methods using long incubation durations. The assay requires incubation times analogous to ELISA, but could be further multiplexed depending on the specificity of antibodies employed.

Finally, employing intrinsically fluorescent beads in a unique way, a fluoro-microbead guiding chip (FMGC)-based sandwich immunoassay for the quantification of biomarkers was investigated by Song et al [48]. The FMGC consists of four immunoassay regions, each containing five gold functional surfaces to support five identical tests performed simultaneously with the quantification of four separate analytes in parallel. The gold surfaces were conjugated to capture antibodies to create a sensing surface, where capture of both antigen and detection antibody was diffusion-driven. Using fluoro-microbeads conjugated to antibody and a fluorescent microscope, a sandwich immunoassay was performed and antigen concentrations determined directly by counting microbeads immobilized on the immunosensing regions. In an assay time of less than one hour cardiac troponin I (cTnI) could be quantified in a range from 0.1-100 ng/mL. With the addition of agitation or convective mixing to increase sample capture and improve sensitivity, its time advantage over ELISA may be maintained.

As illustrated in the sections above, the immunoassay applications achieved using both magnetic and non-magnetic particles as a solid support are diverse. These assays have been tailored to meet the needs particular to their use, which may be increased assay speed, sensitivity, or simplicity of operation. In general, assays that achieved rapid

analysis suffered from limitations in sensitivity. However, assays have not been produced which optimize the relationship between assay speed and ability to detect biomolecules with diverse physiological concentrations. Work done to improve this relationship may be the most promising avenue toward reaching a truly optimized micro-immunoassay, owing to the other advantages inherent to microparticle solid supports such as ease of manipulation, small sample size, and the straightforward coupling to advanced signal processing methods.

3.3 Signal generation by flow conditions

A second major area of interest in micro-immunoassay applications involves those based around the use of flow conditions to produce a quantifiable signal. In this section assays employing microcolumns [51,52] and immobilization on channel walls [53], where target quantification is achieved by the release and flow of a signal-generating agent to a detector, will be discussed. This format has the advantage of allowing rapid quantification times with small sample requirements. Additionally, it is easily adapted to quantify different analytes. However, these assays are limited to a singleplex format and each antigen would require a unique column.

The Hage group from the University of Nebraska has contributed significantly to this area since 2008 [51,52]. One recent study introduced a reverse displacement immunoassay (RDIA) that generates signal by the analyte displacement of a label from a small immobilized analog column [52]. When a complex is formed between analyte and label, a displacement peak is created and the signal is measured allowing analyte quantification (Figure 3.3). Results show the lower limit of detection for RDIA to be around 67µg/mL (27-29 pmol) and the upper limit 400 µg/mL (160-200 pmol) for a 20 µl

sample of mouse IgG F_{ab1}. The total assay analysis time is less than ten minutes, with signal generation occurring within 20-30 seconds after sample application to the column. This rapid analysis, which offers a pronounced time advantage over ELISA, is afforded because no pre-incubation of the sample with label is required. While this assay is limited to a singleplex format, it can be applied to any analyte where an appropriate label and immobilized analog are available or can be generated. Although sensitivity of the assay may be improved by using a larger sample volume, this format is not competitive with those employing incubation steps between sample and detecting agent.

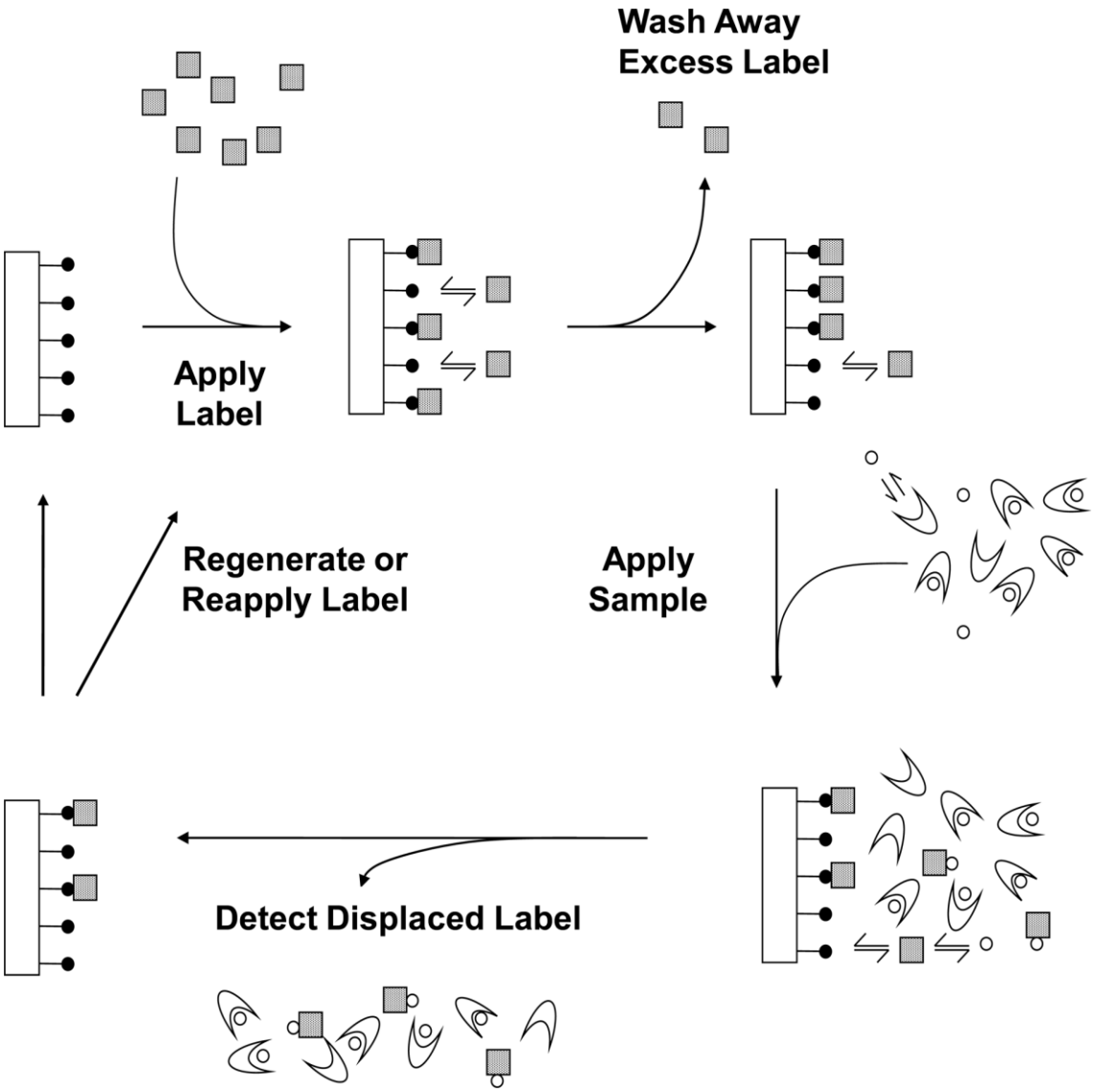

Figure 3.3. Scheme for a reverse displacement Immunoassay. Reprinted with permission from [22] © American Chemical Society (2011).

A second contribution made by this group analyzed the binding and elution of target compounds from IAC/HPIAC (immunoaffinity chromatography/high performance immunoaffinity chromatography) columns in order to understand both association and dissociation efficiencies [51]. Using this format a variety of detection schemes can be used to obtain kinetic and binding information, including fluorescence, mass

spectrometry, and absorbance. The insight gained from this study can be valuable in the design of future solid-phase immunoassays.

A more sensitive flow based assay was described by Liu et al. who published on the development of a poly(methylmethacrylate) (PMMA) microfluidic chip coupled to electrochemical detection for the quantification of α-fetoprotein (AFP) [53]. AFP antibody is immobilized on the poly(ethyleneimine) (PEI)-derived PMMA surface. After antigen and horse radish peroxidase (HRP)-conjugated AFP antibody bind sequentially in the channel, a three-electrode electrical system at the microchip outlet records the reduction in the H_2O_2 current response. Results show a linear response between 1-500 pg/mL with a 1 pg/mL detection limit requiring minimal use of sample in a time of 40 minutes. Although it requires minimal sample and achieves sensitive quantification in under an hour, the assay is not easily adaptable to the analysis of multiple analytes in parallel.

Theoretical work to assist in predictions of device performance was conducted by Sinha et al [54]. A comprehensive model was created to characterize interactions during a flow-through immunoassay. Findings may help provide a rational basis for determining operating conditions in microfluidic IMS devices.

These immunoassays share the ability to achieve the rapid quantification of analytes using minimal sample volumes. This rapid analysis is made possible by the ability to perform the assay without sample pre-incubation steps. The sensitivity of these rapid tests is comparable to many immunoassays employing much longer incubation times [14,41,44], and are easily adaptable to quantify any target compound. However,

since detection is dependent on the measurement of a displacement peak composed of label and antigen, multiplexing this assay format would be challenging.

3.4 Use of a static solid support to trap antigen and generate signal

The use of a solid support provides certain advantages, including the straightforward ability to multiplex and sensitive limits of detection. In this area of research many variations on this traditional "static well" format have evolved. This section discusses techniques that employ antibodies patterned on PDMS [6,7] or in capillary systems [15], as well as antibody microarrays [55], and novel techniques that employ static detection like the surround optical fiber immunoassay (SOFIA) [5] or oligonucleotide-linked immunosorbent assay (OLISA) [56]. These assays offer the advantage of easy and direct multiplexing, often accomplished by the patterning of capture antibodies on a static surface. Many of the assays also offer sensitive limits of detection, owing to long incubation times. The long incubations allow time for sample to interact with antibodies by diffusion, but put a limitation on the potential throughput or ability to track changes in protein levels over time using serial measurements.

Since 2008 many groups have developed new technologies centered around the traditional static solid-phase immunoassay. The Delamarche group from Switzerland has made multiple contributions in this area [6,15]. In one study, the patterning of capture antibodies (cAbs) on PDMS in order to be compatible with capillary systems (CSs) was described [6]. Once cAbs are patterned, the PDMS block is placed on CSs with cAbs oriented perpendicularly to the reaction chambers which produces well-defined areas for analyte capture from solution. These small patterned areas allow one-step fluorescent imaging of all analytes, and the fast reaction is permitted by confining sample to a minute

space as it flows over capture zones. The capillaries allow multiple analytes to be detected from small samples (1 μL or less). This produces a "micro-mosaic assay" with the potential for 96 test sites if used with a chip having six independent reaction chambers. Results show that CRP could be detected to a sensitivity of 0.9 ng/mL in 11 minutes using only 1 μl of sample. While already comparable in sensitivity to ELISA with a much smaller sample and shorter assay duration, the sensitivity of these assays may be further improved by coupling the detection to signal-amplification methods.

In a second contribution the group described a one-step immunoassay using capillary systems [15]. The assay is based on the preloading of freeze-dried detection antibodies (dAbs) into the analyte flow path. After antibody reconstitution and analyte addition, fluorescence detection can be performed downstream on patterned capture antibodies. Results show that within ten minutes analyte concentrations with a lower limit of 3μg/mL could be detected. After 25 minutes of total assay time a decrease in the background noise-(resulting from the decay of unbound dAbs)- allowed concentrations down to 1 μg/mL to be observed. This single-step assay reduces handling overhead for the end-user. Although this assay possesses a higher limit of detection and an equal or longer assay time than the previous work, this study suggests that the positive aspects of CSs previously exploited could potentially be achieved in a one-step immunoassay.

The fluorescent one-step immunoassay platform was further studied by Ruckstuhl et al [57]. In this contribution a system of polymer test tubes with fluorescence collection optics was utilized along with a compact fluorescence reader. The detection technology, based on supercritical angle fluorescence (SAF), allows for the real-time monitoring of surface reactions. Because the intensity of the signal decays exponentially with the

distance from the boundary, surface-selective detection is achieved providing a sensitive readout for immunoassays. In an assay time of only 13 mintues, IL-2 could be quantified with a linear response down to 4.5 pg/mL using a sample volume of 40 µl. This represents advantages compared to the traditional ELISA format, which requires four hours and 100 µL to give a limit of detection of 4 pg/mL, but presents an analogous limitation in terms of multiplexing. The assay, currently taking place in disposable test tubes, may be adapted to a well-plate format but will remain limited to the analysis of one compound per sample.

Other static solid-phase assays produced based on the traditional format continue to employ 96 well micro-titer plates as incubation chambers. Chang et al. reported on the development of SOFIA, which uses 96 well plates for incubations, consuming volumes analogous to commercial ELISA methods [5]. Analysis takes place in a singleplex format using specially designed equipment. Samples are placed in a 100 µl microcapillary and excited in a detection unit by focusing temporally modulated light along the capillary's axis. After light is focused into a single optical fiber and coupled to a low noise photo-voltaic diode, detection takes place using phase sensitive detection employing a lock-in amplifier. The sensitivity was tested using Rhodamine Red and results show a 0.1 attogram limit of detection. Prion proteins from varying species were also investigated and found to have a limit of detection >10 attograms from a sample volume of 100 µl and requiring long incubation times. While this assay offers superior sensitivity and the ability to multiplex, long incubation times and highly specialized equipment increase assay costs and limit sample throughput.

Work done by Han et al. also made use of a 96 well plate to develop a creative variation on traditional ELSIA termed OLISA [56]. It is designed based on a detection antibody tethered to DNA through the incorporation of RNase H mediated signal amplification. Using a fluorescence platform, the limit of detection for OLISA was around 1 ng/mL using 100 µl of sample. This is comparable to the analogous ELISA, although slightly less sensitive. Detection antibodies employing different fluorophore/quencher pairs are employed that have independent spectral ranges for excitation and emission. This allows up to ten analytes to be interrogated in a single sample without signals arising from separate analytes interfering in the quantification of each compound. While this allows multiple analytes to be interrogated from a single sample, sensitivities are not improved relative to ELISA and incubation times, along with sample volumes, remain the same. Adaptations to the 96-well plate to allow nano-scale read volumes were achieved by the use of Siloam technology [58]. Incorporation of a spiral microchannel into each well of a microplate allows samples to be reduced to 5-10 µL and the washing to be reduced while mirroring the standard ELISA steps. The sensitivity of this commercial format is in line with that for OLISA and ELISA (around 1 pg/mL), but is accomplished in a time frame of 90 minutes and can accommodate multiple repeat samples to the same well to increase detection.

The static solid-support format has also been used to develop a fully automated ELISA on a portable disc-based format in work done by Lee et al [59]. In this unique alternative to typical disc systems, fluid transfer occurs through ferrowax microvalves created using low intensity laser light to melt paraffin wax embedded in iron oxide nanoparticles. The paraffin valves allow the full integration of the immunoassay on-disc

starting with a sample of whole blood. The assay is not limited in its number of steps as typically is seen with lab-on-a-disc systems where increasing spin speed is employed for sample transfers. With each disc having three identical units, multiple assays may be performed simultaneously in 30 minutes. The assay speed is afforded by disc rotation while sample is in the mixing chambers with reagents. This allows the assay to overcome time hurdles associated with diffusion-dependent incubations. Using 150 µl of whole blood, results show detection limits for anti-hepatitis B (anti-HBs) and hepatitis B antigen (HBsAg) of 8.6 mIU/ml and 0.51 ng/mL, respectively. This represents limits of detection comparable with ELISA using half the sample size and an assay time with one-fourth the duration. While this device is portable and disposable, assays are limited to the detection of three compounds simultaneously. This, coupled with the need to produce new devices for each assay may result in high costs associated with fabrication. This assay shares similar qualities to the commercially available Gyrolab, which is a completely integrated immunoassay system [60]. Here, 10 µL samples are loaded onto a special compact disk which, through centrifugal force, is pushed into nano-scale channels containing streptavidin-coated bead columns used to trap the immunocomplex. While quantification may take place in one hour, this format is limited to serial measurements and has high costs associated with specialized instrumentation and a single source of reagents.

As an alternative to expensive and complicated fabrication processes associated with many static immunoassays, a low-cost micro-chip based fluorescent immunoassay was presented by Shao et al. for IgG detection [10]. The chip design is composed of four *X*-direction channels and one *Y*-direction channel to form four designated reaction zones (DRZ, Figure 3.4). Areas between the zones were used as negative controls, where no

obvious fluorescence was observed. Results show a limit of detection for IgG to be 5 ng/mL from a 10 µl sample, but this method requires long incubation times. These incubation times (1 hour per step) were required because no agitation or mixing accompanied reaction steps, which were accomplished by diffusion after the initial channel filling. With times comparable to ELISA, this assay requires only one-tenth the sample volume to achieve analogous limits of detection. The same design could be used for the monitoring of multiple analytes with the possible integration of more DRZs without additional technical complexity.

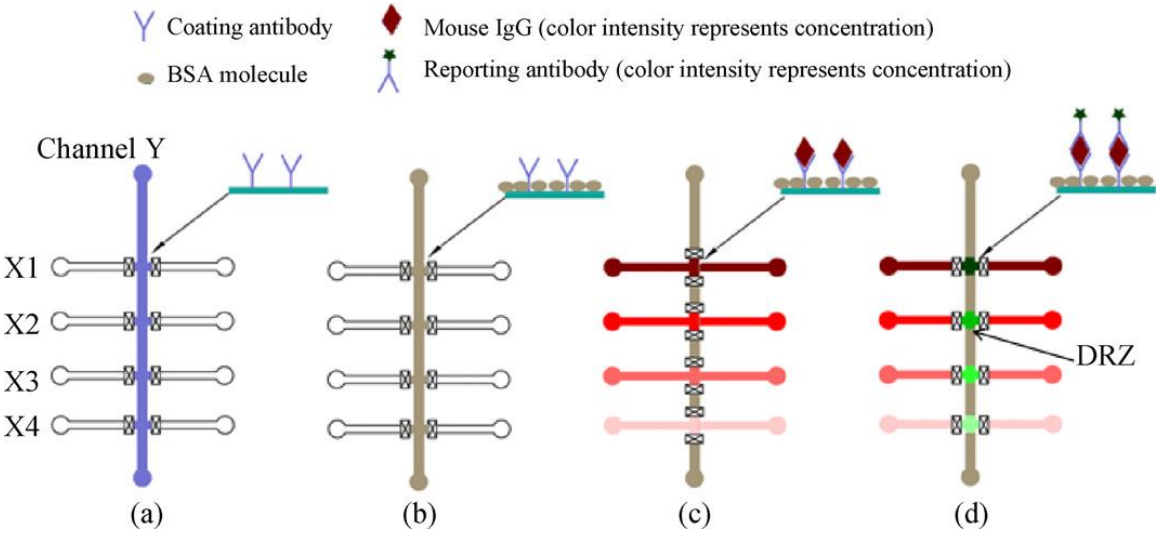

Figure 3.4. On-chip immunoassay protocol. Initially flowing coating antibody and blocking reagent through channel Y prepares the DRZs for the addition of analyte through the independent X channels. A reporting antibody can be delivered to each DRZ by addition through the Y channel, producing four independent DRZs, having negative controls present in the Y channel between reaction zones. The DRZs are prepared by (A) exposing channel Y to a coating antibody and (B) BSA as a blocking agent. (C) After sample addition through each X channel, (D) a reporting antibody can be delivered to each DRZ by addition through the Y channel. This produces four independent DRZs with negative controls present in the Y channel between reaction zones. DRZ: Designated reaction zones.

Although detection took place on a static printed array, Lian et al. describe the use fluorescent nanoparticles (NP) to produce a NP-labeled microarray [55]. In order to

perform a multiplexed assay on the same slide, multiple blocks of capture antibodies were printed as subarrays. After incubation and wash steps occurring at room temperature as well as at 4°C for long time spans (two hours to overnight), select bioterrorism agents could be detected down to 10 pg/mL using 100 µl of sample over the entire array. The detection limits here represent roughly 100-fold improvements over fluorescent ELISA protocols used previously and require minimal sample use. However, equal or longer incubations are necessary which would limit assay throughput and the ability to make serial analyses.

While most static solid-support assays require long incubation times to complete, Li et al. reported on a pre-functionalized PDMS microfluidic chip in an effort to produce an ultrafast heterogeneous immunoassay [7]. Using an antigen-antibody reaction time of 5 minutes, the study found that blocking time had very little effect on the signal-to-noise ratio observed. This implies that nonspecific adsorption is reduced by short immunoreaction times. Results show a limit of detection for IgG of 600 ng/mL in an overall assay time of 19 minutes, while requiring only 10 nl of sample. This assay also offered the ability to quantify 5 analytes in parallel on a single chip. This assay boasts the advantage of completing analysis six times faster than ELISA using one-tenth the sample volume. Since incubation steps are currently defined by diffusion, detection limits may be improved by the introduction of agitation during sample reactions. With the ability to more sensitively quantify many compounds in parallel using small sample volumes and short assay durations, this assay would be competitive with the most optimized formats currently employing mobile solid phases.

With an emphasis on assay sensitivity as opposed to rapid quantification, Lee et al. presented a sensitive total internal reflection fluorescence microscopy (TIRFM) system for the detection of TNF-α on a nanoarray protein chip [17]. Using a homemade experimental system, TNF-α was successfully observed at a concentration of 0.13 fg/mL using a 50 µl sample. The total assay time took two hours to complete, following the preparation of capture protein probe and sample. The assay affords a comparable assay duration to ELISA, but employs half the sample. Although it offers a highly sensitive assay that could be reasonably adapted to quantify multiple analytes, the assay requires sophisticated and specialized equipment.

While most static support immunoassay systems employ fluorescence detection, the Ju group investigated chemiluminescent immunoassay platforms for the near-simultaneous detection of two analytes, CEA and AFP [61,62]. In the first study a modified glass tube with immobilized anti-CEA antibody was incubated with a mixture of the two antigens, their HRP-conjugated detection antibodies, and anti-AFP immobilized on paramagnetic particles [61]. After immunocomplexes were formed, AFP could be separated into an unmodified glass tube. Following separation, near-simultaneous detection with the aid of an optical shutter could be performed. Results show detection limits for CEA and AFP of 0.6 and 0.89 ng/mL from 10 µL of sample, with negligible cross-reactivity, respectively. A later study, based on a system of series-wound immunosensing channels (SWIC), was performed on the same target antigens [62]. With a procedure similar to the one reported previously, the immunoassay could be completed in 27 minutes using 15 µl of sample. Here, the limits of detection for CEA and AFP were reduced to 0.39 and 0.41 ng/mL, respectively. Both assays afford the

advantage of reduced assay duration and sample volume while maintaining comparable limits of detection to reference methods.

Many of the assays discussed in this section require relatively long incubation times and moderate sample volumes. These requirements are similar to those for micro-cantilevers, which offer novel detection modes using elegant physics [63,64]. While simple to operate and capable of attaining clinically relevant sensitivities (0.1 ng/mL), these methods require long incubations and large sample volumes (100 -200 µL). Additionally, due to the detection platform they appear restricted in their ability to adapt to a multiplexed format, limiting their practical utility in diagnostic immunoassay applications.

While many of the methods discussed here have long incubation requirements, in cases where incubation times may be reduced through agitation or mixing this format remains competitive with the on-chip assays utilizing magnetic solid supports. They offer the advantage of straightforward multiplexing and sensitive sample quantification, mostly without introducing complicated reaction processes or detection systems. While currently competitive with mobile solid-support formats these assays rely heavily on detection through static fluorescence measurements. This limits their ability to be coupled with advanced signal processing mechanisms and may restrict their capacity to quantify target compounds at the low end of the physiological range.

3.5 Concluding Remarks

Looking at the literature over this time span, a large number of publications focused on the use of a mobile solid phase, especially those utilizing magnetic micro- or nanoparticles. This emphasis evolved from the ease of manipulation through the

introduction of magnetic forces that allowed for simple wash steps to be performed during the assay. In designs executed entirely on-chip, it also allowed flow conditions to be used for sample and reagent introduction, which drastically cuts overall assay time requirements. While this group of assays have primarily been evaluated in a single-analyte format, alterations allowing analysis of multiple compounds in parallel are straightforward and would not detract from sensitivity. In terms of attaining a fully optimized assay, fully on-chip immunoassays employing magnetic solid supports reduced sample size and time requirements while using simple detection methods and maintaining ease of use. The sensitivity achieved by methods with long incubation times could potentially be reached using convective mixing or slow flow rates to minimize the depletion-layer surrounding the solid surface, all while maintaining rapid analysis. To tailor assays for clinical use techniques must balance incubation durations and limits of detection. In addition, compatibility with the signal processing methods demonstrated to improve detection limits to reach superior sensitivity is ideal to and achieve a fully optimized micro-immunoassay [4,5,21].

Another broad area of research is that using fluorescent microbeads as a solid support, predominantly in the area of FMIA, which has been used successfully to detect up to ten analytes simultaneously with clinically acceptable levels of sensitivity. This approach is obviously useful, as it provides information about multiple analytes in the same sample volume as one traditional assay and could theoretically be used to detect up to 100 compounds in a single run. However, its ultimate limitation is the specificity of antibodies used, and the cross-reactivity this produces between different targets. This could put a practical limitation on the number of compounds quantified simultaneously.

Adaptions to testing for different analytes, while entirely possible, will require intensive assay development to ensure that singleplex assays for each compound give equivalent results to the multiplex assay used diagnostically. Additionally, due to the diffusion-mediated incubations, long assay durations are required to achieve acceptable limits of detection and this format is not readily capable of coupling to sophisticated signal processing methods. Nonetheless, in terms of practical immunoassay requirements these tests can achieve the required level of multiplex capabilities and offer reasonable limits of detection (ng/mL to pg/mL) for most analytes.

Finally, the micro-mosaic assays offer the advantage of easy multiplexing and simple fabrication. They also produce low limits of detection, although they require moderate sample volumes and long incubation times resulting from the diffusion-mediated sample adsorption required using this format. Similarly, the flow-through assays allow simple sample analysis. These assays also produce rapid results using moderate sample volumes. However, unlike the micro-mosaic assays they do not lend themselves easily to multiplexing.

3.6 Future Perspectives

While many of the assay formats described here were successful in improving upon one or more of the areas required for developing an optimized clinical test, none have been able to fully reach that mark. Today, the same issues challenging immunoassays development remain. These issues consist of finding the appropriate balance between rapid analysis and sensitivity using techniques capable of coupling to signal processing methods, which may enhance detection limits. New techniques, in addition to consuming limited quantities of sample, should be currently capable of, or

easily adaptable to, multiplexing without the requirement for highly specialized detection equipment. While various techniques have their specific advantages, a combination of aspects from multiple approaches appears to hold the greatest promise if a truly optimized assay is to be found.

With an increased understanding of reaction principles and conditions leading to superior sensitivity, immunoassay techniques continue to improve and progress toward optimization. Additionally, the now more familiar process of microfabrication enables the realistic implementation of many on-chip methods through large scale photolithographic or injection mold production. In this arena techniques will benefit from simple chip designs to ensure technical reproducibility. More development on this front over the next few years is poised to provide immunoassays well-tailored to their specific needs, which may be rapid analysis of samples taken on-site, or the ability to detect minute fluctuations in biomarkers over time indicative of disease states.

3.7 References

[1] Engvall E, Jonsson K, Perlmann P., *Biochimica et Biophysica Acta.* 1971, *251*, 427-434 .

[2] Hahn YK, Park JK., *Lab Chip.* 2011, *11*, 2045-2048.

[3] Ranzoni A, Sabatte G, van Ijzendoorn LJ, Prins MWJ., *ACSnano*. 2012, *6*, 3134-3141.

[4] Mahanti P, Taylor T, Hayes MA, Cochran D, Petkus MM., *Analyst*. 2011, *136*, 365-373.

[5] Chang B, Gray P, Piltch M, *et al*., *J. Viro. Met.* 2009, *159*, 15-22.

[6] Ziegler J, Zimmermann M, Hunziker P, Delamarche E., *Anal. Chem.* 2008, *80*, 1763-1769.

[7] Li P, Abolmaaty A, D'Amore C, Demming S, Anagnostopoulos C, Faghri M., *Microfluid Nanofluid*. 2009, *7*, 593-598.

[8] Peyman SA, Iles A, Pamme N., *Lab Chip*. 2009, *9*, 3110-3117.

[9] Sasso LA, Under A, Zahn JD., *Microfluid Nanofluid*. 2010, *9*, 253-265.

[10] Shao G, Wang J, Li Z, Saraf L, Wang W, Lin Y, *Sensors and Actuators B.* 2011, *159*, 44-50.

[11] Do J, Ahn CH. , *Lab Chip.* 2008, *8*, 542-549.

[12] Langenhorst RJ, Lawson S, Kittawornrat A, *et al., Clin. Vacc. Immunol.* 2011, *19*, 180-189.

[13] Lawson S, Lunney J, Zuckermann F, *et al., Vaccine.* 2010, *28*, 5356-5364.

[14] Cao Z, Li H, Lau C, Zhang Y. , *Analytica Chimica Acta*. 2011, *698*, 44-50.

[15] Zimmermann M, Hunziker P, Delamarche E., *Biomed. Microdevices.*2009, *11*, 1-8.

[16] Pesce AJ, Michael JG., *J. Immunol. Met.* 1992, *150*, 111-119.

[17] Lee S, Cho NP, Kim JD, Jung H, Kang SH, *Analyst*. 2009, *134*, 933-938.

[18] Vignali DAA.,. *J.Immunol. Met.* 2000, *243*, 243-255.

[19] Allinson JL., *Bioanalysis.* 2011, *3*, 2803-2816.

[20] Verch T, Bakhtiar R., *Bioanalysis.* 2012, *4*, 177-188.

[21] Hayes MA, Petkus MM, Garcia AA, Taylor T, Mahanti P., *Analyst.* 2009, *134*, 533-541.

[22] Watson DS, Reddy SM, Brahmakshatriya V, Lupiani B., *J. Immunol. Met.* 2009, 340, 123-131.

[23] Kellar KL, Douglass JP., *J. Immunol. Met.* 2003, *279*, 277-285.

[24] Clavijo A, Hole K, Li M, Collignon B., *Vaccine.* 2006, *24*, 1693-1704.

[25] Ravindran R, Khan IH, Krishnan VV, *et al., J. Immunol. Met.* 2010, *363*, 51-59.

[26] Svateck RS, Shah JB, Xing J, *et al., Cancer.* 2010, *116*, 4513-4519.

[27] Smith J, Samons D, Robertson S, Biagini R, Snawder J., *Toxic. Mech. Meth.* 2010, *20*, 587-593.

[28] Kuriakose T, Hilt DA, Jackwood MW. , *Avian Diseases*. 2012, *56*, 90-96.

[29] Pochechueva T, Chinarev A, Spengler M, *et al., Analyst*. 2011, *136*, 560-569.

[30] Ji XH, Cheng W, Guo F, *et al., Lab Chip.* 2011, *11*, 2561-2568.

[31] Talat N, Shahid F, Perry S, *et al., Cytokine.* 2011, *54*, 136-143.

[32] Bin Z, Ke W, Jian J, *et al., Food. Anal. Meth.* 2011, *4*, 228-232.

[33] Cauchon E, Liu S, Percival MD, *et al., Anal. Biochem.* 2009, *388*, 134-139.

[34] Li Z, Zhang QY, Zhao LX, *et al., Sci. China. Chem.* 2010, *53*, 812-819.

[35] Sista RS, Eckhardt AE, Srinivasan V, Pollack MG, Palanki S, Pamola VK., *Lab Chip.* 2008, *8*, 2188-2196.

[36] Lacharme F, Vandevyver C, Gijs MAM. , *Microfluid Nanofluid*. 2009, *7*, 479-487.

[37] Dupont EP, Labonne E, Vandevyver C, Lehmann U, Charbon E, Gijs MAM., *Anal. Chem.* 2010, *82*, 49-52.

[38] Kim JI, Wang C, Kuizon S, *et al., Neuroimmunol* 2005, *158*, 112-119.

[39] Proczek G, Gassner AL, Busnel JM, Girault HH., *Anal. Bioanal. Chem.* 2012, *402*, 2645-2653.

[40] Lacharme F, Vandevyver C, Gijs MAM. , *Anal. Chem.* 2008, *80*, 2905-2910.

[41] Piao Y, Jin Z, Lee D, *et al.*, *Biosens.Bioelectron.* 2011, *26*, 3192-3199.

[42] Soh N, Tanaka M, Hirakawa K, *et al.*, *Anal. Sci.* 2011, *27*, 1069-1076.

[43] Gao D, Li HF, Guo GS, Lin JM., *Talanta.* 2010, *82*, 528-533.

[44] Chen H, Abolmatty A, Faghri M., *Microfluid. Nanofluid.* 2011, *10*, 593-605.

[45] Squires TM, Messinger RJ, Manalis SR., *Nat. Biotechnol.* 2008, *26*, 417-426.

[46] Sivagnanam V, Song B, Vandevyver C, Gijs MAM., *Anal. Chem.* 2009,*81*, 6509-6515.

[47] Sivagnanam V, Bouhmad A, Lacharme F, Vandevyver C, Gijs MAM., *Microelectron. Eng.* 2009, *86*, 1404-1406.

[48] Song SY, Han YD, Kim K, Yang SS, Yoon HC., *Biosens. Bioelectron.* 2011, *26*, 3818-3824.

[49] Afshar R, Moser Y, Lehnert T, Gijs MAM., *Anal. Chem.* 2011, *83*, 1022-1029.

[50] Fu Z, Shao G, Wang J, Lu D, Wang W, Lin Y., *Anal. Chem.* 2011, *83*, 2685-2690.

[51] Pfaunmiller E, Moser AC, Hage DS., *Methods* 2012, *56*, 130-135.

[52] Schiel JE, Tong Z, Sakulthaew C, Hage DS., *Anal. Chem.* 2011, *83*, 9384-9390.

[53] Liu Y, Wang H, Huang J, Yang J, Liu B, Yang P., *Anal. Chim. Acta* 2009, *650*, 77-82.

[54] Sinha A, Ganguly R, Puri IK., *J. Appl. Phys.* 2010, *107*, 034907-1-034907-6.

[55] Lian W, Wu D, Lim DV, Jin S., *Anal. Biochem.* 2010, *401*, 271-279.

[56] Han KC, Ahn DR, Yang EG., *Bioconjugate Chem.* 2010, *21*, 2190-2196.

[57] Ruckstuhl T, Winterflood CM, Seeger S., *Anal. Chem.* 2011, *83*, 2346-2360.

[58] Kai J, Puntambekar A, Sehy D, Brescia P, Banks P, *Gen. Engineer. Biotechnol. News.* 2011, *31*, 26-27.

[59] Lee BS, Lee JN, Park JM, *et al.*, *Lab Chip.* 2009, *9*, 1548-1555.

[60] Roman J, Qiu J, Dornadula G, *et al.*, *J. Pharm. Toxic. Meth.* 2011, *63*, 227-235.

[61] Yang Z, Liu H, Zong C, Yan F, Ju H., *Anal. Chem.* 2009, *81*, 5484-5489.

[62] Yang Z, Zong C, Yan F, Ju H., *Talanta*. 2010, *82*, 1462-1467.

[63] Xue C, Zhao H, Liu H, *et al.*, *Sens.Actuators B.* 2011, *156*, 863-866.

[64] Tan W, Huang Y, Nan T, *et al.*, *Anal. Chem.* 2010, *82*, 615-620.

Websites

[101] RNase H1Antibody (5D10). www.novusbio.com/H00246243-M01

CHAPTER 4

OFF-CHIP MAGNETIC MICROBEAD IMMUNOASSAY FOR THE DETECTION OF MYOGLOBIN, CARDIAC TROPONIN, AND FATTY ACID BINDING PROTIEN

4.1 Introduction

Due to their high sensitivity, biosensors have become a popular diagnostic tool for both early and rapid disease detection. Rapid detection is particularly important in cases of acute myocardial infarction (AMI) where prompt diagnosis is crucial for patient survival. The biomarker targeted by the biosensor is of key importance and the characteristics an ideal cardiac marker have recently been defined [1]. These include both the rapid release of the biomarker into the blood for early detection and prolonged elevation for later assessment and confirmation, along with the quantitative assay possessing a high clinical sensitivity and specificity. The American College of Cardiology (ACC) and the American Heart Association (AHA) currently recognize a biomarker panel composed of myoglobin, cardiac troponins (cTnI), and creatine kinase MB (CK-MB) for the diagnosis of AMI [2,3]. However, because CK-MB has a low sensitivity for AMI within six hours after an incident and cTnI is better at detecting minor cardiac damage, it was not evaluated in this study [2]. Instead, heart-type fatty acid binding protein (H-FABP) was included due to its early release following cardiac injury and potential when used as part of a panel with cTnI [4-7].

Myoglobin is an oxygen-binding protein found in both cardiac and striated muscle, and is currently used as a routine biomarker for AMI [8,9]. Its early release into the blood (increasing 1-3 hours within the onset of myocardial necrosis), as well as

relatively high plasma reference concentration (34 μg/L) illustrate several of the qualities desired in an ideal cardiac marker [9]. However, because it may also indicate skeletal muscle damage, by itself myoglobin has shown a sensitivity of 75.9%, and a clinical specificity of only 25.0% for AMI diagnosis. In recent years H-FABP has also shown promise as an early cardiac injury marker in plasma [4,7,10,11]. Owing to its lower concentration in skeletal muscle compared to myoglobin, rapid release into circulation, and potential to predict patient prognosis, H-FABP has received considerable attention [5-7,12,13]. Still, due to its release in other medical conditions, H-FABP alone shows only a 64% sensitivity [5,14]. While no single marker has shown adequate diagnostic accuracy for AMI, a high sensitivity and specificity has been achieved using myoglobin and H-FABP as part of a biomarker panel along with cTnI [5,8,10,12,14-16]. Even using biomarker panels, there still exists a need for more sensitive assays capable of analyzing multiple markers in a short time enabling serial measurements to be practically evaluated in a clinical setting. This capability would be beneficial not only in the diagnosis of AMI, but for the early detection of many diseases which could greatly improve prognosis.

Over the last few years a great deal of research has been devoted to the development of micro-immunoassay platforms allowing for the sensitive quantitation of varied target biomarkers [17-25]. A particularly interesting subset of this research incorporates the use of magnetic micro- or nano-particles as the solid surface employed for primary antibody fixation and target trapping [26-34]. Use of magnetic particles permits easy sample manipulation and separation from interfering species, as well as straightforward coupling to signal amplification and signal processing.

This work describes the development of a micro-immunoassay platform allowing for extremely sensitive quantitation. This system directly and indirectly addresses many the six metrics of an optimized immunoassay: increased sensitivity, reduced analysis time, reduced cost, lower sample volumes, ability to multiplex and operational simplicity [35]. The primary focus of this study is the improvement of quantitative sensitivity for the assay platform, and emphasis has been placed on optimizing this feature. However, additional metrics are addressed using this protocol, including the requirement for low sample volumes and potential to reduce the analysis time. While the studies here are performed on an AMI biomarker panel composed of myoglobin, cTnI and H-FABP, this format is easily adaptable to the detection of limitless targets and may be incorporated as a detection method into a micro-total analysis system (μTAS) for the parallel detection and quantification of biomarker panels.

4.2 Experimental

4.2.1 Myoglobin Detection Antibody Conjugation to Fluorescein-5-EX, Succinimidyl Ester

Fifty micrograms (50 μL; 1 mg/mL) of polyclonal rabbit anti-human myoglobin reconstituted in DI H_2O (LSBio, Seattle, Washington) was added to 50 μL of 1 M sodium bicarbonate in a 1.5 mL capped vial. One milligram of fluorescein-5-EX, succinimidyl ester (FEXS, Invitrogen) was dissolved in 0.1 mL dimethyl sulfoxide (DMSO) and added dropwise to the polyclonal antibody (Pab) solution at room temperature. This was reacted in darkness at room temperature for 3 hours on a stir plate (Corning) and then placed at 4°C to continue the reaction overnight. The crude reaction mixture was added to a purification column with a 15,000 Dalton molecular weight cut-off (Invitrogen). The

fluorescently labeled antibody was separated on-column from unbound dye using 10 mM PBS with 0.15 M NaCl and 0.2 mM NaN_3, pH 7.2 and collected in a single fraction. The purified FEXS-Pab solution was analyzed for absorbance measurements at 280 and 494 nm (BioTeck Synergy HT Multi-Mode Microplate Reader). These measurements were used to determine the quantity of antibody present and extent of FEXS conjugation [36].

4.2.2 cTnI and H-FABP Detection Antibody Conjugation to NHS-Fluorescein

250 μg (250 μL; 1 mg/mL) of polyclonal goat anti-human cTnI and 100 μg (100 μL; 1 mg/mL) polyclonal rabbit anti-human FABP were used as purchased in PBS buffer (cTnI: 0.1% NaN_3; FABP: 0.02% NaN_3, 0.1% BSA), pH 7.2. NHS-Fluorescein (Thermo Scientific) was dissolved in DMSO to a concentration of 10 mg/mL and added dropwise to the Pab solutions at room temperature (24 μL and 40 μL, respectively). This was reacted in darkness at room temperature for two hours on a shaker (Southwest Science LabMini MiniMixer). The crude reaction mixtures were added to dialysis cups (Thermo Scientific) with a molecular weight cut-off of 3,500 Daltons. The labeled protein was dialyzed in 100 mM PBS with 0.02% NaN_3 and 0.1% Tween 20, pH 7.2 overnight. The dialyzed NHS-Fluorescein-Pab solutions were analyzed for absorbance measurements utilizing the same method as for anti-human myoglobin Pab.

4.2.3 Preparation of Capture Antibody and Particles

Biotinylated anti-myoglobin Mab (bMab; 100 μL; 1.4 mg/mL; LSBio) was incubated with 3 μL of BioMag paramagnetic particles having an average diameter of 1.6 μm and ranging in diameter from 1.0-2.0 μm (Quagen, Inc.). The total reaction volume was diluted to 300 μL with PBS at pH 7.2 containing 5% BSA, 0.1% Tween-20, and 0.1% NaN_3. This was incubated for 3 hours on a shaker (Southwest Science LabMini

MiniMixer) at room temperature and then stored at 4°C until used. Biotinylated anti-cTnI Mab (50 µL, 2 mg/mL, LSBio) and biotinylated anti-FABP Mab (45 µL, 2.33 mg/mL, LSBio) were prepared in the same way.

4.2.4 Sandwich Immunoassays

Purified human myoglobin (7.33 mg/mL) was purchased from MyBioSource, LLC (San Diego, California). Standards ranging in concentration from 0.62 fg/mL to 25 ng/mL (36 aM to 1.5 nM) were created through serial dilution of the stock myoglobin. Following sample preparation 30 µL of each Mb standard was mixed with 30 µL of the bMab-BioMag colloid and incubated at room temperature on a shaker for 1 hour. Following the incubation, 4 µL of the detection polyclonal antibody-FEXS solution was added to each sample and incubated in the dark at room temperature for 1 hour with shaking. After the incubation, samples were washed 3 times using 60 µL of PBS buffer and then exchanged to a final volume of 30 µL. Three separate 10 µL droplets were analyzed for each sample, with a total of ten analyses performed for each concentration. Purified human cTnI (1.07 mg/mL) and H-FABP (2.2 mg/mL) were purchased from Life Diagnostics (West Chester, Pennsylvania). Standards ranging in concentration from 10 fg/mL to 10 ng/mL (0.42 fM to 0.42 nM) for cTnI and from 1 fg/mL to 10 ng/mL (67 aM to 0.67 nM) for H-FABP through serial dilution of the initial stock solutions. Following sample preparation samples were prepared and analyzed in the same way as myoglobin.

4.2.5 Data Collection

Data were collected using an Olympus IX70 inverted microscope with a charge coupled device (CCD) camera connected to a computer capable of image-capture (Q-Imaging, Surrey, BC). Capture settings for the CCD camera were optimized for the

observation of strong fluorescent signal clusters with minimal contribution from background pixels through studies utilizing biotinylated fluorescein (Sigma-Aldrich) as a positive control. Biotinylated fluorescein was chosen as a control due to the strong binding relationship between biotin and the streptavidin on the BioMag particles and a common fluorophore with the experimental immunoassays. Offset was adjusted to minimize background of a washed sample without reducing pixel intensity from signal, values between −1120 to 440 were tested. With the offset held constant at 100, gain values between 4.7 to 15.0 were explored to maximize the sensitivity of the assay without compromising the dynamic range. Optimal image quality was observed at an offset of 100 and gain of 13.8. Once established, capture settings were held constant for all experiments performed on cardiac targets.

Multiple 10 µL-sized droplets were analyzed for each sample concentration using a microscope slide having a small hydrophilic zone encompassed by a hydrophobic Teflon coating (Tekdon Inc., Myakka City, Florida). A cylindrical rare earth magnet (2.5 cm diameter, 0.3 cm thick) placed 2 cm above the droplet was used to generate the magnetic field (Magcraft, Vienna, VA) and collect structures for ~30s. Supraparticle structures approximately 15 µm in length were observed. The magnet was secured to a DC motor by a 7 cm metal shaft allowing for rotation and controlled via a USB 4-motor stepper controller (Trossen Robotics). The controller was connected to the motor through a ribbon wire to protect it from fluids used during the experiment. The magnet was rotated at a constant velocity during assays (30 rpm), and illumination from a mercury lamp (Olympus) was passed through the appropriate filter cube and a LCPlanFl 40X/0.60

objective to excite the assay. Emitted fluorescence was collected using the QIACAM FAST cooled Mono 12-bit (QImaging) CCD camera and stored as video files.

4.2.6 Data Analysis

Video was analyzed using Image J (National Institute of Health, Bethesda, Maryland). The images (492 x 396) were captured at an exposure time of ~120 ms (gain, 13.8; offset, 100) which translates to a rate of ~12 frames/s. Fluorescence intensity measurements were collected by manually selecting all rotors (areas of interest, ROI) within a video frame and summing the fluorescence intensity. This was performed for ten randomized frames per video and the resulting intensities were averaged to attain a single average fluorescence intensity value for a given trial. Ten trials per sample concentration were averaged per experiment.

4.3 Results and Discussion

4.3.1 Assay Optimization and Protein Detection

Three human cardiac biomarkers, myoglobin, cTnI, and H-FABP, were quantified using a singleplex immunoassay detection system. Proteins were detected by adjusting the hardware settings such that images with visible, yet unsaturated, signal clusters with minimal background contribution were captured. Using an exposure time of 120 ms, signals generated from low concentrations of proteins (down to 36 aM of myoglobin) were detected above the background intensity (Figure 4.1).

Control experiments were performed at a zero antigen concentration, exposing paramagnetic particles with immobilized capture antibody to fluorescently-labeled detection antibody. Dark structures resulted, with minimal diffuse fluorescence suggesting that little or no nonspecific binding is present. The average fluorescence

intensity of the entire image was noted (including pixels from all areas, including diffuse fluorescence between rotors) since distinct signal clusters were not visible. This is a more stringent test for background quantification, since the noise from all pixels is included.

At low sample concentrations, below 360 aM for myoglobin, the signal becomes highly variable and the uncertainty in the measurements was greater than 10%. When the uncertainty in a measurement falls below 10% the signal may not only be detected, but quantified with a reasonable level of certainty [37]. This distinction is important as it differentiates a qualitative positive result from the ability to distinguish when a biomarker is present in concentrations that correspond to diagnostic cut-off values. For the optimization of a clinical assay it is the quantitation limit that is of interest.

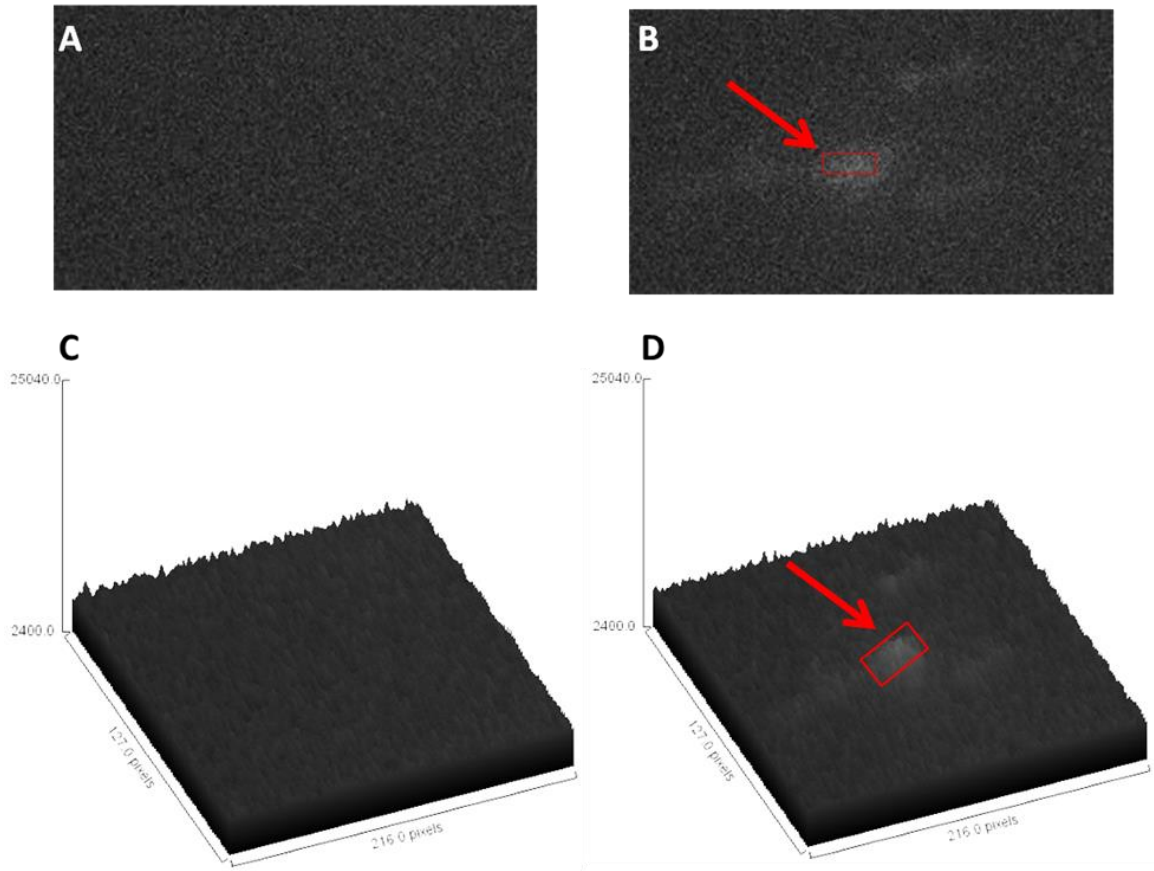

Figure 4.1 (**A and B**) Images showing fluorescence of high sensitivity immunoassays at the detection limit (below the limit of quantification) for 36 aM myoglobin (**B**) compared to background (**A**). (**C and D**) Surface plots illustrating the difference in fluorescence intensity between background (zero concentration, **C**) and signal clusters representing specific signal (36 aM myoglobin, **D**). While the signal clusters are not as distinct as those observed for higher target concentrations, this represents the lower limit detectable above zero concentration.

4.3.2 Quantitation Limit

Measurements of cardiac targets permitted the quantitation of myoglobin to a minimal concentration of 360 ± 2.5 aM with an observed detection limit of 36 ± 2.5 aM, and a linear standard curve from 360 aM to 14 fM (R^2 = 0.996; Fig. 2A). H-FABP and cTnI were quantified to limits of 67 ± 3 fM and 42 ± 0.01 fM, with linear standard curves from 67 fM to 67 pM and 42 fM to 42 pM, respectively (R^2 = 0.998; Fig. 2B and R^2 = 1; Fig. 2C). The optimized collection of the video sets allowed for improvement in detection

over several orders of magnitude compared to previously collected myoglobin data, from 50 pM to 36 aM (Table 4.1) [30]. The limits of quantitation observed in the present work compare favorably to the metrics of a fully optimized immunoassay, achieving detection on the same order of magnitude as fundamental limitations. At low numbers of molecules, quantification becomes impossible due to Poisson statistics [37]. While targets may be observed below this limit, they may not be quantified due to high levels of uncertainty in the measurements made.

	Previous Studies[30]	**Commercial Techniques[38,39]**	**Present Work**	**Optimized Values**	**Plasma Concentration[40]**
Myoglobin	50 pM	1.5 nM	360 ±2.5 aM	33 aM	2.5 nM
H-FABP	--	6.7 pM	67 ± 3 fM	33 aM	110 pM
cTnI	--	83 pM	42 ± 0.01 fM	33 aM	62.5 pM

Table 4.1 Quantitation limits for immunoassay techniques. Optimized values represent the limit to immunoassay quantitation in a 10 μL sample volume.

Several differences exist in both the data acquisition and data analysis performed in this work that account for the observed improvement in quantitation ability compared to previous studies [30]. In terms of data acquisition, previous work noted differences in signal strength depending on their location in the field of view, increasing variation in both signal and noise. The changes to optics and acquisition conditions eliminated this issue, producing rotors with similar signal intensities independent of their location. Optimizing acquisition conditions through control studies with b-Fluorescein resulted in an increase in exposure time from 50 to 120 ms, as well as reductions in gain (from 2000 to 13.8) and offset (from 2600 to 100) [30]. The increase in exposure time still allowed clear visualization of rotor rotation while reducing the impact on noise compared with a

shorter exposure. With a lowered gain, the amplification of the image collected by the CCD camera is reduced. Since both the signal and noise are reduced, this lowered value will improve the signal-to-noise ratio (S/N) and reduce the background intensity and noise while specific signal remains visible. By contrast, reducing the offset allows lower intensity values for both specific signal and background fluorescence to be captured. While this increases both the background intensity and noise as well as signal intensity and noise, this minimal value assures that clusters from low signal concentrations may be observed. By improving the signal-to-noise ratio of the captured video files lower intensity signals may be differentiated from background noise, improving assay sensitivity.

Along with the changes made to data acquisition conditions, the process of data analysis has also been altered to increase the signal power obtained from each sample [30]. In previous work a small region of each image (150 x 120 pixels), containing roughly two of the 10-15 signal clusters present overall, was analyzed. Additionally, while signal clusters contributed to less than 30% of the region selected, the average pixel intensity was calculated for the entire selected area, including both signal and noise [41]. Signal processing studies performed on this data conclude that by calculating pixel intensity for the entire image selection, and by only two of the signal clusters contributing to target quantification, a large portion of the signal power is lost while the noise power is increased [41]. By manually segmenting data and selecting all rotors in each frame (492 x 396 pixels) as was done in this work, both issues observed with previous analysis methods are solved. The overall noise power is reduced while signal power is increased

[41]. This, coupled to the increase in S/N through optimal data acquisition conditions, allowed for a five-fold improvement in assay sensitivity.

In terms of the mass action equilibrium and detection, sensitivity is maximized by using an excess of both primary and secondary antibodies, and heavy labeling of secondary antibodies (average among all targets of 4 labels per antibody). Given that the paramagnetic particles have a binding capacity of 8.2 nmol/mL (manufacturer specifications), the binding capacity for the primary antibody preparation is 82 nM. Using fundamental relationships from basic immunology the equilibrium reaction between the protein and primary antibody can be described as

$$K_{eq} = \frac{[AgAb1]}{[Ag][Ab1]} \qquad (4.1)$$

where [*AgAb1*] is the concentration of bound antigen, [*Ag*] is the concentration of antigen, [*Ab1*] is the concentration of primary antibody, and K_{eq} is the equilibrium constant. Given a K_{eq} of 10^9 M^{-1}, the equilibrium concentration of bound antigen for a myoglobin sample at a concentration of 3.6 fM is 0.3 pM, about one hundred times the concentration of target present. A similar calculation can be performed for the reaction of bound antigen with secondary antibody, giving an equilibrium concentration of [*AgAb2*] in the nM range. With these experimental conditions it can be determined that nearly all antigen is bound in the sandwich immunoassay, resulting in a linear response for the portion of the sigmoidal immunoassay curve examined.

At myoglobin concentrations below 360 aM, uncertainty is too high in the measurement achieve satisfactory quantitation. Although the lowest concentrations detected could not be quantified due to high variations in signal, the potential exists to

improve quantitative sensitivity through coupling to available signal processing approaches [41]. Using this approach, the detection limit of previously published data has been improved by a factor of 100. If the same factor of improvement and reduction in uncertainty for a given sample was realized for the data collected in this work, quantitation of the lowest sample data collected would be possible.

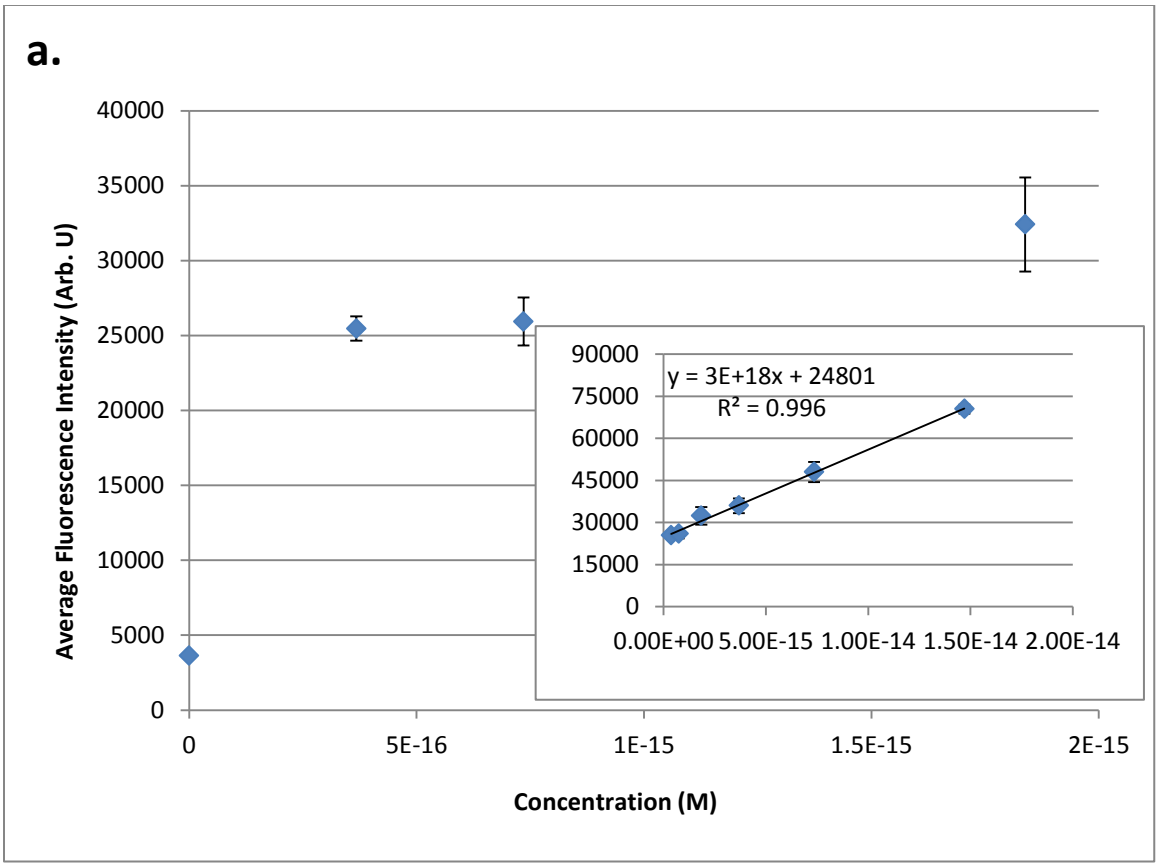

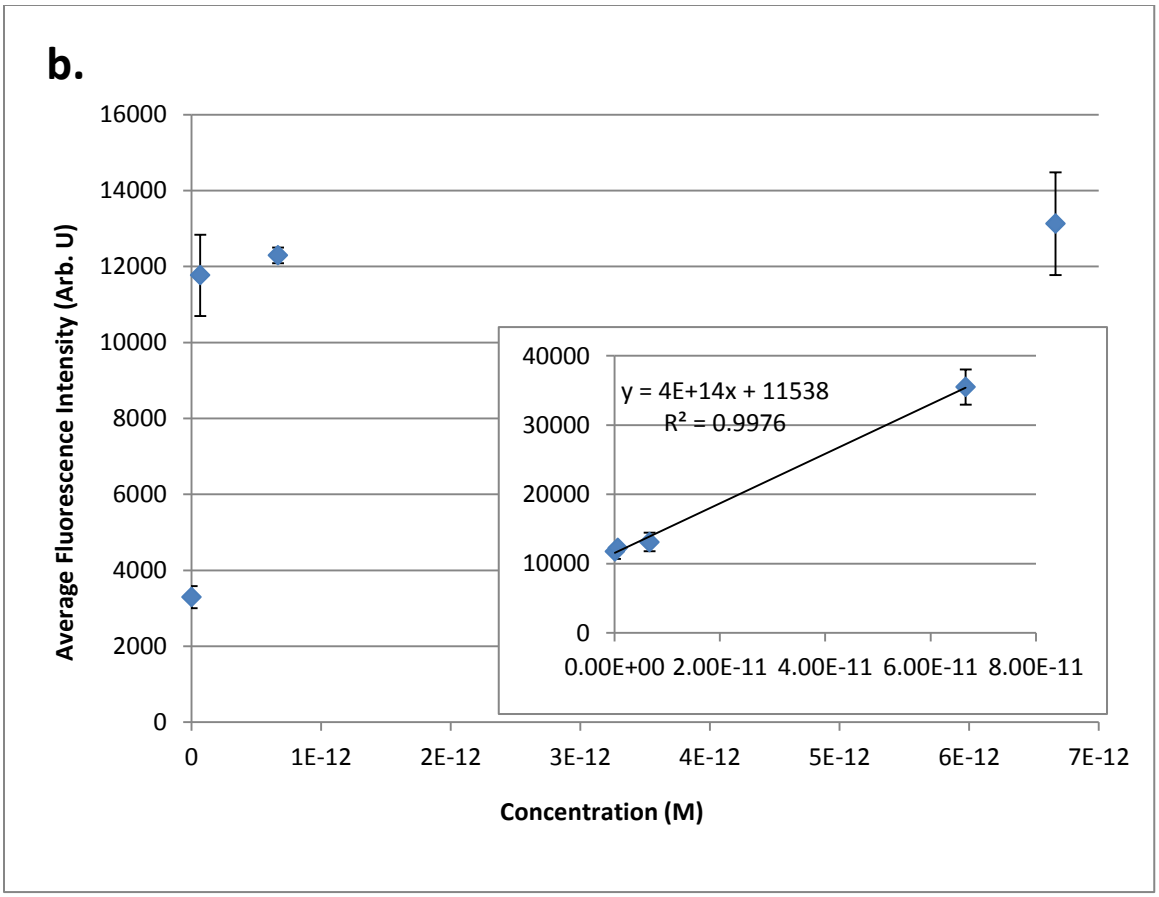
b.
Average Fluorescence Intensity (Arb. U)
16000
14000
12000
10000
8000
6000
4000
2000
0
0
1E-12
2E-12
3E-12
4E-12
5E-12
6E-12
7E-12
Concentration (M)
40000
30000
20000
10000
0
y = 4E+14x + 11538
R² = 0.9976
0.00E+00 2.00E-11 4.00E-11 6.00E-11 8.00E-11

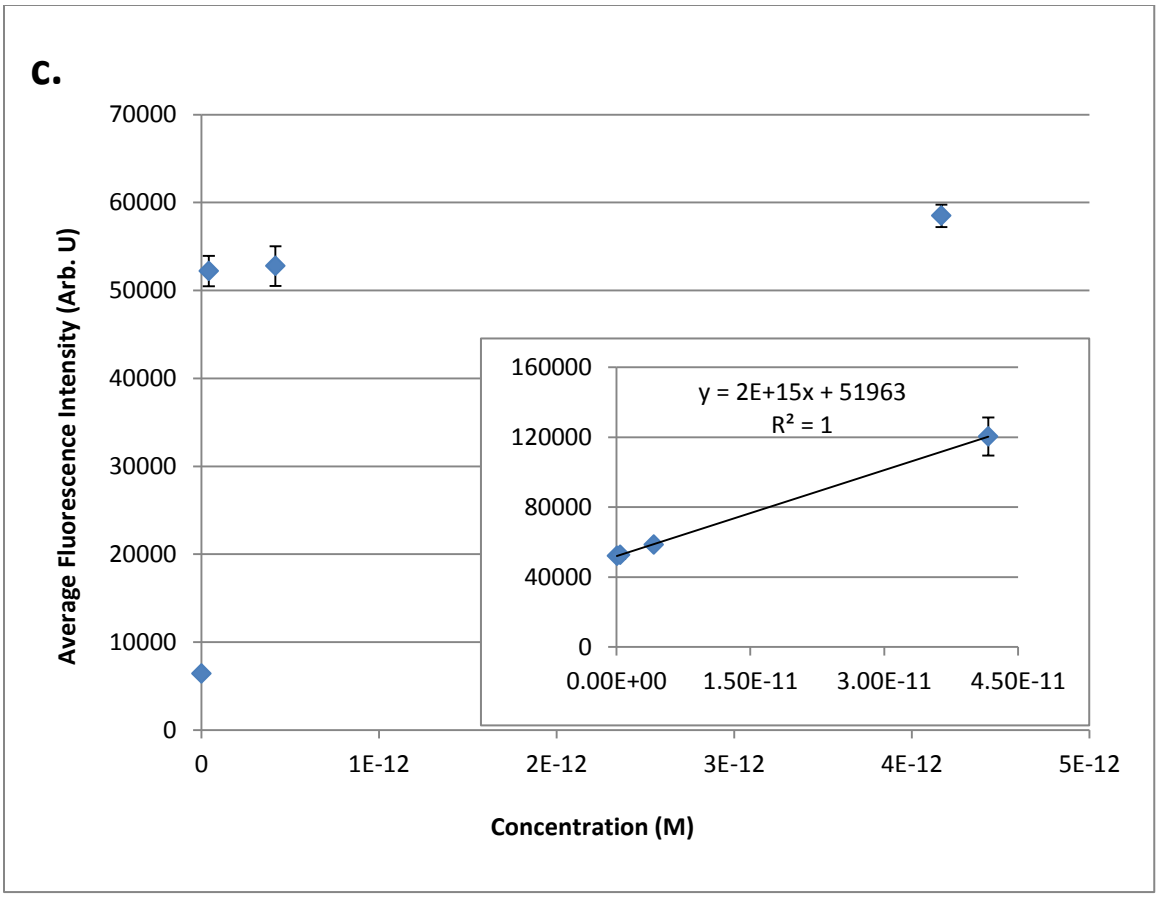

Figure 4.2 Standard curves showing fluorescence intensity data for the sandwich immunoassays performed on cardiac biomarker targets. **a.** Plot showing the quantitation of Myoglobin down to a minimal concentration of 360 aM. Inset shows the linear range to 14.7 fM. **b.** Plot showing the quantitation of h-FABP to a minimal concentration of 67 fM with inset showing the linear range to 67 pM. **c.** Plot showing the quantitation of cTnI to a minimal concentration of 42 fM with inset showing the linear range to 42 pM.

Repeated experiments exhibit a similar result. Figure 3 shows the average fluorescence intensity of data collected from four separate experiments with independent dilutions of a myoglobin stock sample. Error bars show the standard deviation of each data set. Differences in overall fluorescence intensity were observed between experiments, due to aging of the mercury lamp used to illuminate samples. Even when differences in fluorescence intensity were observed between days, the same linear relationship was observed.

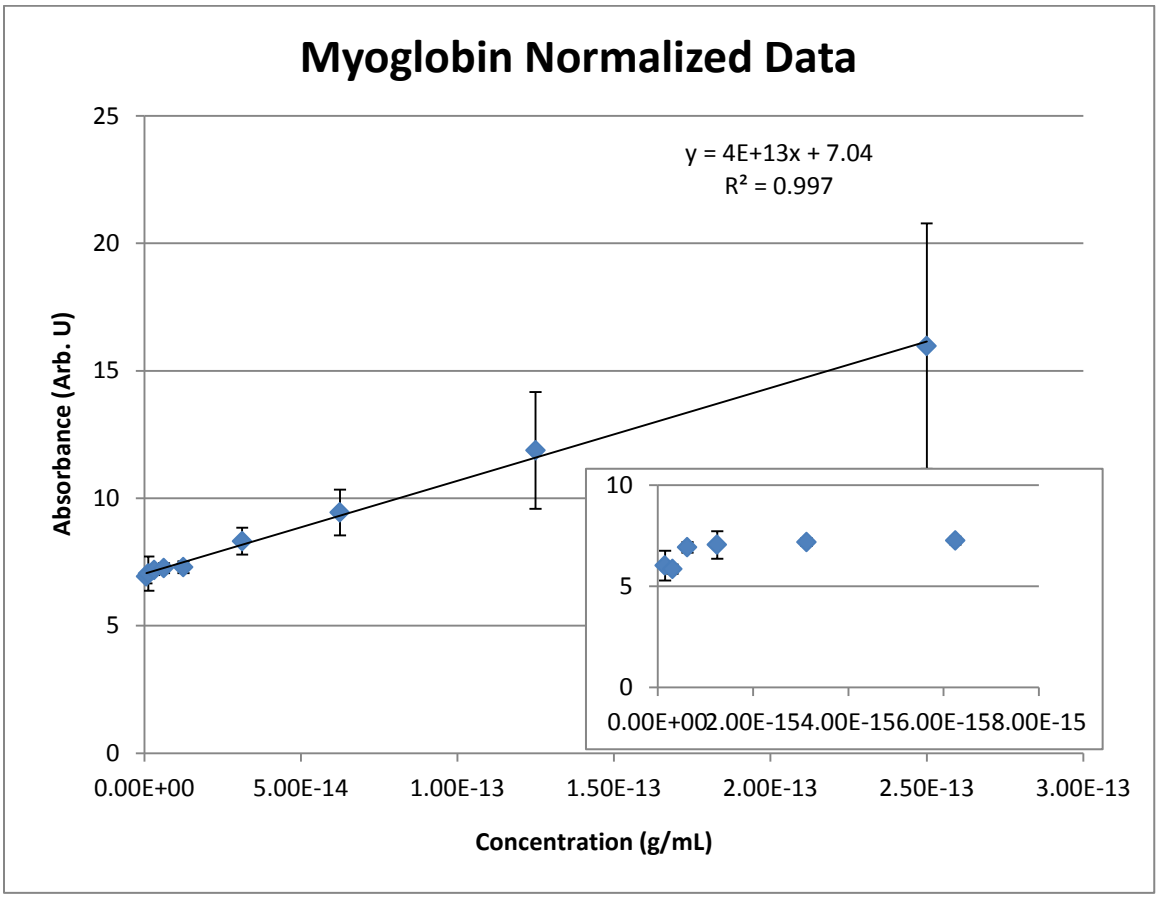

Figure 4.3 Standard curve showing the average fluorescence intensity versus concentration for the myoglobin sandwich immunoassay for four different experiments using the target protein. The inset shows the lower concentrations on the standard curve, error bars represent the standard deviation among data sets. Fluorescence intensity has been normalized to the background intensity (zero concentration) for each data set.

4.3.3 Assay Evaluation

As has been noted previously, in static immunoassays background fluorescence is a serious concern that limits the ability to differentiate specific signal from noise. Signal processing strategies offer the potential to improve detection limits through the identification of specific signal generating surfaces and reduction of background elements to reduce the variation observed in signal intensity for low concentration samples [41]. Surface localization is of use in image processing because it creates distinct signal objects

that are easier to detect and quantify compared to signal spread over the entire field of view. Creating these distinct signal objects allows for segmentation of collected images and the quantitation of fluorescent species bound in the immunoassay without the influence of diffuse background fluorescence.

The potential to optimize quantitation capabilities also exists through the use of new signal input patterns. Lock-in amplification is a commonly employed method to recognize a specific input signal in the presence of noise [42]. This method allows an input signal modulated in amplitude to be matched to a reference signal with the same periodicity and amplified while background noise is not recognized and is effectively removed. It has been used in previous work to achieve detection limits in the pM range [30,32]. However, because the reference signal generated by lock-in amplification is a sine wave, its correlation with the input wave is imperfect and signal power is lost. This has been addressed in part by the development of a new signal processing method that maintains the input signal modulation but uses a new waveform as the reference signal [37]. While this approach was successful in improving quantitation, using autocorrelation analysis to recognize more complicated input patterns could improve the distinction between signal and noise and increase the slope of the regression line at low sample concentrations.

Other immunoassay techniques have worked on improving quantitative sensitivity for protein targets [17,23-25,33,34]. Compared to those studies that were performed using traditional laboratory equipment [23-25,33,34], the assay investigated in this work achieved superior sensitivity (aM to fM range compared with typical nM sensitivity) using shorter incubation times. Incubation times could potentially be reduced further for

this assay as the dispersed magnetic microbead surface offers an advantage during analyte capture. Unlike static assay surfaces that are subject to depletion zones and relaiant on diffusion for target capture, the solid microbead surface is constantly in motion throughout incubations. Another study discussed the development of a microchip-based immunoassay for cTnI detection [17]. Movement to the chip format allowed for shorter analysis times and easy adaptability to portable devices and multiplexed analysis. While offering an improvement over this work in terms of analysis time, the sensitivity achieved in this work was superior (fM compared with pM) using a comparable sample volume.

Many studies have reported on the improved sensitivity of cardiac diagnostic ability with the use of a biomarker panel as opposed to a single target [5,8,10,12,14-16]. One consequence of this is that parallel detection of targets from a single sample is desirable. Along with the potential to optimize this immunoassay platform for sensitive analyte quantitation, the use of magnetic microparticles offers the ability to move from the batch incubation assay conducted within this work to one performed on a microchip as part of a total sample analysis system. Easy manipulation of the magnetic solid surface through an applied magnetic field allows for the containment of surfaces functionalized for the capture of different targets in separate regions of the microchip. Following target isolation on chip through separation science techniques, individual species may be flushed into appropriate detection chambers and quantified. The linear range of this technique may also be extended through the dilution of samples investigated, or use of smaller sample volumes, allowing the assay to be tailored to meet detection needs as required for diagnostic or disease monitoring purposes.

4.4 Concluding Remarks

Dispersed magnetic beads were utilized in a batch incubation format to conduct sandwich immunoassays on three cardiac biomarker targets. Following sample preparation 10 μL droplets were manipulated through variations in an applied magnetic field, and the periodic change in observed fluorescence was captured as a video file. Analysis of video utilizing ImageJ allowed the superior detection of myoglobin (360 aM), H-FABP (67 fM) and cTnI (42 fM) compared to previous results.

Thus, a magnetic bead immunoassay platform was demonstrated utilizing simple batch incubation and a modified microscope slide. This platform has the potential to be incorporated into a full sample analysis chip as a quantification method for biomarker panels while maintaining sensitive detection capabilities, and offers the ability to couple results to more sophisticated signal processing approaches for the detection of low sample concentrations independently from background noise. In its current form this system directly addresses many of the six metrics of an optimized immunoassay. Incorporation of the assay into a μTAS could further these efforts by affording the ability to multiplex and further reduce analysis times while maintaining the high sensitivity, low sample volume, and operational simplicity achieved herein. Doing so has the potential to produce a platform optimized for the diagnosis of myocardial infarction in emergency rooms as previously defined: sensitivity allowing quantification of samples below the pM range using fingerprick blood and the ability to quantify 3 targets simultaneously in under 30 minutes without the requirement for expensive, complicated or bulky instrumentation. Not only could these advances produce a testing platform tailored to emergency

diagnostics, but reaching immunoassay optimization of all six metrics would allow the application of this technique to other biological and medical issues.

4.5 References

[1] Qureshi, A., Gurbuz, Y., Niazi, J.H., *Sensors and Actuators B*, 2012, *171-172*, 62-76.

[2] ACC and Cardiac Biomarkers, 2014, http://www.acc.org/education-and-meetings/image-and-slide-gallery/media-detail?id=d9c880ce33f3482f993161076a32990a

[3] Vasan, R. S., *Circulation*, 2006, *113*, 2335-2362.

[4] Kakoti, A., Goswam, P. i, *Biosensors and Bioelectronics*, 2013, *43*, 400-411.

[5] Ishii, J., Wang, J.H., Naruse, H., Taga, S., Kinoshita, M., Kurokawa, H., Iwase, M., Kondo, T., Nomura, M., Nagamura, Y., Watanabe, Y., Hishida, H., Tanaka, T., Kawamura, K., *Clinical Chemistry*, 1997, *43*, 1372-1378.

[6] Huang, C.H., Tsai, M.S., Chien, K.L., Hsu, C.Y., Chang, W.T., Wang, T.D., Chen, S.C., Huei-Ming Ma, M., Chen, W.J., *Clinica Chimica Acta*, 2014, *435*, 7-13.

[7] Glatz, J.F., Renneberg, R., *Clinical Lipidology*, 2014, *9*, 205-220.

[8] Macdonald, S.P.J., Nagree, Y., Fatovich, D.M., Phillips, M., Brown, S.G.A., *Emergency Medicine Journal*, 2012, *30*, 149-154.

[9] Liao, J., Chan, C.P., Cheung, Y., Lu, J., Luo, Y., Cautherley, G.W.H., Glatz, J.F.C., Renneberg, R., *International Journal of Cardiology*, 2008, *133*, 420-423.

[10] Tonomura, Y., Matsushima, S., Kashiwagi, E., Fujisawa, K., Takagi, S., Nishimura, Y., Fukushima, R., Torii, M., Matsubara, M., *Toxicology*, 2012, *302*, 179-189.

[11] Inoue, K., Suwa, S., Ohta, H., Itoh, S., Maruyama, S., Masuda, N., Sugita, M., Daida, H., *Circulation Journal*, 2011, *75*, 2813-2820.

[12] Molin, S.Da., Cappellini, F., Falbo, R., Signorini, S., Brambilla, P., *Clinical Biochemistry*, 2014, *47*, 247-249.

[13] Setsuta, K., Seino, Y., Mizuno, K., *International Journal of Cardiology*, 2014, *176*, 1323-1325.

[14] McMahon, C.G., Lamont, J.V., Curtin, E., McConnell, R.I., Crockard, M., Kurth, M.J., Crean, P., Fitzgerald, S.P., *American Journal of Emergency Medicine*, 2012, *30*, 267-274.

[15] Gnedenko, O.V., Mezentsev, Y.V., Molnar, A.A., Lisitsa, A.V., Ivanov, A.S., Archakov, A.I., *Analytica Chimica Acta*, 2013, *759*, 105-109.

[16] Body, R., McDowell, G., Carley, S., Wibberley, C., Ferguson, J., Mackway-Jones, K., *Resuscitation*, 2011, *82*, 1041-1046.

[17] Song, S. Y., Han, Y. D., Kim, K., Yang, S. S., Yoon, H. C., *Biosensors and Bioelectronics*, 2011, *26*, 3818-3824.

[18] Casolari, S., Roda, B., Mirasoli, M., Zangheri, M., Patrono, D., Reschiglian, P., Roda, A., *Analyst*, 2013, *138*, 211-219.

[19] Tian, J., Zhou, L., Zhao, Y., Wang, Y., Peng, Y., Hong, X., Zhao, S., *J Fluoresc*, 2012.

[20] Lin, D., Wu, J., Wang, M., Yan, F., Ju, H., *Analytical Chemistry*, 2012, *84*, 3662-3668.

[21] Liang, G., Liu, S., Zou, G., Zhang, X., *Analytical Chemistry*, 2012, *84*, 10645-10649.

[22] Spindel, S., Sapsford, K.E., *Sensors*, 2014, *14*, 22313-22341.

[23] Ammar, M., Smadja, C., Phuong, G.T., Azzous, M., Vigneron, J., Etcheberry, A., Taverna, M., Dufour-Gergam, E., *Biosensors and Bioelectronics*, 2013, *40*, 329-335.

[24] Caulum, M.M., Murphy, B.M., Ramsay, L.M., Henry, C.S., *Analytical Chemistry*, 2007, *79*, 5249-5256.

[25] Park, M., Bong, J.H., Chang, Y.W., Yoo, G., Jose, J., Kang, M.J., Pyun, J.C., *Analytical Methods*, 2014, *6*, 1700-1708.

[26] Han, J., Zhang, J., Xia, Y., Li, S., Jiang, L., *Colloids and Surfaces A: Physiochem. Eng. Aspects*, 2011, *379*, 2-9.

[27] Proczek, G., Gassner, A. L., Busnel, J. M., Girault, H. H., *Anal. Bioanal. Chem.*, 2012, *402*, 2645-2653.

[28] Ranzoni, A., Sabatte, G., van Ijzendoorn, L. J., Prins, M. W. J., *ACS Nano*, 2012, *6*, 3134-3141.

[29] Hahn, Y. K., Park, J. K., *Lab Chip* 2011, *11*, 2045-2048.

[30] Hayes, M.A., Petkus, M.M., Garcia, A.A., Taylor, T., Mahanti, P., *Analyst*, 2009, *134*, 533-541.

[31] Zhang, Y., Zhou, D., *Expert Reviews Ltd*, 2012, *ISSN 1473-7159*, 565-571.

[32] Petkus, M.M., McLauchlin, M., Vuppu, A.K., Rios, L., Garcia, A.A., Hayes, M.A., *Analytical Chemistry*, 2006, *78*, 1405-1411.

[33] Zhu, Y.D., Peng, J., Jiang, L.P., Zhu, J.J., *Analyst*, 2014, *139*, 649-655.

[34] Sakamoto, S., Omagari, K., Kita, Y., Mochizuki, Y., Maito, Y., Kawata, S., Matsuda, S., Itano, O., Jinno, H., Takeuchi, H., Yamaguchi, Y., Kitagawa, Y., Handa, H., *Clinical Chemistry*, 2014, *60*, 610-620.

[35] Woolley, C.F., Hayes, M.A., *Bioanalysis*, 2013, *5*, 245-264.

[36] Fluorescein-EX Protein Labeling Kit, 2004, http://tools.invitrogen.com/content/sfs/manuals/mp10240.pdf.

[37] Currie, L.A., *Analytical Chemistry*, 1968, *40*, 586-593.

[38] Cardiac Marker ELISA Kits, 2013, http://www.calbiotech.com/products/elisa-kits/human-elisa-kits/cardiac-marker-elisa-kits.

CHAPTER 5

THEORETICAL LIMITATIONS OF QUANTIFICATON FOR NONCOMPETITIVE IMMUNOASSAYS

5.1 Introduction

Immunoassays are invaluable tools for the detection and quantification of important biomolecules and many other chemical compounds at low concentrations. Antibodies bind to target structures with large binding constants, which enable selective detection at low analyte concentrations. Since immunoassays were first introduced, attempts to optimize the assay process have persistently focused on improving the limit of detection (LOD) [1,2]. This focus on low LOD's has been stimulated largely by the desire for earlier therapeutic intervention through the detection of diagnostic markers at lower concentrations or from smaller volumes [3]. Over the years these efforts have resulted in the shift away from radioimmunoassays to enzyme-linked immunosorbent assays [4,5], and in the exploration of signal amplification approaches to improve detection of antibody-antigen binding [6-18].

The LOD is an important figure of merit for determining an immunoassay's quality and is frequently used to compare competing methods [19,20]. The term, LOD, is often used interchangeably in the immunoassay literature with the limit of quantification (LOQ), causing some confusion as to the reported capabilities of different assays [21-23]. As defined by Currie in 1968, the LOD corresponds to the presence of any detectable signal from the specific instrumental configuration that can be assigned to the target under study. The LOD is used as a demarcation of the presence or absence of an analyte (the L_d term in reference) and has high quantitative uncertainty at low sampling numbers

(reaching 100%), which undermines its use as an indicator of presence/absence. The LOQ is the level at which measurements have sufficient precision for quantitative determination [23]. The distinction between LOD and LOQ highlights that while single molecule immunoassays can detect the presence of one (or very few) putative signal generating molecules, detection at this level is highly qualitative. For immunoassays aimed at the quantification of minute amounts of proteins indicative of disease states, detection near the LOD is not adequate. Therefore, it is necessary to define the true LOQ for an immunoassay in terms of a statistical assessment and not instrumental factors.

The LOD for most immunoassays has been limited primarily by the signal-to-noise ratio provided by the instrument used to detect antibody-antigen binding or by nonspecific binding (NSB) [24,25]. With improving detection technology capable of routine single molecule detection, the instrumentation to detect antibody-antigen binding is no longer a fundamental factor that defines LOD's for immunoassays. It is well known that NSB often limits the LOD for immunoassays [19,26-31]; however, if an immunoassay method is optimized to reduce NSB to insignificant levels, the LOD that can be obtained with an immunoassay are then limited by antibody-antigen binding and fundamental statistical limitations.

Detection of a single molecule is an irresistible objective for analytical chemists. Recently, so-called 'single molecule immunoassay' techniques have been introduced [26-28]. Much of this work demonstrates the detection of individual signals associated with distinct putative binding events, but detection limits do not approach single molecule for the antigen [26-28]. These techniques have relied on the use of chemically-linked fluorophores to secondary (or tertiary) antibodies with detection schemes able to sense a

single fluorphore (or activity of a single enzyme). The signals from the individual counting of presumed immune complexes are averaged, summed or provided other data-processing mechanisms to generate an estimate of antigen concentration. These studies, while counting distinct signals assumed to be individual immune complexes, required the averaging of many individual signals to produce a quantitative measurement with a satisfactory coefficient of variation (<10%) [32,33]. The requirement for averaging many individual signals demonstrates that while singular complexes have been, in fact, detected using immunoassay techniques, the certainty with which they are detected is not sufficient for quantification of an analyte. Therefore, the true limits of quantification lie at higher levels than a single molecule. For any analytical immunoassay measurements approaching single antigen molecule detection, the LOD is ultimately bound by 'molecular' shot noise – the absolute floor of the limit of detection, which is a statistical sampling effect that follows a Poisson distribution [34].

In this work, relationships based on the law of mass action are used to model the theoretical limit of quantification for immunoassays. Most commercial immunoassay methods currently use P4-P5 fittings (four or five parameter mathematical fittings of resulting sigmoidal curves with no connection to fundamental interactions) to model the sigmoidal immunoassay response curves for quantitative analysis because of the difficulty of implementing theoretical models based on the law of mass action with many parameters [35]. These P4-P5 fittings are useful for practical quantitative analysis with immunoassays, but they cannot be used to explore the fundamental limit of quantification for immunoassays. The focus of this work is the ultimate limitations of immunoassays, mostly centered on molecular shot noise. However, without comparing and contrasting

this limit with other effects, it cannot be put in proper context. The LOQ for immunoassays is considered using theoretical models based on the law of mass action for three situations: when the limit of quantification is defined by 1) instrumental limitations, 2) non-specific binding—the most common case, and 3) conditions where statistical sampling theory is the only limit, so-called molecular shot noise.

5.2 Theory

5.2.1 Fundamental Relationships

Using equations from basic immunology and describing reaction schemes according to the law of mass action, the first incubation in the sandwich-type immunoassay (Figure 5.1) can be described by

$$K1_{eq} = \frac{[Ab1Ag]}{[Ab1][Ag]} \qquad (5.1)$$

where $K1_{eq}$ is the equilibrium association constant (antibody affinity, M^{-1}) for the capture antibody, [*Ag*] is the concentration of free antigen (M), [*Ab1*] is the concentration of unbound capture antibody (M), and [*Ab1Ag*] is the concentration of the antibody-antigen complex formed during the reaction (M) [36]. Modeling the reaction this way requires several assumptions to be made: (i) the interaction of antigen and antibody can be described using a single equilibrium constant, (ii) binding of antibody to a solid surface (or fluorophore or enzyme) doesn't affect binding characteristics, and (iii) wash steps separating bound and free antigen don't disturb the equilibrium reached [36].

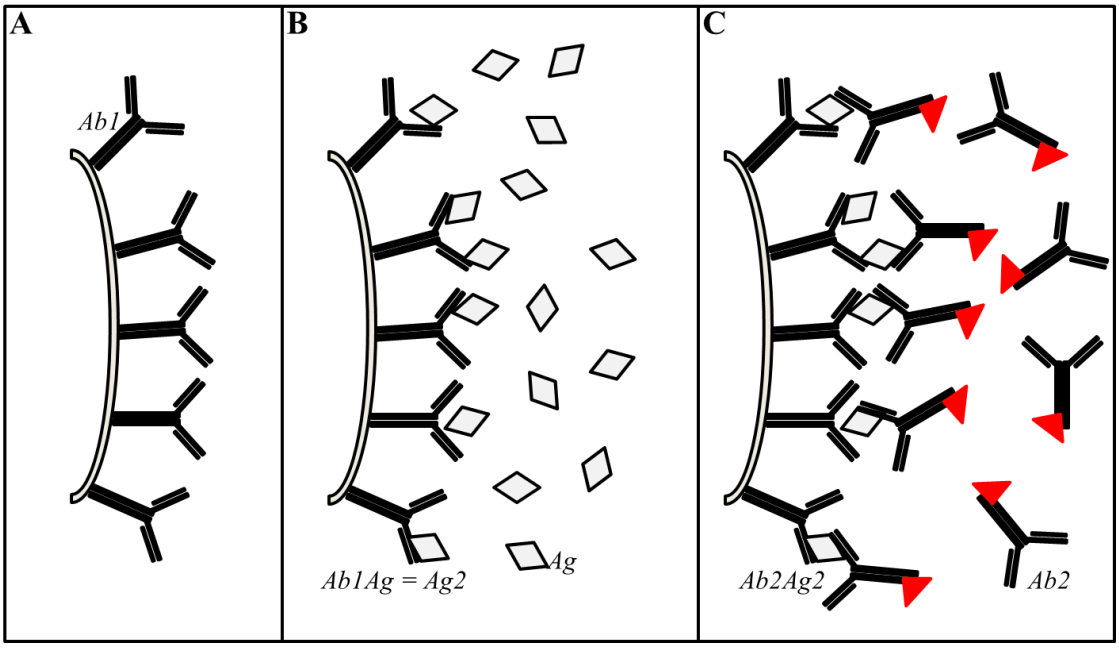

Figure 5.1 Schematic of the sandwich immunoassay format. A) The primary antibody ([*Ab1*]) is bound to a solid support forming a reaction capture area. B) The target analyte ([*Ag*]*)* is incubated with the primary antibody and captured to the surface (forming [*Ab1Ag*] which is equivalent to [*Ag2*]). After washing to remove any unbound species in the sample volume, C) incubation with the secondary detection antibody ([*Ab2]*) and removal of the unbound antibody allows detection of a signal and quantification of the bound analyte ([*Ab2Ag2*]).

Given that [$Ab1_{tot}$] is the total concentration of capture antibody, then

$$[Ab1] = [Ab1_{tot}] - [Ab1Ag] \qquad (5.2)$$

From Equation 5.2 we can write

$$[Ab1Ag] = K1_{eq}[Ag]\{[Ab1_{tot}] - [Ab1Ag]\} \qquad (5.3)$$

which can be simplified to [36,37]:

$$[Ab1Ag] = \frac{K1_{eq}[Ab1_{tot}][Ag]}{(1 + K1_{eq}[Ag])} \ . \qquad (5.4)$$

A plot of [*Ab1Ag*] with respect to log [*Ag*] is sigmoidal (Equation 5.4, Figure 5.2), with very low [*Ag*] concentrations producing linear changes in [*Ab1Ag*] (Figure 5.2 inset). The shape of the curves can be trivially understood by noting that $1 + K1_{eq}[Ag] \cong 1$ when

[*Ag*] is small, thus making eq. 5.4 a linear relationship and when [*Ag*] is very large $1 + K1_{eq}[Ag] \cong K1_{eq}[Ag]$ and the relationship becomes concentration independent.

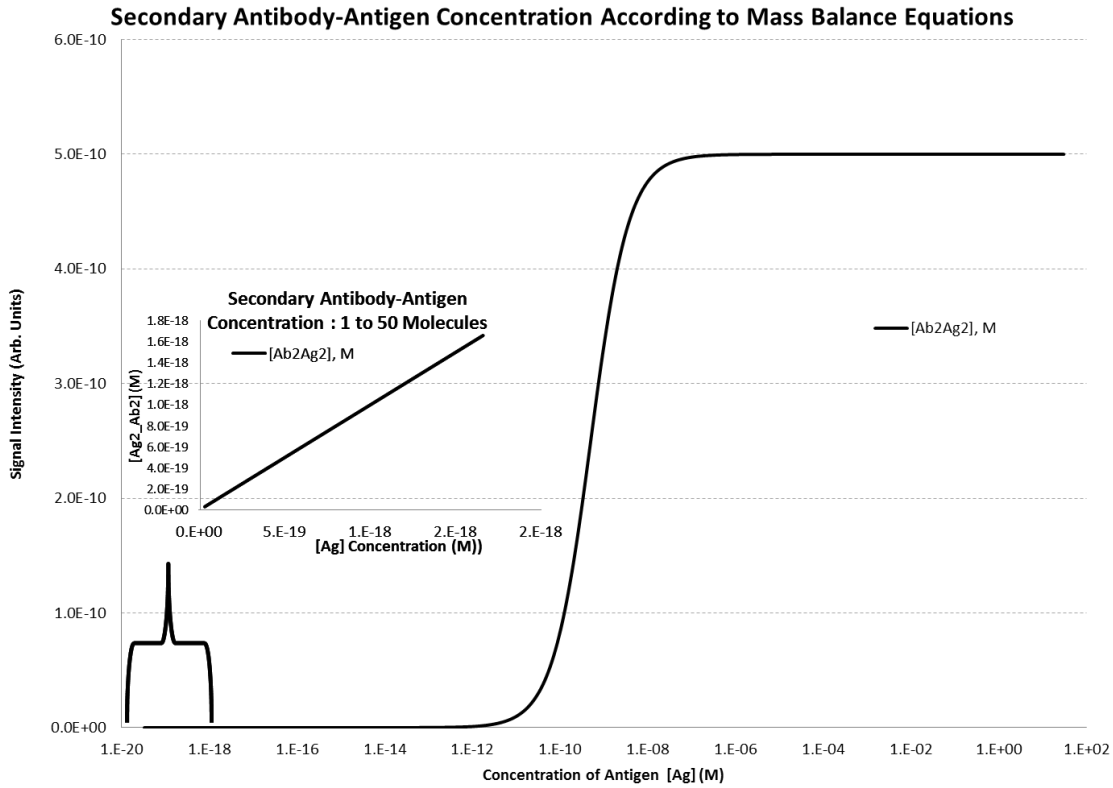

Figure 5.2. Log plot showing the concentration of antigen (log[*Ag*]) bound ([*Ab1Ag*]) to primary antibody from a sample across approximately seventeen orders of magnitude (equation 5.4). This response is a typical sigmoidal-shaped response from the laws of mass action, which is commonly interpreted with four and five parameter sigmoidal fitting models (P4, P5) disconnected from core equilibrium relationships. Inset: Concentration of bound antigen ([*Ab1Ag*]) to primary antibody at low numbers of antigens ([*Ag*]), from single molecule to 600 molecules in 50 microliters (30 zeptomolar to 20 attomolar). Note that across these low concentrations the relationship is linear (inset).

5.2.2 Second Equilibrium, Completion of the Sandwich Assay

For the second step of the sandwich assay, where the detection antibody (labeled appropriately) is introduced, the final complex from step one [*Ab1Ag*] becomes the target antigen for step two. Therefore the bound antigen concentration [*Ab1Ag*] is set equal to the antigen concentration [*Ag2*] as the target of the second incubation. Maintaining the

assumptions outlined during the first incubation process, and going through the same algebraic strategy, from equation 5.4, the amount of antigen present in the second incubation ([*Ag2*]) is equal to the amount bound to the primary antibody in the first incubation ([*AgAb1*]).

$$[AgAb_1] = \frac{K1_{eq}[Ab1_{tot}][Ag]}{(1+ K1_{eq}[Ag])} = [Ag_2] \qquad 5.5$$

From basic immunology equations, the equilibrium constant for the second incubation ($K2_{eq}$) is given in the same format as that for the first incubation ($K1_{eq}$).

$$K2_{eq} = \frac{[Ag_2Ab_2]}{[Ag_2][Ab_2]} \qquad 5.6$$

Given that

$$Ab_2 = [Ab_{2TOT}] - [Ag_2Ab_2] \qquad 5.7$$

we can write

$$[Ag_2Ab_2] = K2_{eq}[Ag_2][Ab_{2TOT} - Ag_2Ab_2] \qquad 5.8$$

which simplifies to

$$[Ag_2Ab_2] = \frac{K2_{eq}[Ab_{2TOT}][Ag_2]}{(1+K2_{eq}[Ag_2]} \qquad 5.9$$

Substitution of equation 5.6 results in the concentration of the signal generating species [*Ab2Ag2*] (M) to be given by

$$[Ag_2Ab_2] = \frac{K2_{eq}[Ab_{2(tot)}]\frac{K1_{eq}[Ab1_{tot}][Ag]}{(1 + K1_{eq}[Ag])}}{(1 + K2_{eq}\frac{K1_{eq}[Ab1_{tot}][Ag]}{(1 + K1_{eq}[Ag])})} \qquad (5.10)$$

where $K2_{eq}$ is the equilibrium association constant (antibody affinity, M^{-1}) for the detection antibody, and [$Ab2_{tot}$] is the total concentration of the secondary antibody (M).

5.2.3 Single Molecule Detection and Fundamental Sources of Noise

Regardless of the detection modality, issues of signal-to-noise, bias and variance can be generalized for any system that has the appropriate conditions to sense the presence of a signal-generating species consistent with a single molecule. Each system will generate a characteristic bias, variance and sensitivity (amplification). To attain 'single molecule sensitivity' (I_{SM}), a signal strength more than to six times the standard deviation (σ) of the noise ($I_{SM}>6\sigma_{noise}$) above the I_{bl} is considered to be unequivocal evidence of distinct signal above noise, generating a 99.73% probability that it statistically represents a positive result (a single molecule is present) if a normal distribution is assumed [38]. To generalize this assessment and examine the best case scenario, the only noise considered is Johnson-Nyquist; an unavoidable fundamental source of noise for all instrumentation [39-41]. Additional fundamental sources of noise (flicker, shot, etc.) can be added to this by summing bias (as expressed by intensity, I, (equal to ΣI_{noise})) and variance (variance is the square of the standard deviation (σ^2), equal to $\Sigma\sigma^2_{noise}$). Other sources of instrumental bias and variance (dark current, environmental noise, etc.) can be similarly summed, the specific values depending on the details of the specific system. The baseline intensity (bias, I_{bl}), in the case of Johnson-Nyquist noise, defines the variance, σ_{bl}^2, by

$$\sigma_{bl}^2 = \sqrt{2qI_{bl}\Delta f} \qquad (5.11)$$

Where q is the charge of an electron, and Δf is the bandwidth (in Hz). Variance also increases with signal intensity, I_s, with the same function, but it is added separately: $\sigma_s^2 = \sqrt{2qI_s\Delta f}$.

5.2.4 Instrumental Background and Noise

There is a broad range of conditions where the relatively high instrument intensity, I_{bl} (and the resulting variance, σ_{bl}^2), or low amplification (ξ) defines the limit of detection. Either the amplification can be insufficient or the instrumental bias and variance may be too high. Whichever effect is the cause, the result is the same. Under these conditions the limit of detection is set at $I_s > 3\sigma_{bl}$, per standard analytical assessment.

5.2.5 Non-Specific Binding

Non-specific binding can influence the LOQ through one of two forms: those arising from the binding of antigen directly to the solid assay surface (and subsequently binding the signaling antibody) and signal antibody binding to the surface independent of the antigen. This source of noise will also have characteristic intensity (bias, I_{NSB}) and variance (σ^2_{NSB}) defined as in equation 5.11. In addition, for very low numbers of molecular interactions, this form of noise can also add molecular shot noise (a minor, rare situation—not considered further).

The sum of the sources of noise and background (E_{system}) in any system gives the relationship

$$E_{system} = I_{bl} + I_{NSB} + \sqrt{\sigma_{bl}^2 + \sigma_{NSB}^2 + \sigma_s^2} \qquad (5.12)$$

where I_{bl} and σ_{bl}^2 are empirically defined functions of the instrumentation used, and I_{NSB}, σ_{NSB}^2, and σ_s^2 are a function of the amplification and binding properties of a system.

5.2.6 Molecular Shot Noise

In an ideal case where instrument noise is minimized and NSB is eliminated, the LOQ is set by Poisson noise (molecular shot noise). This limit arises from the fact that biomolecules are discrete entities and their binding is of a quantum nature, which produces an unavoidable source of error in any detection system, a fundamental signal-to-noise boundary for any assessment. This adds to the variance according to [34]:

$$\frac{\sigma_A}{n_A} = \frac{1}{\sqrt{n_A}} \ . \qquad (5.13)$$

This source of error follows a Poisson statistical distribution for a small number of targets where σ_A is the standard deviation (variance is σ_A^2) of the number of molecular signatures detected (n_A). When NSB and extraneous sources of fluorescent signal are eliminated, the molecular signature is only from the actual number of antigen molecules detected. Improvement in the precision of sampling dilute targets requires the generation and averaging of multiple unique samples, since strongly fluorescent signals from non-antigen specific events may significantly impact the background sampling noise [34]. This sampling statistical effect is different from statistical fluctuations in signal (variance), and represents an intrinsic limit on detection capabilities for a liquid-phase immunoassay (Figure 5.3). This source of error is beyond and separate from the instrumental sources of background (bias) and noise (variance). The sum of the error in any system may be described as:

$$E_{TOT} = E_{MSN} + \frac{E_{system}}{I_{TOT}} \qquad (5.14)$$

where E_{MSN} is error associated with molecular shot noise and I_{TOT} is the total fluorescence intensity detected. Percent error (or uncertainty), $E_{percent}$, is defined:

$$E_{percent} = E_{TOT} * 100 = \left(\frac{1}{\sqrt{N_A}} + \frac{I_{bl} + \sqrt{\sigma_s^2 + \sigma_{bl}^2}}{\xi[Ag] + I_{bl} + \sqrt{\sigma_s^2 + \sigma_{bl}^2}} \right) * 100 \quad (5.15)$$

5.3 Results

The immunoassay signal response was calculated for assays detecting between 1 and $6.7x10^4$ molecules (between 33 zM and 2.2 fM in a 50 µL sample volume). Equilibrium constants were fixed for both $K1_{eq}$ and $K2_{eq}$ at 1.0 x 10^9 M^{-1} to model levels typical of monoclonal antibodies [43,44]. Calculations included elements for instrument bias (background) and variance (noise), non-specific binding, and molecular shot noise. These calculations were used to examine the LODs and LOQs for the three limiting conditions for an immunoassay.

To understand the limits on quantification for immunoassay, three domains are identified, which allow for direct comparison with the ultimate MSN limits. Depending on which source of noise dominates, each imposes limitations on assay quantitation under differing conditions (Table 5.1).

Limiting Factor	Criteria	Assay Limit of Quantitation	Type of Assay
Instrument background noise	$\frac{I_{SM}}{(6\sigma_{bl} + I_{bl})} < 1$	11,000 molecules (0.36 fM)	Traditional laboratory assays
Non-specific binding noise	I_{NSB} is present	~150 molecules and up (5 aM)	Traditional laboratory assays
Molecular shot noise	$I_{SM} > 6\sigma_{bl} + I_{bl}$	~131 molecules (3.7 aM)	Optimized high-sensitivity assay

Table 5.1 shows the limitations of assays based on the type of noise that is responsible for limiting quantitation. When one source of noise is minimized or eliminated quantitation becomes more sensitive until reaching a finite statistical limitation bound by error (uncertainty) due to molecular shot noise. Concentrations are reported for a sample volume of 50 μL.

Table 5.1, along with equation 5.14 (and equation 5.12), demonstrates that different factors can dominate the noise observed in assays depending on experimental conditions. If insensitive or noisy detection instrumentation is used, the background from these machines will dictate the minimum amount of sample that can successfully be quantified. If those limitations are overcome with the incorporation of sensitive detection equipment, assays are typically limited to quantitation in the nano- to picomolar range by NSB effects. NSB creates a minimal background signal that is detected under an assay format without sample present and limits the minimal quantitation that can take place. While it is observed that overall noise increases as signal size increases, the intensity of the noise compared to the intensity of the signal becomes proportionately smaller, resulting in a smaller coefficient of variation (CV) and a greater ability to quantitate the population of specific analytes present.

Since MSN limitations are observed under ideal assay conditions and represent a best case scenario, the impact of MSN on the LOQ is addressed first. Following this, influences from NSB and instrumental background, sources of uncertainty that must be

minimized or eliminated to observe the effects of MSN, are analyzed to illustrate further limitations on the LOQ that may be present in experimental immunoassays.

When detection systems used are capable of single molecule recognition ($I_{SM} > (6\sigma_{noise} + I_{bl})$) and NSB is eliminated, the effects of molecular shot noise are apparent (Figure 5.3). Plots were generated to explore conditions where assay quantification is limited only by molecular shot noise (Equation 5.13). Beyond defining the ultimate LOD and LOQ, operating in the regime required for single molecule sensitivity does not influence the rest of the classic sigmoidal curve, except that it may limit the dynamic range of the overall measurement due to instrumental linearity being exceeded by operating in a high amplification mode. Plotting the percent error normalized to the first data point intensity (error bars = $E_{percent}$ x total intensity (one molecule)) (Figure 5.3 inset) as error bars on the Total Intensity values gives an indication of the accuracy with which measurement can be made. Along with total intensity, the signal and instrument background and noise are plotted. While the detection limit is set to single molecule limit, the uncertainty (expressed as error) of the measurement still contributes finite error.

Another method to examine the same calculations is to plot contributions to percent error ($E_{percent}$) for the different sources at low molecule counts (Figure 5.3, bottom). The signal intensity is linear with increasing concentration, whereas the error in the measurement grows dramatically at low molecular counts, dominated by molecular shot noise with some influence from residual instrumental variance. Under these conditions, the LOD is one molecule (30 zM) and LOQ is 131 molecules (3.7 aM). Note to effectively eliminate the instrumental influence, the amplification must be increased two-hundred-fold or instrument bias and variance must decrease by a thousand-fold.

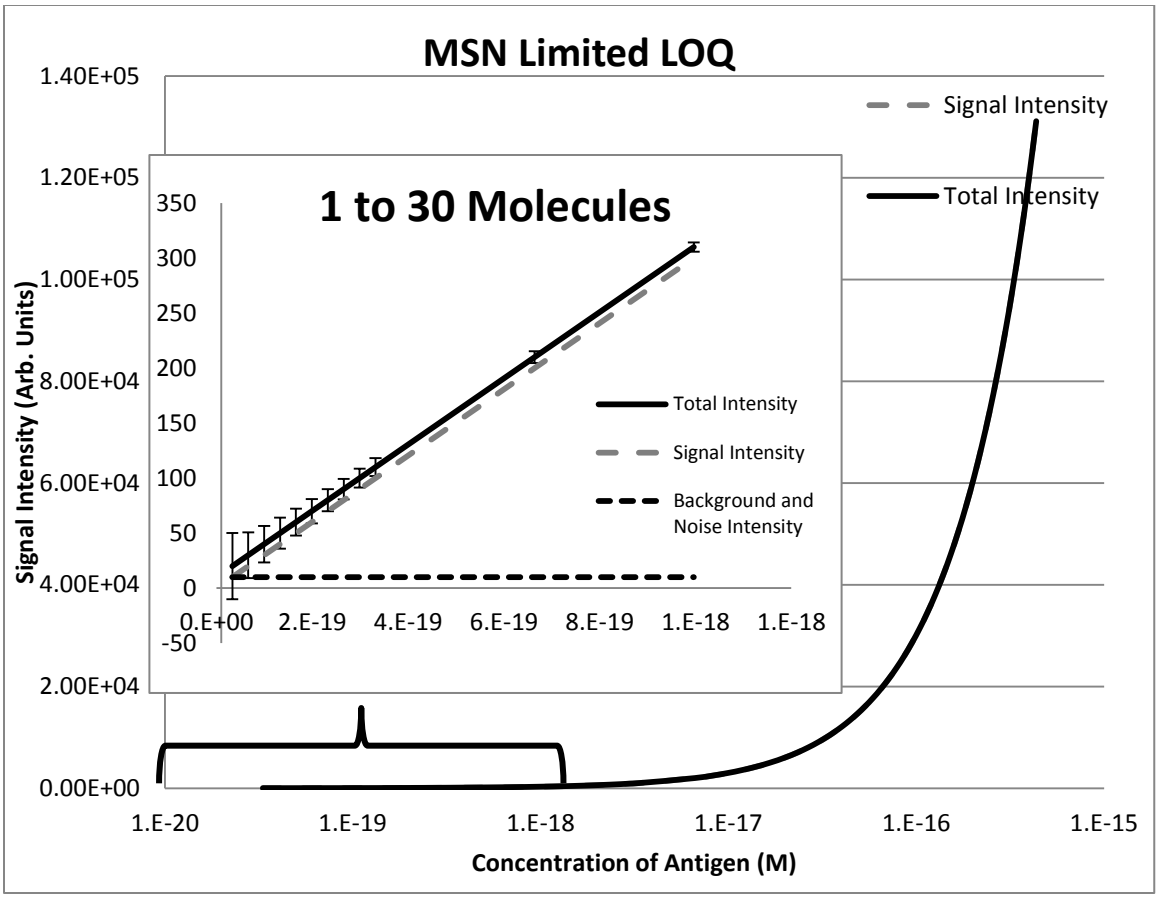
MSN Limited LOQ
1.40E+05
1.20E+05
1.00E+05
8.00E+04
6.00E+04
4.00E+04
2.00E+04
0.00E+00
Signal Intensity (Arb. Units)
1.E-20
1.E-19
1.E-18
1.E-17
1.E-16
1.E-15
Concentration of Antigen (M)
Signal Intensity
Total Intensity
1 to 30 Molecules
350
300
250
200
150
100
50
0
-50
0.E+00
2.E-19
4.E-19
6.E-19
8.E-19
1.E-18
1.E-18
Total Intensity
Signal Intensity
Background and Noise Intensity

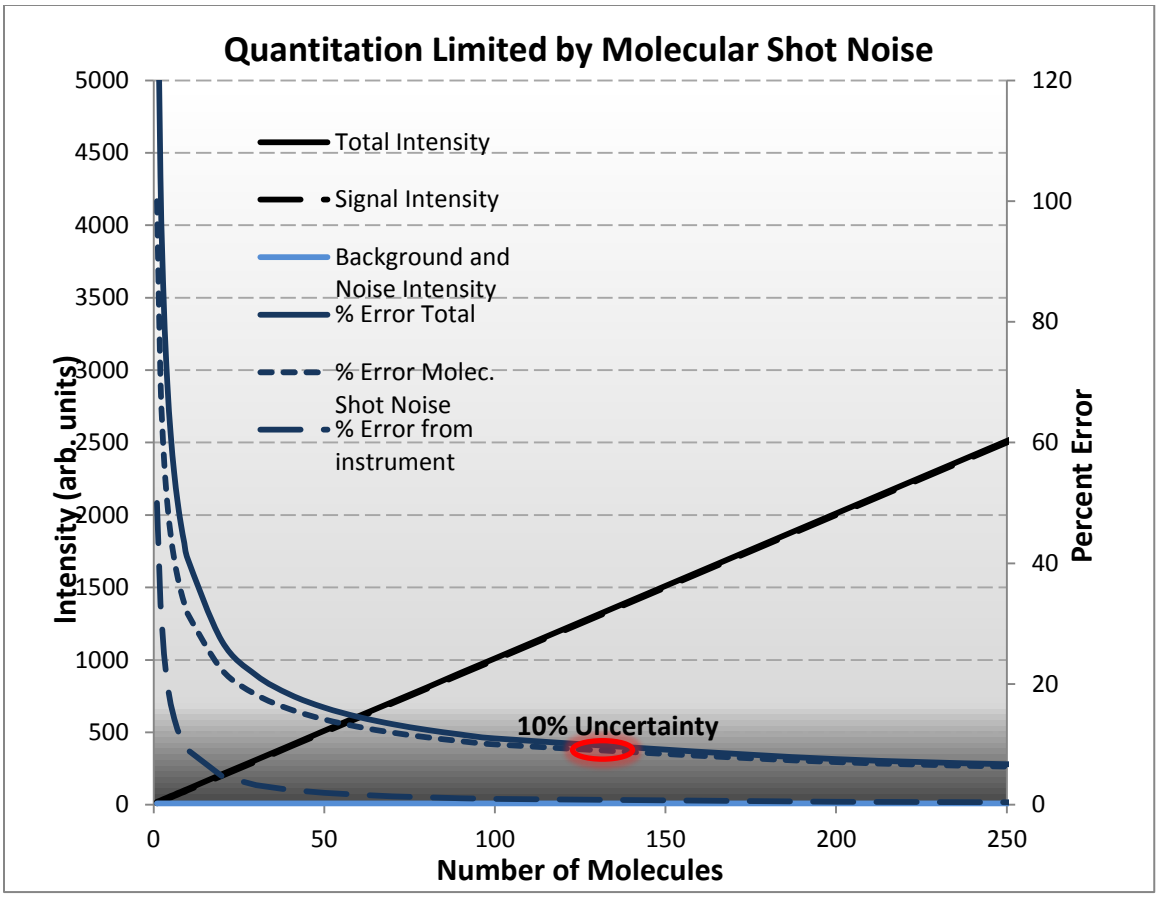

Figure 5.3 Plots illustrating the impact of error from molecular shot noise and residual instrumentation effects on LOD and LOQ. Total Intensity (Equation 5.10 + Equation 5.12), Signal Intensity (Equation 5.10) and Background and Noise Intensity (Equation 5.12) were plotted. Variables set at I_{bl}=10, σ_{bl}=2.38x10^{-4}, and ξ=(I_{bl}+6σ_{noise})=10. Error bars represent percent error. Top: large range of concentration of antigen to emphasize that most of the curve is not influenced by molecular shot noise (signal intensity and total intensity lines overlap). Inset: molecular shot noise generates significant error for small numbers of molecules, error bars are equivalent to the percent error associated with the measurement multiplied by the intensity of a single molecule and reach an acceptable %CV (below 10% error) at 131 molecules. Note instrumentation bias and variance contributes a minor, almost negligible, error. Bottom: Plot of the assay-specific signal intensity (Equation 5.10) the total intensity of the assay (Equation 5.10 + Equation 5.12) and the baseline intensity (Equation 5.12) (left-axis) versus the assay variance from molecular shot noise (Equation 5.13 * 100%) the total variance in signal intensity (Equation 5.15 * 100%) and the variance from the instrument (Equation 5.15 * 100% with MSN equal to 0; right axis). Darker background indicates increase error in the measurement. Total assay variation reaches a level of 10% error when there are fewer than ~131 molecules (approximately 3.7 attomolar in 50 μL) in a sample.

While typical conditions were used for the investigation of MSN (detection system capable of single molecule detection, equilibrium constants of monoclonal antibodies held at 1.0 x 10^9 M^{-1} for both $K1_{eq}$ and $K2_{eq}$) to provide a representative analysis of immunoassay capabilities, antibody properties do influence the fundamental LOQ (Table 5.2). Increasing the equilibrium constant of one or both antibodies can improve the limit of quantitation to approximately 113 molecules. Increases in the equilibrium constant beyond that do not impact this fundamental limit strongly (increasing both $K1_{eq}$ and $K2_{eq}$ to 1.0 x 10^{11} M^{-1} only lowered the limit of quantitation to 111 molecules). The effects of antibody properties are greater when antibodies with below average equilibrium constants are used. By using only one antibody with a K_{eq} of 1.0 x 10^8 M^{-1} raised the LOQ to 277 molecules (9.2 aM in 50 μL). Based on the assumptions stated previously by modeling an immunoassay based on the laws of mass action, systems are considered to be at equilibrium [36]. An excess of both capture and detection antibody are used such that it is determined that all antigen in a system is bound and dissociation is not assumed to occur on the time scale of the experiment. If dissociation of the target compounds does occur after either wash step in a typical assay, the limit of quantitation would increase. Under optimal circumstances 131 molecules must be specifically detected to afford quantitation with a CV below an acceptable threshold (<10%).

$K1_{eq}$	$K2_{eq}$	LOQ (number of molecules)
1X	1X	131
10X	1X	113
1X	10X	113
10X	10X	112
0.1X	1X	277
1X	0.1X	277
0.1X	0.1X	1371

Table 5.2 shows the influence of antibody equilibrium constants on the limit of quantitation. Here, X is defined as $1.0 \times 10^{9}\ M^{-1}$, representing the typical equilibrium constant of a monoclonal antibody [43,44]. The impact on the LOQ when this value is increased or decreased by a factor of 10 for one or both of the antibodies used in a sandwich immunoassay is demonstrated.

When NSB has not been effectively eliminated from an immunoassay system, it can limit the LOD and LOQ if the bias and variance of the signal from the NSB exceeds the instrumental bias and variance. To examine this, amplification was placed at single molecule sensitivity (ξ=10). NSB can be introduced into a system at any level, and here will be considered at levels between 30 zM and 0.33 fM (1 and 10,000 molecules in 50 μL) being non-specifically adsorbed and detected (Figure 5.4). With a target concentration held constant at 1 fM, above the range where MSN and instrument background (capable of single molecule detection) influence impact quantitation, NSB was plotted between 30 zM and 0.33 fM. While it is observed that the intensity of the signal produced from NSB is much lower than the intensity of the specific signal, 10% uncertainty is reached with the addition of 83 aM (2500 molecules) non-specifically binding (Figure 5.4, top). This selection of sample concentration was an arbitrary value emphasizing that any and all NSB will decrease detection limits compared to single molecule detection, both in terms of false positive and increased molecular shot noise error. This influence can be similarly observed by comparing the influence of the number

of molecules NSB on the number of specific sample targets required to achieve quantitation (Figure 5.4, bottom).

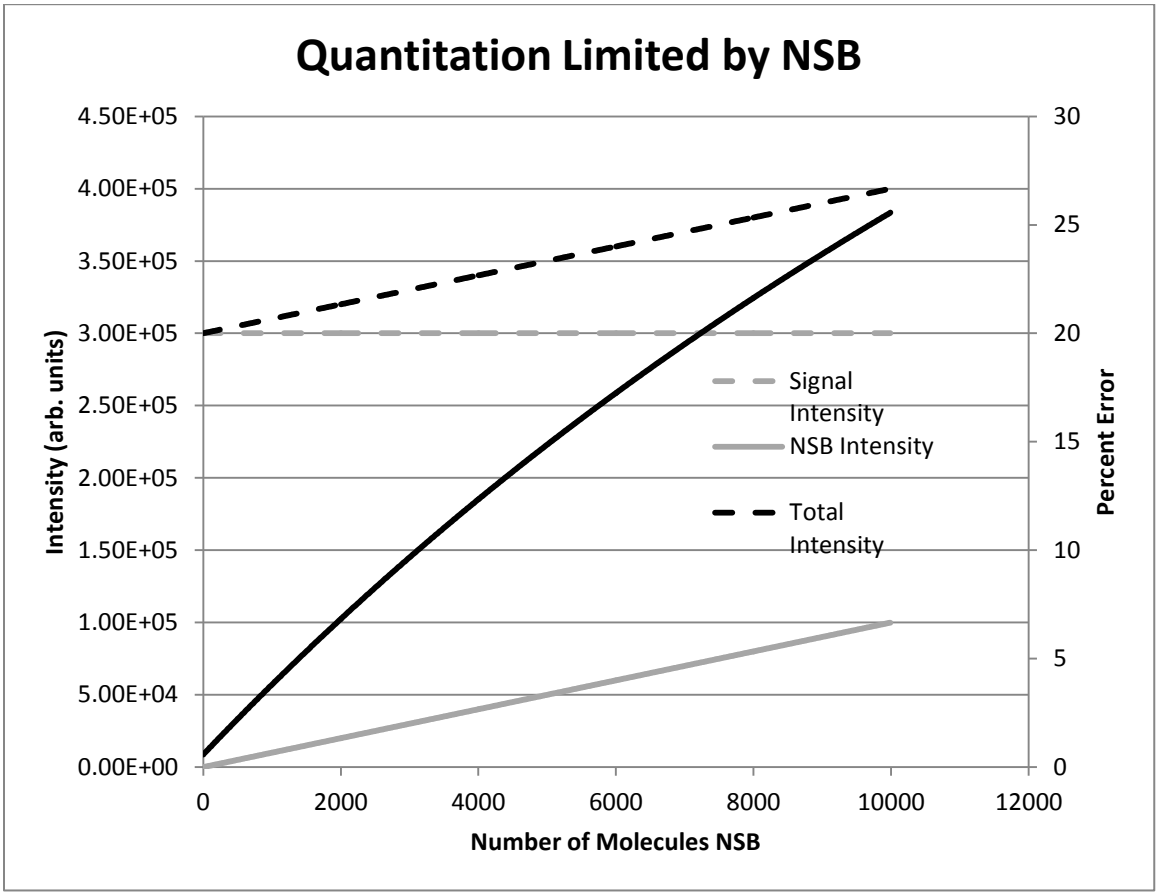

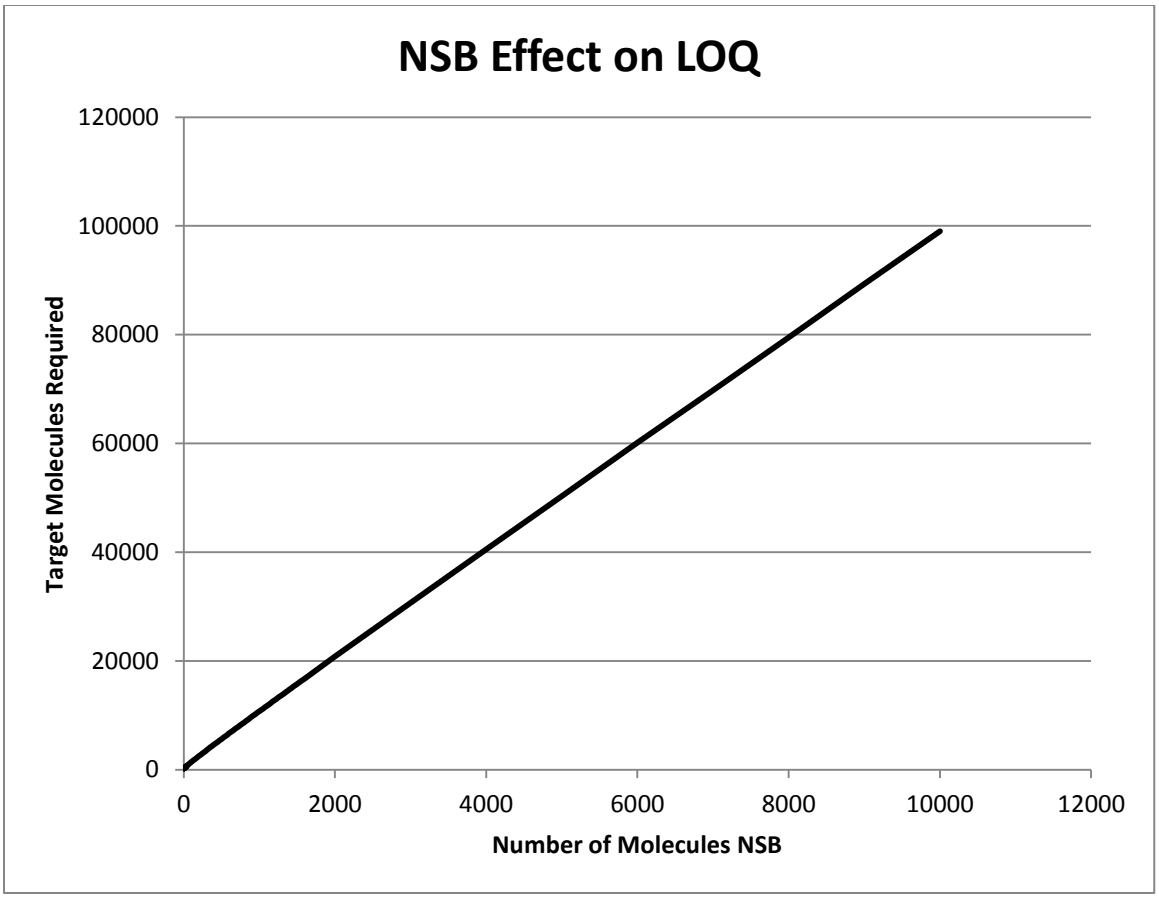

Figure 5.4 Plot illustrating LOD and LOQ defined by non-specific binding properties. Variables set at I_{bl}=10, σ_{bl}=2.38x10^{-4}, and ξ=(I_{bl}+6σ_{noise})=10 and modeled for a specific target concentration of 1 fM. The intensity (bias, I_{NSB}) and standard deviation (noise, σ_{NSB}) were modeled for values between 0 and 10^4 molecules NSB and included according to Equation 5.12. Top: The Signal Intensity (Equation 5.5), Total Intensity (Equation 5.10 + Equation 5.12), and NSB (I_{NSB}) were plotted and compared to Percent Error (Equation 5.10). Note the signal from NSB influences quantification far beyond the number adsorbed entities, reaching the LOQ at 2500 molecules (83 aM) non-specifically absorbed. Bottom: As the number of molecules non-specifically binding increases, the concentration of target molecules required to reach the LOQ increases.

Historically, the LOD and LOQ were determined by the capabilities of the detection system, generating low amplification of signal or high instrument bias and variance (Figure 5.10). Reducing the amplification (ξ) or increasing the background (I_{bl}) of the instrument produced a similar impact on quantitation abilities. This relationship between signal amplification and background is modeled considering Johnson noise only

to examine the best case scenario as described previously where $I_{SM} > 6\sigma_{noise}$ above I_{bl} and noise is modeled according to equation 5.11. The transition towards instrumentation capabilities being the limiting factor occurs when $\xi/(\frac{I_{bl}}{6}+\sigma_{bl}) = \xi/(\frac{I_{bl}}{6} + \sqrt[4]{2qI_{bl}\Delta f}) = 6$. When the ratio is less than six, the signal from a signal molecule is no longer distinguishable above noise and the system is limited by instrumental considerations. For this data, the ratio was set at 1/1000th of the transition value (I_{bl}=10, σ_{bl}=2.38x10^{-4}, $\xi=(I_{bl}+6\sigma_{noise})/1000$=0.01). Any value less than six can illustrate this point, but this value minimum that gave clear and instructive graphical information over a range of antigen concentrations. For these conditions, the LOD was ~1100 molecules (37 aM) and LOQ was 1.1x10^4 molecules (0.36 fM).

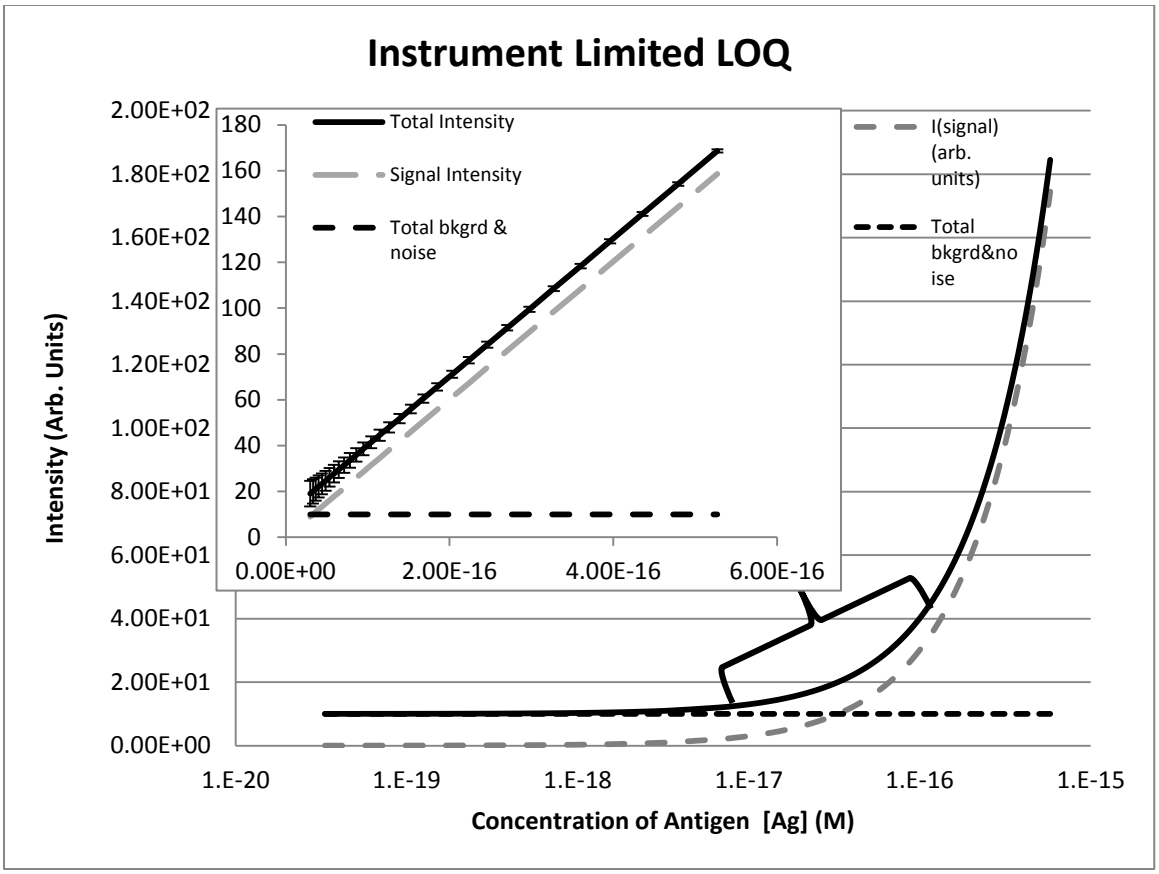

Figure 5.5 Plot illustrating limited amplification or increased background bias and variance resulting in LOD and LOQ being defined by the characteristics of instrumentation. Total Intensity (Equation 5.10 + Equation 5.12), Total Background and Noise (Equation 5.12), and Signal Intensity (Equation 5.10) were plotted versus antigen concentration [*Ag*] (M). Plot shows signal intensity versus antigen concentration according to immunoassay system of equations. Variables set at I_{bl}=10, σ_{bl}=2.38x10^{-4}, and $\xi=(I_{bl}+6\sigma_{noise})/1000$=0.01.

5.4 Discussion

It is commonly accepted that the sandwich-type immunoassay allows for the most sensitive detection among immunoassay formats [30]. With optimal instrumental detection capabilities, the theoretical quantification limit of the sandwich assay depends on the reaction binding constant, the percent of the reaction volume required for measurement, and the precision associated with the measurement made [16]. Precision in these measurements and the statistical limitations of certainty are important points to

consider in the distinction between the LOD and LOQ. The focus on the LOQ is to ensure that the relative error in a sample measurement remains less than a logical pre-determined fraction of the total signal (<10%) [22,23,25,44].

Practically, the LOQ is affected by both constant and variable sources of noise which must be accounted for in determining finite immunoassay capabilities. The constant sources of noise, arising from detection elements, signal processing, molecular shot noise, thermal noise and Johnson noise will be present throughout any measurement at a defined intensity for a particular system. Variable noise arises predominantly from NSB, which can occur at each step in immunocomplex formation with differing effects. Although binding of the non-target species is less probable than the specific binding of an analyte, in the event that the target compound is present at a low concentration, or in a biological sample, non-specific binding will be a significant contributor to the overall signal [25].

Plots based on the law of mass action were used here to illustrate three sets of conditions dictating the LOQ for immunoassays: a) molecular shot noise, b) non-specific binding, or c) the baseline signal intensity arising from measurement instrumentation. While the focus of this work is the determination of the LOQ based on the sources of uncertainty present in a system, and variation in signal response increases with increasing analyte concentrations [44], above the LOQ the signal-to-noise ratio (SNR) increases and the noise factor ($\frac{total\ output\ noise\ power}{output\ noise\ power\ due\ to\ input\ source}$) decreases [25]. These findings demonstrate that while there may be more total variation in signal at higher analyte concentrations, this variation represents a smaller percentage of the overall signal than fluctuations produced at low sample concentrations. The mass action law was used in

this case to gain insight into fundamental limitations of immunoassay systems. While P4 and P5 fitting models are useful in that they provide reasonable estimates of analyte concentration by back-fitting collected data without incorporating too many parameters, their estimates of error are less reliable than using the law of mass action and they do not allow the ultimate LOQ to be determined [1,35].

More recent models of detection statistics have relied on models built from Bayes' theorem to define the LOD as both the probability that it exceeds a signal for a zero dose and its probability density [1,45]. While the accuracy of determining the LOQ is greatest using a dose-response curve based on the law of mass action, and this analysis allows the determination of fundamental limitations that may not be surpassed, models built from Bayes' theorem provide more rigid requirements for the interpretation of data as a part of routine laboratory analysis compared with traditional P4 or P5 fittings [1]. These models not only use back-fitting, but also right-skewed probability densities to determine the extent of error both in blank calibration samples and those with target analyte present.

When the signal from instrument background is minimized and non-specific binding is effectively eliminated, molecular shot noise is responsible for establishing the fundamental statistical LOQ for immunoassay. In this case uncertainty associated with sample heterogeneity at low analyte concentrations dictates the ultimate limit of quantification (Figure 3, Equation 10). The assay plots show that regardless of sample volume, in order to establish certainty in the quantification of an analyte, there must be a minimum of 131 molecules specifically detected. Because the error associated with molecular shot noise, coupled with a minimal variance from the instrument and baseline,

below this number of molecules corresponds to a coefficient of variation greater than 10% the sample may only be potentially detected, not quantified. Establishing a fundamental limitation to the LOQ is important both in the design of immunoassay platforms and the evaluation of existing techniques. As detection instrumentation has improved to the point where sensing a single molecule is possible, many claims of single-molecule immunoassays have been made [26-28]. However, despite using instrumentation capable of sensing individual signals, the actual limits of quantitation are much higher, falling in the aM range and reaching a minimum of 800 molecules quantified [28]. While claims of single molecule detection have not yet successfully approached the fundamental LOQ imposed by MSN, it is necessary to quantitatively establish this absolute limit and assess the impact of additional noise sources that may be present in an experimental immunoassay such that new assays may be appropriately designed to meet the quantitation requirements of specific target species.

Beyond the limitations imposed by MSN, quantification can be impacted by uncertainty bias and variance introduced through non-specific binding. Non-specific binding must always be considered when discussing limit of quantitation for immunoassay. While MSN imposes a fundamental LOQ for immunoassays that cannot be improved, NSB is likely to occur to some extent in experimental immunoassay systems. It is particularly relevant in assays used for medical diagnostics, where desired targets are of relatively low concentration and present in a highly complicated sample. When present, NSB will impose a further limit on the minimal concentration quantified by a given system. This can be observed in that when even one molecule binds non-specifically the LOQ increases from 4.3 to 5.0 aM (Figure 4, bottom).

When background noise from the instrument is higher than the signal intensity arising from molecular shot noise or non-specific binding, the limit of quantification is dependent only upon what can be effectively distinguished from this baseline signal. When the LOQ is dictated by the instrumentation, the effects of MSN are of minimal importance due to the higher numbers of target analyte required for a sample to be recognized above the background noise. For a given instrumental system this background noise is a constant source and cannot be altered by adjusting experimental parameters. However, with the use of a highly sensitive detection instrument capable of sensing the presence of a single molecule, background noise can be sufficiently lowered leading to quantitation bound by the limits of the assay itself.

5.5 Concluding Remarks

Due to the high specificity of the interaction between antibodies and antigens, immunoassays provide a valuable tool when sensitive detection is required. Often, these assays are used to determine the concentration of a particular biologically relevant target. When used as a quantitative tool, the limitations of immunoassays have a theoretical floor bound by molecular shot noise. While detection may still take place below this limit, it can only be considered *qualitative* since the uncertainty (error) associated with the measurement becomes too great (above 10%). While practical limitations, like non-specific binding or baseline instrumental noise, may result in a higher LOQ for experiments, there cannot be *quantitation* with acceptable certainty if samples contain fewer than 131 detected antigen target molecules since signal outputs will be formed from rare events and be subject to statistical sampling effects. Therefore, true

quantification limits lie not at the single molecule level, but in the atto- to femtomolar, or poorer, range.

The models employed here to establish the fundamental qualitative ability for noncompetitive sandwich immunoassays can be employed to assess the ability of an experimental design to quantify targets under the parameters that will be used. This provides a valuable tool for predicting the utility of an assay for its intended application, as well as an aid in the assay design process.

5.6 References

[1] Brown, E. N., McDermott, T. J., Bloch, K. J., McCollom, A. D., *Clinical Chemistry* 1996, *42*, 893-903.

[2] Ekins, R., Kelso, D., *Clin. Chem.* 2011, *57*, 372-375.

[3] Cook, D. B., Selt, C. H., *Clinical Chemistry* 1993, *39*, 965-971.

[4] Miles, L. E. M., Hales, C. N., *Nature* 1968, *219*, 186-189.

[5] Ishikawa, E., Hashida, S., Kohno, T., Hirota, K., *Clinica Chimica Acta* 1990, *194*, 51-72.

[6] Ylander, P. J., Hanninen, P., *Biophysical Chemistry* 2010, *151*, 105-110.

[7] Klenin, K. V., Kusnezow, W., Langowski, J., *J. Chem. Phys.* 2005, *122*, 214715-1-214715-11.

[8] Rodbard, D., Feldman, Y., *Immunochemistry* 1978, *15*, 71-76.

[9] Sadana, A., Chen, Z., *Biosensors and Bioelectronics* 1996, *11*, 17-33.

[10] Werthen, M., Nygren, H., *Journal of Immunological Methods* 1988, *115*, 71-78.

[11] Nygren, H., Werthen, M., Stenberg, M., *Journal of Immunological Methods* 1987, *101*, 63-71.

[12] Nygren, H., Stenberg, M., *Immunology* 1989, *66*, 321-327.

[13] Stenberg, M., Nygren, H., *J. theor. Biol.* 1985, *113*, 589-597.

[14] Stenberg, M., Stiblert, L., Nygren, H., *J. theor. Biol.* 1986, *120*, 129-140.

[15] Beumer, T., Haarbosch, P., Carpay, W., *Anal. Chem.* 1996, *68*, 1375-1380.

[16] Pesce, A. J., Michael, J. G., *Journal of Immunological Methods* 1992, *150*, 111-119.

[17] Stenberg, M., Nygren, H., *Journal of Immunological Methods* 1988, *113*, 3-15.

[18] Rodbard, D., Feldman, Y., Jaffe, M. L., Miles, L. E. M., *Immunochemistry* 1978, *15*, 77-82.

[19] Jackson, T. M. , Ekins, R. P., *Journal of Immunological Methods* 1986, *87*, 13-20.

[20] Glass, T. R., Ohmura, N., Saiki, H., *Anal. Chem.* 2007, *79*, 1954-1960.

[21] Seth, J., *Clinical Chemistry* 1990, *36*, 178.

[22] Kalman, S. M., Clark, D. R., Moses, L. E., *Clin. Chem.* 1984, *30*, 515-517.

[23] Currie, L. A., *Analytical Chemistry* 1968, *40*, 586-593.

[24] Yalow, R. S., Berson, S. A., *Nature* 1959, *184*, 1648-1649.

[25] Hassibi, A., Vikalo, H., Hajimiri, A., *Journal of Applied Physics* 2007, *102*, 014909-1-014909-12.

[26] Rissin, D. M., Kan, C. W., Campbell, T. G., Howes, S. C., Fournier, D. R., Song, L., Piech, T., Patel, P. P., Chang, L., Rivnak, A. J., Ferrell, E. P., Randall, J. D., Provuncher, G. K., Walt, D. R., Duffy, D. C., *Nature Biotechnology*, 2010, *28*, 595-599.

[27] Tessler, L. A., Mitra, R. D., *Proteomics* 2011, *11*, 4731-4735.

[28] Schmidt, R., Jacak, J., Schirwitz, C., Stadler, V., Michel, G., Marme, N., Schutz, G. J., Hoheisel, J. D., Knemeyer, J. P., *Journal of Proteome Research* 2011, *10*, 1316-1322.

[29] Hashida, S., Ishikawa, E., *J. Biochem.* 1990, *108*, 960-964.

[30] Ohmura, N., Lackie, S. J., Saiki, H., *Anal. Chem.* 2001, *73*, 3392-3399.

[31] Chang, L., Rissin, D. M., Fournier, D. R., Piech, T., Patel, P. P., Wilson, D. H., Duffy, D. C., *Journal of Immunological Methods* 2012, *378*, 102-115.

[32] Shalev, A., Greenberg, A. H., McAlpine, P. J., *J. Immunol. Meth.* 1980, *38*, 125-39.

[33] Harris, C. C., Yolken, R. H., Krokan, H., Hsu, I. C., *Proc. Natl. Acad. Sci. USA* 1979, *76*, 5336-5339.

[34] Hungerford, J. M., Christian, G. D., *Anal. Chem.* 1986, *58*, 2567-2568.

[35] Diamandis, E.P., Christopoulos, T.K., *Immunoassay* (theory of immunoassays CH 3) 1996, 25-49.

[36] Ezan, E., Tiberghien, C., Dray, F., *Clin. Chem.* 1991, *37*, 226-230.

[37] Yalow, R., *Diabetes*, 1961, *10*, 339-344.

[38] Ractliffe, J. F., *Elements of Mathematical Statistics*, (the normal distribution CH 7) 1967, 51-68.

[39] Ewing, G.W., *Chemical Instrumentation: XXXIX. Signal to Noise Optimization in Chemistry.* Chemical Education, 1968. *45*(7): p. A533-A544.

[40] Johnson, J.B., *Thermal Agitation of Electricity in Conductors.* Physical Review, 1928. *32*(1): p. 97-109.

[41] Nyquist, H., *Thermal Agitation of Electric Charge in Conductors.* Physical Review, 1928. **32**(1): p. 110-113.

[42] Abcam plc., 2015, http://www.abcam.com/index.html?pageconfig=resource&rid=15749&source=pagetrap&viapagetrap=kd.

[43] Voet, D., Voet, J.G., Pratt, C.W., *Fundamentals of Biochemistry* (Antibodies Section 7.3) 2008, 209-215.

[44] Guo, Y., Harel, O., Little, R. J., *Epidemiology* 2010, *21*, S10-S16.

[45] O'Malley, A.J., Deely, J.J., *Aust. N.Z. J. Stat.*, 2003, *45*, 43-65.

CHAPTER 6

IMMUNOASSAY TARGET SAMPLE PREPARATION USING DC GRADIENT INSULATOR DIELECTROPHORESIS

6.1 Introduction

Early illness intervention requires the capability of monitoring relatively small concentration changes in disease indicated species. Because it contains the most comprehensive depiction of the physiological state of an individual, blood, and in particular plasma, has become the primary sample fluid used in clinical diagnostics [1-3]. However, owing to a high dynamic range spanning over 10 orders of magnitude, as well as the presence of a few high abundance proteins (albumin, immunoglobulins, transferrin, haptoglobin, and lipoproteins), detection of species related to specific disease states is challenging [2-4]. Beyond the complexity of the plasma proteome, whole-blood samples also contain cells (platelets, red blood cells, and white blood cells) that may interfere with specific target detection if not removed [5].

Many clinical diagnostic methods rely on biological recognition, through the use of immunoassay techniques [6,7]. The specific interaction between the target molecule and antibody allows for quantitative testing to take place. However, in the use of whole-blood or plasma one-step assays without prior sample simplification cross-reactivity limits the LOQ to the nM to μM range [8,9,10]. With the effective removal of contaminating species, highly sensitive quantitation of target analytes is possible [11-13]. Specific detection at this level is sufficient to quantify the low abundance proteins that are of interest in diagnostics [1,3].

Currently, centrifugation is most commonly used to eliminate cells from a blood sample [14,15]. Sample testing is primarily performed in centralized clinical laboratories and requires relatively large volumes of blood (mL) as well as long analysis times [16]. By moving from a centralized laboratory to portable micro-total analysis systems (μTAS), it is possible to incorporate a separations based strategy such that more information (both from blood cells and protein analysis) can be extracted from a minimal sample volume in a short analysis time. Achieving this minimally invasive, rapid diagnostic ability while maintaining high sensitivity requires sample preparation steps prior to detection. Separation techniques not only allow the removal of cross-reactive species for more sensitive quantitation, but provide the potential for multiplex detection.

Many experimental microfluidic techniques exist for the separation of blood cells from plasma. These technologies include manipulation and separation based on mechanical, inertial, hydrodynamic, optical, magnetic and electrical methods [14,17-20]. Particularly appealing among these techniques is the use of dielectrophoresis (DEP) because it allows the rapid and selective manipulation of neutral (as well as charged) bioparticles in a label-free system [17,21]. When species are introduced into a non-homogeneous electric field they are exposed to a DEP force according to the relation [22]:

$$F_{DEP} = 2\pi\varepsilon_m R^3 CM(\nabla E^2) \qquad \text{Eq. 6.1}$$

where ε_m is the permittivity of the medium the species is placed in, *R* is the radius of the particle, *CM* is the Clausius-Mossotti factor related to the permittivity of the particle compared to that of the medium and *E* is the amplitude of the electric field. While this equation includes some simplifications, assuming that the particle is homogeneous and

uncharged while the induced polarization once the field *E* is applied takes the form of a dipole moment, it is able to accurately predict the reaction of species to the DEP force. DEP has been used successfully to isolate yeast cells [23], prostate cancer cells [24], ccf-DNA [25], and red blood cells [26].

Here, insulator-based DEP (iDEP) was performed in a microchannel with insulating sawtooth features along the channel sides to create an inhomogeneous electric field. The device used is the second-generation iteration of that described in previous work [26], and was employed to remove red blood cells from a sample containing heart-type fatty-acid binding protein (H-FABP) or myoglobin to model the simplification of a blood sample prior to cardiac biomarker detection. Progressive changes to the distance between teeth (gate width) create increasing field strength along the length of the channel. When the magnitude of the DEP force is great enough to counter the effects of the electroosmotic flow (EOF) and electrophoresis (EP) forces driving analyte movement down the channel, species will be trapped. Effective trapping of the red blood cells without affecting protein movement through the channel suggests that this technique could be valuable as a first step in a μTAS system for the analysis of whole-blood where centrifugation is not practical due to the small scale of the system. The small sample volumes required by downstream detection methods are compatible in scale with the volume requirements needed for RBC removal by incorporating iDEP as an initial sample preparation step in a μTAS. This approach allows downstream analysis of proteins using sensitive immunoassay techniques without interference from abundant blood cells and with small sample volume requirements that allow complete analysis of limited samples or routine serial-monitoring of disease progression without becoming invasive.

6.2 Materials and Methods

6.2.1 Microdevice Fabrication

The sawtooth geometry of the microchannel has been previously described (Figure 6.1) [26]. In these experiments the channel length was 4 cm, with a uniform depth of 20 μm. The initial gate width was 73.3 μm and the final gate width was 25.3 μm. The device was fabricated using standard soft lithography techniques. Briefly, the channel was designed using Adobe Illustrator (Adobe Systems Inc., San Jose, CA) and printed onto a chrome-glass photomask (JD Photo-Tools LTD., Oldham, Lancashire, UK). A silicon wafter was made from the photomask using photolithography and dry etching techniques. From the silicon wafer, PDMS casts were made using a Sylgard 184 silicone elastomer kit (Dow Corning Corp., Midland, MI, USA). Access holes were generated using a 3 mm Harris Uni-Core punch (Shunderson Communications Inc., Orleans, Ontario, Canada). Casts were stored at -20°C until use. Prior to device assembly, PDMS casts were washed with isopropanol, acetone, and 18 mΩ water, then sonicated for 30 seconds (Aquasonic ultrasonic cleaner, VWR International, Radnor, PA, USA). Similarly, glass microscope slides (VWR International) were washed and sonicated for 10 seconds. Slides and PDMS casts were dried using N_2 gas and treated with a high level of O_2 plasma for 60 seconds (Plasma Cleaner, Harrick Plasma, Ithaca, NY, USA) before contact sealing. Once sealed, the channel was rinsed with 115 mM sodium phosphate buffer at pH 7.4 and treated with 4 mg/mL BSA to reduce electroosmotic flow (EOF) and prevent nonspecific absorption prior to sample introduction.

6.2.2 Red Blood Cell and Protein Labeling

Fresh whole blood was obtained through fingerstick from a human donor and suspended in 1 mL of isotonic buffer with 1.8 mg/mL ethylenediaminetetraacetic acid (EDTA). The sample was immediately centrifuged and pelleted red blood cells (RBCs) were resuspended in buffer. After three wash steps to remove plasma, the RBC sample was stained as previously described [26]. The final cell pellet was resuspended in 115 mM sodium phosphate buffer at pH 7.4 with a cell count at 111 cells/nL based on the presumed mean corpuscular volume (MCV) of 90 fL [27].

Purified human myoglobin (7.33 mg/mL) was purchased from MyBioSource and used as received. Purified human heart-type fatty acid binding protein (2.02 mg/mL) was purchased from Life Diagnostis and used as recieved. NHS-Rhodamine (Thermo Scientific) was dissolved in DMSO (Invitrogen) to a concentration of 10 mg/mL. Volume of NHS-Rhodamine was added dropwise to myoglobin and the sample was incubated in the dark at room temperature for 1 hour with shaking. Volume of NHS-Rhodamine was added to FABP and reacted in the same manner. Crude reaction mixtures were added to dialysis cups (Thermo Scientific) with a molecular weight cut-off of 3,500 Daltons. Samples were dialyzed in 100 mM PBS, pH 7.2 overnight. Proteins were diluted in the RBCs to ratios of 1:200 μL (MyO) and 3:200 μL (FABP) for analysis in the DEP device.

6.2.3 Experimental

Channels were filled with roughly 10 μL of a mixture of the fluorescently labeled protein and red blood cells and filled through capillary action. Flow was stopped by balancing the menisci at the entrance and exit of the channel through the addition of running buffer to the outlet reservoir. Platinum electrodes (diameter 0.25 mm) were

inserted into the access ports in the PDMS and potentials were applied to the channel using a LabSmith power supply (Series HV5448, LabSmith Inc., Livermore, CA, USA). Potentials ranging from 100 to 500 ΔV were applied globally to the device, resulting in an electric field strength of 25 to 125 V/cm.

Data collection was achieved using an inverted microscope (Olympus IX70) illuminated by a mercury lamp. Light was passed through an Olympus DAPI, FITC, Texas Red triple band-pass cube (Olympus, Center Valley, PA) used for fluorescence microscopy. Video and still images were collected using a CCD camera (QImaging, Inc., Surrey, British Columbia, Canada) connected to image capture software (Streampix 5, NorPix, Montreal, Quebec, Canada). ImageJ (NIH, Bethesda, MD) was used for video analysis. Fluorescence intensity was measured just upstream of gates where capture of RBCs was observed.

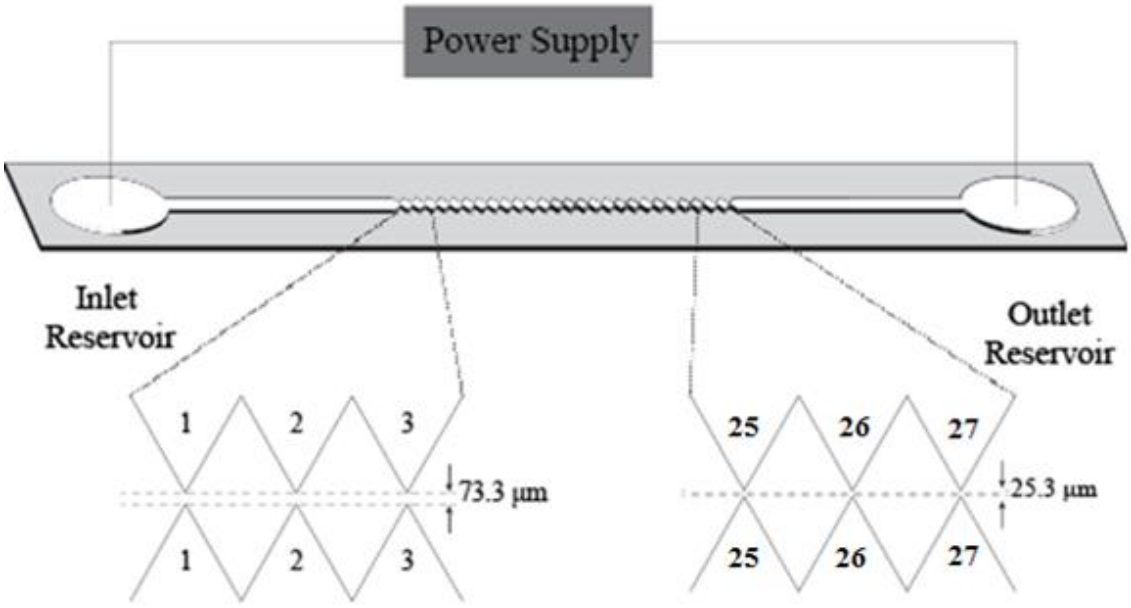

Figure 6.1 Schematic of the iDEP microchannel used. Devices were fabricated from a glass microscope slide and PDMS.

6.3 Results and Discussion

Mixtures of red blood cells with either cardiac biomarker FABP or myoglobin were investigated using the iDEP sawtooth device. The behavior of both species was analyzed at the final set of gates, possessing a gate width of 25.3 μm, and at the end of the microchannel. The magnitude of the electric potential, ranging from 100 to 500 ΔV, was divided by the length of the channel (4 cm) to determine the local electric field strength applied (E_{app}, V/cm).

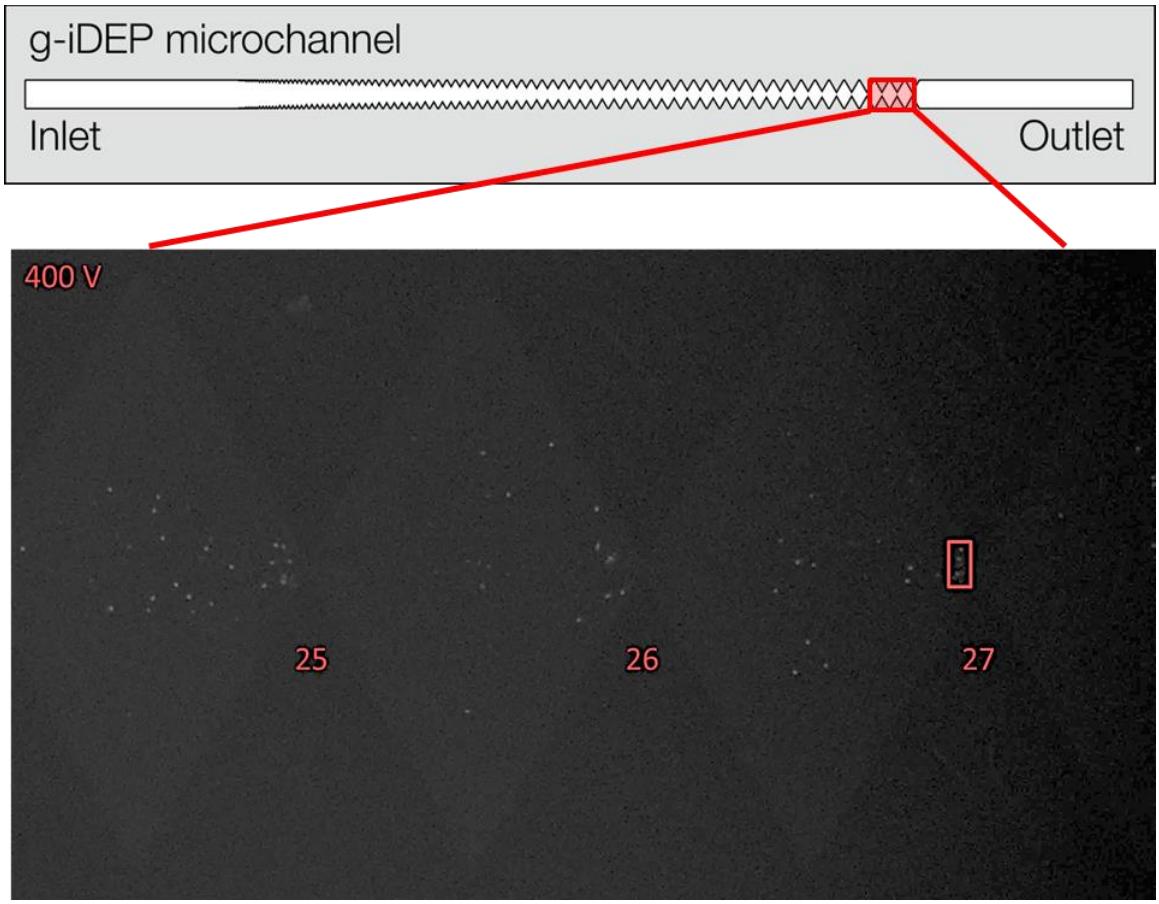

Figure 6.2 Observed capture of RBCs at gate 27 in the presence of H-FABP. Background fluorescence is due to H-FABP while the brightly fluorescent spheres are individual red blood cells. Capture was observed as a cluster of cells immediately upstream from a gate. Red selection shows the region used for fluorescence measurements.

The dielectrophoretic behavior of RBCs was consistent with prior general observations in the sawtooth microchannel [26]. When fluid flow was balanced and potential was applied to the microchannel the bulk motion of particles was oriented toward the outlet reservoir (cathode) due to the combined forces of EP and EOF. Neither RBC or protein capture were observed at any voltage in regions of the channel having a gate width greater than 26.2 μm (size of second-to-last set of gates). In regions with a larger gate width all fluorescent material traveled toward the cathode. Capture was defined by the collection of RBCs immediately prior to a gate (Figure 6.2). As the gate widths become smaller in the microchannel the dielectrophoretic force experienced by the sample increases, reaching a local maxima at the entrance to the gate. Since the negative DEP force opposes the combined forces of EP and EOF, when the DEP force is equal or greater than the combined forces.

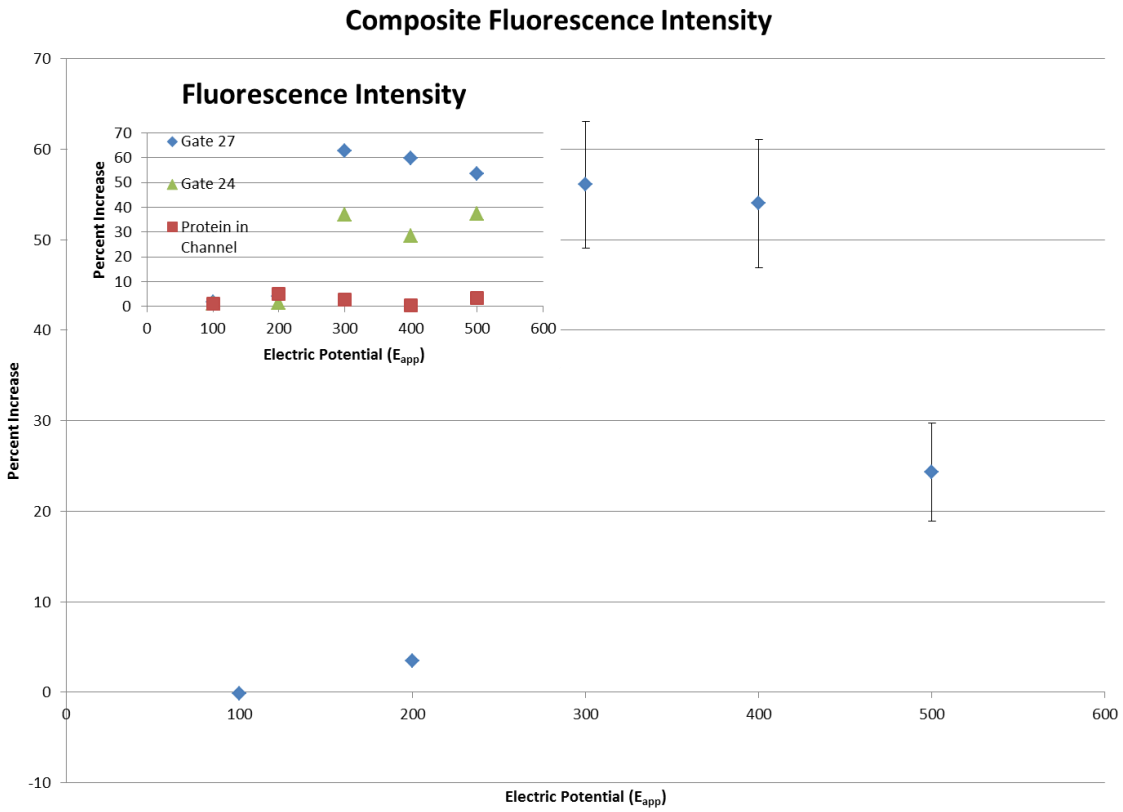

Figure 6.3 Quantitation of red blood cell capture by monitoring fluorescence intensity. Average percent fluorescence increase observed at gates 24 and 27 from 5 different devices and sample preparations of RBCs and FABP. Error bars show the standard deviation. Inset: Percent increase in fluorescence intensity observed at gate 27 after E_{app}. Onset of capture is observed when E_{app} = 300 V (75 V/cm). Capture is observed to a lesser extent at gate 24 with an E_{app} = 300 V. Capture at gate 24 increases with higher E_{app}. At all values of E_{app} the fluorescence intensity of protein within the channel (background fluorescence in channel) is observed to remain unchanged.

The capture of RBCs occurred at 25.3 μm gates with an onset of E_{app} = 300 V applied globally across the device. Capture was observed at 26.2 μm gates minimally at E_{app} = 300 V, with greater material accumulation between E_{app} = 400 and 500 V. The cardiac biomarker proteins were not observed to capture at any E_{app} tested and instead were able to flow freely through the device. Below an E_{app} value of 300 V no capture occurred even at extended time periods of applied voltage. Control studies without protein showed similar capture of RBCs without the diffuse fluorescence observed

throughout the channel in the presence of protein. With an applied voltage meeting the threshold required for RBC capture, material continued to collect during the time voltage was on in regions just prior to a gate. Extent of RBC capture was monitored by determining the local fluorescence intensity increase in regions with observed RBC collection. Repeated experiments show a similar behavior of the RBCs. Figure 6.3 shows the average fluorescence intensity for data collected from 5 different devices with separate preparations of RBCs and H-FABP. Error bars show the standard deviation of data sets.The extent of capture was dependent not only on the E_{app}, but on the location within the channel (Figure 6.3 inset). RBCs were observed to collect at lower voltages and to a greater extent at the smallest gates in the channel before they were captured further upstream. For all values of E_{app} tested, the fluorescence intensity resulting from H-FABP was unchanged. Myoglobin studies produced a similar trend (data not shown). Variables that could not be specifically controlled, such as staining efficiency of the RBCs, contribute to the variance observed between samples. Staining efficiency of the RBCs was determined by inspection of samples at relatively high magnification under both fluorescence and bright-field microscopy. In all cases staining efficiency was observed to be about 45%, but varied between 40% and 50% percent despite identical preparation protocols.

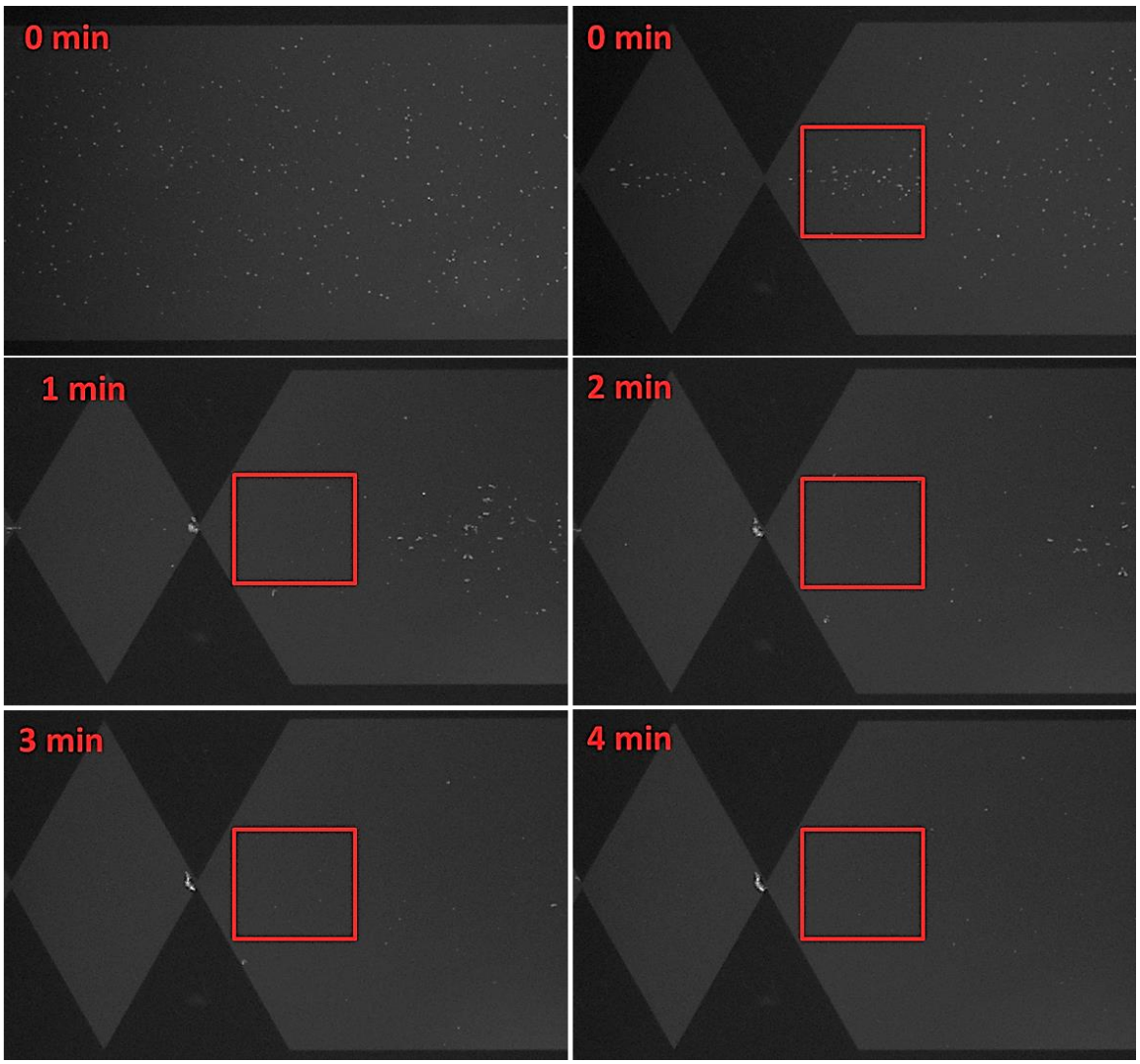

Figure 6.4 Depletion of RBCs in the exit channel beyond the final sawtooth gate. In each image E_{app} is 400 V globally across the device (100 V/cm).

Changes in fluorescence intensity were also measured in a small region directly following the final gate in the microchannel. Using an E_{app} of 400 V to ensure complete capture of RBCs at the 25.3 μm gate, fluorescence was monitored at one minute increments to assess the depletion of RBCs in the sample that could be collected at from the exit reservoir (Figure 6.4). Both visual determination of RBCs present and fluorescence measurements in this region support that, once significant voltage is applied

across the channel, complete capture of RBCs occurs (Figure 6.5). This capture allows simplification of the initial sample, enabling easier quantitation of the protein target in the exit channel.

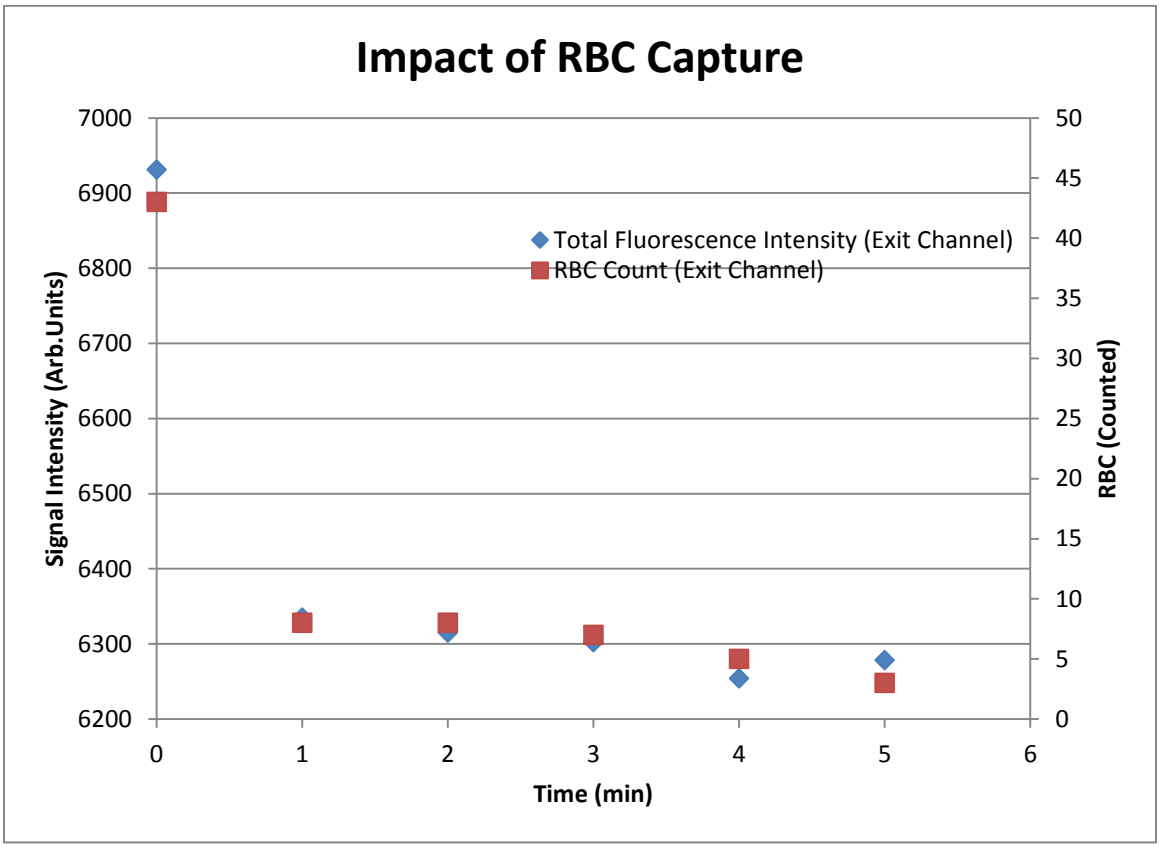

Figure 6.5 A) Fluorescence measurements and **B)** RBC counts present in the exit channel after and E_{app} of 100 V/cm.

Extraction of protein samples was attempted from the exit channel using a hypodermic needle to remove fluid. Under the current configuration of the device, sample removal and quantitation is not practical due to issues in removing a great enough sample volume for off-chip manipulation and detection. While not demonstrated in this work, it is possible that the iDEP channel could be incorporated as the initial sample preparation step in next-generation μTAS for the separation and analysis of complex biological samples. Incorporation of further separation of eluted proteins using electrophoretic

manipulation, which has been demonstrated to be effective in the isolation of charged species [21], as well as on-chip detection through high-sensitivity immunoassay could allow multiplex detection of biomarkers.

6.4 Concluding Remarks

Using an iDEP microdevice with a sawtooth pattern insulated channel the effective removal of RBCs from solutions containing cardiac biomarkers H-FABP or myoglobin. Behavior of the RBCs was consistent with previous observations in an iDEP microchannel [26]. The results shown here indicate that RBCs can be successfully captured using DEP and removed from a sample containing protein species, which were unaffected by the electric potentials applied. Removal of blood cells from plasma samples is a necessary first step in sample preparation prior to quantitative detection in medical diagnostics. While centrifugation techniques are traditionally utilized to achieve cell removal, this method is not practical on a microscale level. Here, it is shown that iDEP can be used as an alternative initial step in sample simplification compatible with incorporation into a μTAS system for the quantitative detection of multiple biomarkers.

6.5 References

[1] Fan, R., Vermesh, O., Srivastava, A., Yen, B.K.H., Qin, L., Ahmad, H., Kwong, G.A., Liu, C.C., Gould, J., Hood, L., Heath, J.R., *Nature Biotechnology*, 2008, *26*, 1373-1378.

[2] Anderson, N.L., Anderson, N.G., *Molecular and Cellular Proteomics*, 2002, *1.11*, 845-867.

[3] Bellei, E., Bergamini, S., Monari, E., Fantoni, L.I., Cuoghi, A., *Amino Acids*, 2011, *40*, 145-156.

[4] Tirumalai, R.S., Chan, K.C., Prieto, D.A., Issaq, H.J., Conrads, T.P., Veenstra, T.D., *Molecular and Cellular Proteomics*, 2006, *2.10*, 1096-1103.

[5] Yan, S., Zhang, J., Alici, G., Du, H., Zhu, Y., Li, W., *Lab Chip*, 2014, *14*, 2993-3003.

[6] Moschallski, M., Evers, A., Brandsetter, T., Ruhe, J., *Analytica Chimica Acta*, 2013, *781*, 72-79.

[7] Moschallski, M., Baader, J., Prucker, O., Ruhe, J., *Analytica Chimica Acta*, 2010, *671*, 92-98.

[8] Martin, R.M., Patel, R., Oken, E., Thompson, J., Zinovik, A., Kramer, M.S., Vilchuck, K., Bogdanovich, N., Sergeichick, N., Foo, Y., Gusina, N., *Plos One*, 2013, *8*, 1-10.

[9] Liang, W., Li, Y., Zhang, B., Zhang, Z., Chen, A., Qi, D., Yi, W., Hu, C., *Biosensors and Bioelectronics*, 2012, *31*, 480-485.

[10] Tachi, T., Kaji, N., Tokeshi, M., Baba, T., *Lab on a Chip*, 2009, *9*, 966-971.

[11] Zhang, B., Liu, B., Zhou, J., Tang, J., Tang, D., *Applied Materials and Interfaces*, 2013, *5*, 4479-4485.

[12] Chandra, P., Abbas Zaidi, S., Noh, H.B., Shim, Y.B., *Biosensors and Bioelectronics*, 2011, *28*, 326-332.

[13] Svateck, R.S., Shah, J.B., Xin, J., *et al*., *Cancer*, 2010, *116*, 4513-4519.

[14] Carlo, D.D., Edd, J.F., Irimia, D., Tompkins, R.G., Toner, M., *Analytical Chemistry*, 2008, *80*, 2204-2211.

[15] Javanmard, M., Emaminejad, S., Gupta, C., Provine, J., Davis, R.W., Howe, R.T., *Sensors and Actuators B*, 2014, *193*, 918-924.

[16] Dimov, I.K., Basabe-Desmonts, L., Garcia-Cordero, J.L., Ross, B.M., Ricco, A.J., Lee, L.P., *Lab on a Chip*, 2011, *11*, 845-850.

[17] Li, M., Li, W.H., Zhang, J., Alici, G., Wen, W., *Journal of Physics D: Applied Physics*, 2014, *47*, 1-30.

[18] Jung, J., Han, K.H., *Applied Physics Letters*, 2008, *93*, 223902-1-3.

[19] Gossett, D.R., Carlo, D.D., *Analytical Chemistry*, 2009, *81*, 8459-8465.

[20] VanDelinder, V., Groisman, A., *Analytical Chemistry*, 2007, *79*, 2023-2030.

[21] Demircan, Y., Ozgur, E., Kulah, H., *Electrophoresis*, 2013, *34*, 1008-1027.

[22] Pethig, R., *Biomicrofluidics*, 2010, **4**, 022811-1-35.

[23] Zhu, H., Lin, X., Su, Y., Dong, H., Wu, J., *Biosensors and Bioelectronics*, 2015, *63*, 371-378.

[24] Huang, C., Liu, H., Bander, N.H., Kirby, B.J., *Biomed Microdevices*, 2013, *15*, 941-948.

[25] Sonnenberg, A., Marciniak, J.Y., Skowronski, E.A., Manouchehri, S., Rassenti, L., Ghia, E.M., Widhopf II, G.F., Kipps, T.J., Heller, M.J., *Electrophoresis*, 2014, *35*, 1828-1836.

[26] Jones, P.V., Staton, S.J.R., Hayes, M.A., *Anal Bioanal Chem*, 2011, *401*, 2103-2111.

[27] Turgeon, M.L., *Clinical Hematology: Theory and Procedures* (Principles of Blood Collection, CH 2), 2004, 18-40.

CHAPTER 7

ISOLATION OF CARDIAC BIOMARKER PROTEINS USING ELECTROPHORETIC EXCLUSION

7.1 Introduction

In clinical diagnostics the parallel detection of biomarker proteins is of particular importance since no single marker has proven to have sufficient diagnostic accuracy for AMI, or a variety of other conditions in which early detection may improve prognosis [1-3]. In the case of clinical diagnostics, plasma has become the primary sample fluid used because it contains the most complete version of the human proteome, including both classical plasma proteins as well as those present from tissue leakage [4-6]. While the protein content in plasma holds great diagnostic potential, protein concentrations in plasma span over 10 orders of magnitude and species of interest such as biomarkers are often present in very low concentrations [5-7]. Multiplex testing has been performed in many cases through batch incubation using monoclonal antibodies specific to each target species [8,9]. However, when the quantification of species from a complex primary sample is required, the potential for cross-reactivity becomes a significant concern [10,11].

In recent years, several microfluidic scale separation-based techniques have been employed as a sample pre-treatment step in the analysis of plasma [12-18]. These techniques include the use of physical barriers to filter the sample [12,13], as well as electrophoretic separation methods [14-18]. Of particular interest among electrophoretic separation techniques are those that operate using counter-flow along with a gradient for the isolation and concentration of target species [16-18]. While counter-flow separations

have been achieved through pH or conductivity focusing, the use of an electric field gradient allows isolation and concentration to occur outside a separation channel.

The use of an electric field gradient as a counter to hydrodynamic flow, termed electrophoretic exclusion, was first used to isolate small molecules [18]. This technique enables the separation of species having different electrophoretic mobilities (μ_a). Assuming that hydrodynamic flow and buffer conditions remain constant throughout sample manipulation, the strength of an applied electric field may be altered to separate target species based on these differences. Exclusion of a target species from a channel is accomplished by maintaining a constant electric field across reservoirs connected to channels in a device and introducing a sharp electric field gradient in microchannels connecting these reservoirs. When the electrophoretic velocity of a target species (v_a), according to:

$$v_a = \mu_a E \qquad 7.1$$

My work was performed as an extension of investigations performed in a microdevice demonstrating the first use of electrophoretic exclusion to separate small molecules on a microscale, as well as the use of a macroscale benchtop device for the manipulation of proteins [18, 19]. The development of a separations-based array previously allowed for the isolation of multiple small molecules and has been shown here to be effective in the exclusion and concentration three cardiac biomarker proteins [20]. The device contains three separation channels connected in parallel to form an array [12]. With electric field gradients applied at the entrance of channels connecting the reservoirs within the array, the magnitude of the electrophoretic velocity can be manipulated until it balances the hydrodynamic flow and prevents the entry of target species resulting in concentration

within a reservoir. The ability to separate and concentrate these target molecules provides a foundation for the development of a micro-total analysis system (μTAS) offering parallel quantitation of biomarker panels from untreated whole blood samples. This method allows downstream analysis of proteins using sensitive immunoassay techniques without interference from abundant plasma proteins and with small sample volume requirements that allow complete analysis of limited samples or routine serial-monitoring of disease progression without becoming invasive.

7.2 Materials and Methods

7.2.1 Microdevice Fabrication

A photograph of the device used for protein separation (top view) and a schematic of the array is shown (Figure 7.1A). The hybrid glass/PDMS array was used for all experiments. Each device contained a large entrance reservoir, three central reservoirs and three exit reservoirs connected by separation channels. The development of this device has been discussed previously [1,2], and is briefly discussed below.

7.2.1.1 PDMS

A single separation array consisted of an entrance reservoir connected to a three central and exit reservoirs through separation channels. The entrance reservoir was 19 mm x 5 mm, all central and exit reservoirs were 5 mm x 5 mm and channels were 1 mm long and 100 μm wide with a uniform depth of 10 μm throughout the device. Masks were designed using Illustrator (Adobe, San Jose, CA, USA) and were printed on a transparency using a resolution of 65,000 dpi (Fine Line Imaging, Colorado Springs, CO, USA). Positive photoresist AZ 4620 was spun onto a silicon wafer and exposed at 500 mJ/cm^2 using an EVG®620 Automated UV-NIL, μ-CP System (EV Group, St. Florian

am Inn, Austria) using the transparency as a mask. The array was then fabricated using common soft lithography techniques. Using Sylgard 184 (Dow Corning, Midland, MI, USA) a 10:1 mass ratio of polymer and curing agent was prepared and poured onto the wafer at a thickness of roughly 5 mm. This was allowed to sit at room temperature for 15 minutes and cured at 70°C for 60 min. The cured PDMS was then removed from the wafer and 3 mm diameter holes were punched in the entrance and exit reservoirs using a Harris Uni-Core punch (Shunderson Communications Inc., Orleans, Ontario, Canada).

7.2.1.2 Electrode Fabrication

Ti/Pt electrodes were plated on standard microscope slides (VWR International). A mask was designed using Adobe Illustrator and printed on transparency using a resolution of 8000 dpi (Fine Line Imaging, Colorado Springs, CO USA). Electrodes were plated 500 μm wide bracketing each reservoir on three sides to produce a flat potential within a reservoir and promote exclusion in channels connecting reservoirs. A schematic of the electrode design is shown (Figure 7.1B). Positive photoresist AZ 4330 was spun onto microscope slides and exposed at 150 mJ/cm^2 with the EVG®620 Automated UV-NIL, μ-CP System using the transparency mask. Electron beam evaporation was used to deposit two layers of metal on the glass microscope slides (PVD75, Kurt J. Lesker Company, Jefferson Hills, PA, USA). A 300 Å layer of Ti was deposited onto the slides followed by 500 Å of Pt. Electric leads were attached at the base of the slide using silver conductive epoxy for connection to an external power supply (Series HV5448, LabSmith Inc., Livermore, CA, USA) through a house-made voltage divider.

7.2.2 Protein Labeling and Sample Preparation

Aspartic acid (Sigma-Aldrich, St. Louis, MO, USA) and DMSO (Mallinckrodt) were used as received. Aspartic acid buffer was prepared at a 5 mM concentration and pH of 2.95 using 18 MΩ Milli-Q water. Purified human myoglobin (7.51 mg/mL) , purified cTnI (1.07 mg/mL) and H-FABP (2.2 mg/mL) were purchased from Life Diagnostics. Myoglobin and H-FABP were used as received in PBS, cTnI was dialyzed to 100 mM PBS, pH 7.2 prior to use. NHS-Fluorescein and NHS-Rhodamine (Thermo Scientific) were dissolved in DMSO to concentrations of 10 mg/mL. 3.0 μL of NHS-Rhodamine was added to myoglobin and the sample was incubated in the dark at room temperature for 1 hour with shaking. NHS-Fluorescein was added to cTnI (1.5 μL) and H-FABP (3.0 μL) and reacted in the same manner. The crude reaction mixtures were added to dialysis cups (Thermo Scientific) with a molecular weight cut-off of 3,500 Daltons. Samples were dialyzed in 100 mM PBS, pH 7.2 overnight. Proteins were diluted with aspartic acid buffer to concentrations of 0.33 mg/mL Myoglobin, 0.2 mg/mL cTnI and 0.22 mg/mL H-FABP prior to analysis.

7.2.3 Experimental

The PDMS layer and glass slide with electrodes were bonded using oxygen plasma operated at high radio frequency (RF) for 60 s (Plasma Cleaner, Harrick Plasma). The array was filled with fluorescently labeled protein samples by pipetting the solution into the entrance reservoir. Channels were filled through capillary action and bulk flow was directed toward the exit reservoirs by the difference in height between the menisci of the entrance and exit reservoirs. A total of 21 μL of solution was added to each device.

Potentials were applied so that exclusion of individual proteins could be observed near the entrance to exit channel 2 and entrance channel 3.

Data collection used an inverted microscope with fluorescence capabilities (IX70, Olympus) using a 100 W high-pressure Hg lamp as the light source. Light was passed through a band-pass filter and 20X microscope objective to the array. Light emitted from the sample was collected through a long-pass dichroic mirror and band-pass filter to a CCD camera capable of image-capture (QICAM, Q imaging, Inc.). ImageJ (NIH, Bethesda, MD) was used for video analysis. The fluorescence intensity was measured in the channel to monitor protein exclusion.

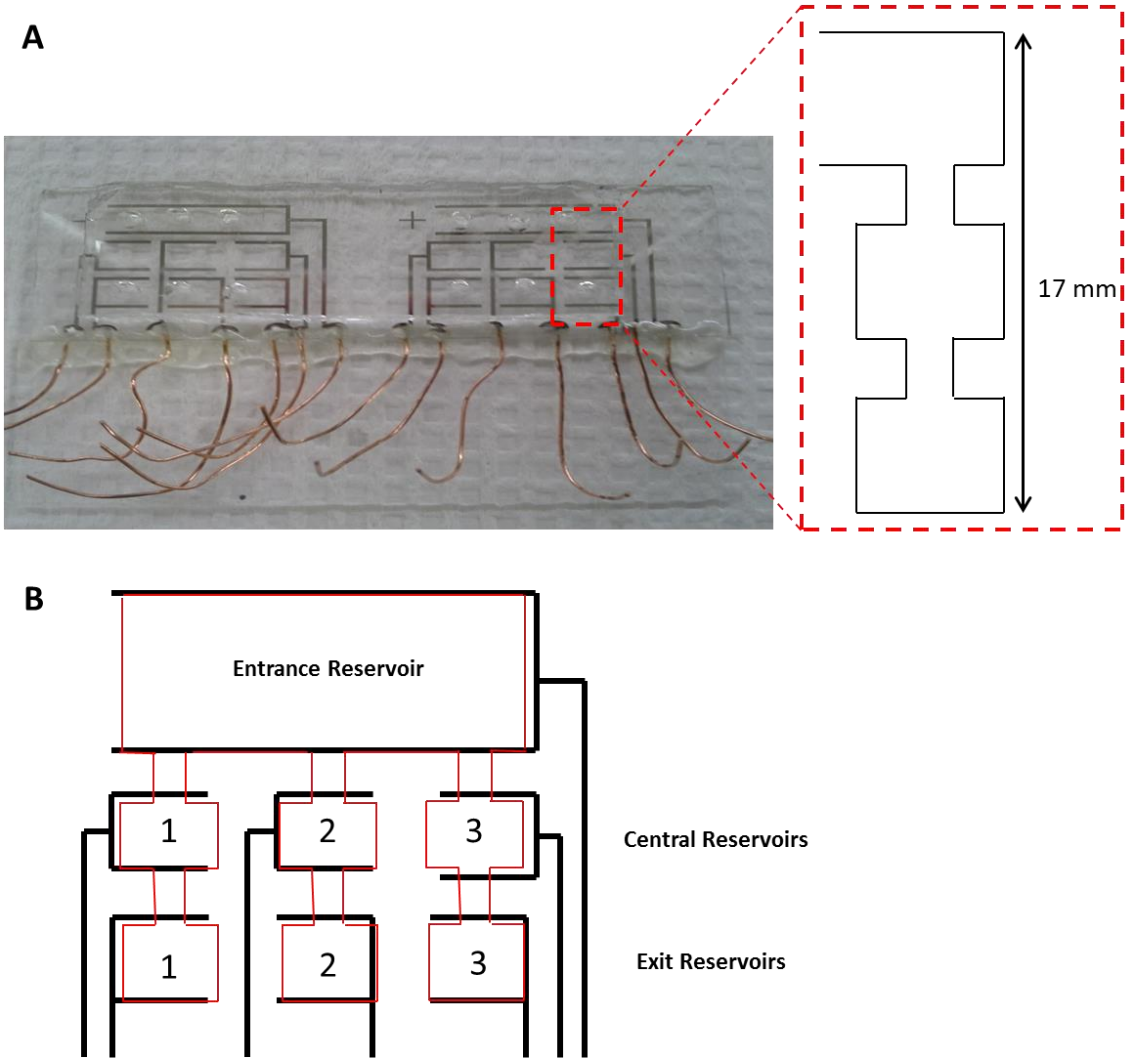

Figure 7.1 Device used for exclusion of protein with schematic of electrode design. **A)** A photograph of the complete chip (glass/PDMS hybrid) with two arrays each containing three channels and a schematic of a single channel used for exclusion. **B)** Schematic showing electrode placement around the reservoirs, promoting exclusion within channels.

7.3 Results and Discussion

When the electrophoretic velocity of a target species is greater than or equal to the hydrodynamic counter flow, electrophoretic exclusion of that analyte is accomplished. If exclusion occurs at the entrance to a channel within the experimental array, that analyte may be separated from other species present in the starting sample. For electrophoretic exclusion to occur three factors must be present: hydrodynamic flow, species having an

electrophoretic mobility, and an applied electric field. With experimental conditions held constant, the hydrodynamic flow and electrophoretic mobility of investigated species are unchanged over the time period of data collection. This allows manipulation of the applied electric field strength such that individual species may be excluded from entering a channel.

The effects of electrophoretic exclusion on cTnI were investigated (Figure 7.2). Briefly, an array is filled with a solution containing the sample of interest (either an individual protein or protein mixture) in aspartic acid buffer (pH 2.95). Initially, no electric field is applied to the array and sample is free to flow from the entrance reservoir towards the exit reservoirs, in the direction of hydrodynamic flow (Figure 7.2A). When an electric field is applied across a channel such that the electrophoretic velocity of the target protein is greater than or equal to the counter-flow, the species is prevented from entering a channel and is concentrated within a reservoir immediately upstream of that channel (Figure 7.2B). Once the electric field is removed, concentrated sample is again allowed to continue in the direction of hydrodynamic flow (Figure 7.2C). The complete exclusion of cTnI from the microchannel with an applied electric field of 65 V/cm demonstrates the potential of this technique to isolate and concentrate proteins from complex samples. cTnI was allowed to collect in the central reservoir over a time of 35 s.

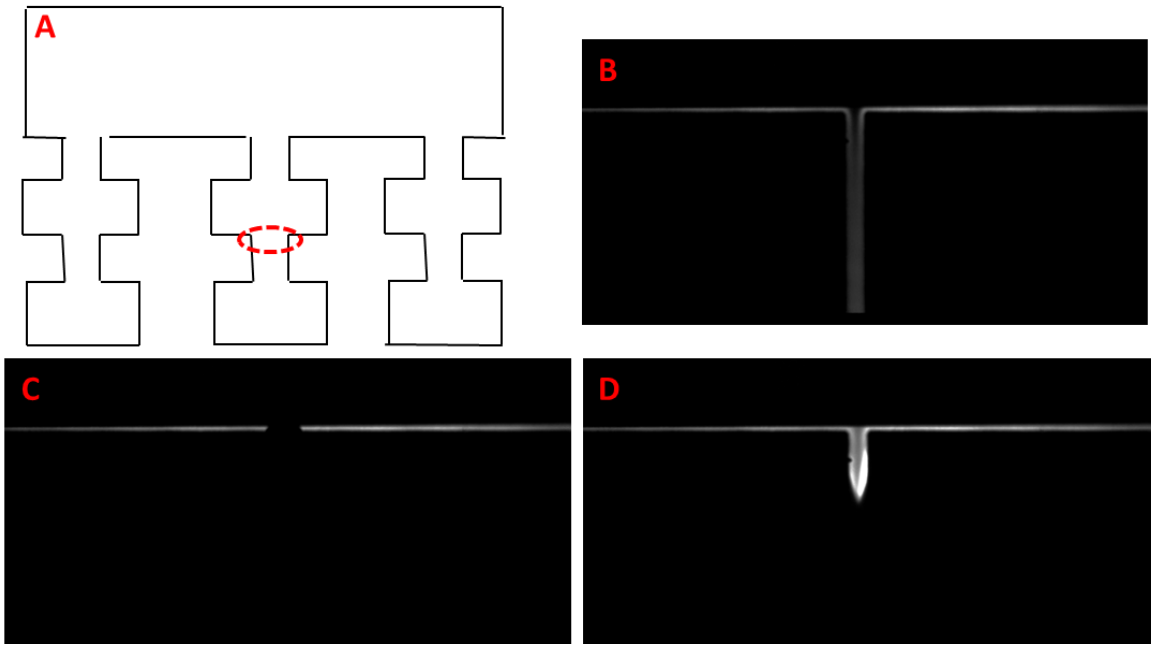

Figure 7.2 Exclusion of cTnI from the entrance to exit channel two. Hydrodynamic flow is from top to bottom. **A)** Graphic illustrating where exclusion behavior is observed on the device. Fluorescence above the microchannel is due to protein, dark band observed in central reservoir 2 is the electrode. **B)** Before an electric field is applied the fluorescently labeled protein travels through the array in the direction of hydrodynamic flow.**C)** Once an electric field is introduced at 65 V/cm the protein is excluded in central reservoir two. **D)** After the field is released the protein may again travel with hydrodynamic flow towards the exit reservoir.

When voltage was released the protein is concentrated compared to the original sample (approximately 3.5 fold). By concentrating samples prior to their quantification, greater sensitivities can be reached. This, in combination with the isolation of species afforded using electrophoretic exclusion, hold potential as a sample pre-treatment step in diagnostic assays requiring multiplex target quantification.

Similar behavior was observed for both myoglobin and H-FABP. Before electric fields were applied to the array, both proteins were allowed to flow freely toward the exit reservoirs. Once electric fields were applied at a channel entrance for 35 s, proteins were observed to collect in the reservoir immediately upstream of that channel. For all target species, once the electric field was removed samples were again able to enter the channel

and move toward the exit reservoirs in the direction of hydrodynamic flow. For studies monitoring individual proteins, the intensity of fluorescence was quantified within the channel. All cases were consistent with complete exclusion of the protein from the microchannel, whereas the electric potential required to achieve this exclusion differs among target species (Figure 7.3). In all cases it is observed that prior to the application of an electric field, the concentration of protein within the channel remains constant. Once potentials were applied to the channel (at t = 10 s) the protein is excluded in the upstream reservoir and prevented from entering the channel. This results in a decrease in fluorescence during the time the potential is applied. Following removal of the electric field (at t = 45 s) the protein is again allowed to enter the channel and an increase in fluorescence is observed.

Four data sets for each protein were analyzed in which the placement of the electrodes was consistent for allowing exclusion behavior to be observed within the channel. The electric field required to exclude each protein under these conditions remained consistent over time. For cTnI an average electric field of 62.5 ± 6.5 V/cm was required for exclusion. For myoglobin and H-FABP 143.8 ± 8.5 V/cm and 87.5 ± 6.5 V/cm were required, respectively.

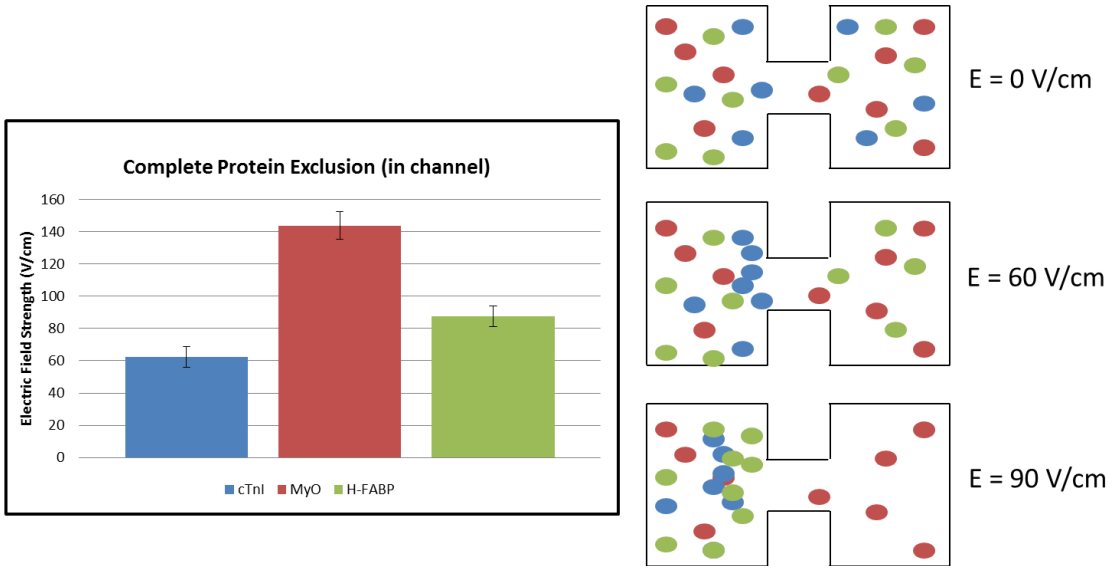

Figure 7.3 Bar graph showing required potential for complete exclusion of protein from a channel. Error bars represent standard deviation between protein preparations and devices, as well as the electric field strength required for protein exclusion.

Alterations in the exclusion behavior (area of exclusion, speed of recovery) were observed with changes in electrode placement between days. The slight movement of electrodes and differences among protein samples account for the deviation in the exclusion potential required for each protein (Figure 7.3). However, even with this variation, the trend in exclusion behavior remained consistent, with cTnI requiring the lowest applied field for complete exclusion and myoglobin requiring the greatest.

Different electric field strengths were applied to determine where the onset of complete exclusion occurred (Figure 7.4). The change in intensity over the length of the channel was calculated as the difference in fluorescence observed when the electric field was applied and immediately following the release of the electric field and return of protein. For cTnI, at field strengths below 55 V/cm, material is either not excluded at all, or incomplete exclusion from the channel is observed. With fields applied below 25 V/cm there is no evidence of exclusion (0 V/cm, 10 V/cm, 12 V/cm), and the characteristic

exclusion curve is no longer observed (inset). Evidence of incomplete exclusion is observed for moderate voltages (25 V/cm and 40 V/cm) showed only the partial exclusion of cTnI from the channel. Following the onset of complete exclusion (62.5 ± 6.5 V/cm), greater voltages produced larger regions of exclusion (data not shown), but did not appear to further concentrate the species and required increasingly long time periods to visualize recovery. Experiments on the exclusion of myoglobin and H-FABP produced similar results (data not shown).

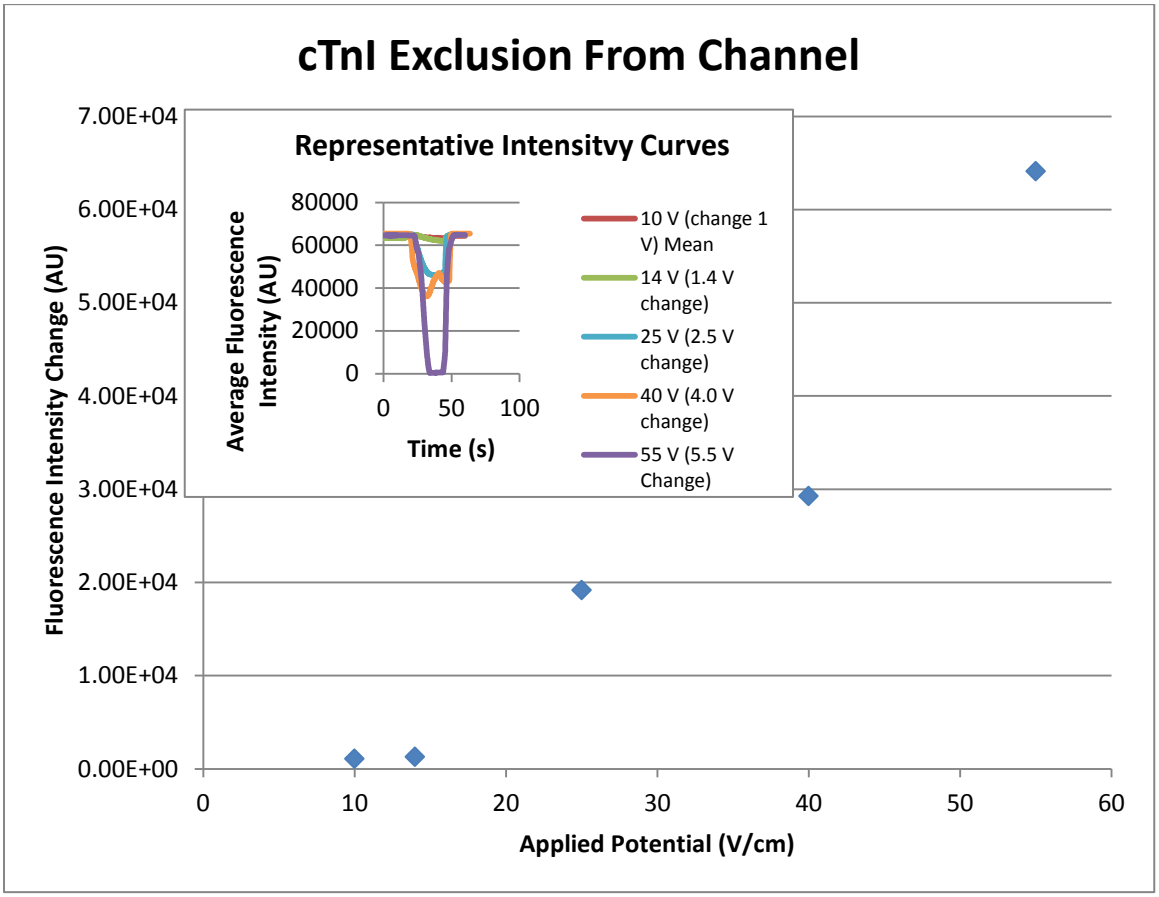

Figure 7.4 Representative change in intensity values for varying electric field strengths over a time of 35 s applied potential for cTnI.

Experiments were performed that demonstrated the ability of electrophoretic exclusion to separate cTnI (green) from myoglobin (red) within the array (Figure 7.5).

Based on the intensity measurements collected in-channel utilizing a blue filter cube, as well as color images obtained from imaging through an Olympus DAPI, FITC, Texas Red triple band-pass cube (Olympus, Center Valley, PA), the separation of species could be clearly visualized. Before the electric field was applied all species were free to flow through the system in the direction of hydrodynamic flow. After a 65 V/cm electric field was applied to the system for 35 s, cTnI was excluded from entering the channel while myoglobin was still able to continue in the direction of bulk flow (observed both visually in color images and through fluorescence intensity measurements filtered for the detection of the NHS-Fluorescein used to label cTnI). Following the release of potential cTnI was again allowed to enter the channel along with the myoglobin.

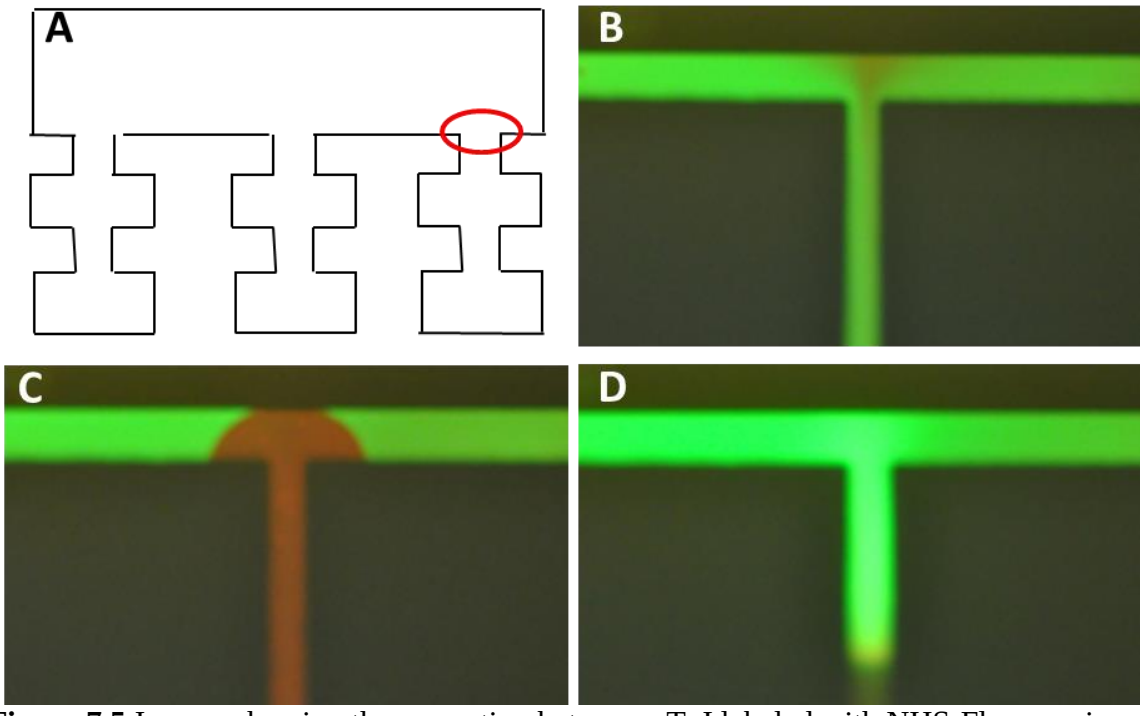

Figure 7.5 Images showing the separation between cTnI labeled with NHS-Fluorescein (green) and Myoglobin labeled with NHS-Rhodamine (red). **A)** Illustration showing the location of protein separation. **B)** Channel before voltage is applied, **C**) separation after 35 s of applied voltage (60 V/cm), and **D)** the channel after the applied voltage is removed.

The difference in electric potentials necessary to attain complete protein exclusion from a channel between the target species investigated suggests that a new design may be produced to exploit these differences and simultaneously isolate, concentrate, and quantify all three proteins within a single device. Separation of two proteins has been accomplished here, representing a first step in that process. Future designs include the incorporation of detection elements to the device such that isolated species may be quantified in a secondary step. A device utilizing voltage gates to separate detection chambers from a central separation channel with well-controlled flow and electric field elements can be designed to allow isolation and detection of desired species from complex samples.

7.4 Concluding Remarks

This work demonstrates for the first time the use of electrophoretic exclusion on a microdevice to manipulate and separate proteins. The exclusion of individual proteins, as well as the direct visualization of protein separation, are significant results. The ability to isolate and concentrate individual target species on a microdevice is an important first step in the development of a μTAS optimized for the quantitation of biomarker panels in clinical diagnostics. By combining the sample treatment step of electrophoretic exclusion with the sensitive and specific quantitation afforded through an immunoassay platform, there exists the potential to create a diagnostic platform that is fully optimized not only for sensitivity and low sample consumption, but for rapid analysis, multiplexed detection and operational simplicity.

7.5 References

[1] Morrow, D. A., Cannon, C. P., Jesse, R. L., Newby, L. K., Ravkilde, J., Storrow, A. B., Wu, A. H. B., Christenson, R.H., *Clinical Chemistry*, 2007, *53*, 552-574.

[2] Macdonald, S.P.J., Nagree, Y., Fatovich, D.M., Phillips, M., Brown, S.G.A., *Emergency Medicine Journal*, 2012, *30*, 149-154.

[3] Molin, S.Da., Cappellini, F., Falbo, R., Signorini, S., Brambilla, P., *Clinical Biochemistry*, 2014, *47*, 247-249.

[4] Fan, R., Vermesh, O., Srivastava, A., Yen, B.K.H., Qin, L., Ahmad, H., Kwong, G.A., Liu, C.C., Gould, J., Hood, L., Heath, J.R., *Nature Biotechnology*, 2008, *26*, 1373-1378.

[5] Anderson, N.L., Anderson, N.G., *Molecular and Cellular Proteomics*, 2002, *1.11*, 845-867.

[6] Bellei, E., Bergamini, S., Monari, E., Fantoni, L.I., Cuoghi, A., *Amino Acids*, 2011, *40*, 145-156.

[7] Tirumalai, R.S., Chan, K.C., Prieto, D.A., Issaq, H.J., Conrads, T.P., Veenstra, T.D., *Molecular and Cellular Proteomics*, 2006, *2.10*, 1096-1103.

[8] Smits, N.G.E., Ludwig, S.K.J., Van der Veer, G., Bremer, M.G.E.G., Nielen, M.W.F., *Analyst*, 2013, *138*, 111-117.

[9] Jayadev, C., Rout, R., Price, A., Hulley, P., Mahoney, D., *Journal of Immunological Methods*, 2012, *386*, 22-30.

[10] Tirumalai, R.S., Chan, K.C., Prieto, D.A., Issaq, H.J., Conrads, T.P., Veenstra, T.D., *Molecular and Cellular Proteomics*, 2006, *2.10*, 1096-1103.

[11] Mitchell, P., *Nature Biotechnology*, 2010, *28*, 665-670.

[12] Camerini, S., Polci, M. L., Liotta, L. A., Petricoin, E. F., Zhou, W., *Proteomics Clin. Appl.*, 2007, *1*, 176-184.

[13] Joglekar, M., Roggers, R. A., Zhao, Y., Trewyn, B. G., *RSC Advances*, 2013, *3*, 2454-2461.

[14] Wang, X., Masschelein, E., Hespel, P., Adams, E., Schepdael, A. V., *Electrophoresis*, 2012, *33*, 402-405.

[15] Jubery, T. Z., Hossan, M. R., Bottenus, D. R., Ivory, C. F., Dong, W., Dutta, P., *Biomicrofluidics*, 2012, *6*, 016503-1-13.

[16] Startsev, M. A., Inglis, D. W., Baker, M. S., Goldys, E. M., *Analytical Chemistry*, 2013, *85*, 7133-7138.

[17] Inglis, D. W., Goldys, E. M., Calander, N. P., *Angew. Chem. Int. Ed.*, 2011, *50*, 7546-7550.

[18] Kenyon, S. M., Weiss, N. G., Hayes, M. A., *Electrophoresis*, 2012, *33*, 1227-1235.

[19] Meighan, M.M., Vasquez, J., Dziubcynski, L., Hews, S., Hayes, M.A., *Analytical Chemistry*, 2011, *83*, 368-373.

[20] Kenyon, S.M., *The Development of a Microfluidic Array for Use in Electrophoretic Exclusion Separations* (Adapting Electrophoretic Exclusion to a Microdevice, Thesis), 2013, 118-140. http://hdl.handle.net/2286/R.A.97689

CHAPTER 8

THE DEVELOPMENT OF A MICROFLUIDIC DEVICE FOR USE IN PARALLEL IMMUNOASSAY QUANTITATION

8.1 Introduction

Previous chapters have addressed the need for a fully optimized immunoassay to aid in disease diagnostics and monitoring. Arising from the necessity to quantify multiple targets in parallel from a single complex sample, separation prior to analysis is an attractive option. As noted previously, electrophoretic exclusion, is a particularly appealing option since it allows for multiple capture zones to be oriented in series or parallel, may be dynamically controlled through adjustment of the applied electric field strength, and affords sample concentration prior to detection through immunoassay.

In addition to allowing multiplexed detection in parallel, sample treatment utilizing electrophoretic exclusion is rapid, can be performed on native species, and avoids the dispersive forces experienced by samples when separation occurs within a channel or column as opposed to at the channel entrance. This concentration of individual target samples is ideal prior to detection through immunoassay as it allows a single, small volume sample to be utilized for the extremely sensitive detection of several targets simultaneously. Concentration of the species relative to the original sample allows even greater improvement to the LOQ than improving on the technique of immunoassay alone, allowing its fundamental limitations of quantitation to be approached in a portable, simple to operate device.

Over the last decade, adaptations have been made to traditional immunoassay formats to allow their compatibility with emerging microfluidic devices. Microscale

devices have been utilized in diverse immunoassay designs for protein quantification including the use of magnetic and non-magnetic microparticles [1-6], as well as the use of a static solid substrate using capillary systems [7,8], modifications on ELISA techniques [9], and the incorporation of designated reaction zones [10]. Notable advantages allowed by the transition to detection on a microdevice include the ability to multiplex [1-5,10], lowered analysis times [7-9], and minimal reagent consumption while maintaining sensitivities comparable to traditional immunoassay formats. Minimizing the consumption of reagents is particularly important when sample volumes are limited, for example in the treatment of infants or during forensic testing. An additional asset of the microchip format is that allows devices that can often be made portable, allowing both bedside testing and use in remote locations [11-14].

Due to the previous success in the separation of proteins observed in a microfluidic device composed of glass and PDMS (Chapter 7), a modified design based on the concept of this array was designed, fabricated and tested. The use of PDMS is appealing because it is optically transparent and is compatible with the fluorescence detection method employed for the immunoassay described throughout this thesis [15]. Modifications were included such that quantitative detection could take place on-chip compared to the original array used in proteins separations. The rest of this chapter focuses on the development of a microfluidic device that could be used for the analysis of complex samples. It has been previously demonstrated that electrophoretic exclusion plays a potentially important role in the pre-treatment of complex samples prior to specific target quantification, and that the sensitive immunoassay described throughout

this work is well suited for incorporation as the detection method. However, a complete device combining these techniques has not been developed.

Here, the preliminary device for sample separation, concentration and quantification is fabricated and tested. Experiments are performed using a mixture of myoglobin and cTnI to evaluate the proficiency of the device in performing separations along the primary *separation* channel (Figure 8.1). Additionally, experiments using a single target are done to assess the ability of the device to isolate and concentrate an individual species in one of the *separation* channel reservoirs prior to quantification. The capacity for quantification, in terms of protein manipulation into the *quantitation* reservoir following concentration, and binding of target species to the magnetic microbeads was also evaluated.

8.2 Materials and Methods

8.2.1 Design and Microdevice Fabrication

Hybrid glass/PDMS devices were used for each experiment and each device contained a single analysis system. A photograph was recorded of the device (view from above) as well as a schematic of a single *isolation* channel (Figure 8.1). The fabrication of this device is analogous to the array design discussed in Chapter 7, where deviations are discussed below.

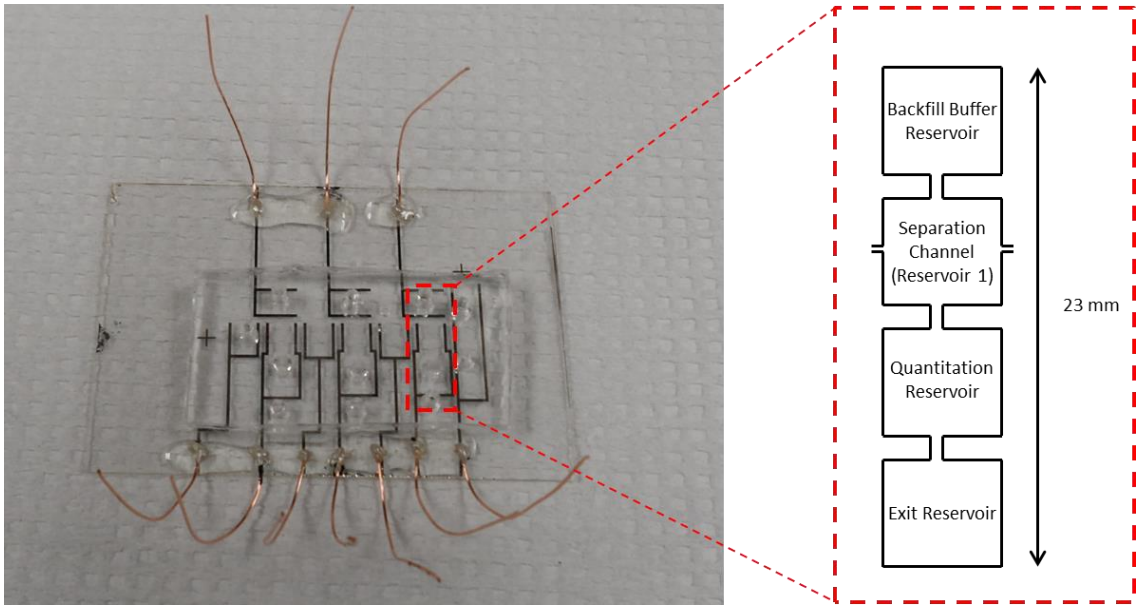

Figure 8.1. Microdevice for protein separation and quantitation by immunoassay. Photograph (left) of the complete microfluidic device with one *separation* channel and three *isolation channels*, and a schematic of a single (right) *isolation* channel explaining terminology used in the device.

8.2.1.1 PDMS

The *separation* channel was 41 mm in length. It contained five central reservoirs for isolation connected to two end reservoirs through a series of short channels. Each central reservoir was 5 mm x 5 mm, end reservoirs were 19 mm x 5 mm and channels were 1 mm by 100 μm having a uniform depth of 10 μm throughout the device. Each *isolation* channel consisted of one of the *separation* reservoirs connected to two end reservoirs and a *quantitation* reservoir through a series of short channels. Each *isolation* channel was 23 mm in length. The size and depth of reservoirs and channels was equivalent to those found in the central reservoirs/channels along the *separation* channel. Masks were designed in AutoCad (Autodesk, Inc., San Rafael, CA) and were printed on a transparency at a resolution of 10,160 dpi (Fine Line Imaging, Colorado Springs, CO, USA). Positive photoresist AZ 4620 was spun onto a silicon wafer and exposed at 750

mJ/cm^2 using an EVG®620 Automated UV-NIL, μ-CP System (EV Group, St. Florian am Inn, Austria) using the transparency as a mask. The system was then fabricated using standard soft lithography techniques as discussed in Chapter 7.

8.2.1.2 Electrodes

Ti/Pt electrodes were plated on 75 x 50 mm microscope slides (Fisherbrand, Waltham, MA, USA) (Figure 8.2, right). A mask was designed in AutoCad (Autodesk, Inc., San Rafael, CA) and printed on a transparency with a resolution of 10,160 dpi (Fine Line Imaging, Colorado Springs, CO, USA). Electrodes were plated 500 μm wide bracketing each reservoir within the *separation* channel, along with the end reservoirs and *quantitation* reservoirs immediately adjacent to the *separation* channel. This was designed to produce flat potentials within reservoirs and promote exclusion at a channel entrance such that separation of proteins can occur and species may be concentrated and isolated within a reservoir. Electron beam evaporation was used to deposit metal onto the slide as previously discussed in Chapter 7. Electric leads were attached at the sides of the slide using silver conductive epoxy for connection to an external power supply (Series HV5448, LabSmith Inc., Livermore, CA, USA) through an in-house produced voltage divider (1:100). A schematic of the electrode and channel design is included (Figure 8.2).

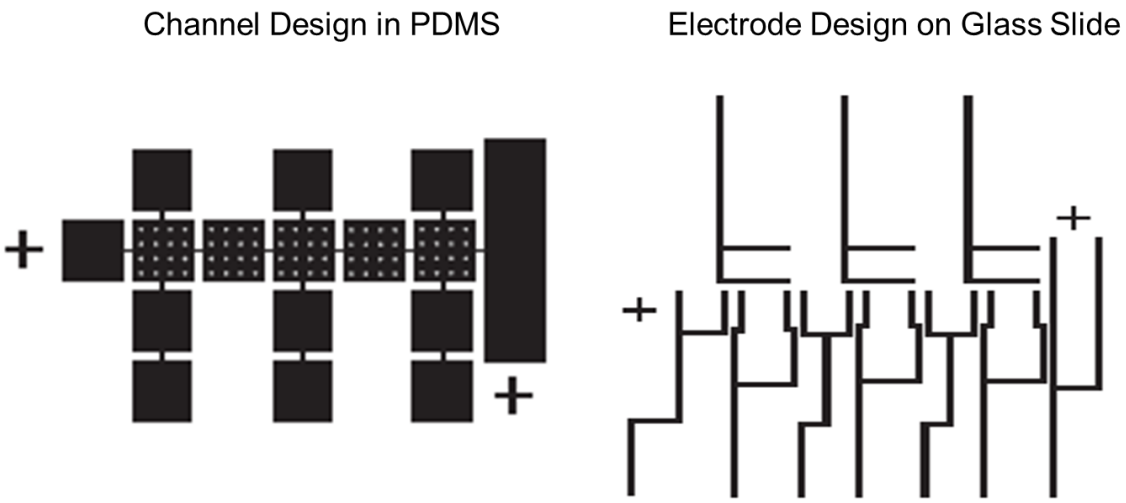

Figure 8.2. Schematic designs of PDMS channel (left) and electrode (right) patterns. The PDMS pattern includes a separation channel where *separation* reservoirs contain posts to support the roof (white circles observed within reservoirs), a large entrance reservoir (far right) and an exit reservoir (far left). Perpendicular to the *separation* channel are three *isolation* channels. Each *isolation* channel consists of a *backfill buffer* reservoir (top), *quantitation* reservoir (below *separation* channel), and an *exit* reservoir (bottom). The electrodes are patterned to surround all reservoirs within the *separation* channel, as well as the *backfill buffer* reservoirs and *quantitation* reservoirs.

8.2.2 Materials

Myoglobin (Life Diagnostics), myoglobin antibody (Lifespan Biosciences, Seattle, WA, USA), cTnI (Life Diagnostics), cardiac troponin antibody (Lifespan Biosciences), NHS-rhodamine (ThermoFisher, Waltham, MA, USA), NHS-fluorescein (ThermoFisher), magnetic microparticles (Qiagen) and DMSO were used as received. PBS buffer was prepared to a 100 mM concentration at a pH of 7.2 with 0.2% NaN_3 and 0.2% Tween 20 using 18 MΩ Milli-Q water. Aspartic acid buffer was prepared to a concentration of 5 mM at a pH of 2.95 using 18 MΩ Milli-Q water. A 10 mg/mL stock solution of NHS-rhodamine was prepared in DMSO and 3.03 μL were added to 13.6 μL of a stock solution of 7.51 mg/mL myoglobin. The mixture was allowed to react at room temperature for 1 hour and dialyzed in PBS overnight to remove unconjugated dye prior

to experiments. The cTnI (1.07 mg/mL; 93.5 μL) was conjugated to 1.5 μL of 10 mg/mL fluorescein in the same way. Magnetic microparticles were diluted in PBS, coated with BSA and functionalized with antibodies before the day of experiments. Protein samples were diluted to concentrations of 0.33 mg/mL (myoglobin) and 0.20 mg/mL (cTnI) in aspartic acid buffer on the day of experiments.

8.2.3 Experimental Setup

The PDMS layer was bonded to the glass slide with the Ti/Pt electrodes using O_2 plasma (Plasma Cleaner, Harrick Plasma) operated at a high RF level for 60 s. The *separation* channel was filled with a protein sample by pipetting the solution into the *entrance* reservoir. The channel was filled by capillary action. The *isolation* channels were filled with buffer by pipetting directly into the *quantitation* reservoir, magnetic microparticles were added by pipetting directly into the *quantitation* reservoir and held in place with a flat, cylindrical rare-earth magnet. Bulk flow along the *separation* channel was induced by the difference in sample meniscus height between the entrance and exit reservoirs. A total of 21 μL of sample solution was pipetted into the *separation* channel. A total of 30 μL of buffer was pipetted into the *isolation* channels. Flow rates for all experiments were held at approximately 10 nL/min. Potential (60 V/cm) was applied using a LabSmith power supply (Series HV5448, LabSmith Inc., Livermore, CA, USA). Eight individual potentials were applied to the channel, one to each electrode pad along the *separation* channel as well as each *isolation* channel. A voltage divider was created in house from 100 kΩ, 120 kΩ, and 1 MΩ resistors as has been discussed elsewhere (Figure 8.3) [16]. Each resistor was connected to a thin wire with a coiled end that would slip over the leads connected to the microscope slide. Output potentials were monitored using

a digital multimeter (Sperry Instruments, Menomonee Falls, WI, USA) throughout the course of the experiment. Output voltages from the voltage divider ranged from 0 to 16 V, providing electric fields between 0 and 160 V/cm.

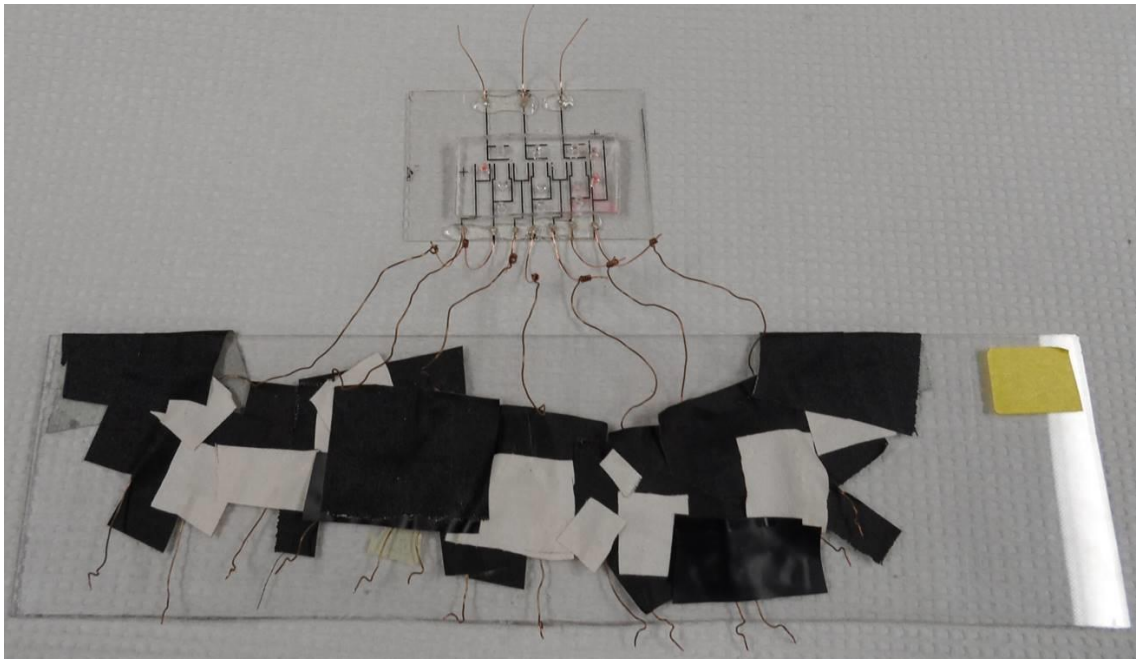

Figure 8.3. Voltage divider (bottom) connected to the microscale analysis system (top). The voltage divider was created from 100 kΩ, 120 kΩ, and 1 MΩ resistors, and each resistor was connected to a thin wire with a coiled end. The coiled end could slip over the leads attached to the device and enabled the precise application of electric fields between 0 and 160 V/cm.

Experiments were monitored using an inverted microscope with darkfield and fluorescence abilities (IX70, Olympus, Center Valley, PA, USA) utilizing a 100 W Hg lamp as the light source. Light from the Hg lamp passed through a band-pass filter and a 1.25X objective to the device during separations. A 40X objective was used during quantitation. During quantitation the rare-earth magnet was rotated to produce an alternating magnetic field and cause formation and rotation of rotors that served as the solid-surface for the immunoassay. The light emitted passed through a long-pass dichromatic mirror and a band-pass filter into the camera port on the microscope for

black and white images. These images were collected digitally using a QICAM CCD camera from Q Imaging, Inc. (Surrey, British Columbia, Canada) that was connected to a computer running Streampix (NorPix, Montreal, Quebec, Canada). Color images were collected from the eyepiece of the microscope using a mounted Nikon D5000 camera (Nikon, Melville, NY, USA). ImageJ (NIH, Bethesda, MD, USA) was used to determine the fluorescence intensity change in the channel reservoirs to assess the extent of concentration in the channel.

All experiments in the system were performed at a pH of 2.95 in aspartic acid buffer to eliminate electroosmotic flow (EOF). Neutralization of proteins was required before binding for quantification, and was performed through the addition of Tris-buffer (pH 8) to the *backfill buffer* and *quantitation* reservoirs.

8.3 Results and Discussion

8.3.1 Device Design

The *separation* channel/quantitation array design was based off the success of the initial array device in separating protein samples (Chapter 7). To allow for quantitation of proteins on chip, additional chamber interfaces were added. Instead of connection in parallel, five *separation* reservoirs were connected in series through short channels to an *entrance* and *exit* reservoir. Connected to three of the central *separation* reservoirs (reservoirs 1, 3 and 5) were perpendicular *isolation* channels composed of a single *backfill buffer* reservoir above the channel, and two reservoirs below the channel, a *quantitation* and *exit* reservoir. These reservoirs were physically open to the channel during separations and controlled using voltage gates. *Separation* reservoirs were connected in series along a single primary channel instead of in an array design for two

reasons; to improve the ability for concentration of each target in a single region of the device, and to enable the easy connection of *quantitation* reservoirs adjacent to the regions of protein concentration. Inclusion of the *isolation* channels provided, for the first time, the ability to manipulate and quantify species following their concentration and isolation through electrophoretic exclusion.

8.3.2 Device Fabrication

Enlarged glass microscope slides (75 x 50 mm) were plated with electrodes to accommodate the size of the microfluidic system. A PDMS layer having reservoirs connected through channels was sealed to the glass slide. Due to the ability of the array described previously (Chapter 7), the same size reservoirs and channels were used in this design. Because electrode width was not an issue in the protein separations performed on the original array, allowed for the easier attachment of the copper leads to the electrodes, and aided in the manual alignment of the PDMS layer, the larger electrode width (500 μm) was again used for this device. The impact of electrode alignment on the separation of both small molecules and proteins has been previously discussed [17].

8.3.3 Operation of the Microfluidic Device

8.3.3.1 Detection of Species

Fluorescence detection was chosen to monitor both the exclusion and direct immunoassay quantitation as it was compatible with the singleplex immunoassay design and allowed highly sensitive detection to be maintained. It also allowed direct visualization of each step in the PDMS/glass hybrid device. Two species, cTnI and myoglobin were chosen for evaluation of the microdevice.

8.3.3.2 Experimental Design

As discussed in chapter 7, electrophoretic exclusion is achieved when the electrophoretic velocity ($\mu_a E$) of a species is greater than or equal to the velocity of hydrodynamic flow through a channel. Balancing these forces prevents a target species from entering a channel and allows concentration of that target in the reservoir immediately upstream of the channel entrance. The microdevice prototype was designed with a total of six interfaces where exclusion could occur along the *separation* channel. Three of these *separation* reservoirs were directly connected to *isolation* channels, and were the intended locations of target protein concentration. The remaining *separation* reservoir/channel interfaces could be programmed to minimize the impact of NSB from potential interfering species in a complex biological sample. The *entrance* reservoir was used for the introduction of sample, while *isolation* channels were used for the introduction of neutralization and wash buffers. Electrodes plated around the reservoirs along the *separation* channel, as well as the *backfill buffer* and *quantitation* reservoirs in the *isolation* channel, were used as voltage gates to control where individual species were excluded and concentrated from the bulk solution.

Protein separation experiments were designed so that cTnI would be captured in *separation* reservoir 1, while myoglobin would continue to move with bulk flow along the channel and be captured in *separation* reservoir 3. A representative sequence of applied potentials is shown (Figure 8.4).

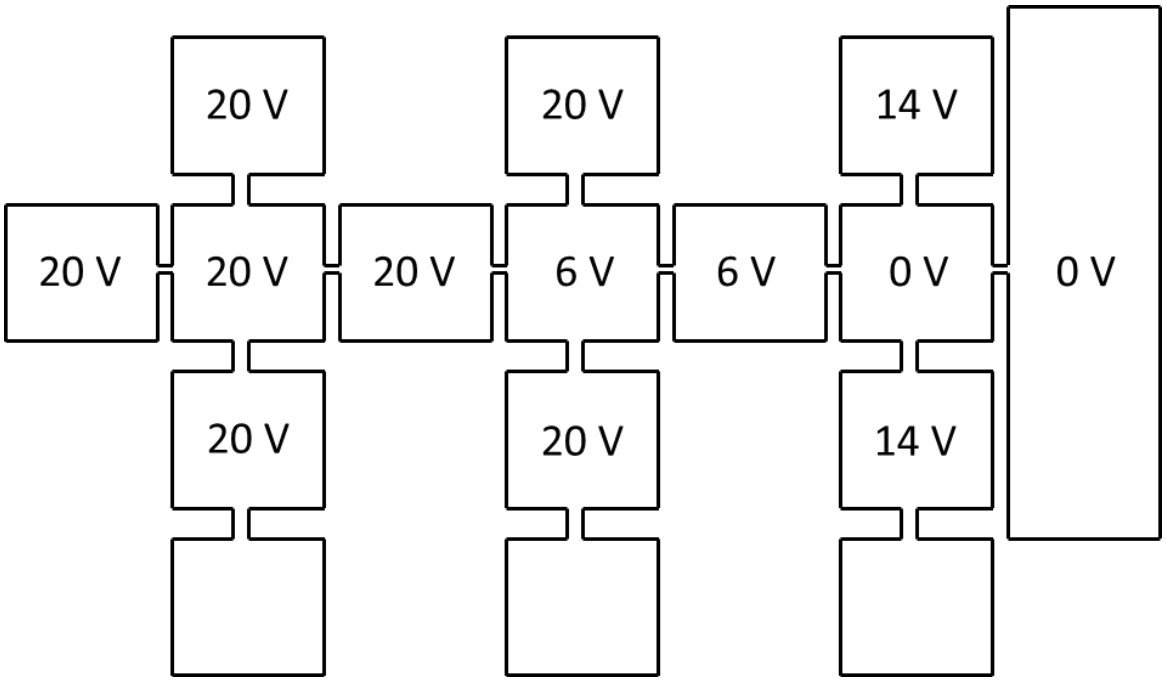

Figure 8.4 Representative values of applied potentials used for the separation of myoglobin and cTnI. With no voltage applied to the entrance reservoir or the first reservoir of the *separation* channel, both species were free to move in the direction of bulk flow. An applied voltage of 6 V (60 V/cm) was used for reservoirs 2 and 3 of the *separation* channel to prevent cTnI from entering *separation* channel reservoir 2 and to concentrate it in *separation* reservoir 1, but allow myoglobin to continue in the direction of bulk flow. 20 V was then applied to reservoir 4 of the *separation* channel to concentrate myoglobin in *separation* reservoir 3. High potential was applied to all *backfill buffer* and *quantitation* reservoirs to remove all protein from the *isolation* channels prior to separation and concentration.

Exclusion of the proteins only occurred when an appropriate electric field was applied across a channel. In instances where there was no field (between *entrance* reservoir and *separation* reservoir 1, as well as between *separation* reservoirs 2 and 3), exclusion was not intended to occur. The progression of a separation experiment is shown in Figure 8.5.

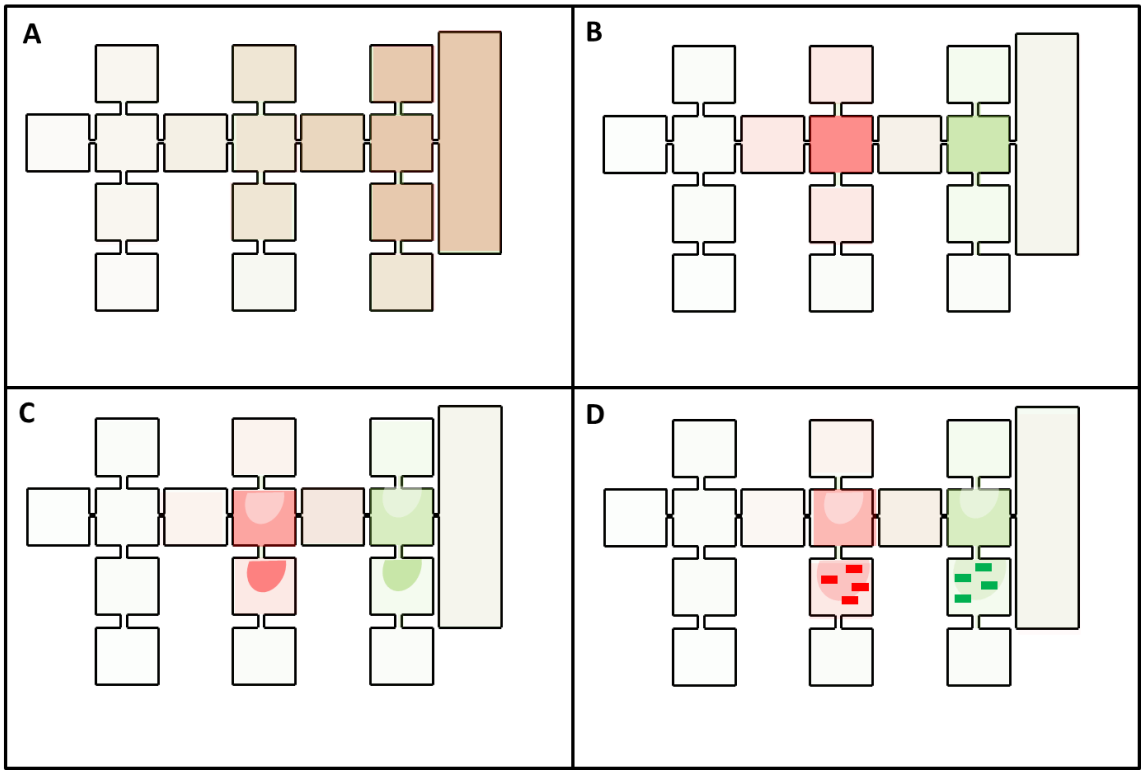

Figure 8.5 Illustrative graphic showing the designed progression of a separation experiment between myoglobin and cTnI. **A.** Filling of the device before any electric potentials are applied. Green indicates the presence of cTnI labeled with NHS-Fluorescein, red indicates the presence of myoglobin labeled with NHS-Rhodamine, saturation of color indicates higher concentration of protein. **B.** Concentration of cTnI in *separation* reservoir 1 and myoglobin in *separation* reservoir 3 after electric potential was applied to the electrodes. **C.** Removal of voltage from the *quantitation* reservoirs and addition of buffer to the *backfill buffer* reservoirs, forcing cTnI and myoglobin into the *quantitation* reservoirs. **D.** Observation of fluorescent supraparticle structures (dark red and green) following the addition of magnetic microparticles to the *quantitation* reservoir and application of a magnetic field.

In the quantification experiments performed with cTnI as a target, following isolation and concentration in *separation* reservoir 1 using electrophoretic exclusion, the addition of a basic Tris buffer (pH 8) was used for neutralization. Neutralization allowed cTnI to bind to magnetic microbeads coated in capture antibodies within the *quantitation* reservoir. The addition of Tris buffer to the *backfill buffer* reservoirs also served to direct flow of the concentrated protein into the *quantitation* reservoir. In the *quantitation* reservoir, a direct immunoassay was performed analogous to that previously described

(Chapter 4), with the exception that convective mixing was used during the incubation as opposed to agitation in a micro-centrifuge tube. The fluorescence intensity of observed rotors was used to monitor protein bound to the surface. The designed progression of a quantitation experiment is demonstrated in Figure 8.6.

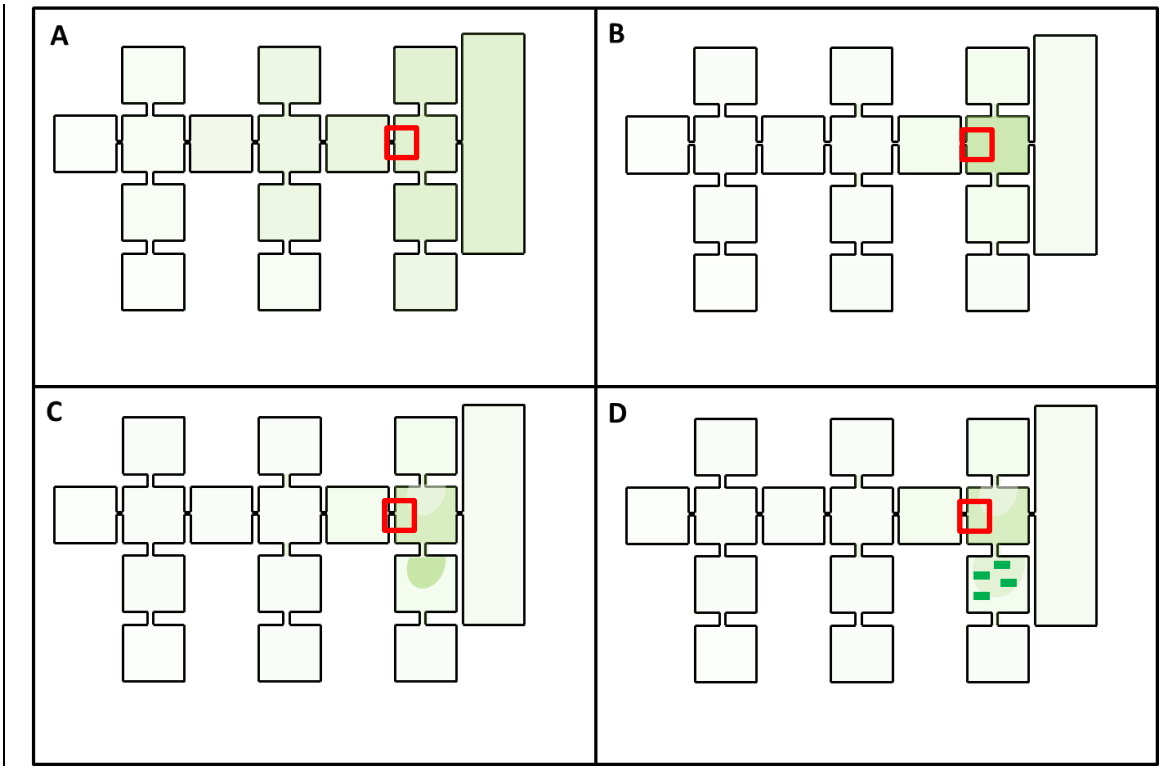

Figure 8.6 Illustrative graphic showing the progression of a quantitation experiment using cTnI. **A.** Filling of the device before any electric potentials are applied. Green indicates the presence of cTnI labeled with NHS-Fluorescein, saturation of color indicates higher concentration of protein. **B.** Concentration of cTnI in *separation* reservoir 1 after electric potential was applied to the electrodes. **C.** Removal of voltage from the *quantitation* reservoir and addition of buffer to the *backfill buffer* reservoir, influencing the movement of cTnI into the *quantitation* reservoir. **D.** Observation of fluorescent supraparticle structures (dark green) following the addition of magnetic microparticles to the *quantitation* reservoir and application of a magnetic field. The red box illustrates the approximate location of the data collected for Figure 8.7.

8.3.4 Results of cTnI and Myoglobin Separation Experiments

The exclusion behaviors of cTnI and myoglobin were consistent with results attained from the array (Chapter 7). With flow directed from right to left across the

device an applied potential of 65 V/cm across the channel between *separation* reservoirs 1 and 2 was used to achieve exclusion of cTnI (and concentration of cTnI in *separation* reservoir 1) while myoglobin was able to flow freely toward the *exit* reservoir (Figure 8.7). Due to sample spreading in the *isolation* channels prior to voltage application, electric potentials of 160 V/cm were applied directly to the *backfill buffer* and *quantitation* reservoirs to remove all material during the time of exclusion.

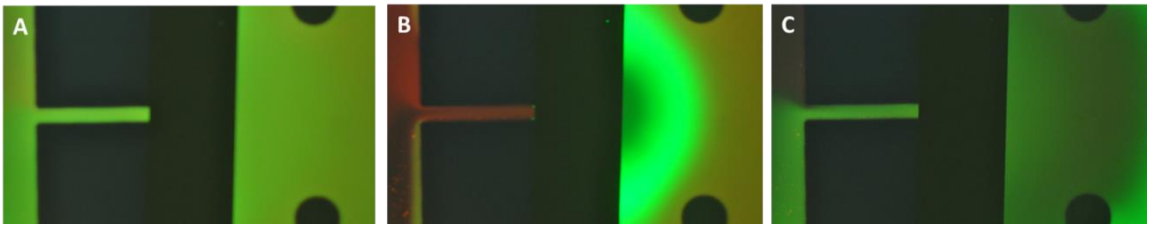

Figure 8.7 Images showing the separation of myoglobin (red) and cTnI (green). Flow is oriented from right to left across the device. The position of data capture is indicated by the red box in Figure 8.6. The dark band immediately to the right of the microchannel is the electrode. **A)** Channel before voltage is applied, **B**) separation after 35 s of applied voltage (65 V/cm), and **C)** the channel after the applied voltage is removed.

During the time voltage is applied, cTnI is excluded from entering downstream channel reservoirs and is concentrated in *separation* reservoir 1. The extent of cTnI concentration was monitored using a blue filter cube to selectively observe the fluorescence caused by the NHS-fluorescein used to label the protein. Repeated trials show consistent results using different preparations of protein and devices over five experiments. With an applied electric field of 65 V/cm within the *separation* channel and fields of 160 V/cm applied to all reservoirs in the *isolation* channel, cTnI was observed to concentrate 4- fold with 35 s of applied voltage. Maintaining the applied electric field for longer time periods increased the protein concentration further. It is observed that after 60 s the fluorescence intensity in the reservoir reaches the maximal pixel intensity that may

be captured using the CCD-camera, representing a 7-fold, or greater, increase in concentration.

8.3.5 Results of cTnI Quantification Experiments

Following the concentration of cTnI in *separation* reservoir 1, material was forced into the *quantitation* reservoir by adding Tris buffer, pH 8.0 to the *buffer backfill* reservoir. Control of material in this way was modeled after the pinched sample injection methods used in microfluidic devices [18-21]. Magnetic microparticles bound to the cardiac troponin capture antibody were pipetted directly into the *quantitation* reservoir and manipulated to achieve convective mixing and promote protein capture (Figure 8.8).

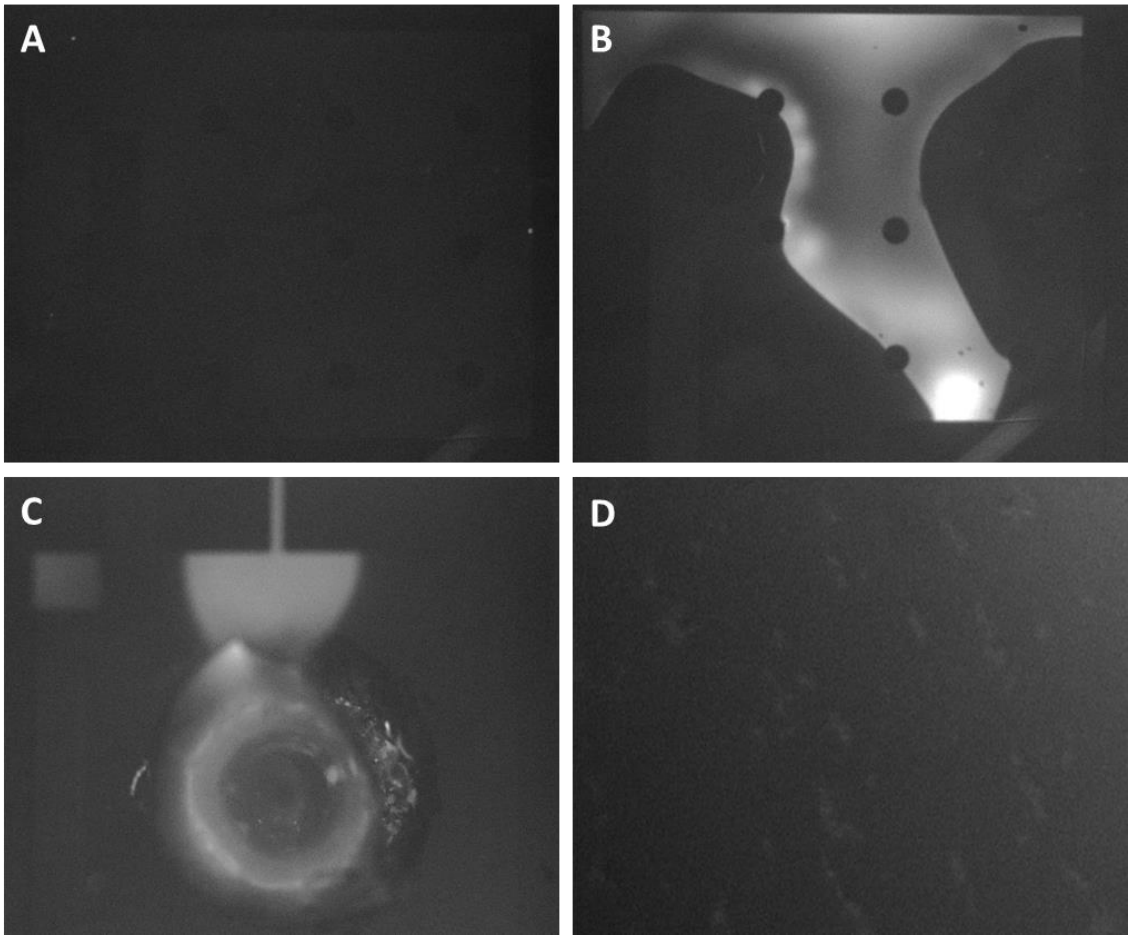

Figure 8.8 Images showing the concentration, manipulation, and quantification of cTnI. **A)** *Separation* reservoir 1 before voltage is applied **B)** *separation* reservoir 1 after 60 s of an applied electric field (note that bubbles formed left and right, limiting the solution to the irregularly shaped center portion, concentration enhancement still occurs) **C)** *quantitation* reservoir 1 after buffer has been added to the *backfill buffer* reservoir **D)** protein bound by the cTnI capture antibody attached to the magnetic microparticles in the presence of a magnetic field.

The concentration of cTnI can be clearly observed in reservoir 1 of the *separation* channel, as evidenced by the increase in fluorescence intensity within the reservoir from 6,600 to 45,000, approximately a 6.7-fold increase (Figure 8.8 A and B), even in the presence of bubbling (dark zones left and right) due to local electrolysis (Figure 8.8B). Following the removal of electric potential to *quantitation* reservoir 1, and the addition of Tris buffer to *backfill buffer* reservoir, material is observed to enter the *quantitation*

reservoir. However, flow into the reservoir is slow, and incomplete over the time course of the experiment (Figure 8.8 C). By increasing the magnification from 1.25 to 20X, the magnetic chains in the *quantitation* reservoir, analogous to those seen in the singleplex immunoassay (Chapter 4) could be observed (Figure 8.8 D).

While some of the cTnI bound to the rotors, based on the fluorescence observed on the chains, there is still a high background fluorescence intensity that indicates not all material is binding. This could be caused by interference in binding sites from the NHS-Fluorescein used to label the cTnI, or the incomplete neutralization of the protein resulting in denatured protein not binding to the rotors.

8.3.6 Assessment of the Initial Design

8.3.6.1 Observed Challenges Preventing Optimal Function

Similar to the previous array this device was able to achieve separation and concentration of proteins. However, to prevent the leakage of material into the *isolation* channels during separation it was necessary to add floating electrodes directly into the *quantitation* and *backfill buffer* reservoirs to ensure the exclusion of material. These floating electrodes were created by inserting platinum wire leads connected to the voltage source directly into the access holes punched in both the *quantitation* and *backfill buffer* reservoirs. Floating electrodes were necessary for several reasons. First, the electrodes plated around the *quantitation* reservoirs are connected to those utilized for the *separation* reservoirs and may not be articulated independently. Additionally, due to the close proximity of electrodes surrounding the *backfill buffer* reservoirs and the reservoirs within the *separation* channel, bubble formation occurred to a greater extent than observed in the previous separation-based array.

An additional issue caused by the current device design is that not all of the target material is concentrated within the desired reservoir of the *separation* channel. Some of the material remained in the *entrance* reservoir, or in the case of myoglobin, in *separation* reservoirs upstream of *separation* reservoir 3, where exclusion and concentration took place. Several alterations could be made in the fabrication of a next generation device in order to eliminate these issues and allow the rapid separation, concentration, and quantification of biomarker panels.

8.3.6.2 Proposed Alterations to Electrode Design

In the initial device used for the separation of proteins, electrode width was not an issue. The larger width of electrodes (500 μm) facilitated the alignment of the PDMS layer and attachment of the copper leads to the electrodes. For these reasons the electrode width was maintained in the design of the current microdevice. However, due to the issues observed both in the ability to articulate *isolation* channel reservoirs independently, bubble formation within the *separation* channel, alterations to the electrode design should be made in a future device. While it is advisable to maintain the width of the electrodes around the reservoirs in the *separation* channel to conserve the advantages noted previously, removing electrodes from the *isolation* channels would improve the ease of use for the device. Incorporating a physical barrier to prevent sample leakage into these reservoirs would aid in the ease of operation, as well as ensure a greater level of purity for the sample detected in each *quantitation* reservoir.

8.3.6.3 Incorporation of Physical Valves

Incorporation of physical valves as a control element within a microfluidic device can aid in the improvement of overall performance [22]. Valves can be designed such

that they are compatible with soft lithography techniques [22-25], and help to improve throughput, sensitivity and the dynamic range capabilities of the device [22]. Incorporation of PDMS valves is an attractive alternative to the use of voltage gates because they are easy to fabricate, maintain a low device fabrication cost, and may easily be scaled to fit the dimensions of system [22]. While voltage gates are also easy to incorporate into a device, the ability to physically control the filling of *isolation* channels using a physical barrier would improve the overall ease of use for the device and increase the sensitivity of detection by ensuring fewer contaminants reach isolated *quantitation* reservoirs.

8.3.6.4 Sample Introduction to the Microdevice

Presently, a solution of buffer containing the sample is directly added to the *entrance* reservoir and used to fill the *separation* channel. Buffer alone is pipetted into *isolation* channels, however, as no physical barrier exists at the time of device filling, the sample is free to flow throughout the device until an electric potential is applied. By instead filling the entire device with buffer and using a microscale peristaltic pumping system to introduce sample at a known flow rate, electric potentials could be applied prior to sample introduction. It would also allow the valves protecting the *isolation* channels to be shut and prevent sample leakage prior to isolation and analysis. Incorporation of a pump would force samples through the device at a higher rate, enabling all protein to move through the *separation* channel and be isolated in the appropriate reservoir such that even very low concentrations of target species may be quantified from complex samples.

8.4 Concluding Remarks

This chapter described the design, fabrication, and evaluation of a microfluidic device. The device was intended for the quantification of a biomarker panel from a complex sample. It was demonstrated that it is possible to isolate and concentrate target proteins in reservoirs along the *separation* channel. Results suggest that creation of a fully optimized device for clinical diagnostics is possible, and this work represents a first step in that direction. Alterations to the electrode layout and sample introduction methods, as well as the incorporation of physical valves, could improve the ease of use, speed, and quantitative ability of the device. By addressing each of these issues systematically, a future design could allow the full optimization of a clinical diagnostic platform allowing the rapid and sensitive quantification of biomarker panels using immunoassay detection in a microscale device.

8.5 References

[1] Cao, Z., Li, H., Lau, C., Zhang, Y., *Analytica Chimica Acta*, 2011, *698*, 44-50.

[2] Lacharme, F., Vandevyver, C., Gijs, M.A.M., *Microfluid Nanofluidics*, 2009, *7*, 479-487.

[3] Li, Z., Zhao, Q.Y., *et al*., *Sci. China Chem.*, 2010, *53*, 812-819.

[4] Proczek, G., Gassner, A.L., Busnel, J.M., Girault, H.H., *Anal. Bioanal. Chem.*, 2012, *402*, 2645-2653.

[5] Song, S.Y., Han, Y.D., Kim, K., Yang, S.S., Yoon, H.C., *Biosens. Bioelectron.*, 2011, *26*, 3818-3824.

[6] Fu, Z., Shao, G., Wang, J., Lu, D., Wang, W., Lin, Y., *Anal. Chem.*, 2011, *83*, 2685-2690.

[7] Ziegler, J., Zimmermann, M., Hunziker, P., Delamarche, E., *Analytical Chemistry*, 2008, *80*, 1763-1769.

[8] Zimmermann, M., Hunziker, P., Delmarche, E., *Biomed. Microdevices*, 2009, *11*, 1-8.

[9] Lee, B.S., Lee, J.N., Park, J.M., *et al*., *Lab Chip*, 2009, *9*, 1548-1555.

[10] Shao, G., Wang, J., Li, Z., Saraf, L., Wang, W., Lin, Y., *Sens. Actuators B Chemistry*, 2011, *159*, 44-50.

[11] Wang, H., Ou, L.M.L, Suo, Y., Yu, H.Z., *Analytical Chemistry*, 2011, *83*, 1557-1563.

[12] Yu, H.Z., Li, Y., Ou, L.M.L., *Accounts of Chemical Research*, 2013, *46*, 258-268.

[13] Tamarit-Lopez, J., Morais, S., Manuis, M.J., Puchades, R., Maquieira, A., *Analytical Chemistry*, 2010, *82*, 1954-1963.

[14] Pallapa, M., Ou, L.M.L., Parameswaran, M., Yu, H.Z., *Sensors and Actuators B*, 2010, *148*, 620-623.

[15] Seia, M.A., Pereira, S.V., Fontan, C.A., DeVito, I.E., Messina, G.A., Raba, J., *Sens. Actuators B, Chemistry*, 2012, *168*, 297-302.

[16] Kenyon, S.M., *The Development of a Microfluidic Array for Use in Electrophoretic Exclusion Separations* (Adapting Electrophoretic Exclusion to a Microdevice, Thesis), 2013, 118-140. http://hdl.handle.net/2286/R.A.97689

[17] Kenyon, S.M., Weiss, N.G., Hayes, M.A., *Electrophoresis*, 2012, *33*, 1227-1235.

[18] Thomas, C.D., Jacobson, S.C., Ramsey, J.M., *Analytical Chemistry*, 2004, *76*, 6053-6057.

[19] Bai, X., Lee, H.J., Rossier, J.S., Reymond, F., Schafer, H., Wossner, M., Girault, H.H., *Lab on a Chip*, 2002, *2*, 45-49.

[20] Alarle, J.P., Jacobson, S.C., Culbertson, C.T., Ramsey, J.M., *Electrophoresis*, 2000, *21*, 100-106.

[21] Ermakov, S.V., Jacobson, S.C., Ramsey, J.M., *Analytical Chemistry*, 2000, *72*, 3512-3517.

[22] Araci, I.E., Quake, S.R., *Lab on a Chip*, 2012, *12*, 2803-2806.

[23] Weaver, J.A., Melin, J. Stark, D. Quake, S.R., Horowitz, M.A., *Nature Physics*, 2010, *6*, 218-223.

[24] Studer, V., Hang, G., Pandolfi, A., Ortiz, M., Anderson, W.F. Quake, S.R., *J. Appl. Phys.*, 2004, *95*, 393-398.

[25] Unger, M.A., Chou, H.P., Thorsen, T., Scherer, A. Quake, S.R., *Science*, 2000, *288*, 113-116.

CHAPTER 9

CONCLUDING REMARKS

9.1 Fundamental Limitations of Quantification for Immunoassay

The sandwich immunoassay is generally considered the most sensitive immunoassay detection platform and has been a fundamental tool for the sensitive detection of proteins for several decades. While several studies have recently claimed single-molecule sensitivity capabilities, all have failed to reach that mark. There exists a fundamental statistical limitation to quantification abilities for immunoassay regardless of sample volume, imposed by molecular shot noise. The development of the theory addressing ultimate quantitation capability has been previously discussed (Chapter 5). Also demonstrated are the other potential influences on the LOQ of experimental immunoassay; NSB and the instrumental background. Ultimate limitations of quantification lie around 131 molecules in a sample (3.7 aM in 50 μL).

9.2 Current Commercial and Experimental Capabilities for Bioanalysis

Many experimental and commercial methods for bioanalysis have been explored in recent years. These methods have improved upon abilities of an immunoassay technique according to one, or more, of the six metrics described for a fully optimized assay; high sensitivity, rapid analysis, cost effective, simple to operate, use of low sample volumes, and the ability to multiplex for parallel detection. While the field has seen general improvements over the last several years, with various assays reaching aM sensitivity, analysis times under a minute, the ability for multiplexed detection, sample volumes around 10 μL, and minimal sample manipulations with the movement to microchip platforms, no single assay has attained complete optimization in all aspects.

9.3 Immunoassay Quantitation of Individual Targets

Although separation and detection of multiple targets in a total analysis system was defined as the ultimate goal, the immunoassay and protein separation studies presented in this dissertation focused mainly on the sensitive detection of individual targets. Earlier work described the use of a microscale batch incubation immunoassay technique sensitively quantify myoglobin, cTnI, and H-FABP individually (Chapter 4). Microchip experiments demonstrated the ability of dielectrophoresis to provide sample preparation, as well as electrophoretic exclusion to separate individual targets (Chapters 6 and 7). These results indicated that the use of electrophoretic exclusion in a separations based device would be useful to isolate targets prior to quantitation using a sandwich immunoassay.

9.4 Potential for Multiplex Immunoassay Utilizing a Microscale Total Analysis System

In addition to the off-chip immunoassay quantitation of individual targets, as well as quantitation of the enrichment of those proteins within an electrophoretic separation array, studies utilizing multiple proteins in the device suggest that electrophoretic exclusion is capable of separating proteins (Chapter 7). A microscale analysis system was designed and tested (Chapter 8) based on the parameters used for the separations based array. Studies indicate that proteins may be manipulated within the channel using electrophoretic exclusion, allowing both the separation and concentration of target species. Further refinement of the system, including incorporation of physical valves to prevent sample leakage into quantification reservoirs prior to analysis, holds the potential

for the development of a system optimized for clinical diagnostics utilizing immunoassay quantitation techniques.

9.5 Future Directions

Rapid analysis of complex biological samples requires the use of sample simplification techniques in combination with sensitive and selective quantitation of specific targets. Immunoassay techniques are attractive for incorporation into total analysis systems because they afford the sensitive detection of target molecules through the specific interaction between antibody and antigen. In terms of sensitivity, techniques exist that are nearing the fundamental limitations of the technique, and significant improvements in this area are unlikely to be realized. However, many challenges remain before an assay fully optimized for clinical diagnostics will exist. These challenges can be addressed through the incorporation of immunoassay detection methods into microscale total analysis systems, allowing the separation and concentration of target species through electrophoretic exclusion prior to detection. This can afford both the ability for multiplexed detection, as well as low sample consumption per analyte investigated. Incubations that rely on convective mixing can combat the long assay times required of traditional, static assays.

In altering the system in which an immunoassay is incorporated many of the obstacles remaining in the early, multiplexed detection of biomarker panels can be eliminated. It is feasible to envision a μTAS system in which an untreated complex sample can be separated as it is introduced and target species may be isolated and concentrated along an initial separations channel. Following rapid separation and concentration, immunoassay detection methods may be employed for rapid quantitation

without necessitating additional sample handling steps. These modifications could allow for near real-time blood testing to take place both in remote settings as well as clinically, achieving rapid diagnostic and disease intervention abilities.

REFERENCES

CHAPTER 1

[1] Zuskin, E., Lipozencic, J., Pucarin-Cvetkovic, J., Mustajbegovic, J., Schachter, N., Mucic-Pucic, B., Neralic-Meniga, I., *Acta Dermatovenerol Croat*, 2008, *16*, 149-157.

[2] Vecchio, I., Tornali, C., Rampello, L., Rigo, G.S., Rampello, L., Migliore, M., Castellino, P., Malta, R., Armocida, G., *Acta Medica Mediterranea*, 2013, *29*, 363-367.

[3] Papavramidou, N., Fee, E., Christopoulou-Aletra, H., *J. Gastrointest. Surg.*, 2007, *11*, 1728-1731.

[4] Loukas, M., Tubbs, R.S., Louis Jr., R.G., Pinyard, J., Vaid, S., Curry, B., *International Journal of Cardiology*, 2007, *120*, 145-149.

[5] Berche, P., *Clinical Microbiology and Infection*, 2012, *18*, 1-6.

[6] Koch, R., *Investigations into the Etiology of Traumatic Infective Diseases (The Relations of Micro-Organisms to Traumatic Infective Diseases)*, 1880, 19-39.

[7] Beale, L.S., *Disease Germs: Their Supposed Nature, an Original Investigation, with Critical Remarks (Disease Germs)*, 1870, 1-13.

[8] Morrow, D. A., Cannon, C. P., Jesse, R. L., Newby, L. K., Ravkilde, J., Storrow, A. B., Wu, A. H. B., Christenson, R.H., *Clinical Chemistry*, 2007, *53*, 552-574.

[9] Dimov, I.K., Basabe-Desmonts, L., Garcia-Cordero, J.L., Ross, B.M., Ricco, A.J., and Lee, L.P., *Lab on a Chip*, 2011, *11*, 845-850.

[10] Woolley, C. F., Hayes, M. A., *Bioanalysis*, 2013, *5*, 245-264.

[11] Cheung, K.T., Trevisan, J., Kelly, J.G., Ashton, K.M., Stringfellow, H.F., Taylor, S.E., Singh, M.N., Martin-Hirsch, P.L., Martin, F.L., *Analyst*, 2011, *136*, 2047-2055.

[12] Policar, C., Birgitta Waern, J., Plamont, M.A., Clede, S., Mayet, C., Prazeres, R., Ortega, J.M., Vessieres, A., Dazzi, A., *Angew. Chem. Int. Ed.*, 2011, *50*, 860-864.

[13] Huth, F., Schnell, M., Wittborn, J., Ocelic, N., Hillenbrand, R., *Nature Materials*, 2011, *10*, 352-356.

[14] Song, S. Y., Han, Y. D., Kim, K., Yang, S. S., and Yoon, H. C., *Biosensors and Bioelectronics*, 2011, *26*, 3818-3824.

[15] Garcia-Valdecasas, S., Ruiz-Alvarez, M.J., Garcia De Tena, J., De Pablo, R., Huerta, M. Barrionuevo, I., Coca, C., Arribas, I., *Acta Cardiol*, 2011, *66*, 315-321.

[16] Liao, J., Chan, C.P., Cheung, Y., Lu, J., Luo, Y., Cautherley, G.W.H., Glatz, J.F.C., Renneberg, R., *International Journal of Cardiology*, 2008, *133*, 420-423.

[17] Berson, S. A., Yalow, R. S., *Nature*, 1959, *184*, 1648-1649.

[18] Long, F., Zhu, A., Shi, H., Sheng, J., Zhao, Z., *Chemosphere*, 2015, *120*, 615-620.

[19] Allinson, J. L., *Bioanalysis*, 2011, *3*, 2803-2816.

[20] Verch, T., Bakhtiar, R., *Bioanalysis*, 2012, *4*, 177-188.

[21] Bellei, E., Bergamini, S., E. Monari, S., Fantoni, L.I., Cuoghi, A., *Amino Acids*, 2011, *40*, 145-156.

[22] Anderson, N.L., Anderson, N.G., *Molecular and Cellular Proteomics*, 2002, *1.11*, 845-867.

[23] Fan, R., Vermesh, O., Srivastava, A., Yen, B.K.H., Qin, L., Ahmad, H., Kwong, G.A., Liu, C.C., Gould, J., Hood, L., Heath, J.R., *Nature Biotechnology*, 2008, *26*, 1373-1378.

[24] Tirumalai, R.S., Chan, K.C., Prieto, D.A., Issaq, H.J., Conrads, T.P., and Veenstra, T.D., *Molecular and Cellular Proteomics*, 2006, *2.10*, 1096-1103.

[25] Mitchell, P., *Nature Biotechnology*, 2010, *28*, 665-670.

[26] Ohmura, N., Lackie, S. J, Saiki, H., *Anal. Chem.* 2001, *73*, 3392-3399.

[27] Diamandis, E. P., Christopoulos, T. K., *Immunoassay* (Theory of Immunoassays CH 3, Interfaces in Immunoassays CH 7), 1996, 25-187.

[28] Duhau, L., Grassi, J., Grouselle, D., Enjalbert, A., Grognet, J. M., *Journal of Immunoassay*, 1991, *12*, 233-250.

[29] Boever, J. D., Kohen, F., Bouve, J., Leyseele, D., Vandekerckhove, D., *Clinical Chemistry*, 1990, *36*, 2036-2041.

[30] Kratzsch, J., Ackermann, W., Keilacker, H., Besch, W., Keller, E., *Experimental and Clinical Endocrinology and Diabetes*, 1990, *95*, 229-236.

[31] Werthen, M., Nygren, H., *Journal of Immunological Methods* 1988, *115*, 71-78.

[32] Stenberg, M., Nygren, H., *Journal of Immunological Methods* 1988, *113*, 3-15.
[33] Stenberg, M., Stiblert, L., Nygren, H., *J. theor. Biol.* 1986, *120*, 129-140.

[34] Nygren, H., Werthen, M., Stenberg, M., *Journal of Immunological Methods* 1987, *101*, 63-71.
[35] Nygren, H., Stenberg, M., *Immunology* 1989, *66*, 321-327.

[36] Ekins, R., Kelso, D., *Clin. Chem.* 2011, *57*, 372-375.

[37] Ishikawa, E., Hashida, S., Kohno, T., Hirota, K., *Clinica Chimica Acta* 1990, *194*, 51-72.

[38] Tian, J., Zhou, L., Zhao, Y., Wang, Y., Peng, Y., Hong, X., Zhao, S., *J Fluoresc*, 2012.

[39] Lee, G. Y., Choi, Y. H., Chung, H. W., Ko, H., Cho, S., Pyun, J. C., *Biosensors and Bioelectronics*, 2013, *40*, 227-232.

[40] Casolari, S., Roda, B., Mirasoli, M., Zangheri, M., Patrono, D., Reschiglian, P., Roda, A., *Analyst*, 2013, *138*, 211-219.

[41] Schiel, J. E., Tong, Z., Sakulthaew, C., Hage, D. S., *Analytical Chemistry*, 2011, *83*, 9384-9390.

[42] Fu, X., Meng, M., Zhang, Y., Yin, Y., Zhang, X., Xi, R., *Analytica Chimica Acta*, 2012, *722*, 114-118.

[43] Sakamaki, N., Ohiro, Y., Ito, M., Makinodan, M., Ohta, T., Suzuki, W., Takayasu, S., Tsuge, H., *Clinical and Vaccine Immunology*, 2012, *19*, 1949-1954.

[44] Lee, W.B., Chen, Y.H., Lin, H.I., Shiesh, S.C., Lee, G.B., *Sensors and Actuators B: Chemical*, 2011, *157*, 710-721.

[45] Song, S. Y., Han, Y. D., Kim, K., Yang, S. S., Yoon, H. C., *Biosensors and Bioelectronics*, 2011, *26*, 3818-3824.

[46] Lee, S., Kang, S.H., *Talanta*, 2012, *99*, 1030-1034.

[47] Sloan, J. H., Siegel, R. W., Ivanova-Cox, Y. T., Watson, D. E., Deeg, M. A., Konrad, R. J., *Clinical Biochemistry*, 2012, *45*, 1640-1644.

[48] Vashist, S. K., *Biosensors and Bioelectronics*, 2013, *4*, 297-302.

[49] Lacharme, F., Vandevyver, C., Gijs, M. A. M., *Microfluid Nanofluidics*, 2009, *7*, 479-487.

[50] Lacharme, F., Vandevyver, C., Gijs, M. A. M., *Analytical Chemistry*, 2008, *80*, 2905-2910.

[51] Petkus, M. M., McLauchlin, M., Vuppu, A. K., Rios, L., Garcia, A. A., Hayes, M. A., *Analytical Chemistry*, 2006, *78*, 1405-1411.

[52] Hayes, M. A., Petkus, M. M., Garcia, A. A., Taylor, T., Mahanti, P., *Analyst*, 2008, *134*, 533-541.

[53] Mahanti, P., Taylor, T., Hayes, M. A., Cochran, D., Petkus, M. M., *Analyst*, 2011, *136*, 365-373.

[54] Woolley, C.F., Hayes, M.A., *Anal. Methods.*, submitted.

[55] Macdonald, S.P.J., Nagree, Y., Fatovich, D.M., Phillips, M., Brown, S.G.A., *Emergency Medicine Journal*, 2012, *30*, 149-154.

[56] Molin, S.Da., Cappellini, F., Falbo, R., Signorini, S., Brambilla, P., *Clinical Biochemistry*, 2014, *47*, 247-249.

[57] Jayadev, C., Rout, R., Price, A., Hulley, P., Mahoney, D., *Journal of Immunological Methods*, 2012, *386*, 22-30.

[58] Pereira, A. T., Novo, P., Prazeres, D. M. F., Chu, V., Conde, J. P., *Biomicrofluidics*, 2011, *5*, 014102-1-014102-13.

[59] Granger, J.H., Granger, M.C., Firpo, M.A., Mulvihill, S.J., Porter, M.D., *Analyst*, 2013, *138*, 410-416.

[60] Proczek, G., Gassner, A. L., Busnel, J. M., Girault, H. H. , *Anal. Bioanal. Chem.* 2012, *402*, 2645-2653.

[61] Camerini, S., Polci, M. L., Liotta, L. A., Petricoin, E. F., Zhou, W., *Proteomics Clin. Appl.*, 2007, *1*, 176-184.

[62] Joglekar, M., Roggers, R. A., Zhao, Y., Trewyn, B. G., *RSC Advances*, 2013, *3*, 2454-2461.

[63] Wang, X., Masschelein, E., Hespel, P., Adams, E., Schepdael, A. V., *Electrophoresis*, 2012, *33*, 402-405.

[64] Jubery, T. Z., Hossan, M. R., Bottenus, D. R., Ivory, C. F., Dong, W., Dutta, P., *Biomicrofluidics*, 2012, *6*, 016503-1-13.

[65] Startsev, M. A., Inglis, D. W., Baker, M. S., Goldys, E. M., *Analytical Chemistry*, 2013, *85*, 7133-7138.

[66] Inglis, D. W., Goldys, E. M., Calander, N. P., *Angew. Chem. Int. Ed.*, 2011, *50*, 7546-7550.

[67] Kenyon, S. M., Weiss, N. G., Hayes, M. A., *Electrophoresis*, 2012, *33*, 1227-1235.

[68] Kenyon, S. M., Keebaugh, M. W., Hayes, M. A., *Electrophoresis*, 2014, *35*, 2551-2559.

CHAPTER 2

[1] Moschallski, M., Evers, A., Brandsetter, T., Ruhe, J., *Analytica Chimica Acta*, 2013, *781*, 72-79.

[2] Wang, H., Ou, L.M.L, Suo, Y., Yu, H.Z., *Analytical Chemistry*, 2011, *83*, 1557-1563.

[3] Farajollahi, M.M., Cook, D.B, Hamzehlou, S., Self, C.H., *Scandinavian Journal of Clinical and Laboratory Investigation*, 2012, *72*, 531-539.

[4] Tamarit-Lopez, J., Morais, S., Puchades, R., Maquieira, A., *Bioconjugate Chemistry*, 2011, *22*, 2573-2580.

[5] Zhang, B., Liu, B., Zhou, J., Tang, J., Tang, D., *Applied Materials and Interfaces*, 2013, *5*, 4479-4485.

[6] FAST® Slide Protein Microarray 2013 KeraFast, Inc. https://www.kerafast.com/c-1-fast-slide-protein-microarray.aspx

[7] Moschallski, M., Baader, J., Prucker, O., Ruhe, J., *Analytica Chimica Acta*, 2010, *671*, 92-98.

[8] Wen, J., Shi, X., He, Y., Zhou, J., Li, Y., *Anal. Bioanal. Chem.*, 2012, *404*, 1935-1944.

[9] Yu, H.Z., Li, Y., Ou, L.M.L., *Accounts of Chemical Research*, 2013, *46*, 258-268.

[10] Imaad, S.M., Lord, N., Kulsharova, G., Liu, G.L., *Lab on a Chip*, 2011, *11*, 1448-1456.

[11] Tamarit-Lopez, J., Morais, S., Manuis, M.J., Puchades, R., Maquieira, A., *Analytical Chemistry*, 2010, *82*, 1954-1963.

[12] Balsam, J., Rasooly, R., Bruck, H.A, Rasooly, A., *Biosensors and Bioelectronics*, 2014, *51*, 1-7.

[13] Cheung, K.T., Trevisan, J., Kelly, J.G., Ashton, K.M., Stringfellow, H.F., Taylor, S.E., Singh, M.N., Martin-Hirsch, P.L., Martin, F.L., *Analyst*, 2011, *136*, 2047-2055.

[14] Pita, I., Hendaoui, N., Liu, N., Kumbham, M., Tofail, S.A.M., Peremans, A., Silien, C., *Optics Express*, 2013, *21*, 25632-25642.

[15] Huth, F., Schnell, M., Wittborn, J., Ocelic, N., Hillenbrand, R., *Nature Materials*, 2011, *10*, 352-356.

[16] Liao, C.R., Rak, M., Lund, J., Unger, M., Platt, E., Albensi, B.C., Hirschmugi, C.J., Gough, K.M., *Analyst*, 2013, *138*, 3991-3997.

[17] Nasse, M.J., Walsh, M.J., Mattson, E.C., Reininger, R., Kajdacsy-Balla, A., Macias, V., Bhargava, R., Hirschmugl, C.J., *Nature Methods*, 2011, *8*, 413-416.

[18] Reddy, R.K., Walsh, M.J., Schulmerich, M.V., Carney, P.S., Bhargava, R., *Applied Spectroscopy*, 2013, *67*, 93-105.

[19] Marcott, C., Lo, M., Kjoller, K., Domanov, Y., Balooch, G., Luengo, G.S., *Experimental Dermatology*, 2013, *22*, 417-437.

[20] Policar, C., Birgitta Waern, J., Plamont, M.A., Clede, S., Mayet, C., Prazeres, R., Ortega, J.M., Vessieres, A., Dazzi, A., *Angew. Chem. Int. Ed.*, 2011, *50*, 860-864.

[21] Mudanyali, O., Tseng, D., Oh, C., Isikman, S.O, Sencan, ., I., Bishara, W., Oztoprak, C., Seo, S., Khademhosseini, B., Ozcan, A., *Lab on a Chip*, 2010, *10*, 1417-1428.

[22] Tseng, D., Mudanyali, O., Oztoprak, C., Isikman, S.O., Sencan, I., Yaglidere, O., Ozcan, A., *Lab on a Chip*, 2010, *10*, 1787-1792.

[23] Zhu, H., Mavandadi, S., Coskun, A.F., Yaglidere, O., Ozcan, A., *Analytical Chemistry*, 2011, *83*, 6641-6647.

[24] Gallegos, D., Long, K.D., Yu, H., Clark, P.P., Lin, Y., George, S., Nath, P., Cunningham, B.T., *Lab on a Chip*, 2013, *13*, 2124-2132.

[25] Balsam, J., Bruck, H.A., Rasooly, A., *Sensors and Actuators B: Chemical*, 2013, *186*, 711-717.

[26] Mudanyali, O., Dimitrov, S., Sikora, U., Padmanabhan, S., Navruz, I., Ozcan, A., *Lab on a Chip*, 2012, *12*, 2678-2686.

[27] Pallapa, M., Ou, L.M.L., Parameswaran, M., Yu, H.Z., *Sensors and Actuators B*, 2010, *148*, 620-623.

[28] Zhu, H., Isikman, S.O., Mudanyali, O., Greenbaum, A., Ozcan, A., *Lab on a Chip*, 2013, *13*, 51-67.

[29] Zeng, Y., Wang, T., *Anal. Bioanal. Chem.*, 2013, *405*, 5743-5758.

[30] Zhu, H., Cox, E., Quian, J., *Proteomics Clin. Appl.*, 2012, *6*, 548-562.

[31] Walsh, M.J., Reddy, R.K., *IEEE Journal of Selected Topics in Quantum Electronics*, 2012, *18*, 1502-1513.

[32] Prashanth, G.R., Goudar, V.S., Raichur, A.M., Varma, M.M., *Sensors and Actuators B: Chemical*, 2013, *183*, 496-503.

[33] Mujawar, L.H., Moers, A., Norde, W., van Amerongen, A., *Anal. Bioanal Chem*, 2013, *405*, 7469-7476.

[34] Mujawar, L.H., Maan, A.A., Khan, M.K.I., Norde, W., van Amerongen, A., *Analytical Chemistry*, 2013, *85*, 3723-3729.

[35] "ONCYTE® Nitrocellulose Film Slides" Grace Bio-Labs, Inc. 2010. http://www.gracebio.com/life-science-products/microarray/oncyte-nitrocellulose-film-slides.html

[36] UniSart® Membranes Consistency by Design http://www.sartorius-stedim.com.tw/Attachment/FCKeditor/Product/file/PDF/lab/filter&membran/Broch_Unisart_Membranes_SL-1522-e.pdf

[37] Zhang, B., Liu, B., Zhou, J., Tang, J., Tang, D., *Applied Materials and Interfaces*, 2013, *5*, 4479-4485.

[38] Peretz-Soroka, H., Pevzner, A., Davidi, G., Naddaka, V., Tirosh, R., Flaxer, Patolsky, F., *NANO Letters*, 2013, *13*, 3157-3168.

[39] Chandra, P., Abbas Zaidi, S., Noh, H.B., Shim, Y.B., *Biosensors and Bioelectronics*, 2011, *28*, 326-332.

[40] Wang, J., Morabito, K., Erkers, T., Tripathi, A., *Analyst*, 2013, *138*, 6573-6581.

[41] Lin, Y.H., Yang, Y.W., Chen, Y.D., Wang, S.S., Chang, Y.H., Wu, M.H., *Lab on a Chip*, 2012, *12*, 1164-1173.

[42] Arnandis-Chover, T., Morais, S., Gonzalez-Martinez, M.A., Puchades, R., Maquieira, A., *Biosensors and Bioelectronics*, 2014, *51*, 109-114.

[43] Disc-shaped Point-of-Care platform for infectious disease diagnosis, K. Mitsakakis, 2014 http://www.imtek.de/laboratories/mems-applications/projects/projects_overview?projectId=8073

[44] Gyrolab Bioaffy CDs 2013 Gyros AB http://www.gyros.com/products/products-optimized/gyrolab-bioaffy-cds/

[45] GenePOC 2014, GenePOC, Inc. http://www.genepoc-diagnostics.com/Technology.shtml

[46] Liu, X.F., Wang, X., Weaver, R.J., Calliste, L., Xia, C., He, Y.J., Chen, L., *Journal of Pharmacological and Toxicological Methods*, 2012, *65*, 107-114.

[47] Guo, Y.J., Sun, G.M., Zhang, L., Tang, Y.J., Luo, J.J., Yang, P.H., *Sensors and Actuators B: Chemical*, 2014, *191*, 741-749.

[48] Clede, S., Lambert, F., Sandt, C., Kascakova, S., Unger, M., Harte, E., Platmont, M.A., Saint-Fort, R., Deniset-Besseau, A., Gueroui, Z., Hirschmugl, C., Lecomte, S., Dazzi, A., Vessieres, A., Policar, C., *Analyst*, 2013, *138*, 5627-5638.

[49] NeaSNOM Microscope, 2013 Neaspec http://www.neaspec.com/products/neasnom-microscope/

[50] Amenabar, I., Poly, S., Nuansing, W., Hubrich, E.H., Govyadinov, A.A., Huth, F., Krutokhvostov, R., Zhang, L., Knez, M., Heberle, J., Bittner, A.M., Hillenbrand, R., *Nature Communications*, 2013, *4*, 1-9.

[51] Govyadinov, A.A., Amenabar, I., Huth, F., Carney, P.S., Hillenbrand, R., *J. Phys. Chem. Lett.*, 2013, *4*, 1526-1531.

[52] Kitsommart, R., Ngerncham, S., Wongsiridej, P., Kolatat, T., Jirapaet, K.S., Paes, B., *Eur J Pediatr*, 2013, *172*, 1181-1186.

[53] StatStrip® Connectivity and StatStrip Xpress Point-of-Care Glucose/Ketone Monitoring Systems 2014 Nova Biomedical Corporation http://www.novabiomedical.com/products/statstrip-glucoseketone-statstrip-xpress-glucoseketone/

[54] Nadeski, M., Frantz , G., The future of medical Imaging http://www.ti.com/lit/wp/slyy020/slyy020.pdf

[55] Cnoga Medical develops diagnostics through skin color, G. Weinreb, 2013 Globes http://www.globes.co.il/serveen/globes/docview.asp?did=1000877563

CHAPTER 3

[1] Engvall E, Jonsson K, Perlmann P., *Biochimica et Biophysica Acta.* 1971, *251*, 427-434 .

[2] Hahn YK, Park JK., *Lab Chip.* 2011, *11*, 2045-2048.

[3] Ranzoni A, Sabatte G, van Ijzendoorn LJ, Prins MWJ., *ACSnano*. 2012, *6*, 3134-3141.

[4] Mahanti P, Taylor T, Hayes MA, Cochran D, Petkus MM., *Analyst*. 2011, *136*, 365-373.

[5] Chang B, Gray P, Piltch M, *et al*., *J. Viro. Met.* 2009, *159*, 15-22.

[6] Ziegler J, Zimmermann M, Hunziker P, Delamarche E., *Anal. Chem.* 2008, *80*, 1763-1769.

[7] Li P, Abolmaaty A, D'Amore C, Demming S, Anagnostopoulos C, Faghri M., *Microfluid Nanofluid*. 2009, *7*, 593-598.

[8] Peyman SA, Iles A, Pamme N., *Lab Chip*. 2009, *9*, 3110-3117.

[9] Sasso LA, Under A, Zahn JD., *Microfluid Nanofluid*. 2010, *9*, 253-265.

[10] Shao G, Wang J, Li Z, Saraf L, Wang W, Lin Y, *Sensors and Actuators B*. 2011, *159*, 44-50.

[11] Do J, Ahn CH. , *Lab Chip.* 2008, *8*, 542-549.

[12] Langenhorst RJ, Lawson S, Kittawornrat A, *et al.*, *Clin. Vacc. Immunol.* 2011, *19*, 180-189.

[13] Lawson S, Lunney J, Zuckermann F, *et al.*, *Vaccine.* 2010, *28*, 5356-5364.

[14] Cao Z, Li H, Lau C, Zhang Y. , *Analytica Chimica Acta*. 2011, *698*, 44-50.

[15] Zimmermann M, Hunziker P, Delamarche E., *Biomed. Microdevices.*2009, *11*, 1-8.

[16] Pesce AJ, Michael JG., *J. Immunol. Met.* 1992, *150*, 111-119.

[17] Lee S, Cho NP, Kim JD, Jung H, Kang SH, *Analyst*. 2009, *134*, 933-938.

[18] Vignali DAA.,. *J.Immunol. Met.* 2000, *243*, 243-255.

[19] Allinson JL., *Bioanalysis.* 2011, *3*, 2803-2816.

[20] Verch T, Bakhtiar R., *Bioanalysis.* 2012, *4*, 177-188.

[21] Hayes MA, Petkus MM, Garcia AA, Taylor T, Mahanti P., *Analyst.* 2009, *134*, 533-541.

[22] Watson DS, Reddy SM, Brahmakshatriya V, Lupiani B., *J. Immunol. Met.* 2009, 340, 123-131.

[23] Kellar KL, Douglass JP., *J. Immunol. Met.* 2003, *279*, 277-285.

[24] Clavijo A, Hole K, Li M, Collignon B., *Vaccine.* 2006, *24*, 1693-1704.

[25] Ravindran R, Khan IH, Krishnan VV, *et al.*, *J. Immunol. Met.* 2010, *363*, 51-59.

[26] Svateck RS, Shah JB, Xing J, *et al.*, *Cancer.* 2010, *116*, 4513-4519.

[27] Smith J, Samons D, Robertson S, Biagini R, Snawder J., *Toxic. Mech. Meth.* 2010, *20*, 587-593.

[28] Kuriakose T, Hilt DA, Jackwood MW. , *Avian Diseases*. 2012, *56*, 90-96.

[29] Pochechueva T, Chinarev A, Spengler M, *et al.*, *Analyst*. 2011, *136*, 560-569.

[30] Ji XH, Cheng W, Guo F, *et al.*, *Lab Chip.* 2011, *11*, 2561-2568.

[31] Talat N, Shahid F, Perry S, *et al.*, *Cytokine.* 2011, *54*, 136-143.

[32] Bin Z, Ke W, Jian J, *et al.*, *Food. Anal. Meth.* 2011, *4*, 228-232.

[33] Cauchon E, Liu S, Percival MD, *et al.*, *Anal. Biochem.* 2009, *388*, 134-139.

[34] Li Z, Zhang QY, Zhao LX, *et al.*, *Sci. China. Chem.* 2010, *53*, 812-819.

[35] Sista RS, Eckhardt AE, Srinivasan V, Pollack MG, Palanki S, Pamola VK., *Lab Chip.* 2008, *8*, 2188-2196.

[36] Lacharme F, Vandevyver C, Gijs MAM. , *Microfluid Nanofluid*. 2009, *7*, 479-487.

[37] Dupont EP, Labonne E, Vandevyver C, Lehmann U, Charbon E, Gijs MAM., *Anal. Chem.* 2010, *82*, 49-52.

[38] Kim JI, Wang C, Kuizon S, *et al*., *Neuroimmunol* 2005, *158*, 112-119.

[39] Proczek G, Gassner AL, Busnel JM, Girault HH., *Anal. Bioanal. Chem.* 2012, *402*, 2645-2653.

[40] Lacharme F, Vandevyver C, Gijs MAM. , *Anal. Chem.* 2008, *80*, 2905-2910.

[41] Piao Y, Jin Z, Lee D, *et al.*, *Biosens.Bioelectron.* 2011, *26*, 3192-3199.

[42] Soh N, Tanaka M, Hirakawa K, *et al.*, *Anal. Sci.* 2011, *27*, 1069-1076.

[43] Gao D, Li HF, Guo GS, Lin JM., *Talanta.* 2010, *82*, 528-533.

[44] Chen H, Abolmatty A, Faghri M., *Microfluid. Nanofluid.* 2011, *10*, 593-605.

[45] Squires TM, Messinger RJ, Manalis SR., *Nat. Biotechnol.* 2008, *26*, 417-426.

[46] Sivagnanam V, Song B, Vandevyver C, Gijs MAM., *Anal. Chem.* 2009,*81*, 6509-6515.

[47] Sivagnanam V, Bouhmad A, Lacharme F, Vandevyver C, Gijs MAM., *Microelectron. Eng.* 2009, *86*, 1404-1406.

[48] Song SY, Han YD, Kim K, Yang SS, Yoon HC., *Biosens. Bioelectron.* 2011, *26*, 3818-3824.

[49] Afshar R, Moser Y, Lehnert T, Gijs MAM., *Anal. Chem.* 2011, *83*, 1022-1029.

[50] Fu Z, Shao G, Wang J, Lu D, Wang W, Lin Y., *Anal. Chem.* 2011, *83*, 2685-2690.

[51] Pfaunmiller E, Moser AC, Hage DS., *Methods* 2012, *56*, 130-135.

[52] Schiel JE, Tong Z, Sakulthaew C, Hage DS., *Anal. Chem.* 2011, *83*, 9384-9390.

[53] Liu Y, Wang H, Huang J, Yang J, Liu B, Yang P., *Anal. Chim. Acta* 2009, *650*, 77-82.

[54] Sinha A, Ganguly R, Puri IK., *J. Appl. Phys.* 2010, *107*, 034907-1-034907-6.

[55] Lian W, Wu D, Lim DV, Jin S., *Anal. Biochem.* 2010, *401*, 271-279.

[56] Han KC, Ahn DR, Yang EG., *Bioconjugate Chem.* 2010, *21*, 2190-2196.

[57] Ruckstuhl T, Winterflood CM, Seeger S., *Anal. Chem.* 2011, *83*, 2346-2360.

[58] Kai J, Puntambekar A, Sehy D, Brescia P, Banks P, *Gen. Engineer. Biotechnol. News.* 2011, *31*, 26-27.

[59] Lee BS, Lee JN, Park JM, *et al.*, *Lab Chip.* 2009, *9*, 1548-1555.

[60] Roman J, Qiu J, Dornadula G, *et al.*, *J. Pharm. Toxic. Meth.* 2011, *63*, 227-235.

[61] Yang Z, Liu H, Zong C, Yan F, Ju H., *Anal. Chem.* 2009, *81*, 5484-5489.

[62] Yang Z, Zong C, Yan F, Ju H., *Talanta*. 2010, *82*, 1462-1467.

[63] Xue C, Zhao H, Liu H, *et al.*, *Sens.Actuators B.* 2011, *156*, 863-866.

[64] Tan W, Huang Y, Nan T, *et al.*, *Anal. Chem.* 2010, *82*, 615-620.

Websites

[101] RNase H1Antibody (5D10). www.novusbio.com/H00246243-M01.

CHAPTER 4

[1] Qureshi, A., Gurbuz, Y., Niazi, J.H., *Sensors and Actuators B*, 2012, *171-172*, 62-76.

[2] ACC and Cardiac Biomarkers, 2014, http://www.acc.org/education-and-meetings/image-and-slide-gallery/media-detail?id=d9c880ce33f3482f993161076a32990a

[3] Vasan, R. S., *Circulation*, 2006, *113*, 2335-2362.

[4] Kakoti, A., Goswam, P. i, *Biosensors and Bioelectronics*, 2013, *43*, 400-411.

[5] Ishii, J., Wang, J.H., Naruse, H., Taga, S., Kinoshita, M., Kurokawa, H., Iwase, M., Kondo, T., Nomura, M., Nagamura, Y., Watanabe, Y., Hishida, H., Tanaka, T., Kawamura, K., *Clinical Chemistry*, 1997, *43*, 1372-1378.

[6] Huang, C.H., Tsai, M.S., Chien, K.L., Hsu, C.Y., Chang, W.T., Wang, T.D., Chen, S.C., Huei-Ming Ma, M., Chen, W.J., *Clinica Chimica Acta*, 2014, *435*, 7-13.

[7] Glatz, J.F., Renneberg, R., *Clinical Lipidology*, 2014, *9*, 205-220.

[8] Macdonald, S.P.J., Nagree, Y., Fatovich, D.M., Phillips, M., Brown, S.G.A., *Emergency Medicine Journal*, 2012, *30*, 149-154.

[9] Liao, J., Chan, C.P., Cheung, Y., Lu, J., Luo, Y., Cautherley, G.W.H., Glatz, J.F.C., Renneberg, R., *International Journal of Cardiology*, 2008, *133*, 420-423.

[10] Tonomura, Y., Matsushima, S., Kashiwagi, E., Fujisawa, K., Takagi, S., Nishimura, Y., Fukushima, R., Torii, M., Matsubara, M., *Toxicology*, 2012, *302*, 179-189.

[11] Inoue, K., Suwa, S., Ohta, H., Itoh, S., Maruyama, S., Masuda, N., Sugita, M., Daida, H., *Circulation Journal*, 2011, *75*, 2813-2820.

[12] Molin, S.Da., Cappellini, F., Falbo, R., Signorini, S., Brambilla, P., *Clinical Biochemistry*, 2014, *47*, 247-249.

[13] Setsuta, K., Seino, Y., Mizuno, K., *International Journal of Cardiology*, 2014, *176*, 1323-1325.

[14] McMahon, C.G., Lamont, J.V., Curtin, E., McConnell, R.I., Crockard, M., Kurth, M.J., Crean, P., Fitzgerald, S.P., *American Journal of Emergency Medicine*, 2012, *30*, 267-274.

[15] Gnedenko, O.V., Mezentsev, Y.V., Molnar, A.A., Lisitsa, A.V., Ivanov, A.S., Archakov, A.I., *Analytica Chimica Acta*, 2013, *759*, 105-109.

[16] Body, R., McDowell, G., Carley, S., Wibberley, C., Ferguson, J., Mackway-Jones, K., *Resuscitation*, 2011, *82*, 1041-1046.

[17] Song, S. Y., Han, Y. D., Kim, K., Yang, S. S., Yoon, H. C., *Biosensors and Bioelectronics*, 2011, *26*, 3818-3824.

[18] Casolari, S., Roda, B., Mirasoli, M., Zangheri, M., Patrono, D., Reschiglian, P., Roda, A., *Analyst*, 2013, *138*, 211-219.

[19] Tian, J., Zhou, L., Zhao, Y., Wang, Y., Peng, Y., Hong, X., Zhao, S., *J Fluoresc*, 2012.

[20] Lin, D., Wu, J., Wang, M., Yan, F., Ju, H., *Analytical Chemistry*, 2012, *84*, 3662-3668.

[21] Liang, G., Liu, S., Zou, G., Zhang, X., *Analytical Chemistry*, 2012, *84*, 10645-10649.

[22] Spindel, S., Sapsford, K.E., *Sensors*, 2014, *14*, 22313-22341.

[23] Ammar, M., Smadja, C., Phuong, G.T., Azzous, M., Vigneron, J., Etcheberry, A., Taverna, M., Dufour-Gergam, E., *Biosensors and Bioelectronics*, 2013, *40*, 329-335.

[24] Caulum, M.M., Murphy, B.M., Ramsay, L.M., Henry, C.S., *Analytical Chemistry*, 2007, *79*, 5249-5256.

[25] Park, M., Bong, J.H., Chang, Y.W., Yoo, G., Jose, J., Kang, M.J., Pyun, J.C., *Analytical Methods*, 2014, *6*, 1700-1708.

[26] Han, J., Zhang, J., Xia, Y., Li, S., Jiang, L., *Colloids and Surfaces A: Physiochem. Eng. Aspects*, 2011, *379*, 2-9.

[27] Proczek, G., Gassner, A. L., Busnel, J. M., Girault, H. H., *Anal. Bioanal. Chem.*, 2012, *402*, 2645-2653.

[28] Ranzoni, A., Sabatte, G., van Ijzendoorn, L. J., Prins, M. W. J., *ACS Nano*, 2012, *6*, 3134-3141.

[29] Hahn, Y. K., Park, J. K., *Lab Chip* 2011, *11*, 2045-2048.

[30] Hayes, M.A., Petkus, M.M., Garcia, A.A., Taylor, T., Mahanti, P., *Analyst*, 2009, *134*, 533-541.

[31] Zhang, Y., Zhou, D., *Expert Reviews Ltd*, 2012, *ISSN 1473-7159*, 565-571.

[32] Petkus, M.M., McLauchlin, M., Vuppu, A.K., Rios, L., Garcia, A.A., Hayes, M.A., *Analytical Chemistry*, 2006, *78*, 1405-1411.

[33] Zhu, Y.D., Peng, J., Jiang, L.P., Zhu, J.J., *Analyst*, 2014, *139*, 649-655.

[34] Sakamoto, S., Omagari, K., Kita, Y., Mochizuki, Y., Maito, Y., Kawata, S., Matsuda, S., Itano, O., Jinno, H., Takeuchi, H., Yamaguchi, Y., Kitagawa, Y., Handa, H., *Clinical Chemistry*, 2014, *60*, 610-620.

[35] Woolley, C.F., Hayes, M.A., *Bioanalysis*, 2013, *5*, 245-264.

[36] Fluorescein-EX Protein Labeling Kit, 2004, http://tools.invitrogen.com/content/sfs/manuals/mp10240.pdf.

[37] Currie, L.A., *Analytical Chemistry*, 1968, *40*, 586-593.

[38] Cardiac Marker ELISA Kits, 2013, http://www.calbiotech.com/products/elisa-kits/human-elisa-kits/cardiac-marker-elisa-kits.

CHAPTER 5

[1] Brown, E. N., McDermott, T. J., Bloch, K. J., McCollom, A. D., *Clinical Chemistry* 1996, *42*, 893-903.

[2] Ekins, R., Kelso, D., *Clin. Chem.* 2011, *57*, 372-375.

[3] Cook, D. B., Selt, C. H., *Clinical Chemistry* 1993, *39*, 965-971.

[4] Miles, L. E. M., Hales, C. N., *Nature* 1968, *219*, 186-189.

[5] Ishikawa, E., Hashida, S., Kohno, T., Hirota, K., *Clinica Chimica Acta* 1990, *194*, 51-72.

[6] Ylander, P. J., Hanninen, P., *Biophysical Chemistry* 2010, *151*, 105-110.

[7] Klenin, K. V., Kusnezow, W., Langowski, J., *J. Chem. Phys.* 2005, *122*, 214715-1-214715-11.

[8] Rodbard, D., Feldman, Y., *Immunochemistry* 1978, *15*, 71-76.

[9] Sadana, A., Chen, Z., *Biosensors and Bioelectronics* 1996, *11*, 17-33.

[10] Werthen, M., Nygren, H., *Journal of Immunological Methods* 1988, *115*, 71-78.

[11] Nygren, H., Werthen, M., Stenberg, M., *Journal of Immunological Methods* 1987, *101*, 63-71.

[12] Nygren, H., Stenberg, M., *Immunology* 1989, *66*, 321-327.

[13] Stenberg, M., Nygren, H., *J. theor. Biol.* 1985, *113*, 589-597.

[14] Stenberg, M., Stiblert, L., Nygren, H., *J. theor. Biol.* 1986, *120*, 129-140.

[15] Beumer, T., Haarbosch, P., Carpay, W., *Anal. Chem.* 1996, *68*, 1375-1380.

[16] Pesce, A. J., Michael, J. G., *Journal of Immunological Methods* 1992, *150*, 111-119.

[17] Stenberg, M., Nygren, H., *Journal of Immunological Methods* 1988, *113*, 3-15.

[18] Rodbard, D., Feldman, Y., Jaffe, M. L., Miles, L. E. M., *Immunochemistry* 1978, *15*, 77-82.

[19] Jackson, T. M. , Ekins, R. P., *Journal of Immunological Methods* 1986, *87*, 13-20.

[20] Glass, T. R., Ohmura, N., Saiki, H., *Anal. Chem.* 2007, *79*, 1954-1960.

[21] Seth, J., *Clinical Chemistry* 1990, *36*, 178.

[22] Kalman, S. M., Clark, D. R., Moses, L. E., *Clin. Chem.* 1984, *30*, 515-517.

[23] Currie, L. A., *Analytical Chemistry* 1968, *40*, 586-593.

[24] Yalow, R. S., Berson, S. A., *Nature* 1959, *184*, 1648-1649.

[25] Hassibi, A., Vikalo, H., Hajimiri, A., *Journal of Applied Physics* 2007, *102*, 014909-1-014909-12.

[26] Rissin, D. M., Kan, C. W., Campbell, T. G., Howes, S. C., Fournier, D. R., Song, L., Piech, T., Patel, P. P., Chang, L., Rivnak, A. J., Ferrell, E. P., Randall, J. D.,

Provuncher, G. K., Walt, D. R., Duffy, D. C., *Nature Biotechnology*, 2010, *28*, 595-599.

[27] Tessler, L. A., Mitra, R. D., *Proteomics* 2011, *11*, 4731-4735.

[28] Schmidt, R., Jacak, J., Schirwitz, C., Stadler, V., Michel, G., Marme, N., Schutz, G. J., Hoheisel, J. D., Knemeyer, J. P., *Journal of Proteome Research* 2011, *10*, 1316-1322.

[29] Hashida, S., Ishikawa, E., *J. Biochem.* 1990, *108*, 960-964.

[30] Ohmura, N., Lackie, S. J., Saiki, H., *Anal. Chem.* 2001, *73*, 3392-3399.

[31] Chang, L., Rissin, D. M., Fournier, D. R., Piech, T., Patel, P. P., Wilson, D. H., Duffy, D. C., *Journal of Immunological Methods* 2012, *378*, 102-115.

[32] Shalev, A., Greenberg, A. H., McAlpine, P. J., *J. Immunol. Meth.* 1980, *38*, 125-39.

[33] Harris, C. C., Yolken, R. H., Krokan, H., Hsu, I. C., *Proc. Natl. Acad. Sci. USA* 1979, *76*, 5336-5339.

[34] Hungerford, J. M., Christian, G. D., *Anal. Chem.* 1986, *58*, 2567-2568.

[35] Diamandis, E.P., Christopoulos, T.K., *Immunoassay* (theory of immunoassays CH 3) 1996, 25-49.

[36] Ezan, E., Tiberghien, C., Dray, F., *Clin. Chem.* 1991, *37*, 226-230.

[37] Yalow, R., *Diabetes*, 1961, *10*, 339-344.

[38] Ractliffe, J. F., *Elements of Mathematical Statistics*, (the normal distribution CH 7) 1967, 51-68.

[39] Ewing, G.W., *Chemical Instrumentation: XXXIX. Signal to Noise Optimization in Chemistry.* Chemical Education, 1968. *45*(7): p. A533-A544.

[40] Johnson, J.B., *Thermal Agitation of Electricity in Conductors.* Physical Review, 1928. *32*(1): p. 97-109.

[41] Nyquist, H., *Thermal Agitation of Electric Charge in Conductors.* Physical Review, 1928. **32**(1): p. 110-113.

[42] Abcam plc., 2015, http://www.abcam.com/index.html?pageconfig=resource&rid=15749&source=pagetrap&viapagetrap=kd.

[43] Voet, D., Voet, J.G., Pratt, C.W., *Fundamentals of Biochemistry* (Antibodies Section 7.3) 2008, 209-215.

[44] Guo, Y., Harel, O., Little, R. J., *Epidemiology* 2010, *21*, S10-S16.

[45] O'Malley, A.J., Deely, J.J., *Aust. N.Z. J. Stat.*, 2003, *45*, 43-65.

CHAPTER 6

[1] Fan, R., Vermesh, O., Srivastava, A., Yen, B.K.H., Qin, L., Ahmad, H., Kwong, G.A., Liu, C.C., Gould, J., Hood, L., Heath, J.R., *Nature Biotechnology*, 2008, *26*, 1373-1378.

[2] Anderson, N.L., Anderson, N.G., *Molecular and Cellular Proteomics*, 2002, *1.11*, 845-867.

[3] Bellei, E., Bergamini, S., Monari, E., Fantoni, L.I., Cuoghi, A., *Amino Acids*, 2011, *40*, 145-156.

[4] Tirumalai, R.S., Chan, K.C., Prieto, D.A., Issaq, H.J., Conrads, T.P., Veenstra, T.D., *Molecular and Cellular Proteomics*, 2006, *2.10*, 1096-1103.

[5] Yan, S., Zhang, J., Alici, G., Du, H., Zhu, Y., Li, W., *Lab Chip*, 2014, *14*, 2993-3003.

[6] Moschallski, M., Evers, A., Brandsetter, T., Ruhe, J., *Analytica Chimica Acta*, 2013, *781*, 72-79.

[7] Moschallski, M., Baader, J., Prucker, O., Ruhe, J., *Analytica Chimica Acta*, 2010, *671*, 92-98.

[8] Martin, R.M., Patel, R., Oken, E., Thompson, J., Zinovik, A., Kramer, M.S., Vilchuck, K., Bogdanovich, N., Sergeichick, N., Foo, Y., Gusina, N., *Plos One*, 2013, *8*, 1-10.

[9] Liang, W., Li, Y., Zhang, B., Zhang, Z., Chen, A., Qi, D., Yi, W., Hu, C., *Biosensors and Bioelectronics*, 2012, *31*, 480-485.

[10] Tachi, T., Kaji, N., Tokeshi, M., Baba, T., *Lab on a Chip*, 2009, *9*, 966-971.

[11] Zhang, B., Liu, B., Zhou, J., Tang, J., Tang, D., *Applied Materials and Interfaces*, 2013, *5*, 4479-4485.

[12] Chandra, P., Abbas Zaidi, S., Noh, H.B., Shim, Y.B., *Biosensors and Bioelectronics*, 2011, *28*, 326-332.

[13] Svateck, R.S., Shah, J.B., Xin, J., *et al*., *Cancer*, 2010, *116*, 4513-4519.

[14] Carlo, D.D., Edd, J.F., Irimia, D., Tompkins, R.G., Toner, M., *Analytical Chemistry*, 2008, *80*, 2204-2211.

[15] Javanmard, M., Emaminejad, S., Gupta, C., Provine, J., Davis, R.W., Howe, R.T., *Sensors and Actuators B*, 2014, *193*, 918-924.

[16] Dimov, I.K., Basabe-Desmonts, L., Garcia-Cordero, J.L., Ross, B.M., Ricco, A.J., Lee, L.P., *Lab on a Chip*, 2011, *11*, 845-850.

[17] Li, M., Li, W.H., Zhang, J., Alici, G., Wen, W., *Journal of Physics D: Applied Physics*, 2014, *47*, 1-30.

[18] Jung, J., Han, K.H., *Applied Physics Letters*, 2008, *93*, 223902-1-3.

[19] Gossett, D.R., Carlo, D.D., *Analytical Chemistry*, 2009, *81*, 8459-8465.

[20] VanDelinder, V., Groisman, A., *Analytical Chemistry*, 2007, *79*, 2023-2030.

[21] Demircan, Y., Ozgur, E., Kulah, H., *Electrophoresis*, 2013, *34*, 1008-1027.

[22] Pethig, R., *Biomicrofluidics*, 2010, **4**, 022811-1-35.

[23] Zhu, H., Lin, X., Su, Y., Dong, H., Wu, J., *Biosensors and Bioelectronics*, 2015, *63*, 371-378.

[24] Huang, C., Liu, H., Bander, N.H., Kirby, B.J., *Biomed Microdevices*, 2013, *15*, 941-948.

[25] Sonnenberg, A., Marciniak, J.Y., Skowronski, E.A., Manouchehri, S., Rassenti, L., Ghia, E.M., Widhopf II, G.F., Kipps, T.J., Heller, M.J., *Electrophoresis*, 2014, *35*, 1828-1836.

[26] Jones, P.V., Staton, S.J.R., Hayes, M.A., *Anal Bioanal Chem*, 2011, *401*, 2103-2111.

[27] Turgeon, M.L., *Clinical Hematology: Theory and Procedures* (Principles of Blood Collection, CH 2), 2004, 18-40.

CHAPTER 7

[1] Morrow, D. A., Cannon, C. P., Jesse, R. L., Newby, L. K., Ravkilde, J., Storrow, A. B., Wu, A. H. B., Christenson, R.H., *Clinical Chemistry*, 2007, *53*, 552-574.

[2] Macdonald, S.P.J., Nagree, Y., Fatovich, D.M., Phillips, M., Brown, S.G.A., *Emergency Medicine Journal*, 2012, *30*, 149-154.

[3] Molin, S.Da., Cappellini, F., Falbo, R., Signorini, S., Brambilla, P., *Clinical Biochemistry*, 2014, *47*, 247-249.

[4] Fan, R., Vermesh, O., Srivastava, A., Yen, B.K.H., Qin, L., Ahmad, H., Kwong, G.A., Liu, C.C., Gould, J., Hood, L., Heath, J.R., *Nature Biotechnology*, 2008, *26*, 1373-1378.

[5] Anderson, N.L., Anderson, N.G., *Molecular and Cellular Proteomics*, 2002, *1.11*, 845-867.

[6] Bellei, E., Bergamini, S., Monari, E., Fantoni, L.I., Cuoghi, A., *Amino Acids*, 2011, *40*, 145-156.

[7] Tirumalai, R.S., Chan, K.C., Prieto, D.A., Issaq, H.J., Conrads, T.P., Veenstra, T.D., *Molecular and Cellular Proteomics*, 2006, *2.10*, 1096-1103.

[8] Smits, N.G.E., Ludwig, S.K.J., Van der Veer, G., Bremer, M.G.E.G., Nielen, M.W.F., *Analyst*, 2013, *138*, 111-117.

[9] Jayadev, C., Rout, R., Price, A., Hulley, P., Mahoney, D., *Journal of Immunological Methods*, 2012, *386*, 22-30.

[10] Tirumalai, R.S., Chan, K.C., Prieto, D.A., Issaq, H.J., Conrads, T.P., Veenstra, T.D., *Molecular and Cellular Proteomics*, 2006, *2.10*, 1096-1103.

[11] Mitchell, P., *Nature Biotechnology*, 2010, *28*, 665-670.

[12] Camerini, S., Polci, M. L., Liotta, L. A., Petricoin, E. F., Zhou, W., *Proteomics Clin. Appl.*, 2007, *1*, 176-184.

[13] Joglekar, M., Roggers, R. A., Zhao, Y., Trewyn, B. G., *RSC Advances*, 2013, *3*, 2454-2461.

[14] Wang, X., Masschelein, E., Hespel, P., Adams, E., Schepdael, A. V., *Electrophoresis*, 2012, *33*, 402-405.

[15] Jubery, T. Z., Hossan, M. R., Bottenus, D. R., Ivory, C. F., Dong, W., Dutta, P., *Biomicrofluidics*, 2012, *6*, 016503-1-13.

[16] Startsev, M. A., Inglis, D. W., Baker, M. S., Goldys, E. M., *Analytical Chemistry*, 2013, *85*, 7133-7138.

[17] Inglis, D. W., Goldys, E. M., Calander, N. P., *Angew. Chem. Int. Ed.*, 2011, *50*, 7546-7550.

[18] Kenyon, S. M., Weiss, N. G., Hayes, M. A., *Electrophoresis*, 2012, *33*, 1227-1235.

[19] Meighan, M.M., Vasquez, J., Dziubcynski, L., Hews, S., Hayes, M.A., *Analytical Chemistry*, 2011, *83*, 368-373.

[20] Kenyon, S.M., *The Development of a Microfluidic Array for Use in Electrophoretic Exclusion Separations* (Adapting Electrophoretic Exclusion to a Microdevice, Thesis), 2013, 118-140. http://hdl.handle.net/2286/R.A.97689

CHAPTER 8

[1] Cao, Z., Li, H., Lau, C., Zhang, Y., *Analytica Chimica Acta*, 2011, *698*, 44-50.

[2] Lacharme, F., Vandevyver, C., Gijs, M.A.M., *Microfluid Nanofluidics*, 2009, *7*, 479-487.

[3] Li, Z., Zhao, Q.Y., *et al*., *Sci. China Chem.*, 2010, *53*, 812-819.

[4] Proczek, G., Gassner, A.L., Busnel, J.M., Girault, H.H., *Anal. Bioanal. Chem.*, 2012, *402*, 2645-2653.

[5] Song, S.Y., Han, Y.D., Kim, K., Yang, S.S., Yoon, H.C., *Biosens. Bioelectron.*, 2011, *26*, 3818-3824.

[6] Fu, Z., Shao, G., Wang, J., Lu, D., Wang, W., Lin, Y., *Anal. Chem.*, 2011, *83*, 2685-2690.

[7] Ziegler, J., Zimmermann, M., Hunziker, P., Delamarche, E., *Analytical Chemistry*, 2008, *80*, 1763-1769.

[8] Zimmermann, M., Hunziker, P., Delmarche, E., *Biomed. Microdevices*, 2009, *11*, 1-8.

[9] Lee, B.S., Lee, J.N., Park, J.M., *et al*., *Lab Chip*, 2009, *9*, 1548-1555.

[10] Shao, G., Wang, J., Li, Z., Saraf, L., Wang, W., Lin, Y., *Sens. Actuators B Chemistry*, 2011, *159*, 44-50.

[11] Wang, H., Ou, L.M.L, Suo, Y., Yu, H.Z., *Analytical Chemistry*, 2011, *83*, 1557-1563.

[12] Yu, H.Z., Li, Y., Ou, L.M.L., *Accounts of Chemical Research*, 2013, *46*, 258-268.

[13] Tamarit-Lopez, J., Morais, S., Manuis, M.J., Puchades, R., Maquieira, A., *Analytical Chemistry*, 2010, *82*, 1954-1963.

[14] Pallapa, M., Ou, L.M.L., Parameswaran, M., Yu, H.Z., *Sensors and Actuators B*, 2010, *148*, 620-623.

[15] Seia, M.A., Pereira, S.V., Fontan, C.A., DeVito, I.E., Messina, G.A., Raba, J., *Sens. Actuators B, Chemistry*, 2012, *168*, 297-302.

[16] Kenyon, S.M., *The Development of a Microfluidic Array for Use in Electrophoretic Exclusion Separations* (Adapting Electrophoretic Exclusion to a Microdevice, Thesis), 2013, 118-140. http://hdl.handle.net/2286/R.A.97689

[17] Kenyon, S.M., Weiss, N.G., Hayes, M.A., *Electrophoresis*, 2012, *33*, 1227-1235.

[18] Thomas, C.D., Jacobson, S.C., Ramsey, J.M., *Analytical Chemistry*, 2004, *76*, 6053-6057.

[19] Bai, X., Lee, H.J., Rossier, J.S., Reymond, F., Schafer, H., Wossner, M., Girault, H.H., *Lab on a Chip*, 2002, *2*, 45-49.

[20] Alarle, J.P., Jacobson, S.C., Culbertson, C.T., Ramsey, J.M., *Electrophoresis*, 2000, *21*, 100-106.

[21] Ermakov, S.V., Jacobson, S.C., Ramsey, J.M., *Analytical Chemistry*, 2000, *72*, 3512-3517.

[22] Araci, I.E., Quake, S.R., *Lab on a Chip*, 2012, *12*, 2803-2806.

[23] Weaver, J.A., Melin, J. Stark, D. Quake, S.R., Horowitz, M.A., *Nature Physics*, 2010, *6*, 218-223.

[24] Studer, V., Hang, G., Pandolfi, A., Ortiz, M., Anderson, W.F. Quake, S.R., *J. Appl. Phys.*, 2004, *95*, 393-398.

[25] Unger, M.A., Chou, H.P., Thorsen, T., Scherer, A. Quake, S.R., *Science*, 2000, *288*, 113-116.

APPENDIX A

PUBLISHED PORTIONS

Chapters 2 and 3 were previously published in the journals referenced below.

Woolley, C. F., Hayes, M. A., *Analyst*. 2014, **139**, 2277-2288.

Woolley, C. F., Hayes, M. A., *Bioanalysis*. 2013, **5**, 245-264.

Chapters 4 and 5 were submitted to the journals referenced below.

Woolley, C.F., Hayes, M.A., *Analytical Methods*, submitted.

Woolley, C.F., Hayes, M.A., Mahanti, P., Gilman, S.D., Taylor, T., *Analytical and Bioanalytical Chemistry*, submitted.

Published portions or portions in preparation were included with the permission of all coauthors.

APPENDIX B

SUPPLEMENTAL INFORMATION

Technique	Applications	Sensitivity	Analysis Time	Equipment/Fabrication Requirements	Single/Poly/ Multiplex	References
Non-magnetic particle assay						
FMIA	Protein/ drug/ small molecule quantification	pg - ng/mL	70min-4 hours	Luminex beads; flow cytometer; Luminex X-map technology	Multiplex	12, 13, 20, 23-30
FIA	Protein quantification	~0.1 ng/mL	1-3 hour	Fluorescent microscope; chip fabrication	Singleplex/ Polyplex	14, 48, 50
AlphaLISA	Protein/ toxin detection	~0.007 ng/mL	1(+) hour	EnVision reader; AlphaScreen beads	Singleplex	32, 33
BD Biosciences	Cytokine quantification	3 pg/mL	3(+) hours	BD FACS array bio-analyzer; CBA kit	Multiplex	31
Off-chip incubation magnetic bead assay						
FIA	Protein/ antibody quantification	~11.5 pg/mL	1-3 hours	Microchip fabrication; fluorescent microscope	Singleplex	4, 21, 36, 39, 101
Electrochemical Detection	Antibody quantification	0.19 ng/mL	~3 hours	Electrochemical sensor; microchip fabrication	Singleplex	41
Chemiluminescent Detection	Protein quantification	0.61 ng/mL	~2 hours	Microchip fabrication	Singleplex	34
On-chip magnetic bead assay						
Manipulation of particles	DNA, antibody, small molecule quantification	~250 ng/mL – 0.1 µg/mL	10 min – 2.5 hours	Fluorescence microscope; microchip fabrication	Singleplex	8, 9, 44
Manipulation of reagents	Protein/ antibody quantification	3.2 fg/mL – 16.4 ng/mL	35min – 3 hours	Microchip fabrication; electrochemical detector; isomagnetophoretic detector	Singleplex/ Multiplex	2, 11, 40, 43
Flow-based assay						
RDIA	Protein quantification	67 µg/mL	<10 min	Analog column; fluorescence detector	Singleplex	51, 52
Electrochemical Detection	Protein quantification	1 pg/mL	40 min	Three-electrode electrical system; microchip fabrication	Singleplex	53
Static solid-support assay						

Capillary systems (CSs)	Protein quantification	0.9 ng/mL – 3 µg/mL	11 – 25 min	Microchip fabrication; fluorescence detector	Multiplex	6, 15
Supercritical angle fluorescence	Cytokine quantification	4 pg/mL	13 min	Microchip fabrication; fluorescence detector	Singleplex	57
SOFIA	Dye/protein quantification	~10 ag/mL	~3 hours	Lock-in amplifier; optical fibers; photo-voltaic diode	Singleplex	5
OLISA	Protein quantification	1 ng/mL	~3 hours	Fluorescence detector; detection antibodies with differing fluorophore/quencher pairs	Multiplex	56
Portable disk automated ELISA	Protein/ antibody quantification	0.51 ng/mL	30 min	Micro-disc fabrication	Polyplex	59
Gyrolab	Protein/ antibody quantification	5 ng/mL	~1 hour	Fluorescent detector; Gyrolab Bioaffy CDs	Singleplex	60
DRZ chip	Protein quantification	5 ng/mL	~3 hours	Fluorescence detector; microchip fabrication	Polyplex	10
NP-labeled array	Small molecule/ protein quantification	10 pg/mL	3(+) hours	Fluorescence detector; microchip fabrication	Multiplex	55
TIRFM system	Cytokine quantification	0.13 fg/mL	2 hours	Microscope; microchip fabrication	Singleplex	17
SWIC system	Protein quantification	0.6-0.89 ng/mL	~27 minutes	Chemiluminescence detector; optical shutter; microchip fabrication	Polyplex	62
Microcantelievers	Small molecule quantification	0.1 – 1 ng/mL	1(+) hour	Photon sensitive detector; flow cell; beam splitter	Singleplex	19, 20

Table 3.1. Provided here is a summary of the techniques described for emerging micro-immunoassays. While this table provides an overview of technologies in the field, they represent average values for each category of assay which give only a gross approximation for the capabilities of each immunoassay technique